β-MSCs: Successful fusion of bone marrow mesenchymal stromal cells with β-cells results in a β-cell like phenotype

Dissertation

zur Erlangung des Grades eines Doktors der Naturwissenschaften

im Fachbereich Biologie/Chemie
der Universität Bremen

vorgelegt von

Master of Science
Zahra Azizivarzaneh

Bremen, im Mai 2015

1. Gutachter: Prof. Dr. Kathrin Maedler

2. Gutachter: Prof. Dr. Elke Oetjen

Erklärung gemäß §6 Abs. 5 der Promotionsordnung

Ich versichere, dass ich die vorliegende Dissertation mit dem Titel " β-MSCs: Successful fusion of bone marrow mesenchymal stromal cells with β-cells results in a β-cell like phenotype " selbständig verfasst und keine anderen als die angegebenen Quellen und Hilfsmittel benutzt habe.

Bremen, den ……..

Zahra Azizivarzaneh

Table of contents

I. Abstract

Diabetes mellitus rapidly becomes an epidemic disorder. According to the international diabetes federation (IDF) report, 387 million people suffer from the disease and every 7 seconds a person dies from diabetes in the world. Type 1 diabetes mellitus (T1D) is caused by autoimmune-mediated destruction of β-cells, leading to an absolute deficiency of insulin and development of hyperglycemia. Type 2 diabetes mellitus (T2D) is characterized by a combination of β-cell failure (loss of mass and function) and insulin resistance. Loss of functional β-cell mass is central to the pathogenesis of both types of diabetes. So far, transplantation of the cadaver pancreas or of purified islets is the only clinically applicable strategy to replace the missing islet cells in T1D, this could also be therapeutically valuable in a T2D individual with a profound reduction of β-cell mass. However, the necessary immunosuppressive therapy, limitations in donor supply, quality of islets and limited survival of transplanted islets remain a barrier to islet transplantation. There is a critical need to develop therapeutic strategies aiming for restoration of functional β-cell mass in both types of diabetes. Making new β-cells by induction of human β-cell proliferation and/or β-cell neogenesis from other cell types such as hepatocytes, alpha or acinar cells as well as multipotent stem cells like mesenchymal stromal cells (MSC) represent a promising therapeutic approach to the treatment of diabetes.

MSCs are an attractive tool in transplantation and regenerative medicine due to the lack of human leucocyte antigen (HLA) class II as well as anti-inflammatory and anti-apoptotic properties. They are easily accessible from bone marrow and rapidly expand in the cell culture system. MSCs possess a broad differentiation potential to form other cell types as well. On the other hand, cell-cell fusion is a natural process and tightly regulated from the fertilization and development in the embryonic stage to tissue repair in adults. Bone marrow MSCs are circulating throughout the body and their spontaneous fusion with injured cells has a significant role in *in vivo*-regeneration.

Abstract

Here, I aimed to establish a fusion protocol of human bone marrow derived MSCs with the rat β-cell line (INS1E) as well as with dispersed human islets in order to generate β-MSCs as a cell-based treatment for diabetes. Human MSCs are characterized based on the expression of CD73, CD105 or CD90 or lack of CD34, CD45 and MHC II. MSCs and INS1E cells were infected with the eGFP-puromycin or mCherry-zeocin lentiviral gene ontology (LeGO) viruses and selected with puromycin or zeocin, respectively in order to generate $eGFP^+$MSCs or $mCherry^+$INS1E expressing stable cells. $mCherry^+$ INS1E or human dispersed islet cells were mixed and cultured with $eGFP^+$ MSCs and treated with phytohemagglutinin (PHA-P) and polyethylene glycol (PEG) to induce fusion. MSCs and fused cells were further selected by puromycin treatment.

We observed 1.44 ± 0.18% spontaneous fusion between human MSCs and rat INS1E cells in culture, which increased to 4.72 ± 0.56% after PEG–fusion induction. 83.04 ± 5.77% of these cells are stable polyploid heterokaryons. With the improved fusion protocol, 29.79 ± 2.92% of all MSCs were fused β-MSC heterokaryons based on double positivity for mCherry and eGFP. Such better MSC/β-cell fusion efficiency was reached by an increased number of β-cells in the mixture at a ratio of 1:11 MSC/INS-1E cells, by pretreatment with 33.3 mM glucose for 8 hours at the PHA-P concentration of 100 µg/ml and by a 2^{nd} addition of 50% W/V PEG to the cell mixture. After fusion and puromycin selection, human *NKX6.1* and *insulin* as well as rat *NeuroD1*, *Nkx2.2*, *MafA*, *Pdx1* and *Ins1* mRNA were highly elevated in fused MSC/INS1E cells, compared to the mixed control population. Indeed, our optimized protocol showed higher levels of the β-cell marker expression, compared with the standard fusion protocol (MSC/INS1E cells ratio of 1:2, 100 µg/ml PHA-P, 50% W/V PEG). Such induction of β-cell markers was confirmed in fused human MSC/human dispersed islet cells, which showed elevated *NEUROD1*, *NKX2.2*, *MAFA*, *PDX1* and *insulin* mRNA compared to mixed control. Fused cells had higher insulin content and insulin positive β-MSCs also expressed nuclear PDX1.

In conclusion, in this doctoral project I established a rapid and virus-free optimized PEG fusion protocol in adherent culture for MSCs and β-cells and show fused β-MSCs which express β-cell markers.

II. Zusammenfassung

Diabetes mellitus ist zu einer Krankheit mit epidemischen Ausmaßen mit steigender Inzidenz und Mortalität avanciert. Nach einer Studie der Internationalen Diabetes Federation (IDF) sind weltweit 387 Millionen Menschen erkrankt und alle 7 Sekunden stirbt ein Mensch an Diabetes. Diabetes mellitus vom Typ 1 (T1D) basiert auf einer autoimmun gesteuerten Zerstörung der β-Zellen und resultiert in einen vollständigen Mangel an β-Zellen und führt somit zum Verlust der körpereigenen Insulinsekretion und Entwicklung einer Hyperglykämie. Typ 2 Diabetes mellitus (T2D) tritt in etwa 90-95% der Diabeteserkrankungen auf und ist durch eine Insulinresistenz sowie einen Insulinmangel (Verlust von β-Zellmasse und Funktion) gekennzeichnet. Beide Hauptgruppen des Diabetes sind durch einen Verlust der funktionellen β-Zellmasse charakterisiert. Nach heutigem Stand ist die Transplantation des Pankreas oder isolierter Insellzellen von Organspendern die einzige Chance, die verlorenen Betazellen im T1D sowie in Fällen von massivem Verlust funktioneller β-Zellmasse bei T2D, zu ersetzen. Die Nebenwirkungen der Immunsuppression sowie die völlig unzureichende Anzahl an Spenderorganen, oft eine zu geringe Qualität der isolierten Inseln und nur kurze Überlebenszeiten nach der Transplantation erfordern neue Strategien zur kausalen Therapie des Diabetes zur Wiederherstellung der funktionellen β-Zellmasse.

Mesenchymale Stammzellen (MSCs) wurden bereits erfolgreich bei Transplantationen sowie in der regenerativen Medizin aufgrund ihrer anti-inflammatorischen sowie anti-apoptotischen Eigenschaften und dem Fehlen der humanen Leukozyten Antigene (HLA) Klasse II, die oft für die Abstoßungsreaktionen verantwortlich sind, eingesetzt. MSCs können aus dem Knochenmark gewonnen und stabil *in vitro* kultiviert werden. Sie besitzen ein breites Differenzierungsspektrum in andere Zelltypen. Die Zell-Zell Fusion ist ein natürlicher Prozess, welcher von der Befruchtung über die embryonale Entwicklung bis hin zu Gewebsreparationsmechanismen streng reguliert wird. MSCs aus dem Knochenmark zirkulieren im Körper und können durch ihre Fähigkeit zur

spontanen Fusion verletze Zellen heilen und spielen daher eine wichtige Rolle bei der *in vivo* Regeneration von Zellen und Organen.

Ziel meiner Arbeit war es, ein Protokoll zur Fusion von MSCs aus humanem Knochenmark mit der Ratten β-Zell Zelllinie INS1E und mit isolierten humanen Langerhansschen Inseln zu etablieren, um funktionelle insulinproduzierende β-MSCs herzustellen als zellbasierte Behandlungsmethode für Diabetes. Die humanen MSCs sind aufgrund ihrer Expression von CD73, CD105 und CD90 sowie das Fehlen von CD34, CD45 und MHC II charakterisiert.

Im Rahmen dieser Arbeit wurden MSCs mit eGFP-Puromycin und INS1E Zellen mit mCherry-zeocin LeGO Viren infiziert und mittels Pyromycin bzw. Zeocin selektioniert, um stabile Zelllinien zu etablieren. Diese $eGFP^+$MSCs wurden mit $mCherry^+$INS1E oder humanen Inselzellen mittels phytohemagglutinin (PHA-P) und Polyethylen Glycol (PEG) fusioniert und $eGFP^+$ Zellen im Anschluss über eine Pyromycin Behandlung selektiert.

Es konnte eine spontane Fusionsrate von 1,44 ± 0,18% zwischen humanen MSCs und Ratten INS1E Zellen ermittelt werden, wohingegen die Fusionsrate in der behandelten Gruppe auf 4,72 ± 0,56% erhöht werden konnte. 83,04 ± 5,77% dieser Zellen wiesen stabile polyploide Zellkerne auf und belegen die Möglichkeiten der im Rahmen dieser Arbeit weiterentwickelten Methode. Weitere Anpassungen konnten die Fusionsrate insgesamt auf 29,79 ± 2,92% mCherry und eGFP positive β-MSCs erhöhen. Dies wurde unter anderem durch ein erhöhtes Mischungsverhältnis von 1:11 MSC/INS1E und eine achtstündige Vorbehandlung mit 33.3 mM Glukose erreicht. Zusätzlich wurde die PHA-P Konzentration auf 100 µg/ml erhöht und die Zellen zweifach mit 50% w/v PEG behandelt. Dadurch wurde eine verstärkte Produktion der Betazellmarker erreicht; humane *NKX6.1* und *Insulin* sowie rattenspezifische *NeuroD1*, *Nkx2.2*, *MafA*, *Pdx1* und *Ins1* mRNAs waren stark erhöht in den fusionierten Zellen. Diese Induktion der Expression der β-Zellmarkergene konnte unter Verwendung von humanen MSCs und humanen Inselzellen bestätigt werden. Hier wurde eine verstärkte Expression von *NEUROD1*, *NKX2.2*, *MAFA*, *PDX1* und *Insulin* mRNA in der nach optimiertem Protokoll behandelten Gruppe erzielt. Des Weiteren

konnte ich nachweisen, dass diese fusionierten Zellen einen höheren Insulingehalt und eine größere Anzahl insulinproduzierender β-MSCs, welche auch positiv für PDX1 waren, aufwiesen.

Zusammenfassend ist es mir gelungen, ein schnelles und virenfreies verbessertes PEG Fusionsprotokoll in adhärenten Zellkulturen von MSCs und β-Zellen zu etablieren, wobei die fusionierten Zellen β-Zellmarker exprimieren.

III. Abbreviations

APC	Antigen presenting cells
ATP	Adenosine triphosphate
BCM	β-cell mass
BMDC	Bone marrow derived cell
MSC	Bone marrow mesenchymal stromal cell
CAT	Catalase
cDC	Classical dendritic cells
C–peptide	Connecting peptide
CVB	Coxsackieviruses B
CX3CL1	CX3C ligand 1
CX3CR1	CX3C receptor 1
CXCL12	CXC ligand 12
CXCR12	CXC receptor 12
ER	Endoplasmic reticulum
ESCs	Embryonic stem cells
FA	Fatty acid
FFA	Free fatty acids
FVIIa	Low–molecular mass factor VIIa
G6P	Glucose-6-phosphate
Gal	Galactose–α1,3–galactose
GLUT–1/2	Glucose transporter–1/2
Glut4	Glucose transporter type 4
GSIS	Glucose–stimulated insulin secretion
HDAC	Histone deacetylase
HFD	High-fat diet

Abbreviation

IAPP	Islet amyloid polypeptide
IBMIR	Blood mediated inflammatory reaction
IFN– γ	Interferon– γ
IFN–γ)	Interferon–gamma
IL–12	Interleukin–12
IL–1β	Interleukin–1 beta
iNKT	Invariant natural killer T cells
INS1E	Rat insulinoma cell line
IPC	Insulin–producing cell
iPGTT	Intraperitoneal glucose tolerance test
iPSC	induced pluripotent stem cells
IRS2	Insulin receptor substrate 2
LeGO	Lentiviral gene ontology
MHC	Autoantigen molecules
Mn^{2+}	Manganese ions
MSC	Mesenchymal stromal cells
MST1	Mammalian sterile 20–like kinase 1
NGN3	Neurogenin3
NKX2.2	Nk family homeobox locus 2
NKX6.1	Nk family homeobox locus 1
NOD	Non–obese diabetic
PANC–1	Pancreatic carcinoma, epithelial-like cell line
PAX4	paired box gene 4
pDC	Plasmacytoid Dendritic cell
Pdx1	pancreatic duodenal homeobox 1
PGE2	Prostaglandin E 2
ROS	Reactive oxygen species

Abbreviation

SOD	Superoxide dismutase
STZ	Streptozotocin
T1D	Type 1 Diabetes
T2D	Type 2 Diabetes
TCA	Tricarboxylic acid cycle
Th1	T helper type 1 cell
TLR	Toll–like receptors
TNF– α	Tumor necrosis factor–alpha
TNF–α	Tumor necrosis factor–α
Treg	Regulatory T cell
TSG–6	TNF–stimulated gene 6 protein
Utf1	Chromatin–associated protein

1. Introduction

1.1. Pancreas: structure and function

The pancreas is a yellowish–pink elongated shaped organ, which is attached to the distal two third of the duodenum from the head and overlaid on the stomach. The tail of the pancreas ends close to the splenic hilus and it is softness varies largely. The pancreas as an exocrine and endocrine gland has two distinct functions:

(1) The exocrine function of the pancreas is performed by grape–like clustered cells, called acinar cells, accumulated around ducts. Acinar cells mainly produce a group of inactive digestive enzyme precursors (zymogens). These precursor enzymes are secreted into lumen of acinus and then accumulate in the pancreatic ducts and finally reach the first segment of intestine, called duodenum, where the zymogens cleaved and activate by enteropeptidase.

(2) The endocrine function of the pancreas is formed by a cluster of cells, called the islets of Langerhans, which constitute about one to two percent of the whole pancreas in vertebrates. Microscopically, the pancreatic islets are well vascularized and are surrounded by mesodermal derived stromal cells. Pancreatic islets contain five major type of cells: β–cells, α–cells, δ–cells, ε–cells and PP–cells that secret insulin, glucagon, somatostatin, ghrelin and pancreatic polypeptide, respectively (Figure 1). All of these are glucoregulatory hormones; they regulate glucose homeostasis and metabolic fuels in the body.

β–cells secrete other hormones such as islet amyloid polypeptide (IAPP) or amylin and C–peptide (Connecting peptide), which are both co–secreted with insulin [1-3].

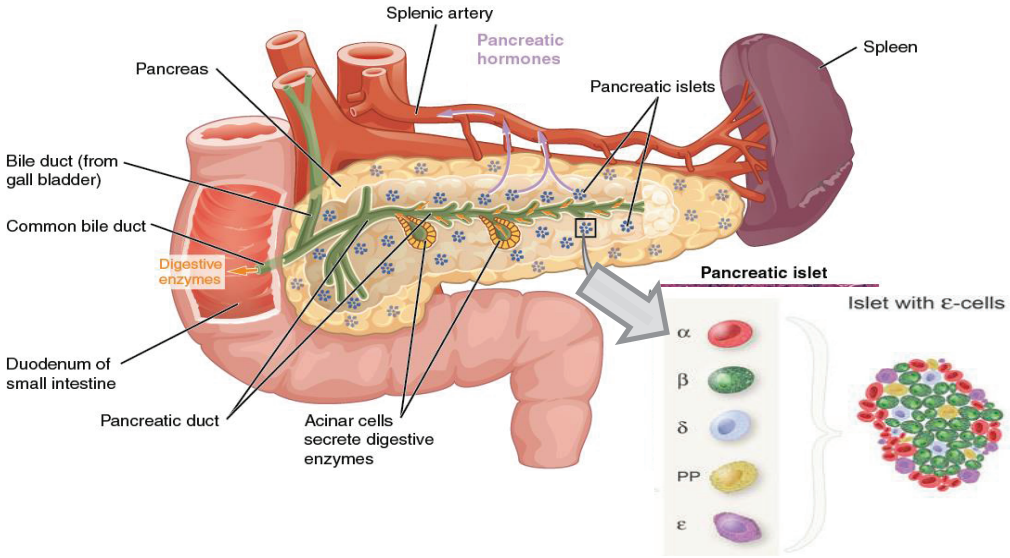

Figure 1 adapted from [1, 2]: Histology of the pancreas: The pancreatic acinar cells secret digestive enzymes like amylase, protease and lipase into duodenum of small intestine via pancreatic duct. The pancreatic islet cells secret insulin (β–cells), glucagon (α– cells), somatostatin (δ–cells), pancreatic polypeptide (pp–cells) and ghrelin (ε–cells). These hormones regulate glucose metabolism in the body.

1.2. Endocrine Pancreatic organogenesis in mammals

Pancreatic organogenesis has three major stages in mammals including primary, secondary and tertiary transitions where progenitor cells differentiate into endocrine committed pancreatic cells.

In the first transition step, the foregut endoderm gets thick and begins to make two buds into surrounding mesenchyme (8.5 to 12.5 days of mouse embryonic day / 2 to 3 weeks of human fetal age [4, 5]). These two buds contain the first pancreatic multipotent progenitor cells (MPCs). MPCs express homeodomain transcription factor pancreatic duodenal homeobox 1 (Pdx1) (4 week in humans) [5]. In humans, the first $PDX1^{+}$ $Insulin^{+}$ cells are observed at 7 weeks [5]. At this stage, bud cells form the first small clusters of secreting $islet^{+}$ cells (10–12 weeks in human [6]). The main hormone

is glucagon in this stage [4]. However, some cells are positive for insulin as well. This is the first wave of endocrine cell differentiation (E11 in mouse [4], 14–15 weeks in human [5]) including “trunk” domain that differentiate into exocrine ducts (express Nkx6.1 [7]) or islet cells (transiently express Neurogenin3 (NGN3) [8]) as well as “tip” domain including multipotent pancreatic progenitor cells (express sox9 [9]) that give rise to proacinar cells [10, 11].

During the second transition step, cells in the tip domain loose multipotency and differentiate into acinar cells [12]. In the trunk domain, $NGN3^+$ endocrine precursors (expressed from E8.5 to E15.5in the mouse [4]) differentiate into five different types of committed endocrine islet cells [11] during this phase (E13.5–E14.5 in mouse) [4]. $NGN3^+$ progenitor cells are detectable for many weeks during pancreas development in humans [13].

NGN3 expression switches on the expression of other transcription factors, such as NeuroD1, Pax4, NKX6.1 and NKX2.2. $NGN3^+$ endocrine progenitor cells move toward a single hormone expressing islet cell [14]. Nk family homeobox locus 2 (NKX2.2), plays an important role in the differentiation into the β-cell fate. NKX2.2 expression is initiated in the dorsal pancreatic epithelium and preserves in mature β- and α-cells. Additionally, Nk family homeobox locus 1 (NKX6.1) and paired box gene 4 (PAX4) are initiated to express in both pancreatic buds and NKX6.1 expression becomes limited to β-cells. It has been shown that the expression of NKX6.1 is essential for proper insulin secretion. The PAX4 expression is also necessary for specification into δ– and β-cell lineages and becomes restricted to β-cells [15, 16]. Additional factors such as PAX6, ARX, and MAFB (for α-cells) and MAFA (for β-cells) control later phases of differentiation into mono-hormone mature islet cells. For instance, the expression of MAFA, the basic leucine-zipper transcription factor, and NeuroD1 is critical for β-cell maturation which persists in mature β-cells [17, 18]. Additionally, the expression of NeuroD1 is required for β-cell glucose responsiveness [19]. It is important to mention that the signal transduction steps for differentiation into β-cells are very similar between β-cell development in the pancreas and the generation of insulin- producing cells in culture [13, 20-23].

The final phase of transition is proliferation and migration of differentiated cells to form the final pancreas structure, which occurs from E16.5 to birth (mouse) or the second trimester of pregnancy in humans (Figure 2) [4, 13, 24].

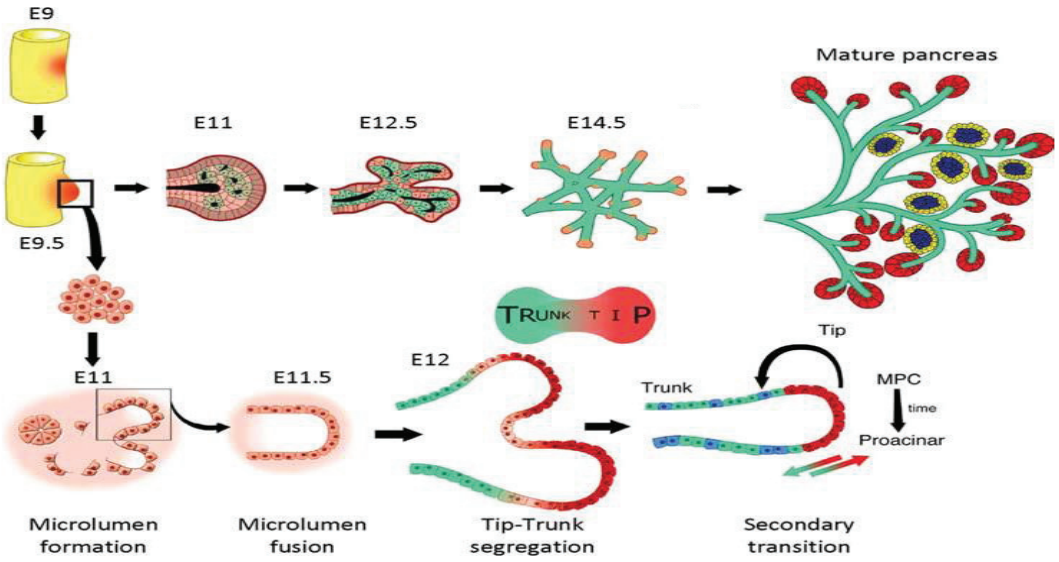

Figure 2 [24]: Mouse pancreas morphogenesis: The schematic picture in the upper panel; it shows the formation of pancreas in three major transition steps and in the lower panel; it depicts the tissue development towards duct (green), acinar (red) or endocrine (blue) lineages in secondary transition step via tip–trunk polarization.

1.3. Insulin: history, structure and secretion

Insulin is the only peptide hormone that can decrease the blood glucose level and is essential to maintain glucose homeostasis in the body. Insulin is a 51–amino acid polypeptide and its localization was detected by immunohistochemistry in pancreatic β–cells by Lacy [25]. The lack of the pancreas results in diabetes; this was the first discovered by group of scientists including Oskar Minkowski, Joseph von Mering and Emmanuel Hédon (1869). Later, Eugen Opie (1901) showed the possible connection of damaged pancreatic islets and human diabetes. Insulin polypeptide is isolated and

used in the market only since 1923, and is one of the most successful scientific achievements of the 20th century, introduced by Banting and Best [26].

Insulin is derived from an inactive precursor proinsulin which undergoes maturation by the prohormone convertases PC1/2 and carboxypeptidase E during a proteolytical process. PC1/2 convertases cleave proinsulin into C–peptide fragment as well as two polypeptide chains A and B which bound together by two disulfide bonds. Mature insulin is finally produced by removing of few amino acids at C–terminal by carboxypeptidase E. The C–peptide has a role, similar to insulin, in maintaining the nutrient levels in the blood plasma. Mature insulin is packed into secretory granules together with C–peptide (ratio of 1:1), stored in the cytoplasmic secretory vesicles near the plasma membrane and will be secreted in response to metabolic signals such increased glucose concentrations (higher than 3mM) into the blood circulation.

Glucose enters the β–cells via the glucose transporter–1/2 (GLUT–1/2) and undergoes glycolysis, yielding two pyruvates that reach the mitochondria. Pyruvate is transformed to acetyl–CoA by pyruvate dehydrogenase complex. Acetyl–CoA entry into tricarboxylic acid cycle (TCA) cycle stimulates mitochondrial oxygen consumption to increase production of adenosine triphosphate (ATP), closure of ATP–sensitive potassium (K^+) channels and cell membrane depolarization. This process leads to a flux of calcium ions (Ca^{2+}) through the voltage–dependent calcium channels as well as their release from the smooth endoplasmic reticulum (ER). Ca^{2+} release triggers exocytosis of insulin granules, insulin release and activating metabolic amplifying pathway. This process is called glucose–stimulated insulin secretion (GSIS) (Figure 3) [27]. A mature β–cell contains about 13 000 secretory granules, which are ready to release insulin to the blood vessels according to changes in nutrient, hormone and transmitter levels to maintain glucose homeostasis [28].

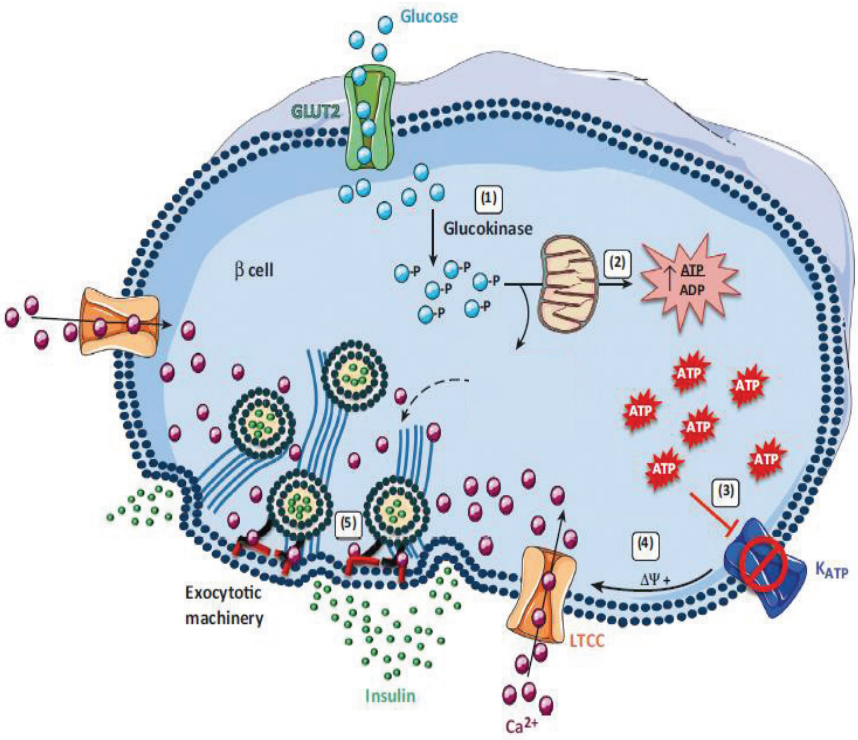

Figure 3 adapted from [27]: Mechanism of GSIS in β–cells: Glucose uptakes through GLUT–2 in a β–cell. Then, glucokinase phosphorylates glucose to produce glucose–6–phosphate (G6P). G6P undergoes glycolysis (energy–releasing pathways) which produces two pyruvates. 1) Pyruvates reach the mitochondria and transformed to acetyl–CoA which entry into TCA cycle and increase the production of ATP. 2) Closure of ATP–sensitive potassium (K^+) channel. 3) Cell membrane depolarization. 4) Influx of extracellular Ca^{2+} ions through the voltage–dependent Ca^{2+}–channel. 5) Insulin granules exocytosis.

1.4. Diabetes Mellitus

Diabetes Mellitus is one of the major disorders in the 21st century. 387 million people in the world suffer from diabetes. The international diabetes federation (IDF) has reported that the number of diabetic patients will be about 592 million by 2035 [29]. Diabetes mellitus is a complex metabolic disorder characterized by abnormalities in insulin secretion and action, which leads to progressive deterioration of glucose tolerance and hyperglycemia. Diabetes is also a heterogeneous disorder and the role of genetic susceptibility and environmental factors in determining diabetes has been reported before [30] .

Two common forms of diabetes are known as Type 1 Diabetes (T1D) and Type 2 Diabetes (T2D). T1D results from the selective destruction of pancreatic β–cells by the autoimmune system and T2D is caused by β–cell failure (loss of mass and function) as well as decrease in insulin sensitivity in the peripheral tissues such as liver, muscles and fat [30, 31] .

1.4.1. Type 1 Diabetes

T1D, also known as insulin–dependent diabetes, is a multifactorial disease characterized by hyper–activation of the autoimmune system resulting in immune cell infiltration into pancreatic islets, local inflammation and β–cell destruction. In T1D, β–cell demise is a non–linear procedure and progression rate of T1D is variable in individual patients [32]. In long-standing T1D patients, no β-cell mass (BCM) is remained [33]. It is possible that a very small subpopulation of proliferative β-cells exist, which -after birth- divide to compensate for insulin demands in the body. However, their expanding rate would not be enough to compensate in severe β-cell failure [34, 35].

Despite genetic factors, the inheritance pattern of T1D is so complicated and this disease rarely develops due to a single gene mutation such as in the HLA locus, PTPN22, IL-2Ralpha, CTLA-4, IFIH [35], Foxp3 transcription factors (which is express in the regulatory T cell (Treg) [36]) or the insulin region on the chromosome [35].

For instance, the susceptibility of T1D in monozygotic twins is much higher (>50%) in compare to zygotic twins (6–10%) [35].

Environmental factors such as lack of vitamin D, enteroviruses especially coxsackieviruses B (CVB) infection and the composition of the gastrointestinal microbiota have been suggested to contribute in the development of T1D [37, 38]. Interestingly, a recent study shows a link between CVB infection and T1D in European countries [37]. It has also been reported that gastrointestinal microflora alterations by antibiotics increased the susceptibility to T1D [38]. Multiple complex environmental factors increase the chance of T1D development [35] .

In T1D patients, the immune system detects β–cells as non–self cells and chronically destroys them by autologous cytotoxic T cells that is mainly observed in children but also affect adolescents [35]. Obtained cytotoxic $CD8^+$T cells from non–obese diabetic (NOD) mice, an established model of T1D, showed more than 60% of these T cells detect G6P catalytic subunit–related protein or insulin [40]. Major targets in autoreactivation of B and T cells in β–cells are glutamic acid decarboxylase–65 /–67, islet antigen–2, islet cell autoantigen of 69 kDa and proinsulin [41, 42]. β–cell autoantigens are released by β–cells through cellular turn–over mechanism or damaged β–cells which will be processed and presented to T cells by Antigen presenting cells (APCs). APCs, such as dendritic cells (DCs) and macrophages are the first cells that are infiltrating to pancreatic islets and present β–cell antigens to Treg cells [43], which are a subgroup of T cells that prevent exceedingly respond of immune system via shut down immune reaction [32]. Finally, pancreatic β–cells become infiltrated by multiple immune cells and these cells are responsible for islet inflammation (insulitis) [35, 44], which leads to β–cell destruction and development of T1D. These infiltrated cells release inflammatory mediators including free oxygen radicals and pro–inflammatory cytokines resulting in β–cells apoptosis [44, 45].

Two mechanisms are proposed for β–cell destruction in T1D: 1) cell–cell contact or recognition–dependent and 2) cytokine activation or recognition–independent [46]. In the cell–cell contact mechanism, autoantigen molecules (MHC) of pancreatic β–cells activate $CD8^+$ T cells, through direct interaction of β–cell MHC and TCR located on T

cells. Such deleterious interaction initiates Fas/FasL interactions and/or the perforin/granzymes system, which induces β–cell apoptosis [35, 47, 48]. In the recognition–independent mechanism, local APCs which have already infiltrated the islets take up pancreatic β–cell autoantigens by phagocytosis and go to pancreatic lymph nodes to recruit activated T cells into islets ultimately leading to β–cell death [35, 45]. In response, β–cells begin to produce high concentration of pro–inflammatory cytokines like interleukin–1 beta (IL–1β), interferon–gamma (IFN–γ) and tumor necrosis factor–alpha (TNF– α) which enhance the recognition of pancreatic β–cells due to cytotoxicity [49].

Furthermore, $CD4^+$ and $CD8^+$ T cells secrete TNF–α or IFN–γ and local APCs produce IL–1β resulted in the acceleration of cell death [50]. In non–diabetic individuals, Treg constantly check potential diabetogenic T cells [43, 49] (Figure4) and it is a claim that T cell mediated–T1D is resistance to response to Treg cells [35, 51].

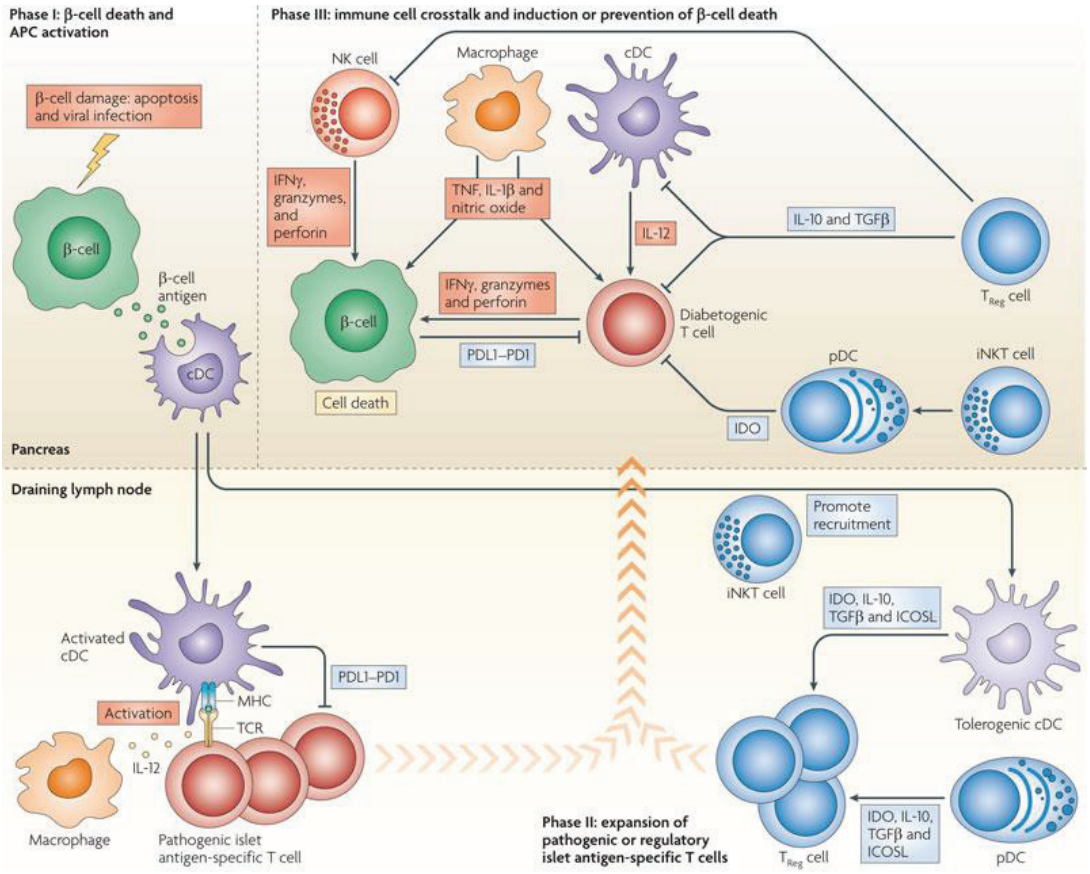

Figure 4 [49]: Different Phases in initiation of T1D: Apoptosis is initiated in β–cells due to viral infection of oxidative stress. Classical dendritic cells (cDC) cells develop the beta–cell antigens in the pancreas resulting in activated cDCs. These cells present β–cell antigens to diabetogenic T cells in the lymph node and the macrophages accelerate this process by interleukin–12 (IL–12) secretion. CDCs can be inhibited via different mechanisms resulted in the suppression loop back of diabetogenic T cells. For instance, invariant natural killer T cells (iNKT) can expand Treg cells via tolerogenic cDCs or plasmacytoid DC (pDC). In the Langerhans islets, the macrophage kills β–cells through secretion of nitric oxide, TNF and IL–1β in addition to IFNγ, perforin and granzymes produced by NK cells and diabetogenic T cells. β–cell destruction loop can be inhibited by Treg.

1.4.2. Type 2 diabetes

T2D is the most common disorder (approximately 90%) among different forms of diabetes, and has a large impact on middle–aged people. T2D is multifactorial disease characterized by combination of β–cell failure (insufficient secretion of insulin due to progressive reduction of β–cell function and mass) as well as insulin resistance (failure of response to the normal action of insulin)[30].

Some factors, such as obesity and the lack of physical activity as well as family history and islet inflammation, strongly contribute towards the development and progression of T2D [30, 52]. The adipose tissues, liver and hypothalamic inflammation promotes insulin resistance and only develops T2D in subjects that are incapable to sustain the β–cell insulin production through compensatory response[30].

Inflammation and elevated free fatty acids (FFA) in T2D individuals inhibits peripheral tissues such as fat and muscle to uptake glucose by blocking cellular insulin signaling which is crucial for insulin–induced glucose transporter type 4 (Glut4) membrane recruitment and localization [53, 54]. Additionally, inflammation decreases glycogen storage and enhances glucose synthesis from non–carbohydrate molecules (gluconeogenesis) and lipogenesis in the liver contributing to hyperglycemia and hyperlipidemia during progression of T2D [53]. In parallel, pro–inflammatory cytokines induce lipolysis in adipose tissues, which results in high concentrations of FFAs in the blood. All of these factors elevate the plasma glucose level, the body demands more insulin to maintain glucose homeostasis and the β–cells try to compensate by increasing their mass and insulin production [55].

Pancreatic β–cells are dynamic cells (Figure 5) and can modulate their mass according to pathophysiological or physiological stages [56, 57] such as obesity, insulin resistance [53] or puberty/pregnancy [58]. β–cell mass adapts in response to high demand of insulin in the body which occurs in two major phases that occur when the body needs to regulate the glucose level.

The First stage (compensation): In order to compensate for higher insulin demand, β–cell increases their mass and/or secretory function. β–cell duplication (hyperplasia) [56], increase in β–cell size (hypertrophy) as well as β–cell neogenesis (forming β–cell from other cell lineages, including duct originated progenitor cells, acinar cells and non–β cells in pancreatic islets, as well as bone marrow cells [57, 59]) are contributing to β–cell boosting in response to metabolic demand. Multiple studies clearly showed such compensatory mechanisms in β–cell adaptive response in rodent models of T2D [60]. But, this still needs to be confirmed in humans (Figure 5).

The Second stage (de–compensation): β–cells produce and secrete high amounts of insulin as a reaction towards hyperglycemia in the early stage of the disease. β–cell failure occurs when islets are unable to maintain β–cell compensation. This functional defect is progressive, particularly after hyperglycemia is established, which ultimately leads to the loss of BCM by apoptosis [57] or de–differentiation [61]. Multiple detrimental factors are involved in the process of β–cell decompensation and loss such as glucotoxicity [62, 63], lipotoxicity [63, 64], proinflammatory cytokines [31, 52], ER stress and oxidative stress [57].

Glucotoxicity or chronically elevated glucose reduces response to stimulus to secrete insulin, and activates ER stress, oxidative stress as well as modifying the gene expression pattern [62, 64]. Extensive metabolism of glucose in the mitochondria can lead to reactive oxygen species (ROS) that damage the cell. ROS are potentially harmful superoxides, which contribute to oxidative stress. Normally, cellular ROS levels are reduced by cellular antioxidant defense system. In chronic hyperglycemia, however, the high amount of glucose in β–cells and overstimulation of the mitochondrial metabolism pathway results in exceedingly high levels of ROS. Therefore, the antioxidant defense system cannot withstand the ROS level and the β–cells undergo damage via lipid peroxidation (oxidative degradation of lipids), protein oxidation and DNA damage [65, 66] as well as the activation of pro–apoptotic cascades [55]. Unlike other cell types like liver cells that can overcome exceedingly high levels of ROS, β–cells are susceptible to oxidative stress mainly because of low expression of antioxidant enzymes like superoxide dismutase (SOD) and catalase

(CAT) [65, 67, 68]. Since, β–cells are almost non–proliferating cells, their apoptosis results in the decrease of total BCM over time (Figure 5) [57].

Chronically high levels of FFAs cause lipotoxicity contributing to the β–cell damage, loss of insulin secretory response and β–cell apoptosis. A high level of intracellular FFAs leads to a higher concentration of fatty–acyl–CoA, malonyl–CoA and fatty acid (FA) peroxidations, as well as ER stress [63, 69]. Unlike of other cell types, such as adipocytes [70] or hepatocytes [71] that can overcome exceedingly high concentration of FFAs, β–cells are sensitive to high levels of FFAs, because β–cells are not specialized cells for metabolizing or sorting lipids [72].

At this stage, insulin biosynthesis and insulin secretion (exocytosis) becomes insufficient in response to glucose stimulus, resulting in imbalanced blood metabolism and hyperglycemia [55, 63, 64]. Patients are fully diabetic when this phase is reached. Other factors such as pro–inflammatory cytokines such as IL–1β are contributing to β–cell dysfunction and apoptosis [31, 52].

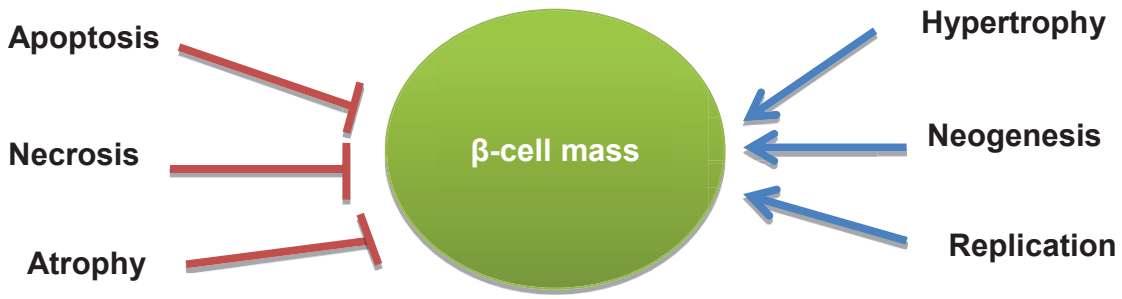

Figure 5 adapted from [57]: BCM changes via different mechanisms: β–cell destruction occurs via apoptosis, necrosis or atrophy, which leads to β–cell loss. On the other hand, BCM can increase via neogenesis, proliferation or hypertrophy.

β-cell failure by apoptosis directly leads to insulin deficiency and development of both types of diabetes (T1D, T2D) [35, 57]. Therefore, apoptosis plays a critical role in the regulation of BCM. Therapeutic strategies aiming for apoptosis blockade would be important in order to restore β-cell function and mass, glucose homeostasis and prevent hyperglycemia in diabetic patients. Therefore, this thesis also aimed to find pharmacological targets for the therapy to maintain BCM and function, since all current drugs in T1D and T2D are only deviating the symptoms and not acting towards the cause of diabetes; the destruction of the β–cells. We identified a pro-apoptotic kinase mammalian sterile 20–like kinase 1 (MST1) as a central target for protecting BCM and function at disease state.

1.5. Mammalian sterile–20 like kinase1 (MST1)

MST1 is a serine/threonine kinase, which regulates cell proliferation, morphogenesis, apoptosis and stress response. This protein is central in apoptotic pathways and acts as a substrate for caspases, through a vicious cycle, MST1 is further activated by cleaved caspase. MST1 autophosporylation activates MST1 resulted in induction of apoptotic machinery including caspase signaling pathways. Upon cleavage, N-terminal fragment of kinase MST1 translocates from cytoplasm to nucleus resulting in phosphorylation of transcription factors that are involved in the apoptotic pathway. The outcome would be DNA fragmentation and apoptosis [73].

Our results show that MST1 is hyperactivated in β–cells under multiple diabetic stimuli, which resulted in activation of mitochondrial–dependent pathway of apoptosis by modulating pro-and anti-apoptotic mitochondrial proteins. We have also discovered that transcription factor PDX1 as a specific MST1 substrate which is ubiquitinated and degraded after activation of MST1 under diabetic conditions. MST1 deletion *in vivo* protects β–cells from STZ-induced hyperglycemia and development of diabetes. The beneficial role of MST1 deletion on β–cell function and survival was further confirmed in HDF mouse model of T2D diabetes. In conclusion, our data showed the strong correlation between MST1 activation and β–cell destruction in diabetic states. Therefore, MST1 inhibition (maybe by developing chemical MST1 inhibitors) would be a good strategy to reduce apoptosis and restore BCM in diabetes [74].

1.6. Diagnosis of Diabetes Mellitus

Diabetes patients are diagnosed with excessive thirst, urination and fatigue [35]. It is a gap between the initiation of β–cell destruction and the appearance of diabetic symptoms. At the time of diagnosis of diabetes, approximately 65% (T2D) or all (T1D) the BCM is lost [33, 75]. Therefore, early diabetes diagnosis is essential to save the remaining β–cells. The best efficient and practical detection tool would be direct measurement of the functional β–cells in the pancreas. Magnetic resonance imaging (MRI) can be a non–harmful tool to scan functional β–cells in the pancreas via the usage of manganese ions (Mn^{2+}) as a contrast agent [76]. Similarly to Ca^{2+} in the β–cells, Mn^{2+} enters through Ca^{2+} voltage–dependent channels [77]. Therefore, the Mn^{2+} signal is glucose dependent in the β–cells and the comparison of Mn^{2+}–enhanced MRI signals before and after glucose injection leads to measurement of functional BCM. For the first time, Antkowiak et al. showed the decrease in Mn^{2+} signals, 5 min after glucose injection in streptozotocin (STZ) mice as a harsh model of BCM loss [78].

In this thesis, we present a significant correlation between functional BCM and Mn^{2+}–enhanced MRI signal shown by GSIS, intraperitoneal glucose tolerance test (iPGTT) and BCM and Mn^{2+} signal in MRI during diabetes development (β–cell compensation and failure stages) in the high–fat diet (HFD) mouse model of T2D. These data were further confirmed by the reduction of MRI signals in STZ induced β–cell destruction. Already after 1 week of HFD a significant increase of MRI signal was measurable in the pancreas suggesting early adaptive response by increasing in the functional BCM. However, the functional BCM measurement needs to be optimized due to the pancreas position in the body and their low contrast between pancreatic islets and peripheral tissues. In conclusion, we establish Mn^{2+}–enhanced MRI *in vivo* imaging as a reliable technique to detect early functional β–cell failure during diabetes progression. This would open the possibility to practically monitor fluctuations of functional BCM during disease and also under therapy. In addition, this method will allow longitudinal studies on the same animals and thus reduce the animals in experiments [79] in accordance with the RRR (replace-reduce-refine) rules of animal experimentations.

1.7. Current therapy of Type 1 diabetes

To date insulin injection is the main treatment for T1D patients. Ideally, personally well–adapted insulin treatment regimen reaches normolglycemia and thus inhibits the risk of hyperglycemia related secondary disorders (neuropathy, retinopathy and nephropathy), but there is a high risk of hypoglycemic events (seizures and coma).

Despite recent efforts on close–loop systems, which can adapt glucose levels to insulin injections, exogenous insulin injections are unable to tightly regulate glucose levels as our body can do under physiologically healthy conditions. Cadaver pancreases or islet cell transplantation is not a feasible cure for these patients. Novel therapeutic strategies have to be used to achieve the goal to restore glucose homeostasis and prevent hyperglycemia in diabetic patients (Figure 6) [80].

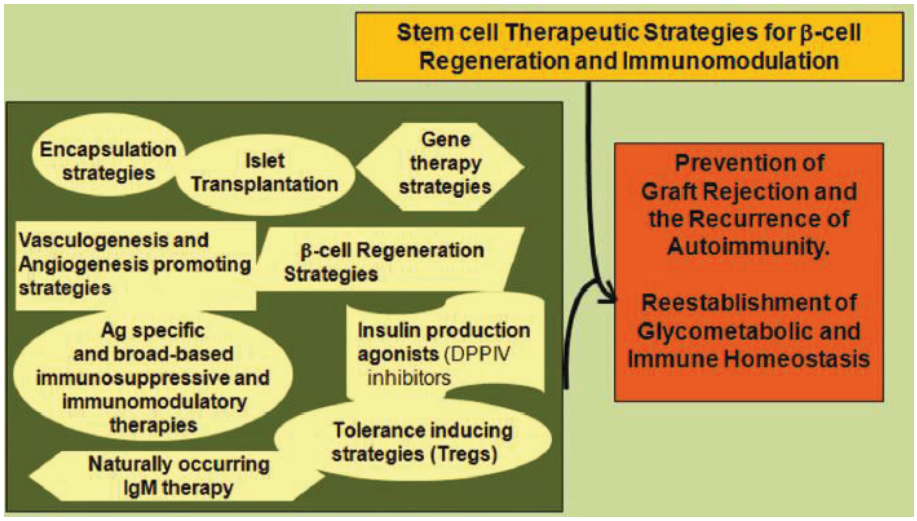

Figure 6 [80]: The combination of different strategies toward treatment of T1D patients.

1.7.1. Pancreas and islet cells transplantation

Pancreas or islet transplantation is a therapeutic tool especially for T1D patients. In 2000, Shapiro and his colleagues reported that two–third of islet transplanted patients were independent from insulin injection for one year by using an improved immunosuppressive regimen after islet cell implantation [81, 82]. They introduced a procedure called “Edmonton protocol” for islet allotransplantation to T1D patients [81]. This approach improves the quality of diabetes patient`s life because they have continuous normoglycemia without insulin injection, at least for some time [83, 84]. However, this curative approach is limited since it needs a large amount of human cadaveric islets (2 cadavers pancreatic islets for one recipient) and ~50% of grafted islets lose their functions in early stage after transplantation due to blood mediated inflammatory reaction (IBMIR) [82]. Autoimmune reactions in T1D patients are high due to autoreaction of lymphocytes to same antigens which express in grafted islets [42]. Follow–up islet treated patients gradually showed a dramatic reduction in insulin independence in most cases during five years [85].

Of note, the Edmonton protocol has been improved by using compounds such as immunosuppressive regimens (everolimus and cyclosporine) and TNF–α blockade (ATG plus etanercept) in the last decade [35, 81]. However, these drugs have a wide range of side effects such as post–transplant neoplasms especially skin cancers in recipients [86]. It has also been shown that autoreactive T cells expand after some immunosuppressive medications, which took place after islet transplantation [35, 87]. Therefore, screening T cell response after islet transplantation is essential to prolong islet transplantation efficiency. Further progress to optimize transplant setting before (isolation, purifications, preparations of islets transplantation procedure, overexpression or suppression of specific genes, which have an impact on negative feedback loop to control insulin–signaling pathway or decrease immune response or treatment of islets with stimuli to maintain cell survival) (Figure 7) [88] and after transplantation (immunosuppression regimen, post graft screening) would be necessary to achieve higher islet post–implantation efficiency [82, 88, 89]. For instance, it has been reported that overexpression of insulin receptor substrate 2

(IRS2) in islets improved the efficiency of transplantation in the mouse model [90]. In another study, *in vitro* data showed that the inhibition of low–molecular mass factor VIIa (FVIIa) reduced IBMIR by inhibiting the activation of 47 kDa transmembrane glycoprotein tissue factor [91, 92].

A. Isolation of human pancreatic islets

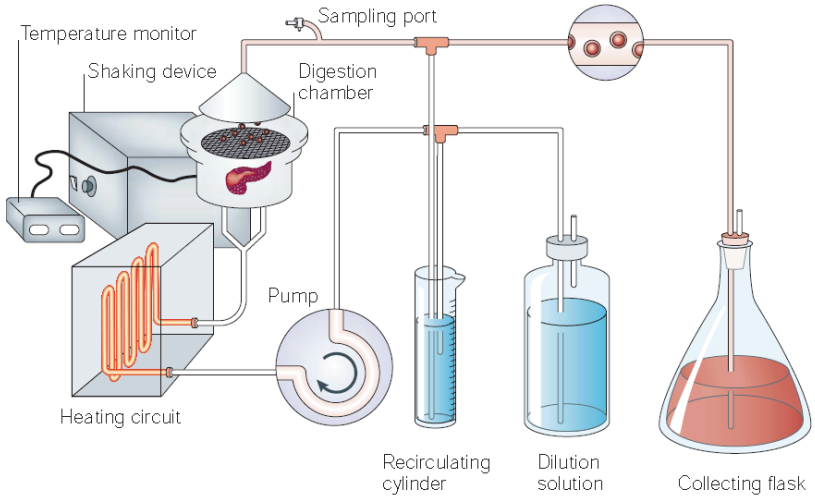

B. Islets purification by density–gradient separation

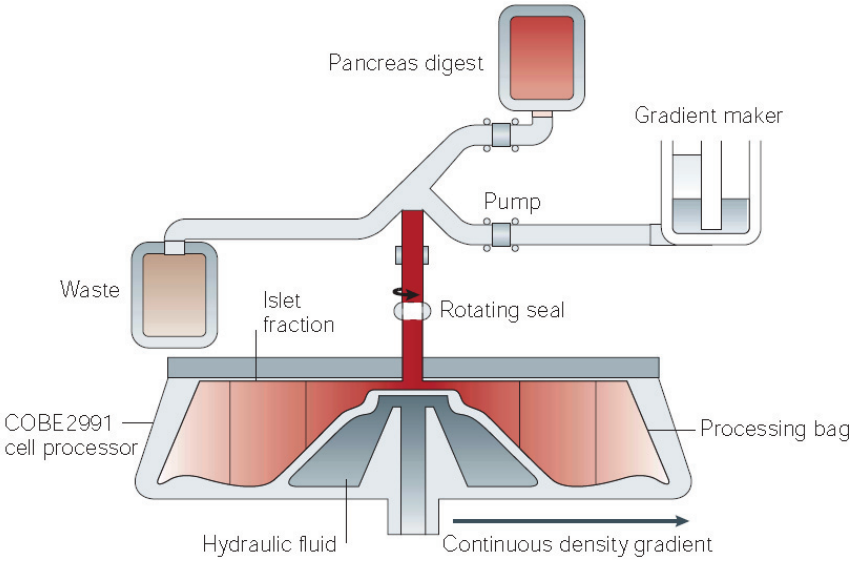

Figure 7 [82]: current automated method to prepare human pancreatic islet clusters for transplantation: A) after injection of enzymes blend such as librase, continuous flow in the digestion chamber improves the efficiency. Blocking the digestion process via cooling, results in less fragmented islet clusters. B) Islet purification is achieved by density–gradient separation (COBE2991 cell processor).

1.7.2. Xenotransplantation

Xenotransplantation is transplantation of living cells or organs from one species to another. Islet xenotransplantation from animals such as pig (Sus scrofa) into humans provides an alternative source for patients with T1D [41, 93]. The instant blood mediated inflammatory reaction (IBMIR) is the main obstacle in both xenografted pancreas as well as adult, neonatal or fetal islet cells [41]. For instance, galactose–α1,3–galactose (Gal) is the most problematic antigen in xenotransplantation rejection since humans naturally have antibodies against Gal. It is expressed in high levels in porcine endothelial cells and neonatal islets. One advantage is that it is lower in mature pig islet cells [94, 95]. Notably, grafted Gal–knockout pig islets to nonhuman primate results in less immune response [41, 95, 96].

Mature pig islets isolation is more difficult than human islets especially then they are younger than two years due to smaller size which makes them susceptible to fragmentation during isolation [97]. Neonatal pig islets have some advantages compared to mature ones such as higher resistance under hypoxic conditions and higher rate of proliferation as well as more successful purification. However, necessity of at least four weeks to become fully functional cells after transplantation is their disadvantage [41, 93].

Alternative places have been tried for islet transplantation in order to minimize IBMIR. These include portal veins [41], gastric submucosal space [98], intramuscular transplantation [99] and abdominal muscle site which showed efficient metabolic improvement in allotransplantation [100]. However, the preferable transplantation site is still under debate. Recent studies have focused on multiple line of studies such as suitable anatomical place for transplantation, local immunosuppression via genetic manipulation as well as reduction of humoral rejection (due to the stimulation of anti–pig antibodies or encapsulation of islets) to overcome some challenges such as capsule degradation and prolonging viability of encapsulated islets. Xenotransplantation is still in trial phase and further studies need to done for possible future application [41, 93, 101].

1.7.3. Cell–based therapy

The limitations of accessible islet sources as well as side effects of immunosuppression regimen bring a new idea: “cell–based therapy” in this field. Stem cells are the main source to reach insulin–producing cells (IPCs). However, different cell sources can be used to achieve this goal (figure 8). There are three distinct experimental methods for achieving this aim: overexpression of transcription factors, addition of chemical compounds like growth factors and cell–cell fusion or cell fusion [102, 103] in which, not terminally differentiated cells will be committed into IPCs [102].

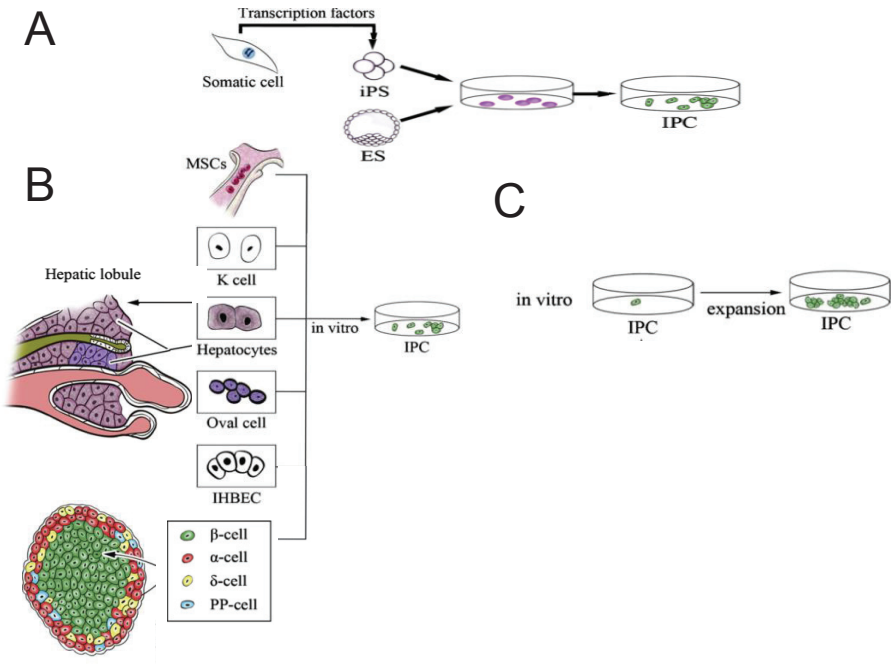

Figure 8 adapted from [102]: Scheme of strategies to generate IPCs *in vitro*: A) Differentiation of pluripotent cells into IPC. B) Transdifferentiation of multipotent cells (MSCs) as well as somatic cells into IPC. C) The aim is the expansion of IPCs in the culture.

1.7.3.1. Stem cells

"*The stem cell is the origin of life*".[1] Stem cells are unspecialized cells that can unlimitedly proliferate (self–renewal character). Based on their origins, there are two main stem cells: embryonic stem cells (ESCs) (originated from Morula or Blastula stages), or adult stem cells (originated from each adult tissue like mesenchymal or hematopoietic bone marrow stem cells and adult–derived pancreatic stem cells) (figure 9) [104]. Based on their plasticity, stem cells are classified to three main categories: totipotent stem cells (can differentiate into all kinds of cells in the body plus extra–embryonic placenta), pluripotent stem cells (can differentiate into all kinds of cells in the body like ESCs and induced pluripotent stem cells (iPSC) and multipotent stem cells (can differentiate into several kinds of cells in the body like mesenchymal stromal cells (MSCs)). Although, high plasticity makes ESCs a powerful tool for regenerative medicine, they have some ethical concern (due to their embryo origin) as well as immunological rejection concern (due to difference in immunogenicity between ESCs donor and recipient) [104, 105]. Therefore, many scientists focused on pluripotent and multipotent stem cell studies to avoid these obstacles in ESCs.

Here, I review the two most commonly used "stem cells" in cell–based therapies: iPSCs and bone marrow MSCs.

MSCs are mesenchymal cells, since they origin from the mesoderm and act as connective tissue. They are stromal cells because they form the supportive structure for the other cells in the tissue. Finally, they are multipotent cells, because they cam differentiate into various cell types, but they are not pluripotent, because they can not form an entire organ Of note, there is still a debate on whether MSCs should be called mesenchymal stem cells, or mesenchymal stromal cells,since they are not fully defined as stem cells and it is still a question mark whether they are able to transdifferentiate into nonmesenchymal cells [106].

[1] Stewart Sell

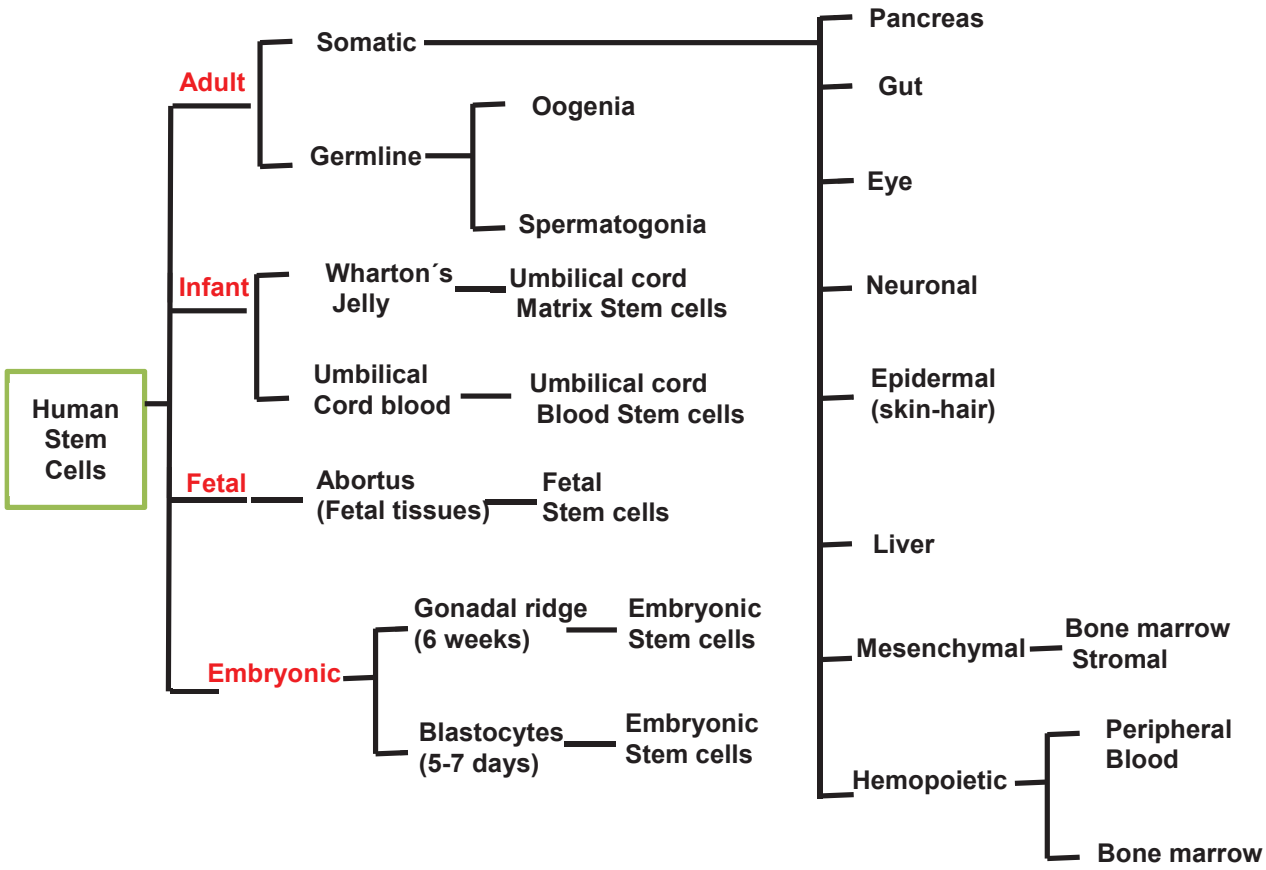

Figure 9 adapted from [104]: Human stem cells categories.

1.7.3.1.1. Induced pluripotent stem cells (iPSCs)

In 2006, Takahashi and Yamanaka first reported that adult mouse fibroblast cells reprogram into iPSCs via the overexpression of specific transcription factors [107]. This report made a new hope for making pluripotent cells from differentiated adult cells. IPSCs are an ideal source of pluripotent stem cells that are derived from any cell types and transplantable without immune rejection in autologous recipient. In parallel, individual patient derived–iPSCs are a useful tool for disease modeling in order to investigate cellular and molecular mechanisms of diseases.

Over the last few years, various range of cells reprogrammed via introducing a combination of transcription factors to make iPSCs. For instance, Stadtfeld *et al*.

introduced iPSCs derived pancreatic β–cells in 2008 [108]. IPSCs are generated by delivery of three/four genes or microRNA (miR) clusters (which are essential for maintenances of pluripotency and self–renewal such as Sox2, c–Myc, Klf4, Nanog, Oct3/4, Lin28 and/or miR302/367) to push somatic cell reprogramming [107, 109].

There are some critical issues regarding iPSCs. The first issue is the efficiency of iPSCs generation since higher number of efficient iPSCs potentially lead to higher number of efficient differentiated colonies. Different methods were applied for delivery of reprogramming factors into somatic cells which are plasmid [107], virus [110], miRNA [111], protein [112] and chemical compounds [113]. Plasmid transfection is an inefficient method (≤0.0002%) compared to viral infection (≤0.2%). Indeed, this efficiency is 10-fold lower than the same method applied for human fibroblast cells compared to mouse fibroblast cells [114]. Although non–integrated strategies were less efficient before, recent studies reported much improved non–integrated protocols [114, 115]. Rais, in 2013, reported that nearly 100% of somatic cells are reprogrammed to iPSCs via depletion of Mbd3 (a molecule that is involved in nucleosome remodeling and deacetylation) in both human and mouse in 5 days [115]. Furthermore, some other factors like cell types, origins and age directly affect the quality and efficiency of the reprogramming and differentiation stages [116].

Safety is the second important issue in using iPSCs for clinical applications. Chang and Sommer independently provided poly–cistronic lentiviral vectors in which all four reprogramming factors were introduced in a single lentiviral vector construct, since infection with a single lentiviral is safer than four vectors [110, 117]. Furthermore, safe transgene–free iPSCs were generated via a cocktail of novel molecules or chemical compounds such as histone methyltransferase inhibitors (BIX01294, BayK8644) [113], histone deacetylase inhibitors (valproic acid [118], butyrate [119]) or chromatin–associated protein (Utf1) as well as anti–p53 specific siRNA combinations [111, 112]. Some of these inhibitors switch on epigenetic regulators like G9a histone methyltransferase inhibitor [113, 116, 120] and deacetylase inhibitors [116, 121, 122] resulted in the high plasticity of iPSCs with the low quality of iPS–differentiated cells [123].

The third issue for using of iPSCs in clinics is immunogenicity. Recently, Araki and Guha independently found that transplantation of differentiated iPSCs to autologous recipients can be tolerated in some tissues due to negligible immunogenicity [124-126]. In another study, transplanted differentiated cells derived from iPSCs provoked immune response in a synergic mouse model due to abnormal gene expression in differentiated iPSCs, compared to ESCs [127].

The fourth major issue is tumorigenicity. Oncogenes such as C–Myc, Klf4 or the loss of tumor suppressor p53 are the oncogenic key factors to make iPSCs and they are being used to maintain survival and proliferation of iPSCs. It has been reported that simultaneous overexpression of C-Myc and KLf4 together with p53 knockdown resulted in a synergistic induction in reprogramming efficiency in fibroblasts-but all those are the factors which potentially make tumors [114, 128, 129]. iPSCs have been proposed but still have a long way to be clinically used in cell therapies.

1.7.3.1.2. Bone marrow mesenchymal stromal cells (MSCs)

For the first time, Friedenstein *et al*. introduced and characterized mouse bone marrow derived cells in 1966 [130]. They showed a group of bone marrow cells that have a potential to differentiate into multilineages and they are called “bone marrow mesenchymal stromal cells” based on their origins in bone marrow, fibroblast–shaped in the culture and no evidence of self–renewal properties *in vivo* [130]. Recent studies showed that MSCs can be found in the most of tissues such as skin, muscle, pancreas and adipose tissues [104, 131, 132]. Current studies also showed that MSCs have the capacity of self–renew *in vivo* [133, 134]. MSCs are easily accessible from the bone marrow. Plastic–adherence and colony forming unit–fibroblasts are the first MSCs characters in the culture. Bone marrow has approximately 0.01–0.001% MSCs that it is not enough for most research purposes [135]. However, these cells rapidly proliferate in the culture and their proliferation rate even accelerates using a platelet lysate instead of preselected FCS [136] or low oxygen tension due to the mimicry of their native microenvironment [137].

In 2006, the international society for cellular therapy has introduced minimal criteria to recognize MSCs by the positivity for surface antigens CD73 (identified by the MAb SH3 and SH4), CD90 and CD105 (identified by the MAb SH2) or the negativity for surface antigens CD34 (primitive hematopoietic progenitors marker), CD45 (pan–leukocyte marker), CD19 and CD79a (B cells marker), CD14 and CD11b (monocytes and macrophages marker) and HLA class II markers as well as the possibility of differentiation into chondrogenic, osteogenic and adipogenic lineages [138].

MSCs circulate through the body via blood stream, migrate and home into injured tissues. Multiple studies showed that the transplantation of MSCs in injured mice improves their recovery [139-141] by the modulation of immune response as well as transdifferentiation (more evidence) or fusion (less evidence) with target cells in injured tissues [141, 142]. MSCs have not only the potential to transdifferentiate into different lineages *in vitro* [143, 144], but also, they can fuse with somatic cells *in vitro* as well as *in vivo* [145-147].

1.7.3.2. MSCs and immune system

MSCs have been proposed as an immunomodulator through direct mechanisms by cell–cell contact, or indirectly, by secretion of growth factors and cytokines [148]. The interaction between MSCs and immune cells affect both innate and adaptive immune response through inhibition of monocyte maturation, T/B lymphocytes proliferation and switching pro– to anti–inflammatory state by modulation of cytokine production [149]. Activated MSCs terminate proinflammatory signals by two mechanisms: 1) Activated MSCs change the phenotype of “killer” M1 macrophage to “healer” M2 macrophage via secretion of prostaglandin E2 (PGE2). 2) Activated MSCs produce a TNF–stimulated gene 6 protein (TSG–6) that interacts with a glycoprotein (CD44) on the surface of M1 macrophages to decline TLR2/NF–kappaB signaling pathway results in reduction of proinflammatory molecules. The outcome is decreasing inflammation [150]. Additionally, the lack of donor antigens, low level of HLA class I and the absence of HLA class II make allogeneic MSCs a suitable source for transplantation [135, 151, 152].

1.7.3.3. MSCs in clinic

In 2002, Bartholomew *et al*. reported that the skin graft survives for a longer time by allogeneic MSCs injection in primates [152]. Later, Yuehua and coworkers showed that injected BMDCs into blastocyst could proliferate and differentiate into all organs in response to the tissue´s specific signals. Unlike ESCs, they did not observe any teratomas after intravenous MSC injection into immunodeficient mice [153]. Another report showed that BCM increase after MSC injection in STZ-induced diabetic mice [154]. Other studies showed that BMDCs circulate and home in different tissues after transplantation. For instance, this has been proven by detection of green fluorescent labeled BMDCs detected in pancreatic islets after injection of GFP^+ bone marrow [155]. Co–transplantation of MSCs with different cells improves and prolongs the transplantation efficiency. For instance, transplantation of pancreatic islets with MSCs prolonged islet survival and improved their functions in a diabetic mouse model [156]. The impact of MSC co–transplantation with islets are summarized in figure 10. Further studies showed MSCs express a set of chemokine receptors such as CX3C receptor 1 (CX3CR1) and CXC receptor 12 (CXCR12), which are attracted by pancreatic islets by expression of CX3C ligand 1 (CX3CL1) and CXC ligand 12 (CXCL12) [157]. Therefore, MSCs would be an attractive vehicle for effective drug, gene or protein delivery to targeted cells [158]. For example, Wu *et al*. showed that co–transplantation of $HGF^+IL–IRa^+$ MSCs with islets improved the efficiency of islet transplantation [159].

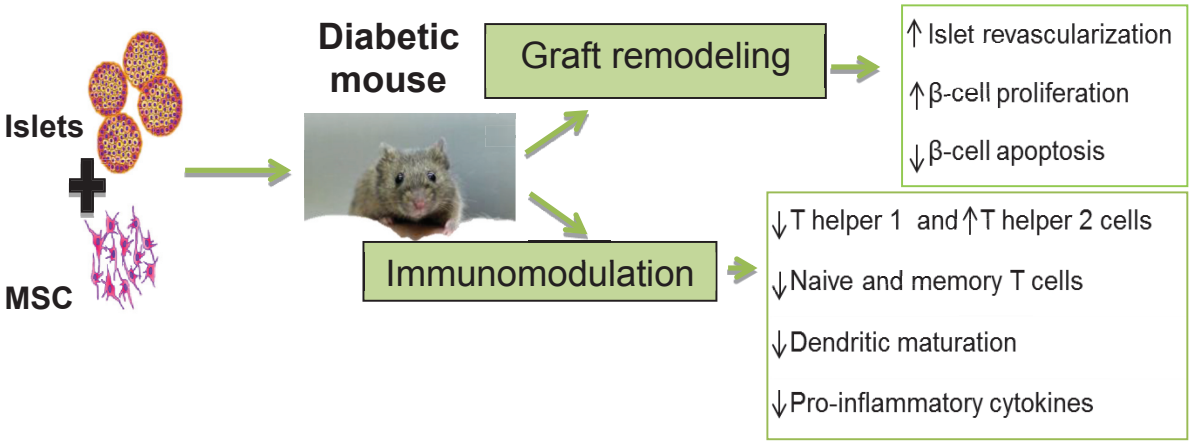

Figure 10 adapted from [160]: The positive impact of MSCs on grafted islets in diabetic mouse model: the co–transplantation of MSCs and islets results in significantly improvement of islet transplantation via graft remodeling and immunomodulation.

Although, Melton and his colleagues showed that the proliferation of β–cells is the main source of new β–cells rather than cell differentiation [56], other studies showed the capacity of MSCs transdifferentiation into β–cells *in vitro* [161, 162] as well as *in vivo* [59, 163]. In summary, MSCs are important cells in clinics because of multiple advantages such as:

1- Source accessibility
2- Anti-inflammatory and, anti– apoptotic properties
3- Capability to differentiate into multilineages like adipocytes, neurons and pancreatic β–cells.
4- Lack of teratomas formation *in vivo* [164].

1.7.3.4. MSCs in regenerative medicine

Over the last three decades, many studies showed that MSCs are an important tool in regenerative medicine [142, 165]. Blau and her coworkers showed transplanted bone

marrow cells which contain different cell types including MSCs (BMDC) contribute to generate myoblast cells in injured mice. In this process, BMDCs first acquire the muscle diploid stem cell fate called satellite cells and later they contribute to generate mature polyploid myofibers [166]. In another study, Hess *et al*. showed lower blood glucose levels in BMDCs injected nonobese diabetic mice; they reported more pancreatic β–cells in BMDCs injected mice suggesting that BMDCs indirectly transdifferentiate into vascular endothelial cells which resulted in higher rate of pancreatic progenitor cell proliferation [162, 163]. Indeed, PDX1–expressing MSCs could be transformed into β–cells and displayed insulin content, glucose–stimulated insulin secretion and reduced hyperglycemia in diabetic mice [165]. Prockop and his colleagues reported a sub-population of differentiated epithelium like cells in the mixture of injured epithelial cells and MSCs in the culture. This result confirmed this idea that some of MSCs transdifferentiated into epithelium like cells. Interestingly, they demonstrated that fusion was a frequent phenomenon and up to 1% of the MSCs were epithelial^{+} polyploid cells [142]. Therefore, it is possible that BMDCs transdifferentiate directly or indirectly after cell fusion with impaired cells in injured tissue *in vivo*.

1.8. Cell fusion as a unique tool

One of the first cell fusion reports was by Sorieul and Ephrussi in 1961. These scientists co–cultured two mouse cell lines constantly. After three months, they observed approximately 10% derived hybrid cells according to chromosome variations due to spontaneous fusion [167]. Later on, Harris *et al*. discovered that UV–inactivated Sendai virus could induce fusion phenomenon in the culture. They fused the mammalian Hela cells with chicken erythrocytes. The chromosome of birds' erythrocytes is condensed and inactive. Interestingly, they observed that interspecies heterokaryons express chicken specific RNA. Therefore, DNA and RNA synthesis had been activated in the chicken nuclei after fusion [168].

Three fundamental methods induce cell fusion in culture; (1) inactivated viruses, (2) chemical agents including PEG and (3) electric pulse [168-170]. Fusion can happen

between the same or different cells and results in transient homokaryons or heterokaryons. Cell fusion has three distinct outcomes; heterokaryon or homokaryon, synkaryon and hybrid (Figure 11). During fusion, the plasma membranes of cells (two or more) that are in contact to each other are merged; cytoplasms distribute, and make a cell with two or more nuclei and one cytoplasm called heterokaryon (in case of different nuclei in 1 cell) or homokaryon (in case of two or more identical nuclei in 1 cell). This cell is a polyploid non–dividing cell and frequently transient, if their nuclei fuse resulting in a polyploid synkaryon (a cell with one nucleus). The nucleus of a synkaryon is a combined chromosome pool of all nuclei. Proliferative synkaryons make hybrids. During cell fusion, epigenetic and genetic information of different cell types would be combined which would lead to modification of the cell expression pattern. This event starts in few hours in the heterokaryon state by remodeling in the chromatin resulting in switch on trans–acting regulators at key loci [171, 172]. Fusion between some interspecies cells, like rat and human, significantly increases the formation of stable interspecies heterokaryons. So that, the nuclei in interspecies heterokaryons would not be combined. This phenomenon brings a unique opportunity to trace the variation of chromosome pool in an intact nucleus after the fusion event. Therefore, these cells are used extensively in epigenetic studies, iPSCs generation [171, 173] as well as in the differentiation field [174]. Studies revealed that the cell fate could be bidirectional after fusion; however, cell fate is fixed to only one of the parental cell fate finally [175]. The dominant cell fate after fusion of one pluripotent with one somatic cell is pluripotency [103]. The dominant cell fate after fusion of two somatic cells depends on cell types; always one of these fates overcomes the other. For instance, Blau and her colleagues indicated that heterokaryons derived from human keratinocytes and mouse myotubes have a more keratinocyte fate [175]; though, subcloning of mouse melanoma–rat hepatoma hybrid produced melanin and albumin but not at the same time [176]. The new cell fate in heterokaryons is determined by the change of structural information in the chromosomes such as DNA methylation and demethylation patterns lead to repression and activation of specific genes. The dominant cell type nuclei would transfer this information to recessive cell type nuclei

via cytoplasm. Moreover, mouse myotubes/human B–lymphocytes heterokaryons are expressing both of these phenotypes in the presence of histone deacetylase (HDAC) inhibitor resulted in blocked gene suppression. It means that dominant and recessive fates ratio is changeable after fusion [177].

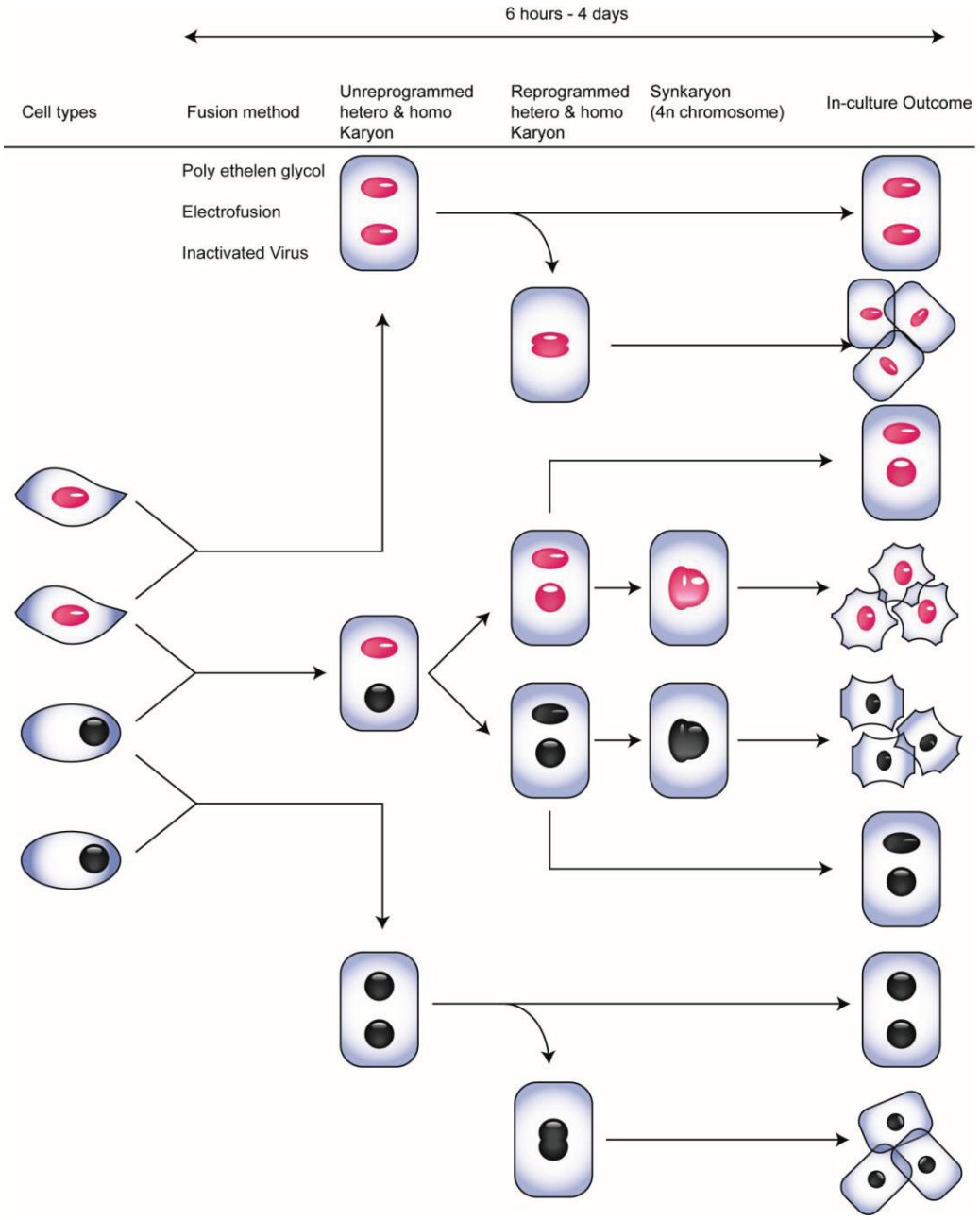

Figure 11: Cell fusion outcomes *in vitro*: Fusion occurs between one cell type or more resulting in homokaryons or heterokaryons. If the nuclei of polyploid cells combine, synkaryons will be generated. Finally, proliferative synkaryons produce hybrids.

1.8.1. BMDCs and cell fusion *in vivo*: A new opportunity for tissue regeneration

Life begins with cell fusion. During fertilization, the membrane of sperm and egg fuse. Fusion is happening repeatedly during developmental process. Later, this phenomenon happens in adults such as macrophage fusion at infectious conditions [172]. In early 2002, Terada *et al*. reported the spontaneous fusion of mouse BMDCs with other cell types in the culture and they also showed that fused cells adopt their phenotype to the recipient cells [178].

Unlike two reports that have not observed any evidence of transdifferentiation via cell fusion to β-cells *in vivo* in humans [179] or in mice [180], many studies indicated BMDCs turn into a new phenotype mainly via cell–fusion *in vivo*. For instance, BMDSCs transdifferentiation was traced by Cre–loxP system in mice after bone marrow transplantation. Data showed that bone marrow cells transdifferentiate into cardiac, lymphatic and kidney tissues and surprisingly, cell fusion was the ubiquitous phenomenon. Monitoring these cells for five months indicated that fused cells do not show any cancer signs [181]. However, spontaneous cell fusion is a rare phenomenon *in vivo* unless under inflammatory conditions within injured tissues [142, 147, 172] and the ratio of spontaneous fusion increases with age and with time after transplantation [182]. Therefore, cell fusion can be a vehicle to transfer an intact chromosome to a damaged cell, which leads to tissue regeneration.

After BMDCs transplantation, the frequency of fusion towards purkinje neurons, skeletal myotubes, cardio myocytes and hepatocytes is higher due to larger cytoplasmic volume of these cells in compare to BMDCs [172]. The outcome is reprogrammed stable heterokaryons [182]. However, the most *in vivo*–cell fusion reports used rodent as a model organism [147, 182-184]. The first report in human is from a woman cerebellar tissue autopsy who received a man and woman bone marrow transplants. Confocal microscopy showed 0.1% of her purkinje neurons were tetraploid (XXXX) or contained both X and Y chromosome (XXXY) resulted in cell fusion between male bone marrow samples and her neurons [182]. Butler and

colleagues indicated the same results. They analyzed 11 individuals' human pancreas sections who received mismatch–sex cord blood cells. They observed that 1.5% of insulin$^+$ cells are diploid with opposite sex cells resulting from differentiation of transplanted cord blood cells to β–cells. Indeed, 0.76% of these insulin$^+$ cells were polyploid cells with three or more sets of sex chromosomes due to fusion of donated cord blood cells and recipient's β–cell [179].

Other studies observed more heterokaryon cells after apoptosis induction [146] or chronic inflammation [147]. But the molecular evidence of reprogramming of transplanted BMDCs still needs to a final proof. The first evidence of *in vivo* reprogramming after fusion was based on condensed or uncondensed chromatin. Blau and coworkers injected GFP$^+$ BMDCs into mice and they observed BMDCs–purkinje binucleated heterokaryons in mouse brain sections. BMDCs chromatin is more compact than purkinje neurons, however, BMDCs nuclei are less compact in binucleated heterokaryons. In support of this, they used L7–GFP–PCP2 BMDCs from transgenic mice. L7 is a specific purkinje neuron promoter that controls PCP2 gene expression. Therefore, when the l7 promoter reactivates via reprogramming in BMDCs, it expresses GFP as well. They injected l7/GFP BMDCs in four mice. The analysis of brain sections showed GFP$^+$ purkinje neurons in each mouse. All GFP$^+$ purkinje cells are binucleated cells [182]. In parallel, a number of studies presented the presence of functional heterokaryons *in vivo* [182, 184]. The full scenario is still unknown.

1.8.2. BMDCs and cell fusion *in vitro*: mimicry of nature for tissue regeneration

Since 1960, different methods were established to induce fusion [168-170] to achieve higher fusion efficiency than spontaneous fusion *in vitro*, but currently the yield is still poor. In 2009, Voldman and his colleagues presented a microfluidic device to improve fusion efficiency in suspension culture [185]. Nevertheless, cell fusion efficiency depends on cell types, *in vitro* age of cells as well as microenvironmental conditions

like TNF–α /INf–δ cytokine pretreatment [183] or apoptotic such as H_2O_2 pretreatment [146]. For example, the fusion of ESCs/MSCs is at least 10x or 50x more efficient than ESCs/neural stem cells or ESCs/adipose tissue–derived cells in the mouse model respectively [186].

The number of fused embryonic fibroblasts is approximately 16 times more in early passages compared to late passages [186]. Yang *et al*. showed that apoptosis induction increase the number of fused cells up to five times. This brings up this idea that fusion can be a main phenomenon to rescue cells in damaged tissues *in vivo* [146]. Flatt and his colleagues introduced a functional human cell line (1.1B4) from the fusion of the epithelial–like cell line, human pancreatic carcinoma, (PANC–1) with human pancreatic islet cells by electrofusion. These studies showed that 1.1B4 hybrid cells have stable characteristics in culture and secrete insulin upon glucose stimulation. Furthermore, the implantation of 1.1B4 cells into STZ–diabetic mice decreases glucose level and resulted in improvement of diabetes [174].

1.9. Aim of the Thesis:

The aim of this thesis is to produce fully functional β-cells by fusion of β-cells with MSCs, which show both cell characteristics to provide a novel transplantable source for β-cell therapy.

Successful reports of the pancreatic islets transplantation bring a new hope to cure both types of diabetes [81-83, 85, 88]. However, human cadaveric islets are a limited source and the side–effects of immunosuppression drugs are risky for patients [187]. Regenerative medicine can overcome these barriers by making new β-cells from patient`s own cell types such as MSCs. Recent studies indicated that co–transplantation of pancreatic islets with MSCs prolongs islet survival due their immunomodulatory effect after transplantation [156, 188] and their potential to differentiate into various cell types [142, 165]. MSCs are also an easily accessible source from the bone marrow and rapidly proliferate in the culture.

Cell-cell fusion is a natural phenomenon which happens in embryonic stages or adults [172, 189] and transplanted bone marrow cells circulate throughout the body and their spontaneous fusion with injured cells makes them an attractive tool for *in vivo*-regeneration [142, 147, 172, 182, 183]. By combining the tissue repair, anti–apoptotic, transdifferentiational, self–renewal, and immunogenic capacity of MSCs [133, 134, 138, 140, 141, 146, 150] with the β–cell characteristics of insulin secretion, I aimed to mimic the fusion phenomenon from the nature and generate a fused human β-cell with a MSC (β-MSC) *in vitro*.

In the first step, I generated polyploid non–dividing β–MSC heterokaryons by fusion of human MSCs and the rat β-cell line INS1E. The formation of these interspecies heterokaryons helped me to precisely count the number of β-MSC fused cells and to optimize the PEG–fusion protocol. Then, rat/human β-MSCs were characterized according to the expression of β-cell markers; human *NKX6.1* and insulin as well as rat *Neurod1, Nkx2.2, MafA, Pdx1* and insulin and insulin content and co-positivity of insulin and PDX1 in insulin^{+} β-MSCs. In the next step, I have used the optimized protocol to fuse human pancreatic dispersed cells with human MSCs to generate

human insulin^{+} β-MSCs which were characterized by the expression of *NEUROD1, NKX2.2, MAFA, PDX1* and *insulin* as well as insulin content and co-positivity of PDX1 in insulin^{+} β-MSCs. I established a rapid virus free fusion protocol of MSCs and β–cells to generate insulin^{+} β-MSCs.

References

1. College CAaPaO. Anatomy & Physiology: CNX Anatomy and Physiology and OpenStax College 2013.
2. cartailler J. 2005 [cited; beta cell consortuim]. Available from: https://www.betacell.org/content/articleview/article_id/13/
3. Gittes GK. Developmental biology of the pancreas: a comprehensive review. *Developmental biology* 2009; **326**: 4-35.
4. Herrera PL, Huarte J, Sanvito F et al. Embryogenesis of the murine endocrine pancreas; early expression of pancreatic polypeptide gene. *Development* 1991; **113**: 1257-65.
5. Piper K, Brickwood S, Turnpenny LW et al. Beta cell differentiation during early human pancreas development. *The Journal of endocrinology* 2004; **181**: 11-23.
6. Polak M, Bouchareb-Banaei L, Scharfmann R, Czernichow P. Early pattern of differentiation in the human pancreas. *Diabetes* 2000; **49**: 225-32.
7. Schaffer AE, Freude KK, Nelson SB, Sander M. Nkx6 transcription factors and Ptf1a function as antagonistic lineage determinants in multipotent pancreatic progenitors. *Developmental cell* 2010; **18**: 1022-9.
8. Villasenor A, Chong DC, Cleaver O. Biphasic Ngn3 expression in the developing pancreas. *Developmental dynamics : an official publication of the American Association of Anatomists* 2008; **237**: 3270-9.
9. Seymour PA, Freude KK, Tran MN et al. SOX9 is required for maintenance of the pancreatic progenitor cell pool. *Proc Natl Acad Sci U S A* 2007; **104**: 1865-70.
10. Benitez CM, Goodyer WR, Kim SK. Deconstructing pancreas developmental biology. *Cold Spring Harb Perspect Biol* 2012; **4**.
11. Arda HE, Benitez CM, Kim SK. Gene regulatory networks governing pancreas development. *Developmental cell* 2013; **25**: 5-13.
12. Zhou Q, Law AC, Rajagopal J et al. A multipotent progenitor domain guides pancreatic organogenesis. *Developmental cell* 2007; **13**: 103-14.
13. Lyttle BM, Li J, Krishnamurthy M et al. Transcription factor expression in the developing human fetal endocrine pancreas. *Diabetologia* 2008; **51**: 1169-80.
14. Gouzi M, Kim YH, Katsumoto K et al. Neurogenin3 initiates stepwise delamination of differentiating endocrine cells during pancreas development. *Developmental dynamics : an official publication of the American Association of Anatomists* 2011; **240**: 589-604.
15. Dohrmann C, Gruss P, Lemaire L. Pax genes and the differentiation of hormone-producing endocrine cells in the pancreas. *Mechanisms of development* 2000; **92**: 47-54.
16. Sander M, Sussel L, Conners J et al. Homeobox gene Nkx6.1 lies downstream of Nkx2.2 in the major pathway of beta-cell formation in the pancreas. *Development* 2000; **127**: 5533-40.

17. Kroon E, Martinson LA, Kadoya K et al. Pancreatic endoderm derived from human embryonic stem cells generates glucose-responsive insulin-secreting cells in vivo. *Nat Biotechnol* 2008; **26**: 443-52.
18. Nishimura W, Kondo T, Salameh T et al. A switch from MafB to MafA expression accompanies differentiation to pancreatic beta-cells. *Developmental biology* 2006; **293**: 526-39.
19. Gu C, Stein GH, Pan N et al. Pancreatic beta cells require NeuroD to achieve and maintain functional maturity. *Cell Metab* 2010; **11**: 298-310.
20. Johannesson B, Sui L, Freytes DO et al. Toward beta cell replacement for diabetes. *The EMBO journal* 2015.
21. Ben-Othman N, Courtney M, Vieira A et al. From pancreatic islet formation to beta-cell regeneration. *Diabetes research and clinical practice* 2013; **101**: 1-9.
22. Liew CG. Generation of insulin-producing cells from pluripotent stem cells: from the selection of cell sources to the optimization of protocols. *Rev Diabet Stud* 2010; **7**: 82-92.
23. Morahan F-XJaG. Pancreatic Stem Cells: Unresolved Business.
24. Pan FC, Wright C. Pancreas organogenesis: from bud to plexus to gland. *Developmental dynamics : an official publication of the American Association of Anatomists* 2011; **240**: 530-65.
25. PE L. Electron microscopic and fluorescent antibody studies on islets of Langerhans. *Experimental cell research* 1959; **7**: 296–308.
26. Luft R. Oskar Minkowski: discovery of the pancreatic origin of diabetes, 1889. *Diabetologia* 1989; **32**: 399-401.
27. Mancini AD, Poitout V. The fatty acid receptor FFA1/GPR40 a decade later: how much do we know? *Trends Endocrin Met* 2013; **24**: 398-407.
28. Olofsson CS, Gopel SO, Barg S et al. Fast insulin secretion reflects exocytosis of docked granules in mouse pancreatic B-cells. *Pflugers Archiv : European journal of physiology* 2002; **444**: 43-51.
29. International Diabetes Federation. *Diabetes Atlas* 2014.
30. Ashcroft FM, Rorsman P. Diabetes mellitus and the beta cell: the last ten years. *Cell* 2012; **148**: 1160-71.
31. Ehses JA, Ellingsgaard H, Boni-Schnetzler M, Donath MY. Pancreatic islet inflammation in type 2 diabetes: from alpha and beta cell compensation to dysfunction. *Archives of physiology and biochemistry* 2009; **115**: 240-7.
32. Chatenoud L, Bluestone JA. CD3-specific antibodies: a portal to the treatment of autoimmunity. *Nature reviews Immunology* 2007; **7**: 622-32.
33. Meier JJ, Breuer TG, Bonadonna RC et al. Pancreatic diabetes manifests when beta cell area declines by approximately 65% in humans. *Diabetologia* 2012; **55**: 1346-54.
34. von Herrath M, Sanda S, Herold K. Type 1 diabetes as a relapsing-remitting disease? *Nature reviews Immunology* 2007; **7**: 988-94.
35. van Belle TL, Coppieters KT, von Herrath MG. Type 1 diabetes: etiology, immunology, and therapeutic strategies. *Physiological reviews* 2011; **91**: 79-118.

36. Wallberg M, Cooke A. Immune mechanisms in type 1 diabetes. *Trends in immunology* 2013; **34**: 583-91.
37. Bluestone JA, Herold K, Eisenbarth G. Genetics, pathogenesis and clinical interventions in type 1 diabetes. *Nature* 2010; **464**: 1293-300.
38. Oikarinen S, Tauriainen S, Hober D et al. Virus antibody survey in different European populations indicates risk association between coxsackievirus B1 and type 1 diabetes. *Diabetes* 2014; **63**: 655-62.
39. Vaarala O, Atkinson MA, Neu J. The "perfect storm" for type 1 diabetes: the complex interplay between intestinal microbiota, gut permeability, and mucosal immunity. *Diabetes* 2008; **57**: 2555-62.
40. Lieberman SM, Takaki T, Han B et al. Individual nonobese diabetic mice exhibit unique patterns of CD8+ T cell reactivity to three islet antigens, including the newly identified widely expressed dystrophia myotonica kinase. *Journal of immunology* 2004; **173**: 6727-34.
41. van der Windt DJ, Bottino R, Kumar G et al. Clinical islet xenotransplantation: how close are we? *Diabetes* 2012; **61**: 3046-55.
42. Hilbrands R, Huurman VA, Gillard P et al. Differences in baseline lymphocyte counts and autoreactivity are associated with differences in outcome of islet cell transplantation in type 1 diabetic patients. *Diabetes* 2009; **58**: 2267-76.
43. Coppieters KT, Roep BO, von Herrath MG. Beta cells under attack: toward a better understanding of type 1 diabetes immunopathology. *Seminars in immunopathology* 2011; **33**: 1-7.
44. Eizirik DL, Mandrup-Poulsen T. A choice of death--the signal-transduction of immune-mediated beta-cell apoptosis. *Diabetologia* 2001; **44**: 2115-33.
45. Mathis D, Vence L, Benoist C. beta-Cell death during progression to diabetes. *Nature* 2001; **414**: 792-8.
46. Finegood DT, Scaglia L, Bonner-Weir S. Dynamics of beta-cell mass in the growing rat pancreas. Estimation with a simple mathematical model. *Diabetes* 1995; **44**: 249-56.
47. Kagi D, Vignaux F, Ledermann B et al. Fas and perforin pathways as major mechanisms of T cell-mediated cytotoxicity. *Science* 1994; **265**: 528-30.
48. Thomas HE, Trapani JA, Kay TW. The role of perforin and granzymes in diabetes. *Cell death and differentiation* 2010; **17**: 577-85.
49. Lehuen A, Diana J, Zaccone P, Cooke A. Immune cell crosstalk in type 1 diabetes. *Nature reviews Immunology* 2010; **10**: 501-13.
50. Kulkarni RN. Islet cell growth factors. Austin, Tex.: Landes Bioscience 2011.
51. Schneider A, Rieck M, Sanda S et al. The effector T cells of diabetic subjects are resistant to regulation via CD4+ FOXP3+ regulatory T cells. *Journal of immunology* 2008; **181**: 7350-5.
52. Baker RG, Hayden MS, Ghosh S. NF-kappaB, inflammation, and metabolic disease. *Cell Metab* 2011; **13**: 11-22.
53. Samuel VT, Shulman GI. Mechanisms for insulin resistance: common threads and missing links. *Cell* 2012; **148**: 852-71.

54. Ciaraldi TP, Abrams L, Nikoulina S et al. Glucose transport in cultured human skeletal muscle cells. Regulation by insulin and glucose in nondiabetic and non-insulin-dependent diabetes mellitus subjects. *J Clin Invest* 1995; **96**: 2820-7.
55. Butler AE, Janson J, Bonner-Weir S et al. Beta-cell deficit and increased beta-cell apoptosis in humans with type 2 diabetes. *Diabetes* 2003; **52**: 102-10.
56. Dor Y, Brown J, Martinez OI, Melton DA. Adult pancreatic beta-cells are formed by self-duplication rather than stem-cell differentiation. *Nature* 2004; **429**: 41-6.
57. Lupi R, Del Prato S. Beta-cell apoptosis in type 2 diabetes: quantitative and functional consequences. *Diabetes & metabolism* 2008; **34 Suppl 2**: S56-64.
58. Van Assche FA, Aerts L, De Prins F. A morphological study of the endocrine pancreas in human pregnancy. *British journal of obstetrics and gynaecology* 1978; **85**: 818-20.
59. Ianus A, Holz GG, Theise ND, Hussain MA. In vivo derivation of glucose-competent pancreatic endocrine cells from bone marrow without evidence of cell fusion. *J Clin Invest* 2003; **111**: 843-50.
60. Ackermann AM, Gannon M. Molecular regulation of pancreatic beta-cell mass development, maintenance, and expansion. *J Mol Endocrinol* 2007; **38**: 193-206.
61. Talchai C, Xuan S, Lin HV et al. Pancreatic beta cell dedifferentiation as a mechanism of diabetic beta cell failure. *Cell* 2012; **150**: 1223-34.
62. Thomas HE, McKenzie MD, Angstetra E et al. Beta cell apoptosis in diabetes. *Apoptosis : an international journal on programmed cell death* 2009; **14**: 1389-404.
63. Del Prato S. Role of glucotoxicity and lipotoxicity in the pathophysiology of Type 2 diabetes mellitus and emerging treatment strategies. *Diabetic medicine : a journal of the British Diabetic Association* 2009; **26**: 1185-92.
64. Kim JW, Yoon KH. Glucolipotoxicity in Pancreatic beta-Cells. *Diabetes & metabolism journal* 2011; **35**: 444-50.
65. Rochette L, Zeller M, Cottin Y, Vergely C. Diabetes, oxidative stress and therapeutic strategies. *Biochimica et biophysica acta* 2014; **1840**: 2709-29.
66. Robertson RP. Oxidative stress and impaired insulin secretion in type 2 diabetes. *Current opinion in pharmacology* 2006; **6**: 615-9.
67. Tiedge M, Lortz S, Drinkgern J, Lenzen S. Relation between antioxidant enzyme gene expression and antioxidative defense status of insulin-producing cells. *Diabetes* 1997; **46**: 1733-42.
68. Hou N, Torii S, Saito N et al. Reactive oxygen species-mediated pancreatic beta-cell death is regulated by interactions between stress-activated protein kinases, p38 and c-Jun N-terminal kinase, and mitogen-activated protein kinase phosphatases. *Endocrinology* 2008; **149**: 1654-65.
69. Wilding JP. The importance of free fatty acids in the development of Type 2 diabetes. *Diabetic medicine : a journal of the British Diabetic Association* 2007; **24**: 934-45.
70. Guilherme A, Virbasius JV, Puri V, Czech MP. Adipocyte dysfunctions linking obesity to insulin resistance and type 2 diabetes. *Nature reviews Molecular cell biology* 2008; **9**: 367-77.

71. Gibbons GF, Wiggins D, Brown AM, Hebbachi AM. Synthesis and function of hepatic very-low-density lipoprotein. *Biochemical Society transactions* 2004; **32**: 59-64.
72. Vernier S, Chiu A, Schober J et al. beta-cell metabolic alterations under chronic nutrient overload in rat and human islets. *Islets* 2012; **4**: 379-92.
73. Ling P, Lu TJ, Yuan CJ, Lai MD. Biosignaling of mammalian Ste20-related kinases. *Cellular signalling* 2008; **20**: 1237-47.
74. Ardestani A, Paroni F, Azizi Z et al. MST1 is a key regulator of beta cell apoptosis and dysfunction in diabetes. *Nat Med* 2014; **20**: 385-97.
75. Matveyenko AV, Butler PC. Relationship between beta-cell mass and diabetes onset. *Diabetes, obesity & metabolism* 2008; **10 Suppl 4**: 23-31.
76. Malaisse WJ, Maedler K. Imaging of the beta-cells of the islets of Langerhans. *Diabetes research and clinical practice* 2012; **98**: 11-8.
77. Lin YJ, Koretsky AP. Manganese ion enhances T1-weighted MRI during brain activation: an approach to direct imaging of brain function. *Magnetic resonance in medicine : official journal of the Society of Magnetic Resonance in Medicine / Society of Magnetic Resonance in Medicine* 1997; **38**: 378-88.
78. Antkowiak PF, Vandsburger MH, Epstein FH. Quantitative pancreatic beta cell MRI using manganese-enhanced Look-Locker imaging and two-site water exchange analysis. *Magnetic resonance in medicine : official journal of the Society of Magnetic Resonance in Medicine / Society of Magnetic Resonance in Medicine* 2012; **67**: 1730-9.
79. Meyer A, Stolz K, Dreher W et al. Manganese-Mediated MRI Signals Correlate With Functional beta-Cell Mass During Diabetes Progression. *Diabetes* 2015.
80. Chhabra P, Brayman KL. Stem cell therapy to cure type 1 diabetes: from hype to hope. *Stem cells translational medicine* 2013; **2**: 328-36.
81. Shapiro AM, Lakey JR, Ryan EA et al. Islet transplantation in seven patients with type 1 diabetes mellitus using a glucocorticoid-free immunosuppressive regimen. *The New England journal of medicine* 2000; **343**: 230-8.
82. Ricordi C, Strom TB. Clinical islet transplantation: advances and immunological challenges. *Nature reviews Immunology* 2004; **4**: 259-68.
83. Goss JA, Schock AP, Brunicardi FC et al. Achievement of insulin independence in three consecutive type-1 diabetic patients via pancreatic islet transplantation using islets isolated at a remote islet isolation center. *Transplantation* 2002; **74**: 1761-6.
84. Stock PG, Bluestone JA. Beta-cell replacement for type I diabetes. *Annual review of medicine* 2004; **55**: 133-56.
85. Ryan EA, Paty BW, Senior PA et al. Five-year follow-up after clinical islet transplantation. *Diabetes* 2005; **54**: 2060-9.
86. Wisgerhof HC, van der Boog PJ, de Fijter JW et al. Increased risk of squamous-cell carcinoma in simultaneous pancreas kidney transplant recipients compared with kidney transplant recipients. *The Journal of investigative dermatology* 2009; **129**: 2886-94.

87. Monti P, Scirpoli M, Maffi P et al. Islet transplantation in patients with autoimmune diabetes induces homeostatic cytokines that expand autoreactive memory T cells. *J Clin Invest* 2008; **118**: 1806-14.
88. Chhabra P, Brayman KL. Overcoming barriers in clinical islet transplantation: current limitations and future prospects. *Curr Probl Surg* 2014; **51**: 49-86.
89. Gurevitch D, Boura-Halfon S, Isaac R et al. Elimination of negative feedback control mechanisms along the insulin signaling pathway improves beta-cell function under stress. *Diabetes* 2010; **59**: 2188-97.
90. Hennige AM, Burks DJ, Ozcan U et al. Upregulation of insulin receptor substrate-2 in pancreatic beta cells prevents diabetes. *J Clin Invest* 2003; **112**: 1521-32.
91. Moberg L, Johansson H, Lukinius A et al. Production of tissue factor by pancreatic islet cells as a trigger of detrimental thrombotic reactions in clinical islet transplantation. *Lancet* 2002; **360**: 2039-45.
92. Johansson H, Lukinius A, Moberg L et al. Tissue factor produced by the endocrine cells of the islets of Langerhans is associated with a negative outcome of clinical islet transplantation. *Diabetes* 2005; **54**: 1755-62.
93. O'Connell PJ, Cowan PJ, Hawthorne WJ et al. Transplantation of xenogeneic islets: are we there yet? *Current diabetes reports* 2013; **13**: 687-94.
94. Rayat GR, Rajotte RV, Hering BJ et al. In vitro and in vivo expression of Gal alpha-(1,3)Gal on porcine islet cells is age dependent. *Journal of Endocrinology* 2003; **177**: 127-35.
95. Thompson P, Badell IR, Lowe M et al. Islet xenotransplantation using gal-deficient neonatal donors improves engraftment and function. *American journal of transplantation : official journal of the American Society of Transplantation and the American Society of Transplant Surgeons* 2011; **11**: 2593-602.
96. Good AH, Cooper DK, Malcolm AJ et al. Identification of carbohydrate structures that bind human antiporcine antibodies: implications for discordant xenografting in humans. *Transplant Proc* 1992; **24**: 559-62.
97. Bottino R, Balamurugan AN, Smetanka C et al. Isolation outcome and functional characteristics of young and adult pig pancreatic islets for transplantation studies. *Xenotransplantation* 2007; **14**: 74-82.
98. Echeverri GJ, McGrath K, Bottino R et al. Endoscopic gastric submucosal transplantation of islets (ENDO-STI): technique and initial results in diabetic pigs. *American journal of transplantation : official journal of the American Society of Transplantation and the American Society of Transplant Surgeons* 2009; **9**: 2485-96.
99. Christoffersson G, Henriksnas J, Johansson L et al. Clinical and experimental pancreatic islet transplantation to striated muscle: establishment of a vascular system similar to that in native islets. *Diabetes* 2010; **59**: 2569-78.
100. Berman DM, O'Neil JJ, Coffey LC et al. Long-term survival of nonhuman primate islets implanted in an omental pouch on a biodegradable scaffold. *American journal of transplantation : official journal of the American Society of Transplantation and the American Society of Transplant Surgeons* 2009; **9**: 91-104.

101. Hu Q, Liu Z, Zhu H. Pig islets for islet xenotransplantation: current status and future perspectives. *Chinese medical journal* 2014; **127**: 370-7.
102. Shen J, Cheng Y, Han Q et al. Generating insulin-producing cells for diabetic therapy: existing strategies and new development. *Ageing research reviews* 2013; **12**: 469-78.
103. Yamanaka S, Blau HM. Nuclear reprogramming to a pluripotent state by three approaches. *Nature* 2010; **465**: 704-12.
104. Bongso A, Lee EH. Stem cells : from bench to bedside. Second edition. ed. Hackensack, New Jersey: World Scientific 2011.
105. Jiang Z, Han Y, Cao X. Induced pluripotent stem cell (iPSCs) and their application in immunotherapy. *Cellular & molecular immunology* 2014; **11**: 17-24.
106. Prockop DJ. Repair of tissues by adult stem/progenitor cells (MSCs): controversies, myths, and changing paradigms. *Molecular therapy : the journal of the American Society of Gene Therapy* 2009; **17**: 939-46.
107. Takahashi K, Yamanaka S. Induction of pluripotent stem cells from mouse embryonic and adult fibroblast cultures by defined factors. *Cell* 2006; **126**: 663-76.
108. Stadtfeld M, Brennand K, Hochedlinger K. Reprogramming of pancreatic beta cells into induced pluripotent stem cells. *Current biology : CB* 2008; **18**: 890-4.
109. Anokye-Danso F, Trivedi CM, Juhr D et al. Highly efficient miRNA-mediated reprogramming of mouse and human somatic cells to pluripotency. *Cell stem cell* 2011; **8**: 376-88.
110. Chang CW, Lai YS, Pawlik KM et al. Polycistronic lentiviral vector for "hit and run" reprogramming of adult skin fibroblasts to induced pluripotent stem cells. *Stem Cells* 2009; **27**: 1042-9.
111. Zhao Y, Yin X, Qin H et al. Two supporting factors greatly improve the efficiency of human iPSC generation. *Cell stem cell* 2008; **3**: 475-9.
112. van den Boom V, Kooistra SM, Boesjes M et al. UTF1 is a chromatin-associated protein involved in ES cell differentiation. *J Cell Biol* 2007; **178**: 913-24.
113. Shi Y, Do JT, Desponts C et al. A combined chemical and genetic approach for the generation of induced pluripotent stem cells. *Cell stem cell* 2008; **2**: 525-8.
114. Okita K, Yamanaka S. Induced pluripotent stem cells: opportunities and challenges. *Philosophical transactions of the Royal Society of London Series B, Biological sciences* 2011; **366**: 2198-207.
115. Rais Y, Zviran A, Geula S et al. Deterministic direct reprogramming of somatic cells to pluripotency. *Nature* 2013; **502**: 65-70.
116. Wang J, Gu Q, Hao J et al. Generation of induced pluripotent stem cells with high efficiency from human umbilical cord blood mononuclear cells. *Genomics, proteomics & bioinformatics* 2013; **11**: 304-11.
117. Sommer CA, Sommer AG, Longmire TA et al. Excision of reprogramming transgenes improves the differentiation potential of iPS cells generated with a single excisable vector. *Stem Cells* 2010; **28**: 64-74.

118. Huangfu D, Osafune K, Maehr R et al. Induction of pluripotent stem cells from primary human fibroblasts with only Oct4 and Sox2. *Nat Biotechnol* 2008; **26**: 1269-75.
119. Ware CB, Wang L, Mecham BH et al. Histone deacetylase inhibition elicits an evolutionarily conserved self-renewal program in embryonic stem cells. *Cell stem cell* 2009; **4**: 359-69.
120. Shi Y, Desponts C, Do JT et al. Induction of Pluripotent Stem Cells from Mouse Embryonic Fibroblasts by Oct4 and Klf4 with Small-Molecule Compounds. *Cell stem cell* 2008; **3**: 568-74.
121. Huangfu D, Maehr R, Guo W et al. Induction of pluripotent stem cells by defined factors is greatly improved by small-molecule compounds. *Nat Biotechnol* 2008; **26**: 795-7.
122. Liang G, Taranova O, Xia K, Zhang Y. Butyrate promotes induced pluripotent stem cell generation. *The Journal of biological chemistry* 2010; **285**: 25516-21.
123. Tachibana M, Amato P, Sparman M et al. Human embryonic stem cells derived by somatic cell nuclear transfer. *Cell* 2013; **153**: 1228-38.
124. Araki R, Uda M, Hoki Y et al. Negligible immunogenicity of terminally differentiated cells derived from induced pluripotent or embryonic stem cells. *Nature* 2013; **494**: 100-4.
125. Guha P, Morgan JW, Mostoslavsky G et al. Lack of immune response to differentiated cells derived from syngeneic induced pluripotent stem cells. *Cell stem cell* 2013; **12**: 407-12.
126. Cao J, Li X, Lu X et al. Cells derived from iPSC can be immunogenic - yes or no? *Protein Cell* 2014; **5**: 1-3.
127. Zhao T, Zhang ZN, Rong Z, Xu Y. Immunogenicity of induced pluripotent stem cells. *Nature* 2011; **474**: 212-5.
128. Marion RM, Strati K, Li H et al. A p53-mediated DNA damage response limits reprogramming to ensure iPS cell genomic integrity. *Nature* 2009; **460**: 1149-53.
129. Hochedlinger K, Yamada Y, Beard C, Jaenisch R. Ectopic expression of Oct-4 blocks progenitor-cell differentiation and causes dysplasia in epithelial tissues. *Cell* 2005; **121**: 465-77.
130. Friedenstein AJ, Piatetzky S, II, Petrakova KV. Osteogenesis in transplants of bone marrow cells. *Journal of embryology and experimental morphology* 1966; **16**: 381-90.
131. Crisan M, Yap S, Casteilla L et al. A perivascular origin for mesenchymal stem cells in multiple human organs. *Cell stem cell* 2008; **3**: 301-13.
132. Crisan M, Corselli M, Chen WC, Peault B. Perivascular cells for regenerative medicine. *Journal of cellular and molecular medicine* 2012; **16**: 2851-60.
133. Sacchetti B, Funari A, Michienzi S et al. Self-renewing osteoprogenitors in bone marrow sinusoids can organize a hematopoietic microenvironment. *Cell* 2007; **131**: 324-36.
134. Mendez-Ferrer S, Michurina TV, Ferraro F et al. Mesenchymal and haematopoietic stem cells form a unique bone marrow niche. *Nature* 2010; **466**: 829-34.

135. Verbeek R. Generation of mesenchymal stem cells as a medicinal product in organ transplantation. *Current opinion in organ transplantation* 2013; **18**: 65-70.
136. Lange C, Cakiroglu F, Spiess AN et al. Accelerated and safe expansion of human mesenchymal stromal cells in animal serum-free medium for transplantation and regenerative medicine. *J Cell Physiol* 2007; **213**: 18-26.
137. Grayson WL, Zhao F, Izadpanah R et al. Effects of hypoxia on human mesenchymal stem cell expansion and plasticity in 3D constructs. *J Cell Physiol* 2006; **207**: 331-9.
138. Dominici M, Le Blanc K, Mueller I et al. Minimal criteria for defining multipotent mesenchymal stromal cells. The International Society for Cellular Therapy position statement. *Cytotherapy* 2006; **8**: 315-7.
139. Parr AM, Tator CH, Keating A. Bone marrow-derived mesenchymal stromal cells for the repair of central nervous system injury. *Bone marrow transplantation* 2007; **40**: 609-19.
140. Karussis D, Karageorgiou C, Vaknin-Dembinsky A et al. Safety and immunological effects of mesenchymal stem cell transplantation in patients with multiple sclerosis and amyotrophic lateral sclerosis. *Archives of neurology* 2010; **67**: 1187-94.
141. Rustad KC, Gurtner GC. Mesenchymal Stem Cells Home to Sites of Injury and Inflammation. *Advances in wound care* 2012; **1**: 147-52.
142. Spees JL, Olson SD, Ylostalo J et al. Differentiation, cell fusion, and nuclear fusion during ex vivo repair of epithelium by human adult stem cells from bone marrow stroma. *Proc Natl Acad Sci U S A* 2003; **100**: 2397-402.
143. Galmiche MC, Koteliansky VE, Briere J et al. Stromal cells from human long-term marrow cultures are mesenchymal cells that differentiate following a vascular smooth muscle differentiation pathway. *Blood* 1993; **82**: 66-76.
144. Kopen GC, Prockop DJ, Phinney DG. Marrow stromal cells migrate throughout forebrain and cerebellum, and they differentiate into astrocytes after injection into neonatal mouse brains. *Proc Natl Acad Sci U S A* 1999; **96**: 10711-6.
145. Vassilopoulos G, Wang PR, Russell DW. Transplanted bone marrow regenerates liver by cell fusion. *Nature* 2003; **422**: 901-4.
146. Yang WJ, Li SH, Weisel RD et al. Cell fusion contributes to the rescue of apoptotic cardiomyocytes by bone marrow cells. *Journal of cellular and molecular medicine* 2012; **16**: 3085-95.
147. Johansson CB, Youssef S, Koleckar K et al. Extensive fusion of haematopoietic cells with Purkinje neurons in response to chronic inflammation. *Nature cell biology* 2008; **10**: 575-83.
148. Di Nicola M, Carlo-Stella C, Magni M et al. Human bone marrow stromal cells suppress T-lymphocyte proliferation induced by cellular or nonspecific mitogenic stimuli. *Blood* 2002; **99**: 3838-43.
149. Krampera M. Mesenchymal stromal cell 'licensing': a multistep process. *Leukemia* 2011; **25**: 1408-14.
150. Prockop DJ. Concise review: two negative feedback loops place mesenchymal stem/stromal cells at the center of early regulators of inflammation. *Stem Cells* 2013; **31**: 2042-6.

151. Le Blanc K, Tammik C, Rosendahl K et al. HLA expression and immunologic properties of differentiated and undifferentiated mesenchymal stem cells. *Experimental hematology* 2003; **31**: 890-6.
152. Bartholomew A, Sturgeon C, Siatskas M et al. Mesenchymal stem cells suppress lymphocyte proliferation in vitro and prolong skin graft survival in vivo. *Experimental hematology* 2002; **30**: 42-8.
153. Jiang Y, Jahagirdar BN, Reinhardt RL et al. Pluripotency of mesenchymal stem cells derived from adult marrow. *Nature* 2002; **418**: 41-9.
154. Ezquer FE, Ezquer ME, Parrau DB et al. Systemic administration of multipotent mesenchymal stromal cells reverts hyperglycemia and prevents nephropathy in type 1 diabetic mice. *Biology of blood and marrow transplantation : journal of the American Society for Blood and Marrow Transplantation* 2008; **14**: 631-40.
155. Hasegawa Y, Ogihara T, Yamada T et al. Bone marrow (BM) transplantation promotes beta-cell regeneration after acute injury through BM cell mobilization. *Endocrinology* 2007; **148**: 2006-15.
156. Borg DJ, Weigelt M, Wilhelm C et al. Mesenchymal stromal cells improve transplanted islet survival and islet function in a syngeneic mouse model. *Diabetologia* 2014; **57**: 522-31.
157. Sordi V, Malosio ML, Marchesi F et al. Bone marrow mesenchymal stem cells express a restricted set of functionally active chemokine receptors capable of promoting migration to pancreatic islets. *Blood* 2005; **106**: 419-27.
158. Wu H, Mahato RI. Mesenchymal stem cell-based therapy for type 1 diabetes. *Discov Med* 2014; **17**: 139-43.
159. Wu H, Lu W, Mahato RI. Mesenchymal stem cells as a gene delivery vehicle for successful islet transplantation. *Pharmaceutical research* 2011; **28**: 2098-109.
160. Sordi V, Piemonti L. Mesenchymal stem cells as feeder cells for pancreatic islet transplants. *Rev Diabet Stud* 2010; **7**: 132-43.
161. Jafarian A, Taghikhani M, Abroun S et al. Generation of high-yield insulin producing cells from human bone marrow mesenchymal stem cells. *Molecular biology reports* 2014; **41**: 4783-94.
162. Hess D, Li L, Martin M et al. Bone marrow-derived stem cells initiate pancreatic regeneration. *Nat Biotechnol* 2003; **21**: 763-70.
163. Lechner A, Habener JF. Bone marrow stem cells find a path to the pancreas. *Nat Biotechnol* 2003; **21**: 755-6.
164. Ma S, Xie N, Li W et al. Immunobiology of mesenchymal stem cells. *Cell death and differentiation* 2014; **21**: 216-25.
165. Karnieli O, Izhar-Prato Y, Bulvik S, Efrat S. Generation of insulin-producing cells from human bone marrow mesenchymal stem cells by genetic manipulation. *Stem Cells* 2007; **25**: 2837-44.
166. LaBarge MA, Blau HM. Biological progression from adult bone marrow to mononucleate muscle stem cell to multinucleate muscle fiber in response to injury. *Cell* 2002; **111**: 589-601.
167. Sorieul S, Ephrussi B. Karyological Demonstration of Hybridization of Mammalian Cells in Vitro. *Nature* 1961; **190**: 653-&.

168. Harris H, Watkins JF. Hybrid Cells Derived from Mouse and Man: Artificial Heterokaryons of Mammalian Cells from Different Species. *Nature* 1965; **205**: 640-6.
169. Pontecorvo G. Production of mammalian somatic cell hybrids by means of polyethylene glycol treatment. *Somatic cell genetics* 1975; **1**: 397-400.
170. Teissie J, Knutson VP, Tsong TY, Lane MD. Electric pulse-induced fusion of 3T3 cells in monolayer culture. *Science* 1982; **216**: 537-8.
171. Tsubouchi T, Soza-Ried J, Brown K et al. DNA synthesis is required for reprogramming mediated by stem cell fusion. *Cell* 2013; **152**: 873-83.
172. Ahren B. Are sulfonylureas less desirable than DPP-4 inhibitors as add-on to metformin in the treatment of type 2 diabetes? *Current diabetes reports* 2011; **11**: 83-90.
173. Lluis F, Ombrato L, Pedone E et al. T-cell factor 3 (Tcf3) deletion increases somatic cell reprogramming by inducing epigenome modifications. *Proc Natl Acad Sci U S A* 2011; **108**: 11912-7.
174. McCluskey JT, Hamid M, Guo-Parke H et al. Development and functional characterization of insulin-releasing human pancreatic beta cell lines produced by electrofusion. *The Journal of biological chemistry* 2011; **286**: 21982-92.
175. Palermo A, Doyonnas R, Bhutani N et al. Nuclear reprogramming in heterokaryons is rapid, extensive, and bidirectional. *Faseb J* 2009; **23**: 1431-40.
176. Fougere C, Weiss MC. Phenotypic Exclusion in Mouse Melanoma Rat Hepatoma Hybrid-Cells - Pigment and Albumin Production Are Not Re-Expressed Simultaneously. *Cell* 1978; **15**: 843-54.
177. Terranova R, Pereira CF, Du Roure C et al. Acquisition and extinction of gene expression programs are separable events in heterokaryon reprogramming. *J Cell Sci* 2006; **119**: 2065-72.
178. Terada N, Hamazaki T, Oka M et al. Bone marrow cells adopt the phenotype of other cells by spontaneous cell fusion. *Nature* 2002; **416**: 542-5.
179. Huang CJ, Butler AE, Moran A et al. A low frequency of pancreatic islet insulin-expressing cells derived from cord blood stem cell allografts in humans. *Diabetologia* 2011; **54**: 1066-74.
180. Ianus A, Holz GG, Theise ND, Hussain MA. In vivo derivation of glucose-competent pancreatic endocrine cells from bone marrow without evidence of cell fusion. *J Clin Invest* 2003; **111**: 843-50.
181. Bonde S, Pedram M, Stultz R, Zavazava N. Cell fusion of bone marrow cells and somatic cell reprogramming by embryonic stem cells. *FASEB journal : official publication of the Federation of American Societies for Experimental Biology* 2010; **24**: 364-73.
182. Weimann JM, Johansson CB, Trejo A, Blau HM. Stable reprogrammed heterokaryons form spontaneously in Purkinje neurons after bone marrow transplant. *Nature cell biology* 2003; **5**: 959-66.
183. Kemp K, Gordon D, Wraith DC et al. Fusion between human mesenchymal stem cells and rodent cerebellar Purkinje cells. *Neuropathology and applied neurobiology* 2011; **37**: 166-78.

184. Larsson LI, Bjerregaard B, Talts JF. Cell fusions in mammals. *Histochemistry and cell biology* 2008; **129**: 551-61.
185. Skelley AM, Kirak O, Suh H et al. Microfluidic control of cell pairing and fusion. *Nature methods* 2009; **6**: 147-52.
186. Tat PA, Sumer H, Pralong D, Verma PJ. The efficiency of cell fusion-based reprogramming is affected by the somatic cell type and the in vitro age of somatic cells. *Cellular reprogramming* 2011; **13**: 331-44.
187. Joshi N, Caputo GM, Weitekamp MR, Karchmer AW. Primary care: Infections in patients with diabetes mellitus. *New Engl J Med* 1999; **341**: 1906-12.
188. Wu H, Wen D, Mahato RI. Third-party mesenchymal stem cells improved human islet transplantation in a humanized diabetic mouse model. *Molecular therapy : the journal of the American Society of Gene Therapy* 2013; **21**: 1778-86.
189. Dittmar T, Zanker KS. Cell fusion in health and disease. Volume II: cell fusion in disease. Introduction. *Advances in experimental medicine and biology* 2011; **714**: 1-3.

2. Results

Manuscripts

This thesis is based on the following manuscript that is under submission.

To be submitted to Cell Reports Journal.

β-MSCs: successful fusion of MSCs with β-cells results in a β-cell like phenotype

Zahra Azizi[1, 2], Claudia Lange[2], Federico Paroni[1], Amin Ardestani[1], Anke Meyer[1], Julie Kerr-Conte[3], Francois Pattou[3], Axel Zander[2], Christof Westenfelder[4] and Kathrin Maedler[1]

1Centre for Biomolecular Interactions, University of Bremen, Bremen, Germany

2Center of Bone Marrow Transplantation, University Hospital Hamburg-Eppendorf, Hamburg, Germany

3 European Genomic Institute for Diabetes, Lille, France. INSERM UMR 1190, Lille, France

4Departments of Medicine and Physiology, University of Utah and George E Wahlen Veterans Affairs Medical Centers, Salt Lake City, Utah, USA

β-MSCs: successful fusion of MSCs with β-cells results in a β-cell like phenotype

Bone marrow mesenchymal stromal cells (MSC) have anti-inflammatory, anti-apoptotic and immunosuppressive properties and are a potent source for cell therapy. Cell fusion has been proposed for rapid generation of functional new reprogrammed cells. In this study, we aimed to establish a fusion protocol of bone marrow derived human MSCs with the rat β-cell line (INS-1E) as well as isolated human pancreatic islets in order to generate functional insulin producing β-MSCs as a cell-based treatment for diabetes.

Human eGFP-puromycin^{+} MSCs were co-cultured with either stably mCherry-expressing rat INS-1E cells or human dispersed islet cells and treated with phytohemagglutinin (PHA-P) and polyethylene glycol (PEG) to induce fusion. MSCs and fused cells were selected by puromycin treatment.

With an improved fusion protocol, 29.79 ± 2.92% of all MSCs generated β-MSC heterokaryons based on double positivity for mCherry and eGFP.

After fusion and puromycin selection, human *NKX6.1* and *insulin* as well as rat *Neurod1, Nkx2.2, MafA, Pdx1* and *Ins1* mRNA were highly elevated in fused human MSC/INS-1E cells, compared to the mixed control population. Such induction of β-cell markers was confirmed in fused human MSC/human dispersed islet cells, which showed elevated *NEUROD1, NKX2.2, MAFA, PDX1* and *insulin* mRNA compared to mixed control. Fused cells had higher insulin content and insulin positive β-MSCs also expressed nuclear PDX1.

Our results show an efficient protocol for fusion of human MSCs and β-cells, which resulted in a β-cell like phenotype. This could be a novel tool for cell-based therapies of diabetes.

Keywords: MSC, cell fusion, β-cells, islets, diabetes

INTRODUCTION

Diabetes has become a worldwide health problem in our society and causative therapies to restore the insulin producing β-cells are urgently needed. Destruction and failure of pancreatic β-cells to produce sufficient amounts of insulin to maintain normoglycemia are the main reasons for type 1 diabetes (T1D) as well as type 2 diabetes (T2D). Islet transplantation together with an improved immunosuppressive therapy [1] is one source for new β-cells and a way to restore euglycemia in patients and evades the essential need for exogenous insulin injection, although only for a limited time because of the decline in islet survival with time. Donor islet cells are limited and insufficiently available for diabetes therapy and the necessary immunosuppression is often too risky to justify transplantation in patients with long standing T1D, where infections often occur with increased severity [2].

Current studies show that co-transplantation of MSCs with pancreatic islets prolongs islet survival after transplantation due MSC unique hypo-immunogenic, immunomodulatory, and anti-apoptotic effects [3-5]. MSCs differentiate into mesodermal lineages like osteocytes, chondrocytes, adipocytes, and tenocytes *in vitro* [6] and do not form teratomas *in vivo* [7]. They have been recently suggested as a potential cellular source for regenerative therapy also for diabetes with various mechanisms to support β-cell protection [8, 9]. On the other hand, their immunomodulatory effect through paracrine factors with minimal evidence for homing and no transdifferentiation has been defined in several studies to be the main mode of action [4, 10-12].

MSCs are identified by their cell membrane markers ($CD105^+$, $CD90^+$, $CD73^+$) and by the lack of hematopoietic surface markers and those which activate the host immune system ($HLA\text{-}DR^-$, $CD14^-$, $CD80^-$, $CD86^-$, $CD45^-$, $CD34^-$, $CD79^-$) [13]. They are easy

to isolate from the bone marrow and rapidly expandable *in vitro*. After transplantation, MSCs act as suppressors of immune responses by producing anti-inflammatory cytokines and growth factors which inhibit monocyte maturation and T-/B-cell proliferation but also modulate mitogenesis, apoptosis and cell growth [14-17].

The immunomodulatory effect has been shown in MSC/islet co-transplantation increasing the number of regulatory T cells (Tregs) in rodents and nonhuman primates [3, 19].

Induction of insulin-producing cells out of MSC without gene transfer was observed *in vitro* leading to reduced blood glucose levels after transplantation [20].

Co-transplantation of MSCs together with islets into diabetic mouse models successfully improved islet function and graft survival as well as glycemia [4, 19, 21-25], which were induced by MSC-enhanced tissue repair and improved re-vascularization. MSCs also improved β-cell survival, insulin secretion and insulin sensitivity in a T2D model, mainly through their paracrine effects [26]. Together, these studies show the potential of MSCs for β-cell repair in the pancreas for diabetes therapy. There is still the open question of a possible advantage of β-cell fusion with MSCs.

Cell-cell fusion, when two cells are fused into one, initiates a rapid differentiation process [27]. This phenomenon naturally occurs during development, e.g. the formation of polyploid muscle (myocyte) or bone (osteoclast) cells [28, 29], or in adult tissue repair as well as in immune response [30].

The fusion event is induced through three different methods; physically (electric pulses), chemically (polyethylene glycol; PEG) with random pairing and low efficiency or biologically (inactivated virus) [31-33]. Cell fusion results in three distinct outcomes; heterokaryon or homokaryon, synkaryon and hybrid cells. Heterokaryons are polyploid non-dividing cell and often in a transient state, their nuclei will fuse later resulting in a polyploid synkaryon in which a cell has a nucleus with a combined chromosome pool of all nuclei. Proliferating synkaryons make hybrids. Heterokaryons offer a unique opportunity to trace the variation of chromosome pools in an intact nucleus after the fusion event [34] .

During cell fusion, epigenetic and genetic information of different cell types are combined. When two distinct types of cells fuse, the encoding of a group of genes activates resulting in a modified cellular expression pattern. This event starts within a few hours in the heterokaryon state by remodeling chromatin and switching on trans-acting regulators at key loci [27, 35, 36].

By combining the multipotent, anti-apoptotic, immunogenic and tissue repair capacity of the MSCs with the β-cell specific insulin production, we aimed to establish a stable novel β-cell type. In our study, we established an optimized virus-free cell fusion protocol and produced β-MSC heterokaryons by fusion of human MSCs with rat INS-1E cells or with dispersed human islet cells to generate differentiated β-MSCs.

EXPERIMENTAL PROCEDURES

Cell Culture

Human healthy bone marrow cells from three female donors were isolated at the University Hospital Hamburg-Eppendorf (UKE) and human mesenchymal stromal cells were isolated and purified as described previously [37]. Approval was granted by the UKE ethical committee. Concisely, bone marrow cells were cultured in AlphaMEM medium (Lonza, Basel, Switzerland) supplemented with 5% Platelet lysate [37], 10 I.U./mL heparin (Ratiopharm GmbH, Ulm, Germany) and 1% glutamax (Lonza, Basel, Switzerland). Medium was changed after two days and adherent cells were washed twice with phosphate-buffered saline (PBS) to omit other bone marrow cells. Then, growth medium was changed twice weekly. To identify colony forming unit fibroblasts (CFU-F), cells have been plated in low density, fixed with methanol for 3 min and stained with 1% crystal violet for 5 min after 14 days. Confluent cells (passage 0) were seeded in new plastic adherent flasks till passage 3 and stained for antigen surface marker expressions by flow cytometry or immunostaining. To confirm their capacity of differentiation potential into mesodermal lineages, MSCs were induced to differentiate to adipocytes and osteocytes as described [49].

Human islets and the rat insulinoma cell line (INS-1E) [38] were cultured in their respective medium (CMRL (Invitrogen, Carlsbad, CA, USA), RPMI1640 (PAA))

supplemented with 10% FCS, 1% L-glutamine and 100 U/ml penicillin/100mg/ml streptomycin (all PAA). INS-1E medium was supplemented with 50 µM β-mercaptoethanol (Merck) and 1 mM sodium pyruvate (GIBCO, Carlsbad, CA, USA) and 10 mM HEPES (Sigma-Aldrich). Human islets were isolated from 8 pancreases of healthy organ donors at the University of Lille and Prodo Laboratories (Irvine, CA, USA) as described before [39] and cultured in suspension dishes for 48h. Informed consent was obtained from all subjects. Islet purity was greater than 95% as judged by dithizone staining (if this degree of purity was not achieved by routine isolation, islets were handpicked). To disperse islets into single cells, accutase (Invitrogen) was added at 37°C for 15min and cell suspension mixed.

Amplification of mCherry/eGFP LeGO virus, virus infection and stable cells

EGFP-puromycin and mCherry-zeocin plasmids were used as described previously (http://www.LentiGO-Vectors.de, [40]). To produce the lentiviruses, HEK 293T cells were co-transfected with cell marker drug-resistance vectors (eGFP-puromycin / mCherry-zeocin), Gag/ Pol (viral capsid), Rev (reverse transcriptase) and envelope plasmid via lipofectamine 2000 (Invitrogen) according to the manufacturer's instruction. After 12h incubation, medium was replaced with fresh medium, and supernatant was harvested 12h later. Virus was concentrated by centrifugation for two rounds at 50,000 xg for 2h. MSC or INS-1E cells were infected with eGFP-puromycin (green fluorescence) or mCherry-zeocin (red fluorescence) respectively.

MSC and INS-1E adherent cells were infected with multiplicity of infection (MOI) of 10/20 eGFP-puromycin /mCherry-zeocin lentiviruses respectively in the presence of 8 µg/ml Polybrene (Sigma-Aldrich). Plates were centrifuged at 1000 xg for 1h and cultured. After 24h, media was changed and 72h later, MSCs were treated with 0.5 to 2.5 µg/ml puromycin (Sigma-Aldrich) and INS-1E with 20 to 100 µg/ml zeocin (Invitrogen) antibiotics gradually to obtain $eGFP^+$ or $mCherry^+$ stable cells.

Cell fusion

Cell fusion protocol was adapted from previous standard protocol [41]. Phytohemagglutinin (PHA-P, Sigma-Aldrich) diluted in serum free RPMI1640 at 10

and 100 µg/ml, was added for 30 min and 37°C prewarmed-PEG (Sigma-Aldrich) was added dropwise in the dark at concentrations of 12.5, 25 and 50%W/V for 40s. PEG was diluted gradually by adding drop-by-drop serum free RPMI1640 medium to diminish the effect of osmotic pressure variations on cells. In some experiments, PEG was added another time after 30 min (2XPEG).

Stable eGFP^{+}MSCs were mixed with dispersed human islets and treated with PEG added for 30 min and 37°C prewarmed-PEG (Sigma-Aldrich) was added dropwise in the dark at concentrations of 50%W/V for 50s. To select β-MSC heterokaryons and MSCs, non-fused INS-1E cells/human dispersed islets were eliminated at 36h after PHA-P/PEG treatment by adding 2.5 or 10 µM puromycin to the media for 4 or 7days respectively.

Immunofluorescence

To evaluate the surface antigen expression, MSCs were Bouin-fixed, pelleted in 1% agarose and paraffin-embedded as described before [42]. After deparaffinization and high pH antigen retrieval solution (vector labs, CA, USA), MSC sections were stained with rabbit anti-CD105 or anti-CD 90, mouse anti-CD73, rabbit anti-IgG or mouse anti-IgG1 (all Abcam, Cambridge, UK) followed by secondary Cy3 donkey anti-rabbit or FITC donkey anti-mouse (all Jackson, ImmunoResearch Laboratories, West Grove, PA).

For characterization of β-MSCs, puromycin selected cells were fixed with 4% paraformaldehyde in PBS for 30 min and permeabilized by 0.5% Triton X100 for 4 min at room temperature. Immunostaining with guinea pig anti-insulin (DAKO, Hamburg, Germany), rabbit anti-PDX1 (Abcam) or rabbit anti-glucagon antibody (DAKO) and Cy3 donkey anti-guinea pig or Cy3 donkey anti-rabbit (all Jackson) was performed as described previously [42]. Nuclei were visualized with 6-diamino-2-phenylindole (DAPI) (Vector labs). Fluorescently stained cells were analyzed with a Nikon MEA53200 microscope (Nikon GmbH, Düsseldorf, Germany) /Zeiss confocal laser scanning microscope (CLSM) 780 with ELYRA PS.1 (Zeiss, Oberkochen, Germany), and images were recorded using NIS-Elements software (Nikon)/ ZEN2011black edition (Zeiss).

Insulin content

Puromycin-selected cells were washed with 1XPBS and insulin extracted with 0.18N HCl in 70% ethanol for 12h at 4°C. Insulin was measured by ultrasensitive mouse insulin ELISA kit (ALPCO Diagnostics, Salem, NH, USA) for MSC-INS-1E and by human insulin ELISA kit (ALPCO) for MSC-human islets. Insulin content was normalized to total protein measured by BCA protein assay kit (Pierce, Rockford, IL, USA) from lysed islets in lysis buffer (20 mM Tris acetate, 0.27 M sucrose, 1 mM EDTA, 1 mM EGTA, 50 mM NaF, 1% Triton X-100, 5 mM sodium pyrophosphate, 10 mM β-glycerophosphate plus protease and phosphatase inhibitors (Pierce)) as described before [43].

Quantitative RT-PCR analysis

After puromycin selection, total RNA was extracted with TRIzol (Invitrogen) according to the manufacturer's protocol and RT-PCR performed as described previously [44]. Rat and human-specific primers were designed using vector NTI advanced ™ 11 Software (Invitrogen) and RT-PCR performed for SYBR Green using 2X PCR Master Mix (Applied Biosystems, Darmstadt, Germany). Primers used were 5/ AAACGGTTCCTTAGGGCAAT3/ 5/CAGTCTCACTGCCCCAACTT3/ (rat *Taf1*) and 5/CCTGTCCCCTCAGTTCATGT3/ 5/CCCATGGTCTTCTTCTGCAT3/ (*mCherry*). TaqMan® Real-time RT-PCR was performed using the 2X TaqMan Universal PCR Master Mix with an ABI StepOne Plus Cycler (Applied Biosystems). Reactions were performed in technical duplicates in a volume of 10 µl with specific primers and probes. TaqMan® primers used were of *PPIA* (Hs99999904_m1), *INS* (Hs02741908_m1), *PDX1* (Hs00426216_m1), *NEUROG3* (Hs01875204_s1), *NKX6.1* (Hs00232355_m1), *NKX2.2* (Hs00159616_m1), *NEUROD1* (Hs01922995_s1), *MAFA* (Hs01651425_s1), *PAX4* (Hs00173014_m1), *Ppia* (Rn00690933_m1) , *2* (Rn02121433_g1), *Pdx1* (Rn00755591_m1), *Slc2a2* (Rn00563565_m1), *Gck* (Rn00688285_m1), *Neurog3* (Rn00572583_s1), *Nkx6.1* (Rn1450076_m1), *Nkx2.2* (Rn04244749_m1), *Neurod1* (Rn00824571_s1), *MafA* (Rn00845206_s1), *Pax4* (Rn00582529_m1) for human/ rat respectively (Applied Biosystems). Results were calculated with the $\Delta\Delta C_T$ method. All gene expression data sets were normalized to

the corresponding puromycin selected non-treated mixed cells or treated dispersed islets and normalized to housekeeping genes human *PPIA* or rat *Ppia*/*Taf1*. Samples were analyzed in duplicates for each transcript. In MSC/INS-1E experiments, it was not possible to measure the target gene in each control mix condition; therefore, we normalized to one single randomly chosen sample. Control experiments were performed with human islet and rat INS-1E cells to confirm rat or human primer specificity.

Fluorescence-activated cell analysis (FACS)

MSCs were trypsinized, washed with PBS and 10^5 cells in each condition were incubated with FITC conjugated anti-CD105, FITC conjugated anti-CD90 and PE conjugated anti-CD73 (positive markers) as well as FITC conjugated anti-MHCII, FITC conjugated anti-CD45, PE conjugated anti-CD34 (negative markers). FITC conjugated anti-IgG1, FITC conjugated anti-IgG2a and PE conjugated anti-IgG1 were used as negative isotype control (all Becton Dickinson Biosciences, Franklin Lakes, New Jersey, USA). 72h after LeGO Virus infection, the number of eGFP positive MSCs was quantified using a 488nm laser and 530/30 bandpass filter by FACS analysis.

To quantify the number of rat/human β-MSC interspecies heterokaryons, live cells in different conditions plus non-infected control MSCs, INS-1E and human islet cells were trypsinized and evaluated by eGFP/mCherry double color on LSRFortessa (Becton Dickinson Biosciences) using 488nm laser and 530/30 bandpass filter (eGFP) and 561nm laser and 610/20 bandpass filter (mCherry) respectively.

For polyploidy FACS, cells were fixed by drop-by-drop adding cold 70% ethanol (10^6 cells/ml) at 4°C overnight. Cells were washed two times with PBS and incubated with 2 µg/ml DAPI plus 5 µg/ml RNase in PBS solution for 30min at 37°C in the dark. Cells were measured with an UV laser (450/50 bandpass filter). The numbers of cells in different samples were counted by LSRFortessa (Becton Dickinson Biosciences). Data were analyzed by BD FACSDiva™ software 6.0 or Cyflogic 1.21.

Statistical analysis:

Data evaluation was done in a randomized manner by a single investigator (ZA) and statistical analyses were performed from at least three independent experiments from

three individual human MSC batches, three different human islet organ donors. Values are presented as means ± SEM. Data were analyzed by student's t-tests. Significance was set at $p < 0.05$.

RESULTS

Generation of rat-human β-MSC heterokaryon cells by PEG-mediated cell fusion

Cell-cell fusion has been established with the aim to reprogram MSCs to β-cells. MSCs from human bone marrow showed CFU-F activity based on crystal violet staining (Suppl.Fig.1A), expressed cluster of differentiation CD105, CD90 and CD73, lacked expression of CD45, CD34 and MHC-II (Suppl.Fig.1A,B) and could differentiate into osteoblasts and adipocytes (Suppl.Fig.1C). To identify and select cells, we infected human MSCs with eGFP-puromycin and INS-1E cells with mCherry-zeocin lentiviral gene ontology (LeGO) viruses and made stable MSCs by puromycin and INS-1E by zeocin mediated antibiotic selection. Percentages of $eGFP^+/mCherry^+$ cells were detected with flow cytometry at 3 weeks after antibiotic selection.

Microscopic and flow cytometry analyses both showed that cells were eGFP labeled MSCs or mCherry labeled INS-1E (Fig.1B, Suppl.Fig.1D). $EGFP^+$MSCs stained positive for CD105, CD73 and CD90 (Suppl.Fig.1E) and $mCherry^+$INS-1E for insulin (not shown). To generate interspecies heterokaryons, we established an optimized cell fusion protocol of MSCs isolated from human bone marrow and the rat INS-1E β-cell line (Fig.1A). We co-cultured ("MIX") $eGFP^+$ human MSCs and $mCherry^+$ rat INS-1E cells in INS-1E medium (Suppl.Fig.1F). After 36 hours, adherent co-cultured cells were induced ("TREAT") with 100 µg/ml PHA-P for 30 min and 50% W/V PEG for 40 seconds to fusion, which resulted in three cell populations; $eGFP^+$MSCs, $mCherry^+$INS-1E and double positive heterokaryons (Fig.1C)

Another 36 hours later, puromycin was added to treated or mixed cells for 4 days (Suppl.Fig.1F) in order to select MSCs and β-MSC fused cells. This resulted in the two main populations; $eGFP^+$MSC and fused $eGFP^+$MSC/$mCherry^+$INS-1E cells. Again, double $eGFP^+/mCherry^+$ cells were seen in the treated but only few in mixed control

cells (Fig.1D). This was confirmed by FACS analysis for eGFP/mCherry, which showed 3-fold more eGFP/mCherry double positive cells (Fig.1E, 2A). The level of mCherry expression was significantly higher in TREAT compared to MIX (Fig.1F). When the same experiment was performed in suspension culture, cells only had a limited capacity to attach to the culture dish and to survive after treatment (not shown). To investigate whether the generated fused cells are polyploid heterokaryons and to confirm the efficiency of fusion, cells were fixed and labeled with DAPI. In contrast to single $eGFP^+$MSCs or $mCherry^+$INS-1E cells, where the majority of cells were diploid, 83.04 ± 5.77% of the treated eGFP/mCherry double positive cells were polyploid based on FACS analysis (Fig.1G). Polyploidy of cells in culture was further confirmed by confocal microscopy (Fig.1H, Suppl.Fig.1G).

Optimization of the PEG-mediated cell fusion for rat-human β-MSC heterokaryons

Because of the known important effects of the ratio of nuclear and cytoplasmic factors [27], we hypothesized that a higher ratio of INS-1E to MSCs may increase the number of puromycin selected fused heterokaryons. Therefore, we co-cultured MSC/INS-1E cells at an increasing ratio (1:2; 1:5 and 1:11) at the control glucose concentration for INS-1E cells. This strategy resulted in a 2-fold further increased number of fused cells at a ratio of 1:11 compared to 1:2, based on eGFP/mCherry double positive cells analyzed by FACS analysis (Fig.2A upper panel, Suppl.Fig.2A), which was confirmed by counting the double positive cells under the microscope (3-fold increase; Fig.2A lower panel). In the next step, we further optimized the fusion protocol at the 1:11 MSC/INS-1E ratio by applying different concentrations of PHA-P, PEG and glucose. 30-min pretreatment of 10 µg/ml PHA-P had no effect, but 100 µg/ml PHA-P resulted in 3-fold increase in eGFP/mCherry double positive cells, compared to control without PHA-P, analyzed by FACS (Fig.2B upper panel, Suppl.Fig.2B), and microscopical analysis (Fig.2B lower panel). The number of eGFP/mCherry double positive cells was further increased by 8-hour pre-treatment with elevated 33.3 mM glucose concentrations compared to 5.5 mM glucose (Fig.2C, Suppl.Fig.2C). Increasing the

concentration of PEG to 50% W/V induced a 4-fold increase in heterokaryons, compared to 12.5% PEG (Fig.2D, Suppl.Fig.2D) and two times 50% W/V PEG treatment further increased the number of double positive cells significantly (Fig.2D, Suppl.Fig.2D).

We chose mild cell starvation before fusion and reduced the FCS concentration from 10% to 3% for 8 hours. This resulted in no change of eGFP/mCherry heterokaryons at 3 compared to 10% FCS pre-culture, nor at 3% FCS under 33.3 mM glucose. But we constantly confirmed the effect of PHA-P as well as 1X and 2XPEG treatment in all conditions, which constantly showed a higher percentage of eGFP/mCherry double positive cells analyzed by FACS analysis (Fig.2E upper panel, Suppl.Fig.2E) and by counting (Fig.2E lower panel), compared to the mix condition. FACS analysis indicated that 29.79 ± 2.92% eGFP/mCherry co-positive MSC in our optimized condition at the MSC/INS-1E cells ratio of 1:11, 100 µg/ml PHA-P, 2X 50% W/V PEG, indicating a 6-fold more heterokaryons compared to the first “standard” fusion protocol (MSC/INS-1E cells ratio of 1:2, 100 µg/ml PHA-P, 50% W/V PEG; Fig.2F).

Our optimized condition resulted in a shift from diploid state (2-4n) in mixed control cells to polyploid state (≥4n) in treated cells (histogram, Fig.2G, Suppl.Fig.2F). In order to investigate all cells, we did not select the cells by puromycin. While almost all untreated cells were diploid, 72.76 ± 9.86% of MSCs, and 85.64 ± 6.47% of INS-1E cells and 44.10 ± 6.02% of the whole cell population ($eGFP^+$MSCs/$mCherry^+$INS-1E/$eGFP^+$-$mCherry^+\beta$-MSC) were polyploid after treatment (Fig.2G). At our optimized conditions of 100 µg/ml PHA-P, 2X 50% W/V PEG, we did not identify any increased cleaved caspase 3, as an apoptotic cell death marker, in the non-selected whole cell population at 8h after fusion (not shown). This indicates that PEG did not induce cell death under the applied conditions and also whole protein content in mixed and PEG treated cells were unchanged (not shown).

Characterization of insulin$^+$human/rat β-MSC heterokaryon cells revealed the expression of human as well as rat beta cell markers

To further characterize the β-MSC heterokaryons, human eGFP$^+$MSCs were mixed with INS-1E cells and treated with standard or optimized protocol. Puromycin selection enabled isolating human MSCs and human/rat β-MSC heterokaryons (Fig.3A).

Although under the optimized 2XPEG fusion protocol we did not see improved fusion by elevated glucose (Fig.2E), the combination of 8-hour pre-culture with 33.3 mM glucose and 10% FCS before fusion under the optimized protocol resulted in higher expression of *MAFA* and *insulin* in human MSC/islet cells (Suppl.Fig.3A) compared to 11.1 mM glucose at 3% or 10% FCS. In order to apply the same pre-culture/fusion protocol to both MSC/INS-1E and MSC/human islets, we selected the glucose pre-culture with the optimized fusion protocol (MSC/β-cell ratio 1:11, 100 µg/ml PHA-P, 2X 50% W/V PEG) for all subsequent experiments as the best condition.

Our results showed eGFP and insulin co-positive heterokaryons (Fig.3B, Suppl.Fig.3B). Staining for PDX1 in red and insulin and DAPI in blue showed quadruple-positive eGFP$^+$DAPI$^+$insulin$^+$PDX1$^+$ cells or triple positive eGFP$^+$DAPI$^+$insulin$^-$PDX1$^+$ (Fig.3C), but no eGFP$^+$DAPI$^+$insulin$^+$PDX1$^-$ cells. All heterokaryons were eGFP$^+$glucagon$^-$ (Fig.3D).

Next, we compared human and rat β-cell gene expression patterns [45] in the fused rat-human β-MSCs subjected to 100 µg/ml PHA-P/ 50% W/V PEG (standard protocol) or to 33.3 mM glucose pre-treatment /100 µg/ml PHA-P/ 2X 50% W/V PEG (optimized protocol). Data from three MSC donors are shown separately in order to see the inter-individual differences (Fig.3E, F, Suppl.Fig.3C,D). β-cell gene expression was not detected in eGFP-MSCs (not shown).

Higher expression of the human β-cell genes *NKX6.1* and *insulin* were observed under optimized compared to standard protocol conditions in all 3 experiments (Fig.3E). Higher mRNA levels of human *PAX4* were detected in two and *Neurogenin3 (NGN3)* in one isolation, while rat *Pax4* and *Ngn3* was not detected in any samples. This suggests the induction of early β-cell markers by human MSCs (Suppl.Fig.3C,D).

Rat *Nd1*, *MafA, Nkx6.1* and *Pdx1* as well as *Slc2a2*, *Ins1* and *Gck* mRNA was increased under the optimized fusion protocol, suggesting that MSCs increased INS-1E-originated markers (Fig.3F, Suppl.Fig.3D; in two out of three experiments). Taken

together, screening of β-cell gene expressions under the optimized fusion condition showed higher expression of β-cell markers compared to the standard protocol. The higher production level of insulin was confirmed by the increased insulin content (Fig.3G) in treated compared to mixed control.

Characterization of insulin$^+$ human β-MSCs

To extend this fusion protocol to fully human β-MSCs, human eGFP$^+$MSCs were cultured with dispersed human islet cells on the 804G matrix [46] with the same optimized fusion protocol (pre-treatment with 33.3 mM glucose and fusion with 100 □g/ml PHA-P/ 2X 50% W/V PEG). 36 hours later, cells were exposed to 10μg/ml puromycin for 7 days which resulted in two main populations; MSCs and fused MSC/islet cells (Fig.4A).

Successful fusion was observed by double-positivity for insulin and eGFP (Fig.4B). Labeling of MSC/islet cells for eGFP, PDX1, insulin and DAPI showed quadruple-positive eGFP$^+$DAPI$^+$insulin$^+$PDX1$^+$ cells or triple positive eGFP$^+$DAPI$^+$insulin$^-$PDX1$^+$, but no eGFP$^+$DAPI$^+$insulin$^+$PDX1$^-$ cells (Fig.4C). These quadruple or triple positive cells appeared as synkaryons which consisted of one single nucleus. We rarely observed insulin$^+$eGFP$^+$ polyploid cells (Fig.4D), which was in contrast to human/rat fused cells, where almost all insulin$^+$eGFP$^+$ were polyploid. Some of them formed islet like clusters (Fig.4E); such structures were observed in all human islet preparations from different donors. Insulin/eGFP double positive cells within the cluster were confirmed by confocal microscopy (Fig.4E). We also observed CD105$^+$insulin$^+$ cells in treated MSC/islet cell sections (Suppl.Fig.4A), while some CD105$^+$insulin$^-$ cells were observed in non-treated human islets (not shown).

We compared expression of human β-cell markers [45] under optimized and standard protocol conditions and observed higher induction of *ND1*, *NKX2.2*, *MAFA* and *INS* under the optimized fusion protocol (Suppl.Fig.4B).

When human β-cell gene expression patterns in the treated conditions were compared with mixed controls, higher expression of the β-cell specific genes *NEUROD1*, *NKX2.2*, *MAFA*, *PDX1* and *insulin* (Fig.4G) as well as increased insulin content (Fig.4I)

was observed in all three independent experiments from different MSCs and islet donors. In order to compare β-cell specific gene expression to mature islets, mRNA of the 3 batches of mixed MSC/islet cells was also normalized to the respective mature control islet expression. Again, data from three MSC and three islet donors are shown separately and are fluctuating in their gene expression. Because of the inter-individual changes in the absolute gene expression as well as the stimulated conditions among the donors, data do not allow any further interpretation. Fused cells under the optimized conditions have a comparable amount of *PDX1* as well as *insulin* mRNA to mature islets, while *NEUROD1* and *MAFA* were increased in two out of three experiments (Fig.4H).

DISCUSSION

Recent investigations have revealed that MSCs have the potential to generate insulin-producing cells [20, 47, 48]. Here, we developed a fusion protocol of human MSCs with rat INS-1E cells and human islet cells. This approach resulted in β-MSC fused cells, which carried β-cell markers. Newly generated insulin-producing polyploid cells expressed nuclear PDX1 and cytoplasmic insulin. Better MSC-rat β-cell fusion efficiency was achieved by an optimized protocol of an increased number of β-cells in the mixture at a ratio of 1:11 MSC/INS-1E cells at PHA-P concentration of 100 □g/ml and a 2nd addition of 50% W/V PEG to the cell mixture. This protocol resulted in 6-fold more heterokaryons.

The improved MSC-rat β-cell fusion highly correlated with increased polyploidy, human β-cell marker expression as well as higher insulin content. In all experiments of fused MSC/rat INS-1E cells or MSC/human islet cells, increased fusion efficiency increased *PDX1* and *insulin* expression.

PDX1 is expressed as the first determination factor towards endocrine lineages. PDX1-expressing cells can differentiate into all pancreatic cell types; exocrine, endocrine and pancreatic ducts and thus serve as multipotent pancreatic progenitor cells [49]. Importantly, PDX1 positive cells have the capacity to proliferate [50]. The 2nd

important factor, which stimulates development into all islet cells, is NGN3 [51]. NGN3 drives expression of additional transcription factors such as PAX4, NEUROD1, NKX6.1, NKX2.2 and MAFA leading to the specific β-cell fate [52-54]. Adult β-cells express all of these factors except NGN3 and PAX4 [45].

NGN3 is only temporarily activated and often expressed at low levels. This could be one reason why we have only detected *NGN3* expression in one single experiment, where its expression was driven by MSCs, as specifically human and not rat *Ngn3* was detected in the optimized protocol. In the same experiment, also elevated *PAX4* expression was observed.

Fusion of rat/human islet cells with hMSCs using the optimized protocol induced human β-cell transcription factor expression *NKX6.1* and *MAFA*, which originated from the human MSCs. Additionally, β-cell transcription factors from rat β-cells (*Neurod1*, *Nkx2.2*, *MafA*, *Pdx1*) and genes related to β-cell function *(insulin*, *Glut2* and *Glucokinase)* were detected [54, 55].

The optimized protocol showed elevated levels of *NEUROD1*, *NKX2.2*, *MAFA* and *insulin* together with increased cellular insulin content also in fused human MSC with dispersed islet cells. The overall β-cell marker expression reached levels of mature islets confirming a human β-cell like phenotype of the fused MSC/islet cells.

In addition, β-cell transcription factor *PDX1* was higher in fused MSC/ dispersed islet cells than in mature islet cells. PDX1 plays a role in transition waves of developmental process as well as in mature β-cells as the promoter for glucose induced insulin transcription [54, 55]. The combination of markers for developmental factors together with those of mature β-cells suggest a mixed population of immature and mature β-like cells. This hypothesis was strengthened by immunostaining of PDX1 and insulin, which also showed two cell populations: insulin$^-$PDX1$^+$ cells and insulin$^+$PDX1$^+$ cells, considered as immature and mature β-like cells, respectively.

The difficulty in our study was the high variation of β-cell marker expression levels in the individual mixed/fused samples from different MSC and islet cells, which did not allow us to obtain a robust transcription marker analysis and conclusions on the cell differentiation state [56]. Nevertheless, our optimized protocol provides a high ratio of

stable interspecies also from human islet cells, which has wide applications for further investigation. While human MSC/rat INS-1E cells showed polyploid heterokaryons, fused human MSC/dispersed islet cells showed more synkaryons, suggesting the possibility of already fused nuclei and development of islet like cluster cells as hybrids. Such hypothesis needs further proof in long-culture experiments as well as *in vivo* by characterization of transplanted fused human β-MSC in healthy and diabetic mice.

The high number of rat-human polyploid cells as stable interspecies heterokaryons provides a model for further investigation of epigenetic and genetic variation during cell differentiation to a β-cell phenotype.

In conclusion, we established a rapid and virus-free optimized fusion protocol of adherent MSCs and β-cells and showed fused β-MSCs that express β-cell markers.

ACKNOWLEDGMENTS

This work was supported by the European Research Council (ERC), The German Center for Diabetes Research (DZD), the German Research Foundation (DFG) and by InsuGen. We thank A. Badbaran (University Hospital Hamburg-Eppendorf) and J. Bergemann (University of Bremen) for technical assistances, Damilola Modupe Dawodu (University of Bremen) for help with the microscopical analyses, J. Ahlstrom (University of Utah and George E Wahlen Veterans) for critical discussion, FACS core facility (University Hospital Hamburg-Eppendorf D. Paulmann (University of Bremen) for help with the FACS analyses, A. Dotzauer for support in the virology laboratory (University of Bremen) and Philippe A. Halban (University of Geneva) for the 804G matrix cells. We greatly appreciate the help and support of B. Fuchs and A. Ellrott (Max Planck Institute for Marine Microbiology) for support with the laser scanning microscopy and analysis and K. Riecken (University Hospital Hamburg-Eppendorf) for providing the lentiviruses. Human islets were provided through the European Consortium for Islet Transplantation, Juvenile Diabetes Research Foundation International.

AUTHOR CONTRIBUTIONS

Z.A. designed and performed experiments, analyzed the data and wrote the paper. C.W conceived and patented the idea of fusion of MSCs with islet cells and coined the "β-MSC" term. A.R.Z., C.L., Fe.P., Fr.P., J.K-C., A.A. and A.M. provided experimental and technical support. K.M. supervised the project and wrote the paper.

COMPETING FINANCIAL INTERESTS

The authors declare no competing financial interests. C.W. and A.R.Z. are the founders of InsuGen now named SymbioCellTech.

REFRENCES

1. Shapiro AM, Lakey JR, Ryan EA et al. Islet transplantation in seven patients with type 1 diabetes mellitus using a glucocorticoid-free immunosuppressive regimen. *The New England journal of medicine* 2000; **343**: 230-8.
2. Joshi N, Caputo GM, Weitekamp MR, Karchmer AW. Primary care: Infections in patients with diabetes mellitus. *New Engl J Med* 1999; **341**: 1906-12.
3. Wu H, Wen D, Mahato RI. Third-party mesenchymal stem cells improved human islet transplantation in a humanized diabetic mouse model. *Molecular therapy : the journal of the American Society of Gene Therapy* 2013; **21**: 1778-86.
4. Borg DJ, Weigelt M, Wilhelm C et al. Mesenchymal stromal cells improve transplanted islet survival and islet function in a syngeneic mouse model. *Diabetologia* 2014; **57**: 522-31.
5. Togel F, Hu ZM, Weiss K et al. Administered mesenchymal stem cells protect against ischemic acute renal failure through differentiation-independent mechanisms. *Am J Physiol-Renal* 2005; **289**: F31-F42.

6. Charbord P, Livne E, Gross G et al. Human bone marrow mesenchymal stem cells: a systematic reappraisal via the genostem experience. *Stem cell reviews* 2011; **7**: 32-42.
7. Ma S, Xie N, Li W et al. Immunobiology of mesenchymal stem cells. *Cell death and differentiation* 2014; **21**: 216-25.
8. Bianco P, Cao X, Frenette PS et al. The meaning, the sense and the significance: translating the science of mesenchymal stem cells into medicine. *Nat Med* 2013; **19**: 35-42.
9. Zander AR, Lange C, Westenfelder C. Mesenchymal stromal cells: main factor or helper in regenerative medicine? *Kidney Int Suppl* 2011; **1**: 74-6.
10. Zorina TD, Subbotin VM, Bertera S et al. Recovery of the endogenous beta cell function in the NOD model of autoimmune diabetes. *Stem Cells* 2003; **21**: 377-88.
11. Lee RH, Seo MJ, Reger RL et al. Multipotent stromal cells from human marrow home to and promote repair of pancreatic islets and renal glomeruli in diabetic NOD/scid mice. *Proc Natl Acad Sci U S A* 2006; **103**: 17438-43.
12. Limbert C, Seufert J. In vitro (re)programming of human bone marrow stromal cells toward insulin-producing phenotypes. *Pediatr Diabetes* 2009; **10**: 413-9.
13. Dominici M, Le Blanc K, Mueller I et al. Minimal criteria for defining multipotent mesenchymal stromal cells. The International Society for Cellular Therapy position statement. *Cytotherapy* 2006; **8**: 315-7.
14. Bernardo ME, Fibbe WE. Mesenchymal stromal cells: sensors and switchers of inflammation. *Cell stem cell* 2013; **13**: 392-402.
15. Nauta AJ, Fibbe WE. Immunomodulatory properties of mesenchymal stromal cells. *Blood* 2007; **110**: 3499-506.
16. Francois M, Romieu-Mourez R, Li M, Galipeau J. Human MSC suppression correlates with cytokine induction of indoleamine 2,3-dioxygenase and bystander M2 macrophage differentiation. *Molecular therapy : the journal of the American Society of Gene Therapy* 2012; **20**: 187-95.

17. Prockop DJ. Concise review: two negative feedback loops place mesenchymal stem/stromal cells at the center of early regulators of inflammation. *Stem Cells* 2013; **31**: 2042-6.
18. Zanone MM, Favaro E, Miceli I et al. Human mesenchymal stem cells modulate cellular immune response to islet antigen glutamic acid decarboxylase in type 1 diabetes. *The Journal of clinical endocrinology and metabolism* 2010; **95**: 3788-97.
19. Berman DM, Willman MA, Han D et al. Mesenchymal stem cells enhance allogeneic islet engraftment in nonhuman primates. *Diabetes* 2010; **59**: 2558-68.
20. Ianus A, Holz GG, Theise ND, Hussain MA. In vivo derivation of glucose-competent pancreatic endocrine cells from bone marrow without evidence of cell fusion. *J Clin Invest* 2003; **111**: 843-50.
21. Figliuzzi M, Cornolti R, Perico N et al. Bone marrow-derived mesenchymal stem cells improve islet graft function in diabetic rats. *Transplant Proc* 2009; **41**: 1797-800.
22. Ito T, Itakura S, Todorov I et al. Mesenchymal stem cell and islet co-transplantation promotes graft revascularization and function. *Transplantation* 2010; **89**: 1438-45.
23. Sordi V, Melzi R, Mercalli A et al. Mesenchymal cells appearing in pancreatic tissue culture are bone marrow-derived stem cells with the capacity to improve transplanted islet function. *Stem Cells* 2010; **28**: 140-51.
24. Sordi V, Piemonti L. Mesenchymal stem cells as feeder cells for pancreatic islet transplants. *Rev Diabet Stud* 2010; **7**: 132-43.
25. Urban VS, Kiss J, Kovacs J et al. Mesenchymal stem cells cooperate with bone marrow cells in therapy of diabetes. *Stem Cells* 2008; **26**: 244-53.
26. Si Y, Zhao Y, Hao H et al. Infusion of mesenchymal stem cells ameliorates hyperglycemia in type 2 diabetic rats: identification of a novel role in improving insulin sensitivity. *Diabetes* 2012; **61**: 1616-25.

27. Palermo A, Doyonnas R, Bhutani N et al. Nuclear reprogramming in heterokaryons is rapid, extensive, and bidirectional. *FASEB journal : official publication of the Federation of American Societies for Experimental Biology* 2009; **23**: 1431-40.
28. Hindi SM, Tajrishi MM, Kumar A. Signaling mechanisms in mammalian myoblast fusion. *Science signaling* 2013; **6**: re2.
29. Vignery A. Macrophage fusion: the making of osteoclasts and giant cells. *The Journal of experimental medicine* 2005; **202**: 337-40.
30. Prockop DJ, Gregory CA, Spees JL. One strategy for cell and gene therapy: harnessing the power of adult stem cells to repair tissues. *Proc Natl Acad Sci U S A* 2003; **100 Suppl 1**: 11917-23.
31. Harris H, Watkins JF. Hybrid Cells Derived from Mouse and Man: Artificial Heterokaryons of Mammalian Cells from Different Species. *Nature* 1965; **205**: 640-6.
32. Pontecorvo G. Production of mammalian somatic cell hybrids by means of polyethylene glycol treatment. *Somatic cell genetics* 1975; **1**: 397-400.
33. Teissie J, Knutson VP, Tsong TY, Lane MD. Electric pulse-induced fusion of 3T3 cells in monolayer culture. *Science* 1982; **216**: 537-8.
34. Ogle BM, Cascalho M, Platt JL. Biological implications of cell fusion. *Nature reviews Molecular cell biology* 2005; **6**: 567-75.
35. Tsubouchi T, Soza-Ried J, Brown K et al. DNA synthesis is required for reprogramming mediated by stem cell fusion. *Cell* 2013; **152**: 873-83.
36. Cell fusion in health and disease : I : cell fusion in health. 1st ed. New York: Springer 2011.
37. Lange C, Cakiroglu F, Spiess AN et al. Accelerated and safe expansion of human mesenchymal stromal cells in animal serum-free medium for transplantation and regenerative medicine. *J Cell Physiol* 2007; **213**: 18-26.
38. Merglen A, Theander S, Rubi B et al. Glucose sensitivity and metabolism-secretion coupling studied during two-year continuous culture in INS-1E insulinoma cells. *Endocrinology* 2004; **145**: 667-78.

39. Oberholzer J, Triponez F, Mage R et al. Human islet transplantation: lessons from 13 autologous and 13 allogeneic transplantations. *Transplantation* 2000; **69**: 1115-23.
40. Weber K, Bartsch U, Stocking C, Fehse B. A multicolor panel of novel lentiviral "gene ontology" (LeGO) vectors for functional gene analysis. *Molecular therapy : the journal of the American Society of Gene Therapy* 2008; **16**: 698-706.
41. Islam MQ, Ringe J, Reichmann E et al. Functional characterization of cell hybrids generated by induced fusion of primary porcine mesenchymal stem cells with an immortal murine cell line. *Cell and tissue research* 2006; **326**: 123-37.
42. Ardestani A, Paroni F, Azizi Z et al. MST1 is a key regulator of beta cell apoptosis and dysfunction in diabetes. *Nat Med* 2014; **20**: 385-97.
43. Schulthess FT, Paroni F, Sauter NS et al. CXCL10 impairs beta cell function and viability in diabetes through TLR4 signaling. *Cell Metab* 2009; **9**: 125-39.
44. Maedler K, Sergeev P, Ris F et al. Glucose-induced beta cell production of IL-1beta contributes to glucotoxicity in human pancreatic islets. *J Clin Invest* 2002; **110**: 851-60.
45. Conrad E, Stein R, Hunter CS. Revealing transcription factors during human pancreatic beta cell development. *Trends in endocrinology and metabolism: TEM* 2014; **25**: 407-14.
46. Lefebvre VH, Otonkoski T, Ustinov J et al. Culture of adult human islet preparations with hepatocyte growth factor and 804G matrix is mitogenic for duct cells but not for beta-cells. *Diabetes* 1998; **47**: 134-7.
47. Jafarian A, Taghikhani M, Abroun S et al. Generation of high-yield insulin producing cells from human bone marrow mesenchymal stem cells. *Molecular biology reports* 2014; **41**: 4783-94.
48. Karnieli O, Izhar-Prato Y, Bulvik S, Efrat S. Generation of insulin-producing cells from human bone marrow mesenchymal stem cells by genetic manipulation. *Stem Cells* 2007; **25**: 2837-44.

49. Gu G, Dubauskaite J, Melton DA. Direct evidence for the pancreatic lineage: NGN3+ cells are islet progenitors and are distinct from duct progenitors. *Development* 2002; **129**: 2447-57.
50. Seymour PA, Freude KK, Tran MN et al. SOX9 is required for maintenance of the pancreatic progenitor cell pool. *Proc Natl Acad Sci U S A* 2007; **104**: 1865-70.
51. Gradwohl G, Dierich A, LeMeur M, Guillemot F. neurogenin3 is required for the development of the four endocrine cell lineages of the pancreas. *Proc Natl Acad Sci U S A* 2000; **97**: 1607-11.
52. Gouzi M, Kim YH, Katsumoto K et al. Neurogenin3 initiates stepwise delamination of differentiating endocrine cells during pancreas development. *Developmental dynamics : an official publication of the American Association of Anatomists* 2011; **240**: 589-604.
53. Naya FJ, Huang HP, Qiu Y et al. Diabetes, defective pancreatic morphogenesis, and abnormal enteroendocrine differentiation in BETA2/neuroD-deficient mice. *Genes & development* 1997; **11**: 2323-34.
54. Ben-Othman N, Courtney M, Vieira A et al. From pancreatic islet formation to beta-cell regeneration. *Diabetes research and clinical practice* 2013; **101**: 1-9.
55. Ziv O, Glaser B, Dor Y. The plastic pancreas. *Developmental cell* 2013; **26**: 3-7.
56. Siegel G, Kluba T, Hermanutz-Klein U et al. Phenotype, donor age and gender affect function of human bone marrow-derived mesenchymal stromal cells. *BMC medicine* 2013; **11**: 146.

LEGEND

Fig.1. Generation of rat-human β-MSC heterokaryons

(A) Schematic illustration of the strategy for generation of human stable eGFP$^+$MSCs and rat mCherry$^+$INS-1E cells that carry antibiotic-selectable markers. Cells were mixed ("MIX") or fusion was induced by treatment with 100 µg/ml PHA-P and 50%W/V PEG ("TREAT"). Interspecies heterokaryons and human MSCs were selected by puromycin. (**B)** Cultured eGFP$^+$MSCs (left), mCherry$^+$INS-1E (middle) and MIX (right; all 100X) and **(C)** mCherry$^+$INS-1E (red arrows), eGFP$^+$MSC (green arrows) and double positive β-MSC (orange arrows) in TREAT condition (400X). **(D-H)** TREAT cells after puromycin selection. **(D)** MIX (control) and TREAT conditions after 4 days puromycin selection, white arrows show eGFP$^+$mCherry$^+$ cells (40X). **(E)** Analysis and quantification (right) of mCherry$^+$eGFP$^+$ cells in MIX and TREAT conditions by FACS analysis. Gating was set up with single mCherry or single eGFP+ cells and conditions kept constant. **(F)** The relative mCherry mRNA expression normalized to INS-1E cells. RT-PCR was normalized to rat *Taf1* **(G)** Polyploidy analysis by FACS of eGFP$^+$MSCs, mCherry$^+$INS-1E (controls) and eGFP$^+$mCherry$^+$ heterokaryons. Gating was set for control non-stained cells and kept constant.**(H)** Image of a polyploid MSC heterokaryon by CLSM (400X). All analyses were performed in at least three independent experiments from three MSC donors and show mean ± SEM. *P< 0.05 Treat compared to Mix. ** Mix compared to mCherry INS-1E alone. +P< 0.05 eGFP$^+$mCherry$^+$β-MSC compared to eGFP$^+$MSC or to mCherry$^+$INS-1E.

Fig.2. Optimization of the PEG-mediated cell fusion for rat-human β-MSC heterokaryons. (A-E) The percentages of MSC/INS-1E cells measured by eGFP$^+$mCherry$^+$ flow cytometry (top) as well as quantitative fluorescent microscopical

analysis (bottom) in MIX and TREAT conditions after puromycin selection. **(A)** The mixture of the 1:2 ratio of MSC/INS-1E cells (standard protocol), 1:5 or 1:11 in mixed cells (MIX) and 50%W/V PEG and 100 µg/ml PHA-P treated cells at 11.1 mM glucose as the control glucose concentration for INS-1E cells. **(B-E)** MSC/INS-1E cells at a ratio of 1:11. **(B)** 50%W/V PEG treated cells were exposed to 0, 10 and 100 µg/ml PHA-P. **(C)** 50%W/V PEG and 100 µg/ml PHA-P treated and untreated mixed cells were pre-incubated for 8 h with 5.5, 11.1 or 33.3 mM glucose. **(D)** 100 µg/ml PHA-P treated were exposed to 12.5, 25 and 50% W/V or twice 50% W/V PEG. **(E)** 1X or 2X 50%W/V PEG and 100 µg/ml PHA-P treated cells and mixed cells were pre-incubated with media including 10%FCS, 3% FCS or 3% FCS/ 33.3 mM glucose. **(F)** Comparison of the number of $eGFP^{+}mCherry^{+}$ MSCs between standard and optimized protocol (1:11 MSC/INS-1E; 2X50%W/V PEG and 100 µg/ml PHA-P) by flow cytometry analysis of mCherry and eGFP (left and middle) and by fluorescence microscopy (40X; right). Arrow bars shows an $eGFP^{+}mCherry^{+}$ MSC in higher magnification (400X) **(G)** Polyploidy analysis by FACS before puromycin selection of mixed and treated cells (left panel) and quantification of polyploid cells within $eGFP^{+}$MSCs or $mCherry^{+}$INS-1E cells alone and the whole population ($eGFP^{+}$MSCs/$mCherry^{+}$INS-1E/$eGFP^{+}$-$mCherry^{+}$β-MSC) (right). Average counted cells were 5000 events per condition. Analyses were performed in at least three independent experiments and show mean ± SEM. *P< 0.05 Treat compared to Mix at the same conditions; **P< 0.05 at the ratio of 1:11 compared to 1:5 **(A)**, 100 compared to 10 µg/ml PHA-P **(B)**, 33.3 compared to 5.5 mM glucose **(C)**, 2X compared to 1X 50% W/V PEG **(D)**, PHA-P/PEG compared to PEG alone, ***P<0.05 2x compared to 1x 50% W/V PEG at the same conditions, $^{-}$P< 0.05 optimized compared to standard protocol;

Fig.3. Characterization of insulin^{+}human/rat β-MSC heterokaryon cells.

(A) Schematic illustration of the strategy for generation of fused human $eGFP^{+}$MSCs/rat $mCherry^{+}$INS-1E cells and their subsequent analysis. **(B-G)** $eGFP^{+}$MSCs and $mCherry^{+}$INS-1E cells were treated with PHA-P and PEG, 4 days

after puromycin selection. **(B)** Triple labeling for insulin, eGFP and DAPI revealed polyploid insulin$^+$eGFP$^+$β-MSCs by fluorescence microscopy (left) or CLSM (right). **(C)** Triple staining for PDX1, DAPI and insulin shows PDX1$^+$eGFP$^+$insulin$^-$ polyploid (left) as well as PDX1$^+$eGFP$^+$insulin$^+$ polyploid cells (right; all 400X). **(D)** All cells were glucagon$^-$, (200X). **(E, F)** RT-PCR analysis of human **(E)** and rat **(F)** specific mRNA sequences of β-cell markers shown from three independent experiments relative to mixed MSC/INS-1E cells and normalized to human **(E)** or rat Cyclophilin A **(F)**. **(G)** Insulin content from mixed and treated cells under the optimized condition normalized to protein concentration and shown as percentage of mixed cells. All analyses are from at least three independent experiments from three different MSC donors shown in separate graphs **(E, F)** or as means ± SEM **(G)**. ND = not detected. *P< 0.05 TREAT compared to MIX.

Fig.4. Fusion of human MSCs with human islet cells results in insulin$^+$β-MSCs.
(A) Schematic illustration of the strategy for generation of fused human eGFP$^+$MSCs/human dispersed islet cells. Mixed cells are treated with PHA-P and PEG (optimized protocol) and MSCs and β-MSCs selected by puromycin and analyzed subsequently. **(B)** Triple positivity for insulin, eGFP and DAPI in a β-MSC (400X). **(C)** PDX1, insulin and DAPI costaining shows a PDX1$^+$eGFP$^+$insulin$^-$ cell and a PDX1$^+$eGFP$^+$insulin$^+$ cell (white arrows) (200X). **(D)** A human eGFP$^+$insulin$^+$β-MS heterokaryon (400X) **(E,F)** Insulin, eGFP, and DAPI triple positive cells in an islet like cluster (100X) by **(E)** fluorescence microscopy and **(F)** CLSM **(G,H)** The relative mRNA expression of human β-cell markers normalized to **(G)** mixed (dotted line) MSC/dispersed islet cells or **(I)** mature islet cells (dotted line) from the same batch. RT-PCR was normalized to human Cyclophilin A and **(I)** insulin protein content treated 8h with 33.3 mM glucose,100 µg/ml PHA-P and 50% W/V PEG, All analyses are from at least three independent experiments from three different islet and MSC donors shown in separate graphs **(G, I)** or as means ± SEM **(H).** *P< 0.05 TREAT compared to MIX.

SUPPLEMENTARY

Suppl.Fig.1. Characterization of human bone marrow MSCs.

(A) Colony Forming Unit-Fibroblast (CFU-F) stained with 1% crystal violet as a marker of MSCs in culture after 1 week (left) and the shape of MSCs in long-term culture of around 3 weeks (right). (40X) as well as CD73 and CD105 staining of paraffin embedded MSC sections (400X).**(B)** Positive (CD105, CD90 and CD73; top) as well as negative (CD45, CD34 and MHC-II; bottom) MSC markers by flow cytometry **(C)** MSC differentiation potential after stimulation (see material and methods) into adipocytes and osteoblasts analyzed by Sudan red B and Silver nitrate, respectively (40X). **(D)** Efficiency of $eGFP^+$MSC and $mCherry^+$INS-1E stable cells shown by flow cytometry. **E)** EGFP, CD105 and CD73 and CD90 staining of paraffin embedded $eGFP^+$MSC sections (400X). **(F)** To select the optimal time point of puromycin ,MSC/INS-1E fused cells were treated with puromycin after 12h or 36h.To select the optimum medium, MSC/INS-1E cells were maintained in AlphaMEM (MSC medium) or RPMI1640 (INS-1E medium) immediately after standard treatment condition for 36h. The percentage of $eGFP^+/mCherry^+$ cells was counted under the fluorescent microscope.(G) Z-stack movie (left) and serial sections (right) from $eGFP^+$MSC homokaryons (0.4 µm) (400X). *P< 0.05 at RPMI1640 to AlphaMEM or 12h RPMI1640.

Suppl.Fig.2. Optimization of cell fusion protocol.

(A-E) Representative scatter plots corresponding to the bar graphs in Fig.2A-E. **(F)** Representative scatter plots corresponding to the bar graphs in Fig.2G. Gating was set for control non-stained cells.

Suppl.Fig.3: Characterization of insulin$^+$ human/rat β-MSC heterokaryon cells.

(A) The relative mRNA expression of *MAFA* and *Insulin* of treated normalized to mixed human MSC/dispersed islet cells and to human Cyclophilin A. **(B)** Z-stack movie (left) and serial sections (right) from a eGFP$^+$insulin$^+$heterokaryon (0.4 μm) from eGFP$^+$MSC/mCherry$^+$INS-1E cells under the optimized fusion protocol. (400X) **(C,D)** Relative mRNA expression of human **(C)** as well as rat β-cell markers **(D)** from treated eGFP$^+$MSC/mCherry$^+$INS-1E cells normalized to mixed control conditions. RT-PCR was normalized to human **(C)** or rat Cyclophilin A **(D)**. Results represent three independent experiments. All analyses are from at least three independent experiments from three MSC donors shown in separate graphs.

Suppl.Fig.4. Characterization of insulin$^+$ human β-MSCs.

(A) Co-staining of human β-MSCs with insulin and CD105 in paraffin sections and fluorescent microscopical analysis. White arrows show double positive cells (300X). **(B)** The relative mRNA expression of human β-cell markers of treated human β-MSC cultures normalized to mixed MSC/dispersed islet cells as control and to human Cyclophilin A. The bar graphs represent three independent experiments from three different MSC and islet donors shown in separate graphs.

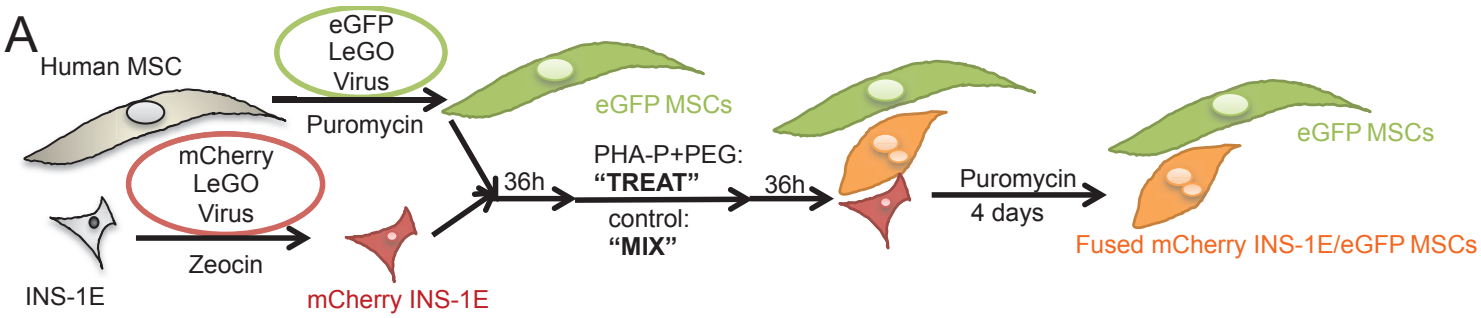
A
Human MSC
eGFP LeGO Virus
Puromycin
eGFP MSCs
mCherry LeGO Virus
Zeocin
INS-1E
mCherry INS-1E
36h
PHA-P+PEG:
"TREAT"
control:
"MIX"
36h
Puromycin
4 days
eGFP MSCs
Fused mCherry INS-1E/eGFP MSCs

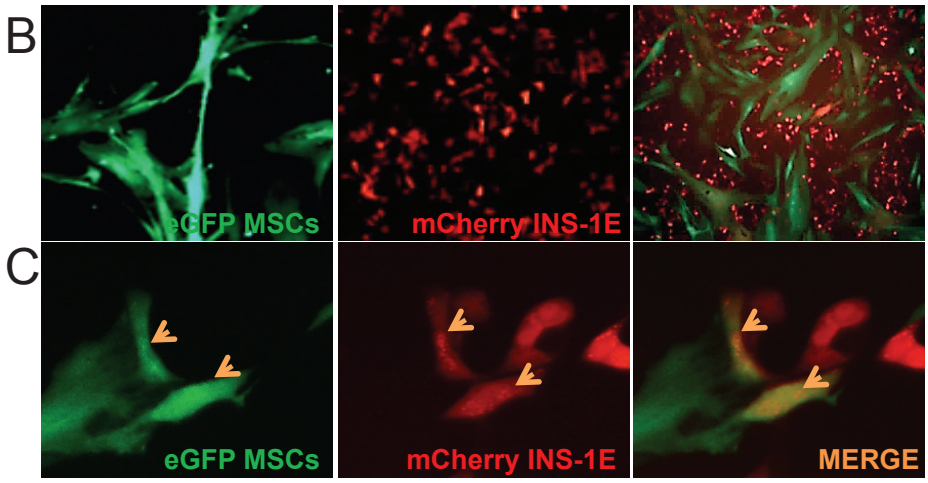
B
eGFP MSCs
mCherry INS-1E
C
eGFP MSCs
mCherry INS-1E
MERGE

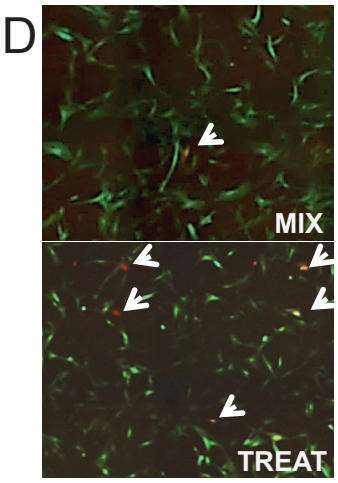
D
MIX
TREAT

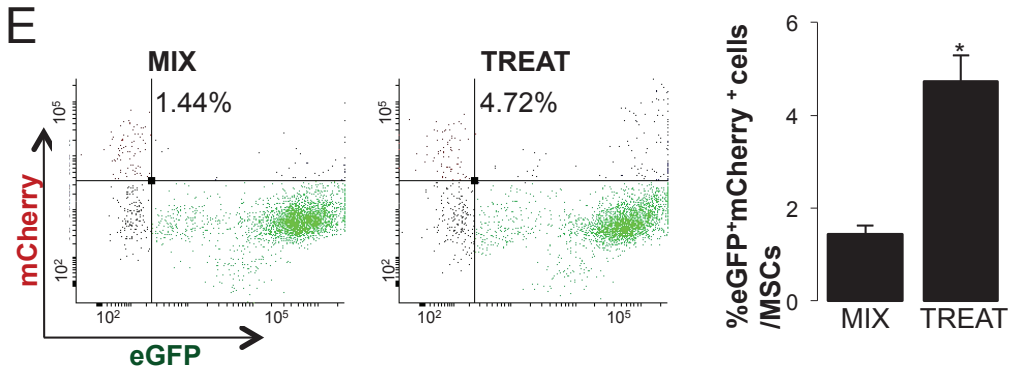
E
MIX
1.44%
TREAT
4.72%
mCherry
eGFP
%eGFP+mCherry+ cells /MSCs
MIX
TREAT

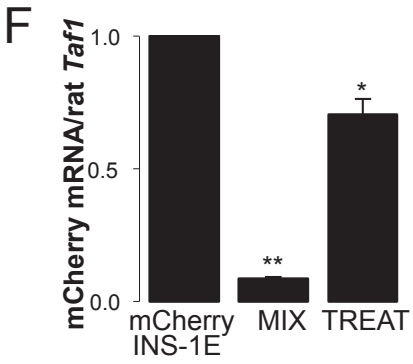
F
mCherry mRNA/rat Taf1
mCherry INS-1E
MIX
TREAT

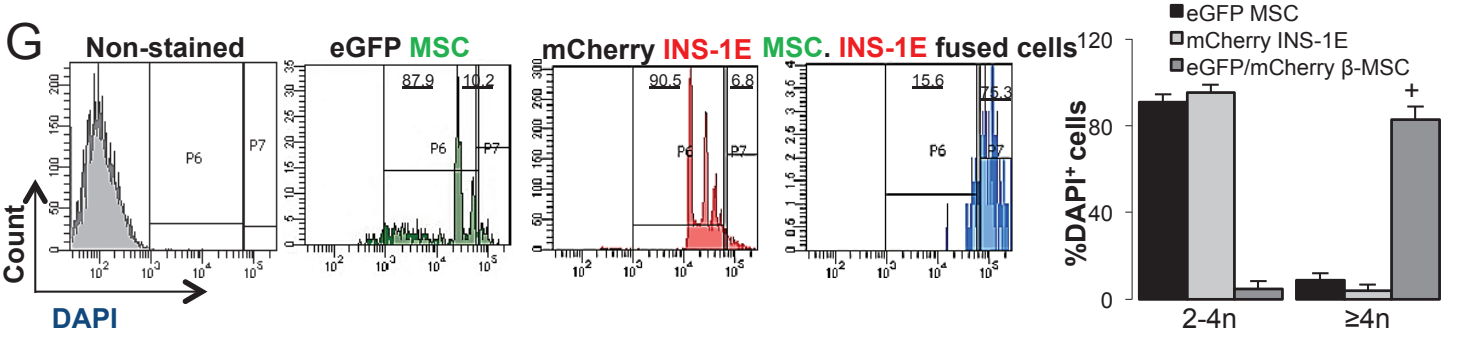
G
Non-stained
eGFP MSC
mCherry INS-1E MSC. INS-1E fused cells
Count
DAPI
eGFP MSC
mCherry INS-1E
eGFP/mCherry β-MSC
%DAPI+ cells
2-4n
≥4n

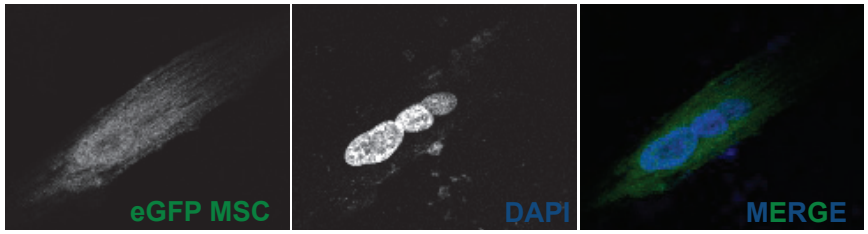
H
eGFP MSC
DAPI
MERGE

Figure 1

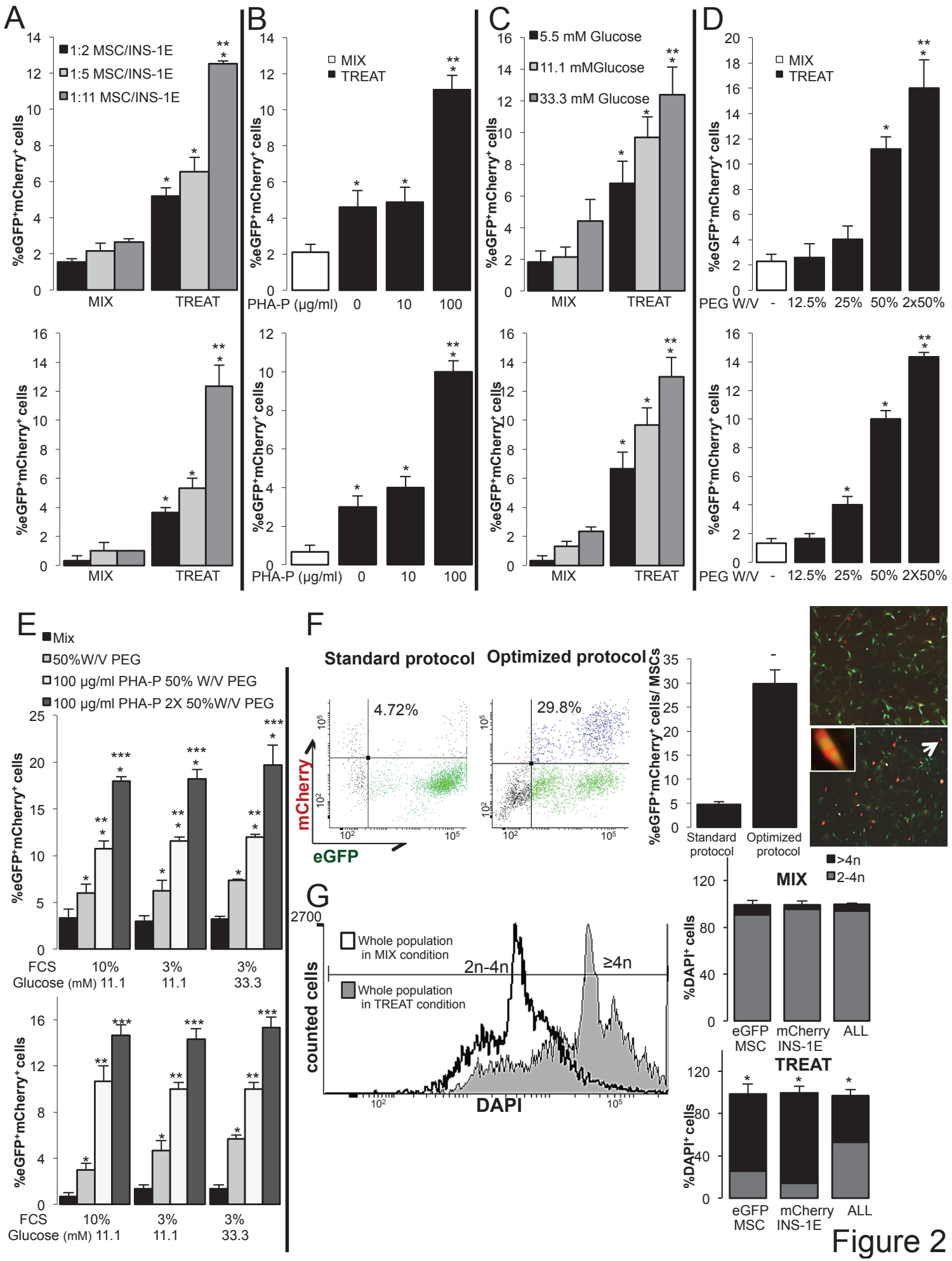
A
1:2 MSC/INS-1E
1:5 MSC/INS-1E
1:11 MSC/INS-1E
%eGFP+mCherry+ cells
MIX
TREAT
B
MIX
TREAT
PHA-P (µg/ml) 0 10 100
C
5.5 mM Glucose
11.1 mMGlucose
33.3 mM Glucose
D
PEG W/V - 12.5% 25% 50% 2x50%
E
Mix
50%W/V PEG
100 µg/ml PHA-P 50% W/V PEG
100 µg/ml PHA-P 2X 50%W/V PEG
FCS 10% 3% 3%
Glucose (mM) 11.1 11.1 33.3
F
Standard protocol
Optimized protocol
4.72%
29.8%
mCherry
eGFP
%eGFP+mCherry+ cells/ MSCs
Standard protocol
Optimized protocol
G
2700
Whole population in MIX condition
Whole population in TREAT condition
2n-4n
≥4n
counted cells
DAPI
>4n
2-4n
MIX
TREAT
%DAPI+ cells
eGFP MSC
mCherry INS-1E
ALL

Figure 2

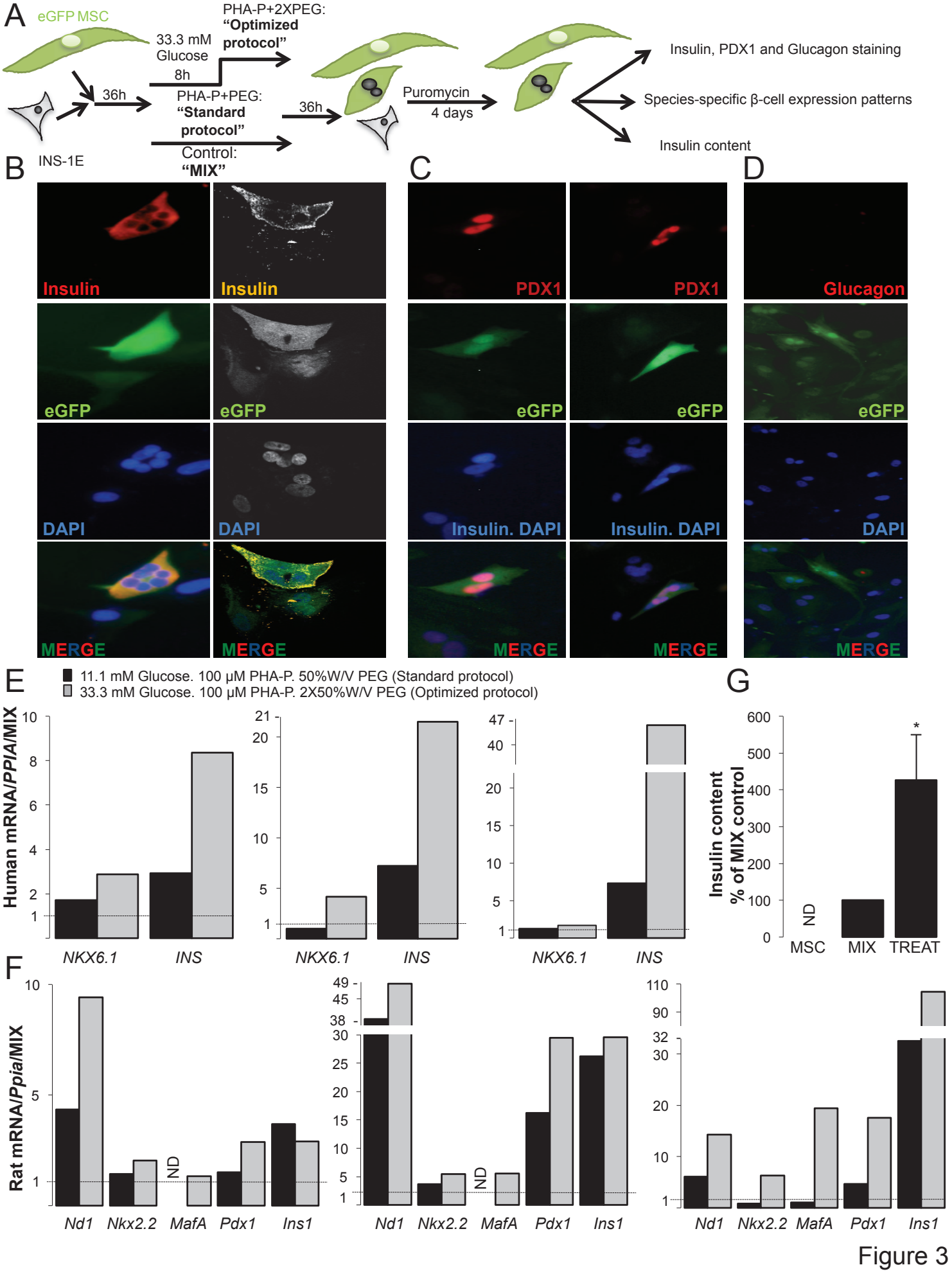
A
eGFP MSC
33.3 mM Glucose
8h
PHA-P+2XPEG: "Optimized protocol"
36h
PHA-P+PEG: "Standard protocol"
36h
Puromycin 4 days
Control: "MIX"
Insulin, PDX1 and Glucagon staining
Species-specific β-cell expression patterns
Insulin content
B
INS-1E
Insulin
Insulin
eGFP
eGFP
DAPI
DAPI
MERGE
MERGE
C
PDX1
PDX1
eGFP
eGFP
Insulin. DAPI
Insulin. DAPI
MERGE
MERGE
D
Glucagon
eGFP
DAPI
MERGE
E
11.1 mM Glucose. 100 µM PHA-P. 50%W/V PEG (Standard protocol)
33.3 mM Glucose. 100 µM PHA-P. 2X50%W/V PEG (Optimized protocol)
Human mRNA/PPIA/MIX
NKX6.1
INS
NKX6.1
INS
NKX6.1
INS
G
Insulin content % of MIX control
ND
MSC
MIX
TREAT
*
F
Rat mRNA/Ppia/MIX
ND
Nd1
Nkx2.2
MafA
Pdx1
Ins1
ND
Nd1
Nkx2.2
MafA
Pdx1
Ins1
Nd1
Nkx2.2
MafA
Pdx1
Ins1

Figure 3

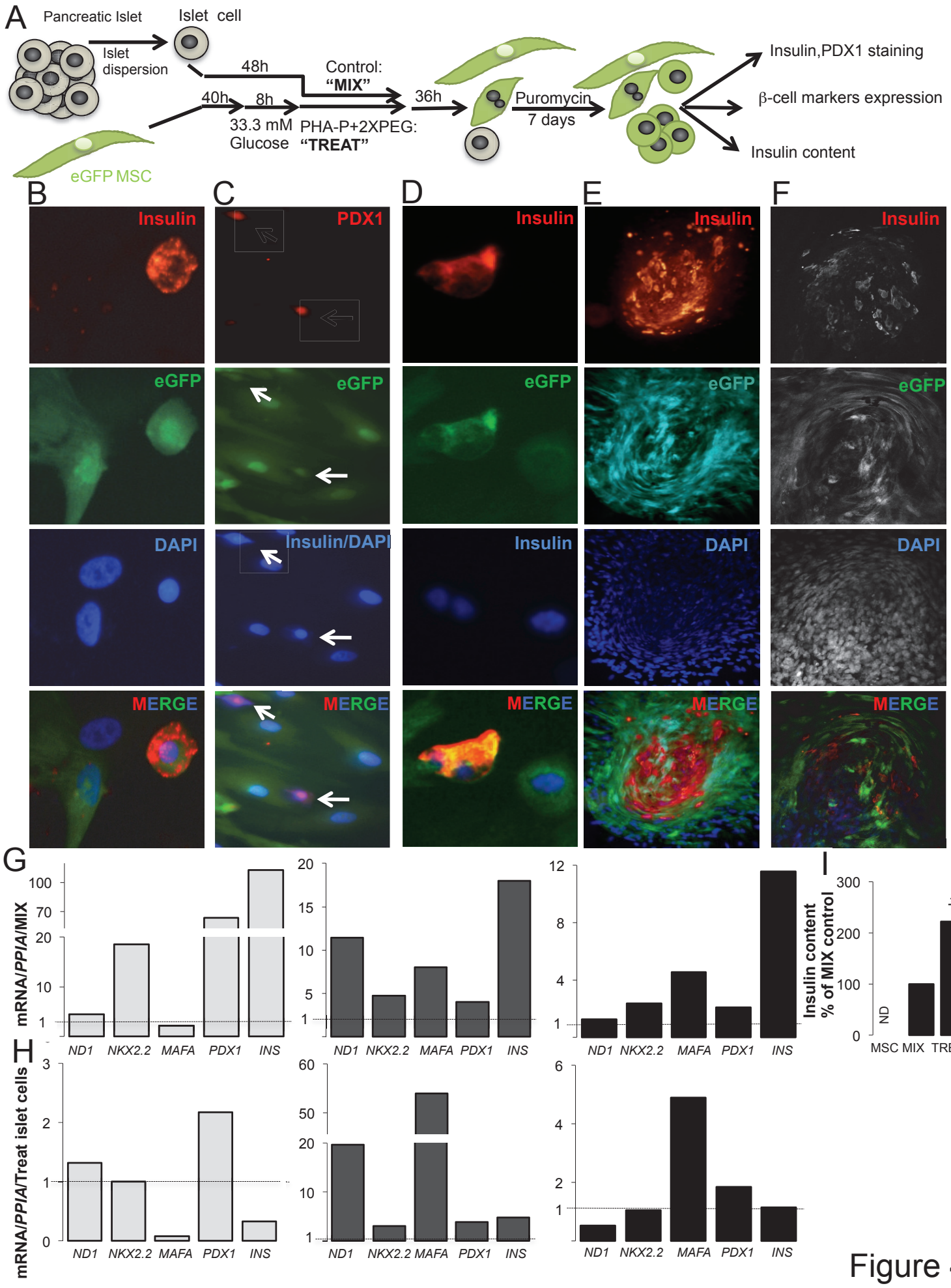
A
Pancreatic Islet
Islet cell
Islet dispersion
48h
Control: "MIX"
40h
8h
33.3 mM Glucose
PHA-P+2XPEG: "TREAT"
36h
Puromycin 7 days
Insulin,PDX1 staining
β-cell markers expression
Insulin content
eGFP MSC
B
C
D
E
F
Insulin
PDX1
eGFP
DAPI
Insulin/DAPI
MERGE
G
mRNA/PPIA/MIX
ND1 NKX2.2 MAFA PDX1 INS
H
mRNA/PPIA/Treat islet cells
I
Insulin content % of MIX control
ND
MSC MIX TREAT
*

Figure 4

supplementary

Suppl.Figure 1

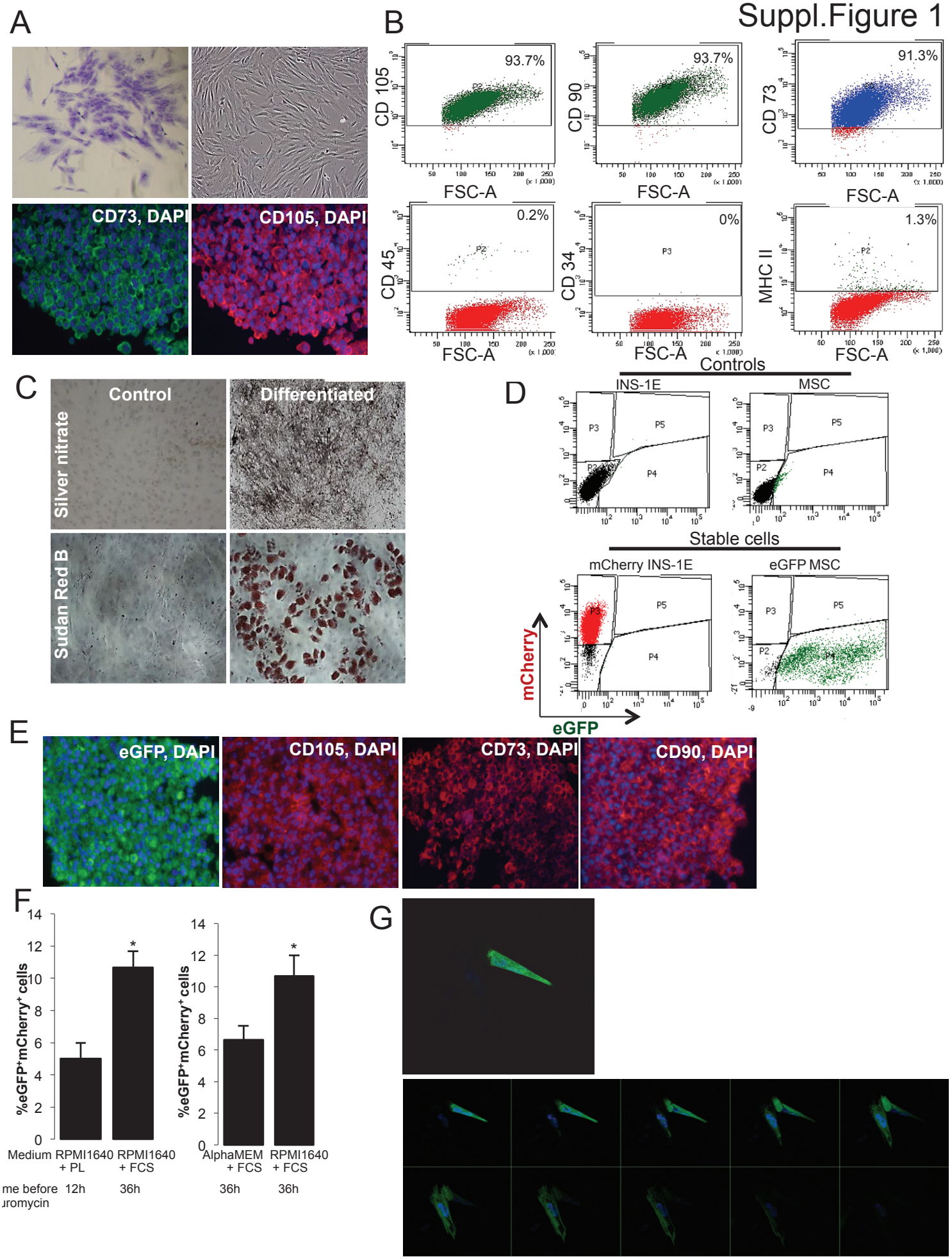

Suppl.Figure 2

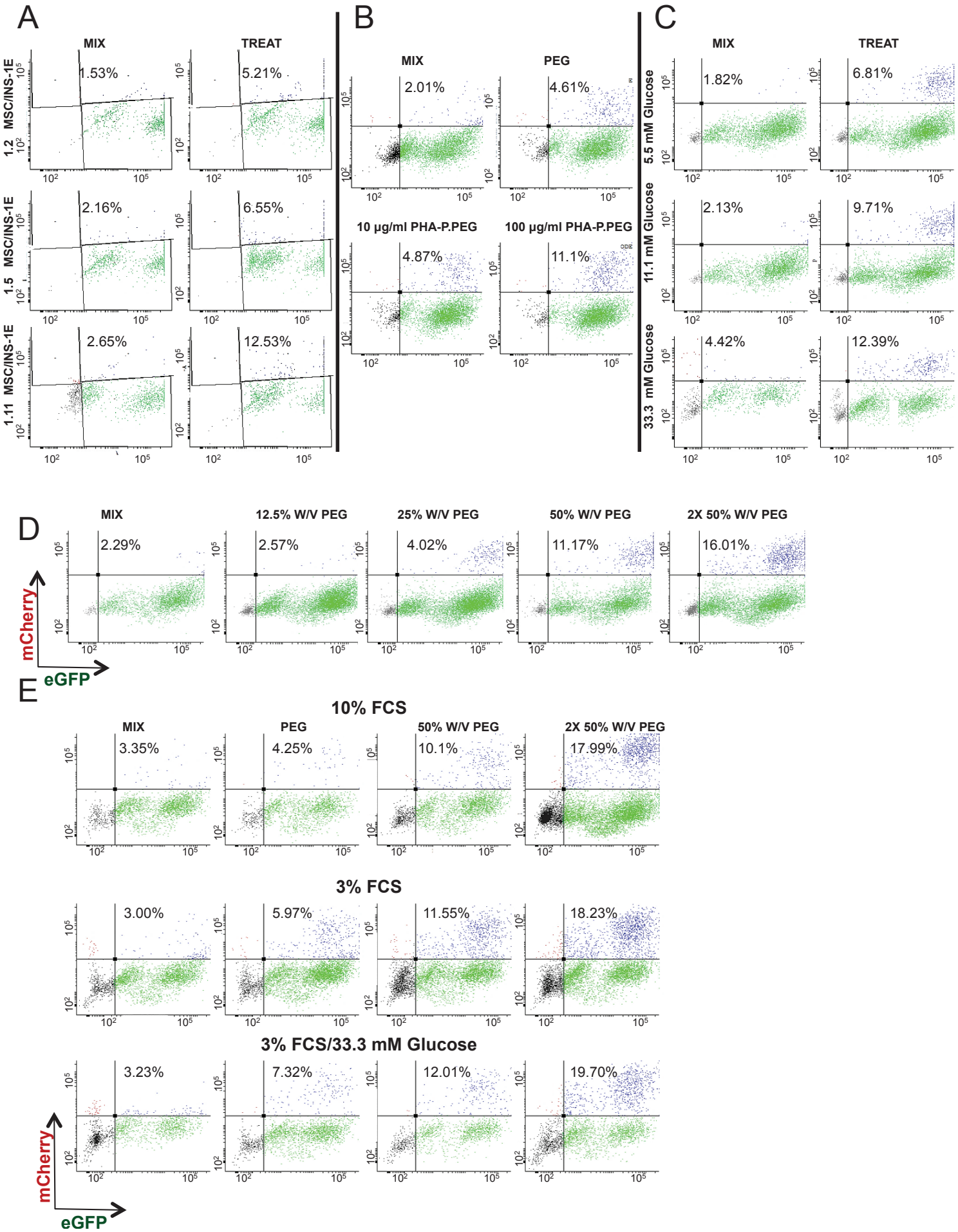

Suppl.Figure 2
continued

F

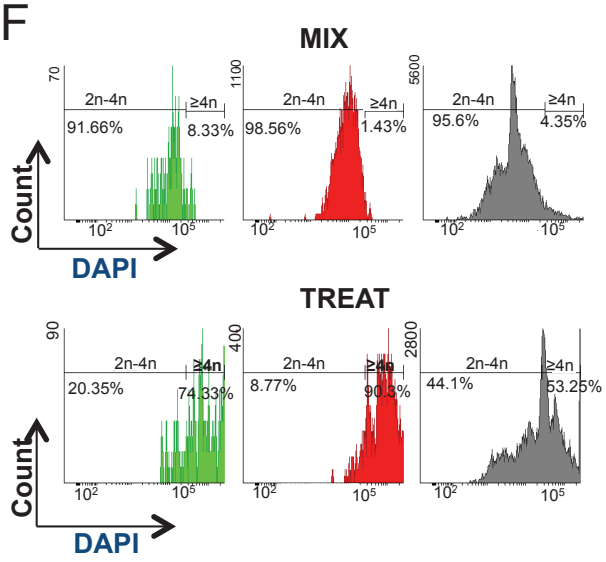

Suppl.Figure 3

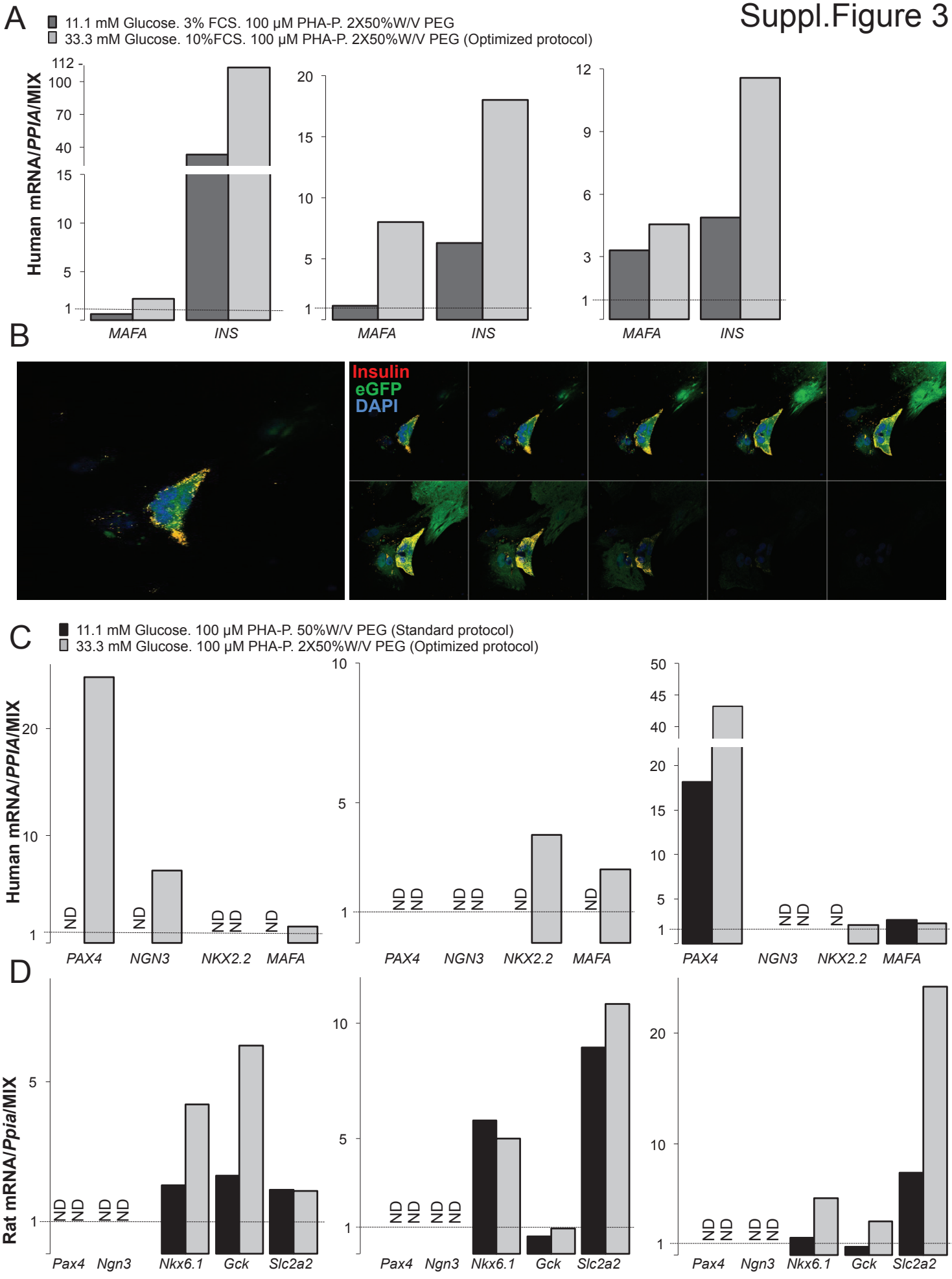

Suppl.Figure 4

A

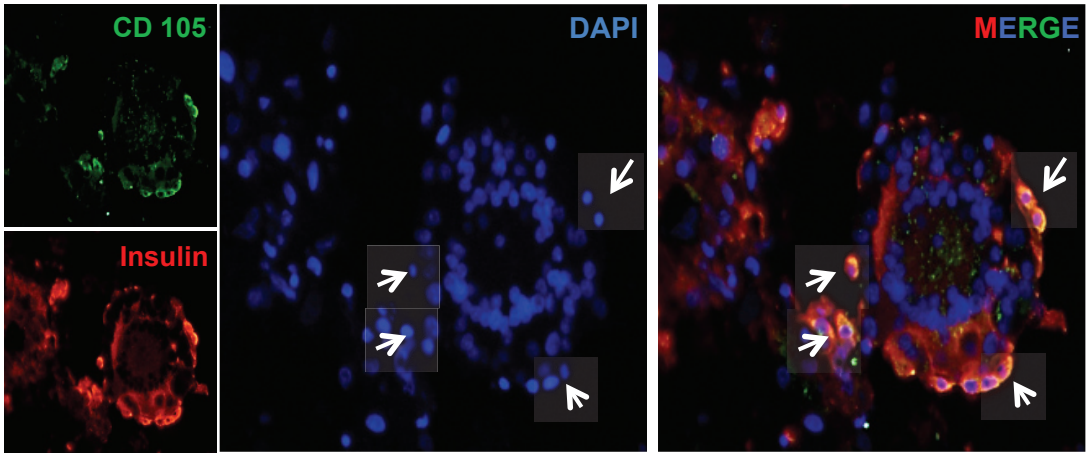

B

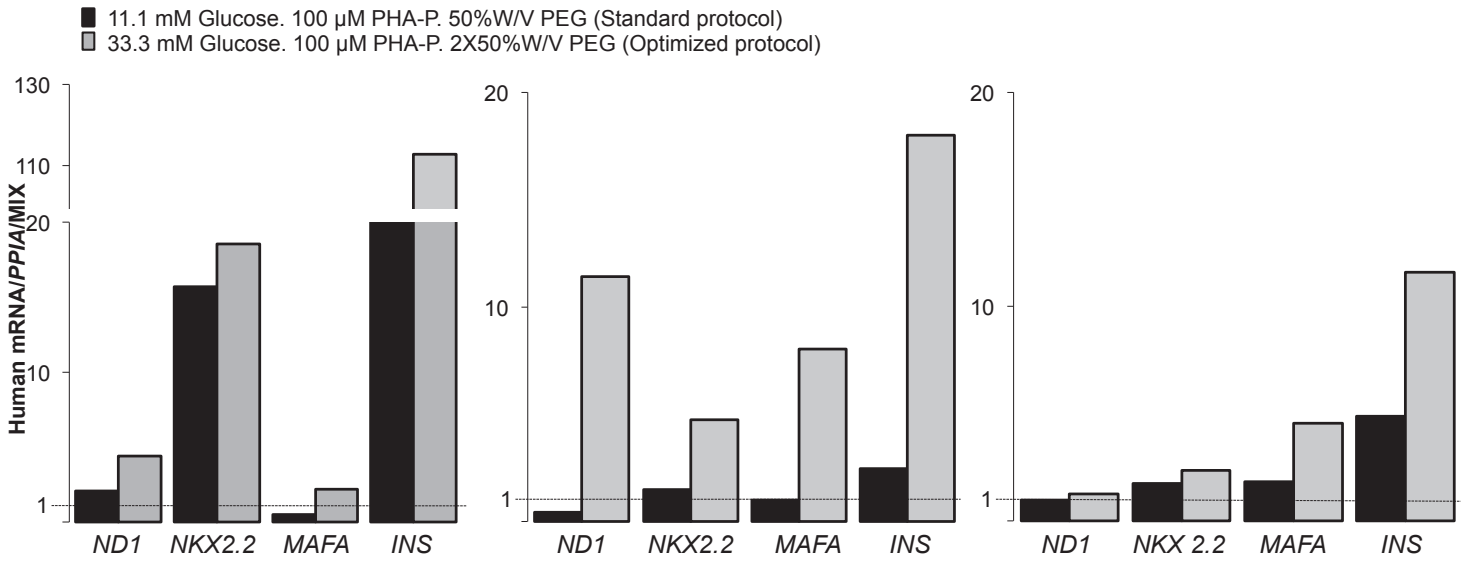

3. Discussion

3.1. Fusion of mesenchymal stromal cells and β–cells in culture

Multiple studies have suggested that injected bone marrow mesenchymal stromal cells (MSC) are a promising strategy to treat various diseases such as prevention of degeneration of retinal cells or normalization of glucose levels in diabetic mice [1-3]. In line of mice data, transplantation of auto- or allograft bone marrow cells has beneficial effects on patients with myocardial infarction or liver cirrhosis [4-7]. Consistently, co-transplantation of MSCs with islets improved both islet viability and graft outcomes over time [3, 8-13]. It has also been shown that engrafted MSCs remarkably normalized hyperglycemia and improved glucose homeostasis in recipient STZ-treated mice as result of increased insulin secretion due to generation of a new source of *in vivo* islet spheroid structure in the body [14]. Different mechanisms have been proposed to explain such restorative effect including inducing β-cell proliferation by MSCs, β-cell neogenesis from MSCs directly [14] or stimulation of other cell types such as duct cells [15, 16] or pancreatic stem cells [17]. Interestingly, another study showed that 1.7-3% of injected bone marrow cells migrated, homed and differentiated to insulin producing beta cells in pancreatic islets according to INS2-eGFP lineage tracing method within 4-6 weeks in mice. These newly formed cells express β-cell markers such as insulin, PAX6, PDX1, SLC2a2, HNF1α, and secret insulin in response to increased glucose concentration [18].

Two major mechanisms have been suggested considering conversion and fate of bone marrow cells upon transplantation: 1) direct transdifferentiation of these cells to other cells [18], 2) fusion of donor bone marrow cells with recipient cell types [19]. Recent reports showed that mouse bone marrow cells convert into particular recipient cells via spontaneous cell-fusion *in vitro*. However, the frequency of this phenomenon is low [20].

During *in vitro* fusion, the plasma membranes of cells are merged and make a cell with two or more nuclei of different cell types and one cytoplasm called heterokaryon. The cell is a polyploid non–dividing cell and frequently transient, if nuclei fuse resulting in a

cell with one polyploid nucleus called synkaryon. Proliferative synkaryons make hybrids.

Different methods are available for screening, and isolation of fused cells in culture [21, 22]. However, these techniques have some limitations. For instance, HAT system (hypoxanthine-aminopterin-thymidine medium) is a genetic selection way which can apply for only special cell types such as isolation of hypoxanthine phosphoribosyl transferase (HPRT) negative, mutant myeloma – B cells hybrids [21]. Herein, we established and optimized a polyethylene glycol (PEG)-fusion protocol for efficiently fusing human MSCs with β–cells (rat INS1E cells or dispersed human islet cells). We initially made polyploid non–dividing β–MSC heterokaryons by fusion of human $eGFP^+$ MSCs and rat $mCherry^+$ INS1E cells. In this system, we could observe spontaneous fusion in the mixture of MSC/IS1E cells based on co-expressing eGFP and mCherry in fused cells. Our preliminary data showed that these cells are polyploid. Generation of non-proliferative polyploid heterokaryon cells between rat and human provide a unique opportunity for screening intact nucleus of MSC after fusion. This method also provides a chance to measure accurate fusion efficiency.

Different approaches such as viral (UV– inactivated Sendai virus) [23], physical (electric pulse) [24] or chemical methods (poly ethylene glycol (PEG)) [25] accelerate the rate of fusion in the *in vitro* setting. Fusion efficiency depends on different factors such as size, type and age of cells [26-28]. For instance, electric pulses make some pores in the plasma membrane resulting in the fusion of two plasma membranes. The threshold voltage depends on the size of the cells and it should be carefully optimized to avoid direct cellular lysis. Another study suggested that viral induced fusion can alter the normal pattern of gene expression in fused cells [29].

PEG is a polymer of ethylene oxide and binds to water molecules resulting dehydration of membranes. PEG can change the configuration and orientation of phospholipid dipoles in the plasma membrane leads to make the pores on the membrane and promote cell membrane fusion of the cells that are in close contact to each other through osmotic pressure [30-32]. The PEG–fusion has been recommended when the two cell types of interest have very different sizes [28]. Here,

we provide a PEG–fusion protocol to generate β–MSCs. The cell fusion was induced by commercially available recrystallized PEG [33].

We mixed eGFP^{+} MSCs with labeled PKH–26 dye (cell membrane marker) INS1E cells, the fusion was induced by PEG and fused cells were observed overtime (data not shown). In agreement with Skelley *et al.* [28], our data showed that cell tracker labeling is not as efficient as the fluorescent–labeled cells due to PKH–26 partial plasma membrane distribution and detection in the MSC/INS1E merged cell. Hence, tracing eGFP–mCherry expressing fused cells is more accurate and feasible compared to cell tracker labeled cells.

In 2008, a microfluidic device was introduced for efficiently fusing suspension cells [28]. Fusion rate is variable due to cell types and passages [26], e.g. NIH3T3 fibroblasts PEG–fusion was optimized from 6 ± 4% fused cells via standard protocol up to 25 ± 5% fused cells after four doses of PEG treatment in microfluidic method [28]. However, our data show higher number of rat/human β–MSCs in the adherent culture compared with suspension culture (data not shown), since suspension fused cells do not attach to the surface of the dish after exposing cells to PEG and they gradually die. Polyploidy in these interspecies β–MSCs were quite high. In a β–MSC heterokaryon, nuclei were not fused which results in an intact genetic pool which allowed us to follow the reprogramming of the human MSC nuclei towards β–cells. A similar system was extensively used for other cell types for monitoring the influence of two different nuclear materials on gene expression [34-38]. However, the optimization of MSC and β–cell fusion protocol was essential before further investigation due to the low number of fused cells in the culture after PEG induction (~5%).

Accordingly, we selected the protocol (100 µg/ml PHA-P, 50% W/V PEG). Introduced and used by Islam et al. for the fusion of mouse MSCs and fibroblasts [39] and we applied it for the fusion of MSC/INS1E cells at the ratio of 1:2 as a standard protocol. Some protocols suggested that phytohemagglutinin (PHA–P) pretreatment can improve PEG–induced fusion efficiency and it allows to decrease PEG concentration without any impact on fusion efficiency [40]. Conversely, others have suggested that PHA–P does not have any effect on the enhancement of fusion efficiency [41]. Our

experiment illustrated that 100 μM PHA–P has a significant effect on fusion rate *in vitro*. Additionally, concentrations lower than 50% W/V PEG in conjugation with 100 μM PHA–P pretreatment decreased the efficiency of fusion dramatically, suggesting that the concentration below 50% W/V PEG is not able to efficiently induce the fusion [40].

Literature data showed that the rate of fusion increases following tissue damage in order to restore the function of impaired tissues. For instance, spontaneous fusion rises up two fold when cells are treated with pro–apoptotic cytokine TNF–α in co-cultured rat bone marrow stromal cells and cardiomyocytes [42]. Fusion frequency also increases from 0.3% to 7.9± 0.3% after H_2O_2 treatment (oxidative stress), which is more than 20-fold fusion induction. Indeed, fused cardiomyocytes-MSCs were morphologically and functionally transdifferentiated cells [42]. Co-cultured human mesenchymal stromal cells with heat shocked–epithelial cells showed a subset of transdifferentiated MSCs, which express the specific epithelial cell markers. Therefore, heat shocked-treatment improved the fusion frequency [43]. Another study showed that the fusion of cardiomyocytes with mesenchymal stromal cells increases in low PH compared to high PH, suggesting the induction of mesenchymal-cardiomyocytes fusion event during ischemia in *in vivo* [44].

Glucose is the major fuel for the β-cell and elevated glucose concentrations have a dual-function, proliferation in the short- apoptosis and functional damage (glucotoxicity) in the long-term [45, 46]. Therefore, we hypothesized that stimulating the β-cells with 33.3 mM glucose may increase the number of β-MSCs. In parallel to other studies, we also observed that 8 hours 33.3 mM glucose (high) compared to 5.5 mM glucose pretreatment increases the number of heterokaryons. However, we didn't detect any fusion induction at high glucose concentration pretreatment when compared to 11.1 mM glucose. Interestingly, we observed higher levels of specific β-cell transcription factors expression in high compared to normal glucose pretreatment. It remains a question how 8-hour glucose pretreatment elevates the insulin$^+$β-MSCs fusion efficiency. Our data also showed that two times 50%W/V PEG treatment as well as increasing the number of β–cells at a ratio of 1:11 MSC/INS1E cells consequently

improved the cell fusion efficiency, since it facilitated cell–cell contact between MSCs and β–cells and raises the possibility of fusion of more than one INS1E cell with one MSC which elevates the chance of β-cell fate dominance, because the access of β-cell nuclear dosage and cytoplasmic factors increase [38].

Altogether, β–MSC fusion efficiency was increased by an optimized protocol (1:11 MSC/INS1E cells, 8 hours 33.3 mM glucose pretreatment, 100 µg/ml PHA–P and a 2nd addition of 50% W/V PEG to the cell mixture), which resulted in a 6–fold more heterokaryons (~30%), compared to standard protocol.

3.2. Generation of Insulin^{+} β–MSCs

The possibility of generating insulin producing cells has been characterized based on nuclear PDX1 and cytoplasmic insulin double positivity in eGFP^{+} polyploid β–MSCs. The staining of polyploid fused cells showed that all nuclei expressed PDX1 due to reprogramming of nuclei originated from MSCs. Therefore, our data are in line with the recent study showing that PDX1 expression is necessary in MSC transdifferentiation into β–like cells as a β–cell differentiation key factor [47]. In addition, our data confirm other studies [37, 38], which show that nuclear reprogramming and phenotype is initiated at the heterokaryon stage. We did not observe any glucagon positive cells as a marker of α–cells, suggesting selective MSCs transdifferentiation into β–cell lineage.

Our data are in the line with other studies, which showed that the reprogramming process in human cells is fast after fusion [35, 36]. However, the initiation time point of reprogramming could not be assessed due to the necessity of puromycin selection. Therefore, it is possible that nuclear reprogramming process started even before this time point (6 days).

Better efficiency of our optimized protocol compared to standard protocol in terms of generating functional β–cells was confirmed by the expression of human and rat β–cell transcription factors, which are involved in determination and specification of β–cell lineage regeneration; PDX1, Neurogenin3 (NGN3), NEUROD1 (ND1), PAX4, MAFA, NKX2.2 and NKX6.1 as well as functional markers; glucose transporter 2 (SLC2a2), glucokinase (GCK) and insulin [48-51]. PDX1 is one of the first endocrine lineage factors and PDX1^{+} cells differentiate into all pancreatic cell types; pancreatic ducts,

endocrine and exocrine cells [52]. A previous study also showed that PDX1–expressing cells are able to proliferate [53]. Our data show strong correlation between fusion efficiency and increased expression of PDX1 and insulin.

NGN3 is an essential transcription factor, which regulates developmental processing into all islet cells [54]. NGN3 drives and stimulates the expression of other transcription factors such as PAX4, ND1, NKX2.2, MAFA and NKX6.1, which is essential for β–cell specification and maturation [48, 55, 56].

NGN3 is a temporary switched–on transcription factor which is expressed at very low level. PAX4 expression is still under debate due to if at all, a low PAX4 expression level in mature β-cell [50, 57]. This may be the reason why we could not detect NGN3 and PAX4 expression in all three individual experiments. Interestingly, human but not rat *NGN3* and *PAX4* expression was detected which originated from MSCs and drives MSCs into β–cell fate.

Rat/human β–MSCs were generated by the optimized protocol compared to standard protocol or mixed condition showed the higher levels of rat β–cell transcription factors expression (*Nd1, Nkx2.2, MafA, Pdx1*) and genes related to β–cell function *(Insulin*, *Glut2* and *Glucokinase)* originated from rat INS1E as well as human β–cell transcription factor expression (*MAFA* and *NKX6.1),* which originated from human transdifferentiated MSCs [48, 49]. It is essential to mention that we could not detect all the human β-cell target genes in each individual mixed condition (control) in three independent batches of MSC/INS1E experiments due to extremely low population of β-MSC in the mixed condition. Hence, we normalized RT-PCR data of treated condition to one single chosen mixed sample [58].

In addition, we counted the number of insulin$^+$ eGFP$^+$ synkaryons in the fused condition. Our data showed that almost all rat/human β-MSC heterokaryons were stable and proliferated only very rarely (data not shown).

In the next step, we used our optimized protocol to generate human β–MSCs. Fusion of human β–MSCs gave rise to higher levels of the β–cell specific markers *ND1, NKX2.2, NKX6.1, MAFA, PDX1* and insulin compared to the mixture of non–treated dispersed islet cells/MSCs. Concomitantly, β–cell transcription factors *ND1, MAFA*

and *PDX1* expression was higher in fused MSC/islet cell than islet cells. This complex network plays a role in transition waves of developmental process as well as mature β–cells [48-50].

The variation of β-cell transcription factor expression in each individual sample compared to insulin expression brought this idea that we have a combination of immature and mature β–like cell populations. This idea was supported by PDX1 and insulin co–staining which showed two cell populations including $PDX1^{+}$ $insulin^{-}$ as well as $insulin^{+}$ $PDX1^{+}$ cells considered as immature and mature β–like cells, respectively. This induction was also confirmed by cellular insulin content in the fused MSC/dispersed islet cells compared to non-treated mix condition which shows the generation of human β–cell like phenotype.

Here, we could not pool our individual analyses since we had a high variation of β–cell marker expression levels in the independent mixed/fused samples from different MSC and islet cells due to donor–to–donor MSC variations, which did not permit us to obtain a robust conclusion on differentiation stages and on raising β–cell transcription marker expression after fusion [59]. Many transcription factors are both involved in β-cell differentiation and specification towards formation of mature β-cells. Kinetics of transcription factor expressions are different in developmental stages and are tightly regulated during pancreas development [49, 50]. So, a comprehensive analysis would have been to monitor transcription factor expression at multiple time points after fusion. This would help to further understand the role of transcription factors during differentiation and whether their expressions are waving and related to a transcriptional network. These experiments were not performed here due to the necessity of long-term puromycin treatment for the complete removal of all non-fused dispersed islet cells.

While our study indicated that the high ratio of rat/human β-MSC cells are polyploid heterokaryons, we observed that fused human MSC/dispersed islet cells are more synkaryons, suggesting the possibility of already combined chromosome pools of MSCs and dispersed islet cells resulting in the formation of islet like cluster cells as

hybrids. Our data is in agreement with studies suggested that a multipotent cell fuses with a somatic cell; the proliferation capacity after fusion is regulated by the multipotent cell [44, 60]. The proliferative capacity needs still to be analyzed after long-term culture of human β-MSC.

In summary, we introduced a non–viral protocol to rapidly generate human insulin–producing cells. However, β-MSCs characterization in long-term culture, the quantification of polyploidy in human β-MSC synkaryons, their ability to respond to glucose and other secretagogues before transplantation as well as their characterization in vivo after transplantation are important questions which are still not answered in this thesis and should be addressed in future studies.

3.3. Conclusion

Here, we showed that stimulated fusion occurs after mixing MSCs and INS1E cells and we established and optimized a PEG–fusion protocol for fusion of β–cells (rat INS1E as well as human islet cells) and human MSCs in adherent culture. We increased the ratio of β–cells (MSC/INS1E:1/11), pretreated the cells for 8 hours with 33.3 mM glucose, added 100 µg/ml PHA–P concentration and a 2nd time of 50% W/V PEG to the cell mixture.

We also showed that interspecies β–MSCs are non-proliferative polyploid cells, which express both rat and human β–cell markers. These markers include transcription factors, which are temporarily involved in β–cell differentiation like NGN3 or expressed in stages of differentiation towards β–cell as well as mature β–cells like NKX6.1, MAFA and PDX1. In addition, we used our optimized protocol to induce fusion of human MSCs and dispersed islet cells, which resulted in insulin-producing β–MSCs.

3.4. Outlook

In this study, we provided a new protocol generating high number of stable interspecies heterokaryons that are not dividing. This efficient protocol could be repurposed as a platform providing a unique chance for rapid epigenetic and genetic variation monitoring during differentiation to β–like cells. For instance, histone tail modifications such as acetylation of K9 in histone 3(H3K9) or investigation of tri–methylation of lysine 27 on histone H3 (H3K27me3) as well as DNA demethylation are important post–translational modifications to regulate the process of open or close chromatin resulted in differentiated β–like cells [61, 62].

This tool can be used for making iPSCs from β–cells [61], providing a possibility to observe the effect of different chemical compounds on β–cell differentiation, understanding the mechanism of fusion of these cells *in vivo* as well as studying the molecular mechanism of MSC plasticity to β–cells *in vitro*. Therefore, this method can help to pave a way for better understanding of β–cell developmental process and the generation of different sources of β–like cells. Also, it is essential to know whether the fusion reprogramming process is partial or completed and how the whole genome epigenetic pattern is regulated under the differentiation process.

On the other hand, human β–MSCs can be a good β–cell candidate source for transplantation. However, it is necessary to monitor these hybrid cells in long–term culture as well as their functional β–cell characteristics such as glucose–dependent insulin secretion. In the next step, human β–MSCs can be transplanted into diabetic STZ–treated mice in order to test their capability to improve glucose homeostasis by production of insulin and graft outcomes over time *in vivo*.

In summary, *in vitro*-imitation of spontaneous *in vivo*–fusion gives hope in regenerative medicine in order to have rapidly differentiated cells *in vitro* and restore damaged cell function after transplantation.

References:

1. Otani A, Dorrell MI, Kinder K et al. Rescue of retinal degeneration by intravitreally injected adult bone marrow-derived lineage-negative hematopoietic stem cells. *J Clin Invest* 2004; **114**: 765-74.
2. Gabr MM, Zakaria MM, Refaie AF et al. Insulin-producing cells from adult human bone marrow mesenchymal stem cells control streptozotocin-induced diabetes in nude mice. *Cell transplantation* 2013; **22**: 133-45.
3. Shen J, Cheng Y, Han Q et al. Generating insulin-producing cells for diabetic therapy: existing strategies and new development. *Ageing research reviews* 2013; **12**: 469-78.
4. Hare JM, Traverse JH, Henry TD et al. A randomized, double-blind, placebo-controlled, dose-escalation study of intravenous adult human mesenchymal stem cells (prochymal) after acute myocardial infarction. *Journal of the American College of Cardiology* 2009; **54**: 2277-86.
5. Meyer GP, Wollert KC, Lotz J et al. Intracoronary bone marrow cell transfer after myocardial infarction: 5-year follow-up from the randomized-controlled BOOST trial. *European heart journal* 2009; **30**: 2978-84.
6. Kharaziha P, Hellstrom PM, Noorinayer B et al. Improvement of liver function in liver cirrhosis patients after autologous mesenchymal stem cell injection: a phase I-II clinical trial. *European journal of gastroenterology & hepatology* 2009; **21**: 1199-205.
7. Bernardo ME, Pagliara D, Locatelli F. Mesenchymal stromal cell therapy: a revolution in Regenerative Medicine? *Bone marrow transplantation* 2012; **47**: 164-71.
8. Duprez IR, Johansson U, Nilsson B et al. Preparatory studies of composite mesenchymal stem cell islets for application in intraportal islet transplantation. *Upsala journal of medical sciences* 2011; **116**: 8-17.
9. Rackham CL, Chagastelles PC, Nardi NB et al. Co-transplantation of mesenchymal stem cells maintains islet organisation and morphology in mice. *Diabetologia* 2011; **54**: 1127-35.
10. Borg DJ, Weigelt M, Wilhelm C et al. Mesenchymal stromal cells improve transplanted islet survival and islet function in a syngeneic mouse model. *Diabetologia* 2014; **57**: 522-31.
11. Kerby A, Jones ES, Jones PM, King AJ. Co-transplantation of islets with mesenchymal stem cells in microcapsules demonstrates graft outcome can be improved in an isolated-graft model of islet transplantation in mice. *Cytotherapy* 2013; **15**: 192-200.
12. King CC. Mesenchymal stem cells: protectors of islets? *Regenerative medicine* 2013; **8**: 20-1.
13. Veriter S, Gianello P, Igarashi Y et al. Improvement of subcutaneous bioartificial pancreas vascularization and function by coencapsulation of pig islets and mesenchymal stem cells in primates. *Cell transplantation* 2014; **23**: 1349-64.
14. Hess D, Li L, Martin M et al. Bone marrow-derived stem cells initiate pancreatic regeneration. *Nat Biotechnol* 2003; **21**: 763-70.

15. Corritore E, Dugnani E, Pasquale V et al. beta-Cell differentiation of human pancreatic duct-derived cells after in vitro expansion. *Cellular reprogramming* 2014; **16**: 456-66.
16. Yatoh S, Dodge R, Akashi T et al. Differentiation of affinity-purified human pancreatic duct cells to beta-cells. *Diabetes* 2007; **56**: 1802-9.
17. Zhang WJ, Xu SQ, Cai HQ et al. Evaluation of islets derived from human fetal pancreatic progenitor cells in diabetes treatment. *Stem cell research & therapy* 2013; **4**: 141.
18. Ianus A, Holz GG, Theise ND, Hussain MA. In vivo derivation of glucose-competent pancreatic endocrine cells from bone marrow without evidence of cell fusion. *J Clin Invest* 2003; **111**: 843-50.
19. Vassilopoulos G, Wang PR, Russell DW. Transplanted bone marrow regenerates liver by cell fusion. *Nature* 2003; **422**: 901-4.
20. Terada N, Hamazaki T, Oka M et al. Bone marrow cells adopt the phenotype of other cells by spontaneous cell fusion. *Nature* 2002; **416**: 542-5.
21. Hakoda M, Hirai Y, Akiyama M et al. Selection against Blood-Cells Deficient in Hypoxanthine Phosphoribosyltransferase (Hprt) in Lesch-Nyhan Heterozygotes Occurs at the Level of Multipotent Stem-Cells. *Human genetics* 1995; **96**: 674-80.
22. Cemazar J, Miklavcic D, Kotnik T. Microfluidic devices for manipulation, modification and characterization of biological cells in electric fields - a review. *Inform Midem* 2013; **43**: 143-61.
23. Harris H, Watkins JF. Hybrid Cells Derived from Mouse and Man: Artificial Heterokaryons of Mammalian Cells from Different Species. *Nature* 1965; **205**: 640-6.
24. Teissie J, Knutson VP, Tsong TY, Lane MD. Electric pulse-induced fusion of 3T3 cells in monolayer culture. *Science* 1982; **216**: 537-8.
25. Pontecorvo G. Production of mammalian somatic cell hybrids by means of polyethylene glycol treatment. *Somatic cell genetics* 1975; **1**: 397-400.
26. Tat PA, Sumer H, Pralong D, Verma PJ. The efficiency of cell fusion-based reprogramming is affected by the somatic cell type and the in vitro age of somatic cells. *Cellular reprogramming* 2011; **13**: 331-44.
27. Kemp K, Gordon D, Wraith DC et al. Fusion between human mesenchymal stem cells and rodent cerebellar Purkinje cells. *Neuropathology and applied neurobiology* 2011; **37**: 166-78.
28. Skelley AM, Kirak O, Suh H et al. Microfluidic control of cell pairing and fusion. *Nature methods* 2009; **6**: 147-52.
29. Targeted Cell Fusion Facilitates Stable Heterokaryon Generation invitro and invivo.
30. Lentz BR. PEG as a tool to gain insight into membrane fusion. *European biophysics journal : EBJ* 2007; **36**: 315-26.
31. Lentz BR. Polymer-induced membrane fusion: potential mechanism and relation to cell fusion events. *Chemistry and physics of lipids* 1994; **73**: 91-106.

32. Ahren B. Are sulfonylureas less desirable than DPP-4 inhibitors as add-on to metformin in the treatment of type 2 diabetes? *Current diabetes reports* 2011; **11**: 83-90.
33. Wojcieszyn JW, Schlegel RA, Lumleysapanski K, Jacobson KA. Studies on the Mechanism of Polyethylene Glycol-Mediated Cell-Fusion Using Fluorescent Membrane and Cytoplasmic Probes. *J Cell Biol* 1983; **96**: 151-9.
34. Blau HM, Blakely BT. Plasticity of cell fate: insights from heterokaryons. *Seminars in cell & developmental biology* 1999; **10**: 267-72.
35. Bhutani N, Brady JJ, Damian M et al. Reprogramming towards pluripotency requires AID-dependent DNA demethylation. *Nature* 2010; **463**: 1042-7.
36. Pereira CF, Terranova R, Ryan NK et al. Heterokaryon-based reprogramming of human B lymphocytes for pluripotency requires Oct4 but not Sox2. *PLoS genetics* 2008; **4**: e1000170.
37. Gridina MM, Serov OL. Bidirectional reprogramming of mouse embryonic stem cell/fibroblast hybrid cells is initiated at the heterokaryon stage. *Cell and tissue research* 2010; **342**: 377-89.
38. Palermo A, Doyonnas R, Bhutani N et al. Nuclear reprogramming in heterokaryons is rapid, extensive, and bidirectional. *FASEB journal : official publication of the Federation of American Societies for Experimental Biology* 2009; **23**: 1431-40.
39. Islam MQ, Ringe J, Reichmann E et al. Functional characterization of cell hybrids generated by induced fusion of primary porcine mesenchymal stem cells with an immortal murine cell line. *Cell and tissue research* 2006; **326**: 123-37.
40. Mercer WE, Schlegel RA. Phytohemagglutinin enhancement of cell fusion reduces polyethylene glycol cytotoxicity. *Experimental cell research* 1979; **120**: 417-21.
41. Pells S. Nuclear reprogramming : methods and protocols. Totowa, N.J.: Humana Press 2006.
42. Yang WJ, Li SH, Weisel RD et al. Cell fusion contributes to the rescue of apoptotic cardiomyocytes by bone marrow cells. *Journal of cellular and molecular medicine* 2012; **16**: 3085-95.
43. Spees JL, Olson SD, Ylostalo J et al. Differentiation, cell fusion, and nuclear fusion during ex vivo repair of epithelium by human adult stem cells from bone marrow stroma. *Proc Natl Acad Sci U S A* 2003; **100**: 2397-402.
44. Kouris NA, Schaefer JA, Hatta M et al. Directed Fusion of Mesenchymal Stem Cells with Cardiomyocytes via VSV-G Facilitates Stem Cell Programming. *Stem cells international* 2012; **2012**: 414038.
45. Maedler K, Sergeev P, Ris F et al. Glucose-induced beta cell production of IL-1beta contributes to glucotoxicity in human pancreatic islets. *J Clin Invest* 2002; **110**: 851-60.
46. Kim WH, Lee JW, Suh YH et al. Exposure to chronic high glucose induces beta-cell apoptosis through decreased interaction of glucokinase with mitochondria: downregulation of glucokinase in pancreatic beta-cells. *Diabetes* 2005; **54**: 2602-11.

47. Yuan H, Liu H, Tian R et al. Regulation of mesenchymal stem cell differentiation and insulin secretion by differential expression of Pdx-1. *Molecular biology reports* 2012; **39**: 7777-83.
48. Ben-Othman N, Courtney M, Vieira A et al. From pancreatic islet formation to beta-cell regeneration. *Diabetes research and clinical practice* 2013; **101**: 1-9.
49. Ziv O, Glaser B, Dor Y. The plastic pancreas. *Developmental cell* 2013; **26**: 3-7.
50. Conrad E, Stein R, Hunter CS. Revealing transcription factors during human pancreatic beta cell development. *Trends in endocrinology and metabolism: TEM* 2014; **25**: 407-14.
51. Cerf ME. Transcription factors regulating beta-cell function. *European journal of endocrinology / European Federation of Endocrine Societies* 2006; **155**: 671-9.
52. Gu G, Dubauskaite J, Melton DA. Direct evidence for the pancreatic lineage: NGN3+ cells are islet progenitors and are distinct from duct progenitors. *Development* 2002; **129**: 2447-57.
53. Seymour PA, Freude KK, Tran MN et al. SOX9 is required for maintenance of the pancreatic progenitor cell pool. *Proc Natl Acad Sci U S A* 2007; **104**: 1865-70.
54. Gradwohl G, Dierich A, LeMeur M, Guillemot F. neurogenin3 is required for the development of the four endocrine cell lineages of the pancreas. *Proc Natl Acad Sci U S A* 2000; **97**: 1607-11.
55. Gouzi M, Kim YH, Katsumoto K et al. Neurogenin3 initiates stepwise delamination of differentiating endocrine cells during pancreas development. *Developmental dynamics : an official publication of the American Association of Anatomists* 2011; **240**: 589-604.
56. Naya FJ, Huang HP, Qiu Y et al. Diabetes, defective pancreatic morphogenesis, and abnormal enteroendocrine differentiation in BETA2/neuroD-deficient mice. *Genes & development* 1997; **11**: 2323-34.
57. Brun T, Gauthier BR. A focus on the role of Pax4 in mature pancreatic islet beta-cell expansion and survival in health and disease. *Journal of molecular endocrinology* 2008; **40**: 37-45.
58. Livak KJ, Schmittgen TD. Analysis of relative gene expression data using real-time quantitative PCR and the 2(-Delta Delta C(T)) Method. *Methods* 2001; **25**: 402-8.
59. Siegel G, Kluba T, Hermanutz-Klein U et al. Phenotype, donor age and gender affect function of human bone marrow-derived mesenchymal stromal cells. *BMC medicine* 2013; **11**: 146.
60. Pomerantz J, Blau HM. Nuclear reprogramming: a key to stem cell function in regenerative medicine. *Nature cell biology* 2004; **6**: 810-6.
61. Graf T. Historical origins of transdifferentiation and reprogramming. *Cell stem cell* 2011; **9**: 504-16.
62. Lluis F, Cosma MP. Resetting epigenetic signatures to induce somatic cell reprogramming. *Cellular and molecular life sciences : CMLS* 2013; **70**: 1413-24.

4. Appendix

Part I

Papers with my contribution:

I.I. MST1 is a key regulator of beta cell apoptosis and dysfunction in diabetes

Amin Ardestani, Federico Paroni*, **Zahra Azizi***, Supreet Kaur*, Vrushali Khobragade, Ting Yuan, Thomas Frogne, Wufan Tao, Jose Oberholzer, Francois Pattou, Julie Kerr Conte & Kathrin Maedler

* Authors contributed equally

Published in Nature medicine journal

My Contribution: Performed β-cell mass and analysis, TUNEL assay and Ki67 staining as markers of apoptosis and proliferation respectively (shown in fig.6)

I.II. Manganese-mediated MRI signals correlate with functional β-cell mass during diabetes progression

Anke Meyer, Katharina Stolz, Wolfgang Dreher, Jennifer Bergemann, Vani Holebasavanahalli Thimmashetty, Navina Lueschen, **Zahra Azizi**, Vrushali Khobragade, Kathrin Maedler*, and Ekkehard Kuestermann*

* Authors contributed equally

Published in Diabetes journal

My Contribution: Performed β-cell mass and analysis, nuclear size analysis and Ki67 staining as a marker of proliferation (shown in fig.3)

I.III. Indicator displacement assays inside live cells

Amir Norouzy, **Zahra Azizi** and Werner M. Nau

Published in Angewandte Chemie international edition journal

My Contribution: Performed image processing and analysis (shown in Fig.1 and Fig.S3), confocal laser scanning microscopy (shown in Fig.S2) experiments and advised the project

nature medicine

MST1 is a key regulator of beta cell apoptosis and dysfunction in diabetes

Amin Ardestani[1], Federico Paroni[1,6], Zahra Azizi[1,6], Supreet Kaur[1,6], Vrushali Khobragade[1], Ting Yuan[1], Thomas Frogne[2], Wufan Tao[3], Jose Oberholzer[4], Francois Pattou[5], Julie Kerr Conte[5] & Kathrin Maedler[1]

Apoptotic cell death is a hallmark of the loss of insulin-producing beta cells in all forms of diabetes mellitus. Current treatments fail to halt the decline in functional beta cell mass, and strategies to prevent beta cell apoptosis and dysfunction are urgently needed. Here, we identified mammalian sterile 20–like kinase-1 (MST1) as a critical regulator of apoptotic beta cell death and function. Under diabetogenic conditions, MST1 was strongly activated in beta cells in human and mouse islets and specifically induced the mitochondrial-dependent pathway of apoptosis through upregulation of the BCL-2 homology-3 (BH3)-only protein BIM. MST1 directly phosphorylated the beta cell transcription factor PDX1 at T11, resulting in the latter's ubiquitination and degradation and thus in impaired insulin secretion. MST1 deficiency completely restored normoglycemia, beta cell function and survival *in vitro* and *in vivo*. We show MST1 as a proapoptotic kinase and key mediator of apoptotic signaling and beta cell dysfunction and suggest that it may serve as target for the development of new therapies for diabetes.

Pancreatic beta cell death is the fundamental cause of type 1 diabetes (T1D) and a contributing factor to the reduced beta cell mass in type 2 diabetes (T2D)[1–4]. In both cases, the mechanisms of beta cell death are complex and as yet not fully defined. Thus, multiple triggering factors have been identified; these factors initiate a variety of signaling cascades that affect the expression of apoptotic genes, leading to subsequent beta cell failure. In T1D, autoimmune destruction of insulin-producing beta cells and critically diminished beta cell mass are hallmarks of the disease[2]. Beta cell destruction occurs through immune-mediated processes; mononuclear cell infiltration in the pancreatic islets and interaction between antigen-presenting cells and T cells lead to high local concentrations of inflammatory cytokines, chemokines, reactive oxygen species and other apoptotic triggers (for example, the perforin and Fas–Fas ligand systems)[2]. In T2D, beta cell dysfunction and reduced beta cell mass are the ultimate events leading to the development of clinically overt disease in insulin-resistant individuals. Beta cell destruction is caused by multiple stimuli including glucotoxicity, lipotoxicity, proinflammatory cytokines, endoplasmic reticulum stress and oxidative stress[5]. Unfortunately, although it has been demonstrated that even a small amount of preserved endogenous insulin secretion has great benefits in terms of clinical outcome[6], none of the currently widely used antidiabetic agents target the maintenance of endogenous beta cell mass.

Beta cells are highly sensitive to apoptotic damages induced by multiple stressors such as inflammatory and oxidative assault, owing at least in part to their low expression of cytoprotective enzymes[7]. The initial trigger of beta cell death still remains unclear; it follows an orchestra of events, which makes the initiation of beta cell death complex and its blockade difficult to successfully achieve *in vivo*. Therefore, the identification of a common key regulator of beta cell apoptosis would offer a new therapeutic target for the treatment of diabetes.

The identification of the genes that regulate apoptosis has laid the foundation for the discovery of new drug targets. MST1 (also known as STK4 and KRS2) is a ubiquitously expressed serine-threonine kinase that is part of the Hippo signaling pathway and involved in multiple cellular processes such as morphogenesis, proliferation, stress response and apoptosis[8,9]. MST1 is a target and activator of caspases, serving to amplify the apoptotic signaling pathway[10,11]. Thr183 in subdomain VIII of MST1 has been defined as a primary site for the phosphoactivation and the autophosphorylation of MST1 and is essential for kinase activation. Both phosphorylation and caspase-mediated cleavage are required for full activation of MST1 during apoptosis. MST1 promotes cell death through regulation of multiple downstream targets such as LATS1 and LATS2, histone H2B and members of the FOXO family, as well as through induction of stress kinase c-Jun-N-terminal kinase (JNK) and activation of caspase-3 (refs. 9,12,13).

Genetic mutations and/or metabolic disturbances can alter protein networks and thereby disrupt downstream signaling pathways that are essential for beta cell survival and function. The transcription factor pancreatic duodenal homeobox-1 (PDX1, previously called IPF1, IDX1, STF1 or IUF1)[14,15] is a key mediator of beta cell development and function[16]. In humans, mutations in the *PDX1* gene can predispose individuals to develop maturity onset diabetes of the young, type 4 (MODY 4)[17], suggesting a critical role for PDX1 in

[1]Centre for Biomolecular Interactions Bremen, University of Bremen, Bremen, Germany. [2]Department of Incretin & Islet Biology, Novo Nordisk A/S, Denmark. [3]State Key Laboratory of Genetic Engineering and National Center for International Research of Development and Disease, Institute of Developmental Biology and Molecular Medicine, Fudan University, Shanghai, China. [4]Division of Transplantation, University of Illinois at Chicago, Chicago, Illinois, USA. [5]INSERM U859 Biotherapies for Diabetes, European Genomic Institute for Diabetes, Lille Regional Hospital Center, University of Lille, Lille, France. [6]These authors contributed equally to this work. Correspondence should be addressed to K.M. (kmaedler@uni-bremen.de) or A.A. (ardestani.amin@gmail.com).

Received 5 December 2013; accepted 21 January 2014; published online 16 March 2014; doi:10.1038/nm.3482

mature beta cells; reduced PDX1 expression affects insulin production and secretion and predisposes to beta cell apoptosis[16,18].

Because MST1 acts as common mediator in multiple apoptotic signaling pathways, we hypothesized that it is an initiating trigger of apoptotic signaling in beta cells. MST1 depletion completely restored normoglycemia and insulin secretion and prevented diabetes progression. These findings suggest that MST1 could be a fundamental target for diabetes therapy.

RESULTS

MST1 is activated in diabetes

To test whether MST1 activation is correlated with beta cell apoptosis, we exposed isolated human and mouse islets and the rat beta cell line INS-1E to a complex diabetogenic milieu. MST1 activity was highly upregulated in these cells under these conditions (created through incubation with the cytokines interleukin-1β (IL-1β) and interferon-γ (IFN-γ) (IL/IF), upon chronic exposure to increasing glucose concentrations (22.2 and 33.3 mM) or palmitic acid, or upon exposure to acute oxidative stress from hydrogen peroxide) (**Fig. 1a–c** and **Supplementary Fig. 1a**,**b**). The upregulation of MST1 occurred by both caspase-mediated cleavage and autophosphorylation (yielding MST1 phosphorylated on T183 (pMST1)). This was accompanied by higher phosphorylation of histone H2B as well as induction of JNK signaling (**Fig. 1a–c**). In contrast, short-term culture with high glucose concentrations (11.2, 22.2 and 33.3 mM) induced neither apoptosis nor MST1 cleavage and phosphorylation (**Supplementary Fig. 1d**). MST1 was also activated in islets from subjects with T2D (**Fig. 1d**), obese diabetic *Lepr^{db}* mice (*db/db* mice, **Fig. 1e**) and hyperglycemic mice fed with a high-fat, high-sucrose diet (HFD) for 16 weeks (**Supplementary Fig. 1c**). This activation correlated directly with beta cell apoptosis as described previously[19], as whenever MSTI was induced, apoptosis was also higher. To confirm the beta cell–specific upregulation of MST1, we performed double immunostaining for pMST1 and insulin in pancreatic islets from subjects with poorly controlled T2D (**Fig. 1d**) and pancreatic islets from *db/db* mice (**Fig. 1e**) and found pMST1 staining in beta cells, whereas there was almost no signal in cells from subjects without diabetes or control mice.

Caspase-3 and JNK act not only as downstream targets but also as upstream activators of MST1 through cleavage- and phosphorylation-dependent mechanisms[12,20], and they may initiate a vicious cycle and a proapoptotic signaling cascade in beta cells. Using inhibitors of JNK (SP600125) and caspase-3 (z-DEVD-fmk) and siRNA to caspase-3, we found that both JNK and caspase-3 were responsible for stress-induced MST1 cleavage by diabetic stimuli in human islets and INS-1E cells (**Supplementary Fig. 1e–h**), suggesting that MST1 induces a positive feedback loop with caspase-3 under diabetogenic conditions.

Because phosphatidylinositol-3 kinase (PI3K)-AKT signaling is a key regulator of beta cell survival and function[21,22] and MST1 signaling is negatively regulated by this pathway in other cell types[23,24], we hypothesized that AKT is an important negative regulator of MST1. Maintaining AKT activation through either exogenous addition of mitogens such as glucagon-like peptide-1 (GLP1) or insulin or overexpression of constitutively active AKT1 (Myr-AKT1, containing a myristoylation sequence and HA tag) inhibited glucose- and cytokine-induced phosphorylation of MST1, MST1 cleavage and apoptosis (**Fig. 1f** and **Supplementary Fig. 2a–d**). As GLP1 and insulin exert their cell survival actions primarily through the PI3K-AKT pathway[21,25], we tested whether inhibition of this pro-survival signaling might enhance MST1 activation. PI3K and AKT were inhibited by LY294002, and triciribine (an AKT inhibitor) led to lower levels of phosphorylation of Gsk3 and Foxo1, two well-characterized AKT substrates, and induced MST1 activation (**Fig. 1g**,**h** and **Supplementary Fig. 2e**). We further corroborated these findings using siRNA against AKT, which led to a critical upregulation of MST1 activity and potentiated cytokine-induced phosphorylation of MST1 and beta cell death (**Supplementary Fig. 2f**). MST1 overexpression also diminished insulin-induced AKT phosphorylation and, conversely, there was higher AKT phosphorylation in MST1-depleted beta cells (**Fig. 1i**). Knockdown of MST1 expression antagonized the apoptotic effect of AKT inactivation in INS-1E cells, implicating endogenous MST1 in the apoptotic mechanism induced by PI3K-AKT inhibition (**Supplementary Fig. 2g**,**h**). In summary, these results suggest that MST1 is activated in prodiabetic conditions *in vitro* and *in vivo*, antagonized by PI3K-AKT signaling and dependent on the JNK- and caspase-induced apoptotic machinery.

MST1 induces beta cell death

MST1 overexpression alone was also sufficient to induce apoptosis in human and rat beta cells (**Fig. 2a–c**). To investigate pathways that potentially contribute to MST1-induced beta cell apoptosis, we overexpressed MST1 in human islets and rat INS-1E cells through an adenoviral system, which efficiently upregulated MST1, activated JNK and induced beta cell apoptosis, as determined by an increased number of TUNEL-positive beta cells as well as caspase-3 activation and cleavage of poly-(ADP-ribose) polymerase (PARP), a downstream substrate of caspase-3 (**Fig. 2a–c**). Previous data proposed a role for the mitochondrial pathway in MST-dependent signaling[26,27]. Evaluation of established mitochondrial proteins in MST1-overexpressing islets and INS-1E cells showed cleavage of the initiator caspase-9, release of cytochrome *c*, induction of proapoptotic BAX and a decline in antiapoptotic BCL-2 and BCL-xL levels (**Fig. 2b**,**c** and **Supplementary Fig. 3a**), which led to a reduction of BCL-2/BAX and BCL-xL/BAX ratios. Notably, MST1-induced caspase-3 cleavage was reduced by treatment of human islets with the Bax inhibitor peptide V5 (**Fig. 2d**), which has been shown to promote beta cell survival[28]; together, these findings emphasize that MST1-induced apoptosis proceeds via the mitochondrial-dependent pathway. We also analyzed the expression of BH3-only proteins as regulators of the intrinsic cell death pathway[29]. Of these, BIM was robustly induced, whereas other BH3-only protein levels remained unchanged (**Fig. 2b**,**c** and **Supplementary Fig. 3b**). To assess whether kinase activity of MST1 is required for altering mitochondrial-dependent proteins and induction of apoptosis, we overexpressed a kinase-dead mutant of MST1 (K59R; dominant-negative MST1 (ref. 30)) in human islets. Unlike wild-type (WT) MST1, MST1-K59R did not change the levels of BIM, BAX, BCL-2, BCL-xL and caspase-3 cleavage (**Supplementary Fig. 3c**). We next determined whether BIM is a major molecule whose action would override the proapoptotic action of MST1. Indeed, BIM depletion led to a significant reduction of MST1-induced apoptosis in human islets (**Fig. 2e**,**f**).

Overexpression of MST1 further potentiated glucose-induced apoptosis in beta cells in a BIM-dependent manner (**Supplementary Fig. 3d**). BIM is regulated by the JNK[31] and AKT[32] signaling pathways. MST1-induced increase in BIM and subsequent caspase-3 cleavage was prevented by JNK inhibition through overexpression of dn-JNK1 (**Fig. 2g**) or by the JNK inhibitor (**Supplementary Fig. 3e**), which suggests that MST1 uses JNK signaling to mediate BIM upregulation and induction of apoptosis. We confirmed the involvement of AKT in the regulation of MST1-induced apoptosis by overexpressing

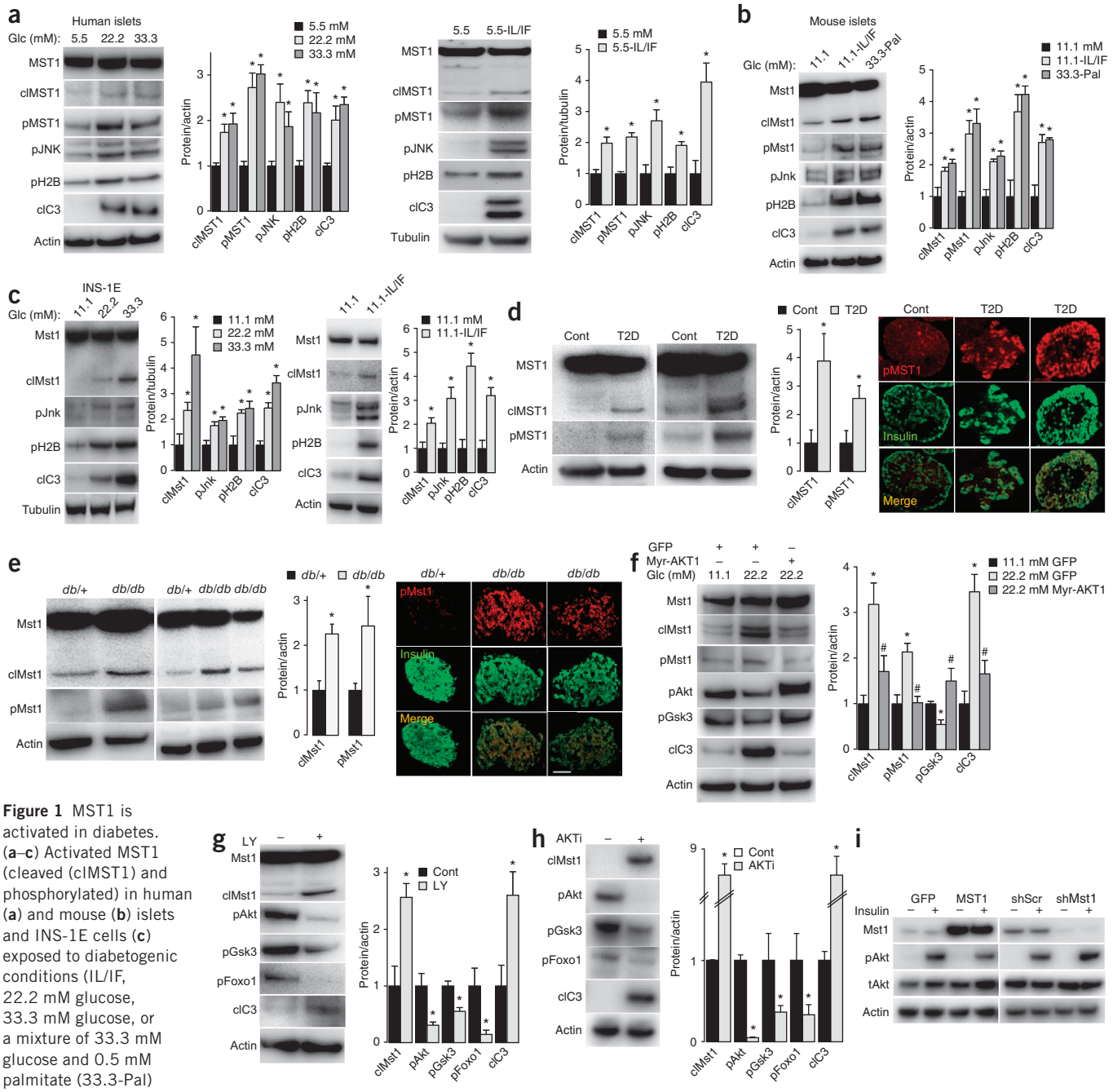

Figure 1 MST1 is activated in diabetes. (**a**–**c**) Activated MST1 (cleaved (clMST1) and phosphorylated) in human (**a**) and mouse (**b**) islets and INS-1E cells (**c**) exposed to diabetogenic conditions (IL/IF, 22.2 mM glucose, 33.3 mM glucose, or a mixture of 33.3 mM glucose and 0.5 mM palmitate (33.3-Pal) for 72 h). Western blots of MST1, pMST1, pJNK, pH2B and caspase-3 cleavage (cIC3) and densitometry analyses are shown. Cont, control; Glc, glucose. (**d**,**e**) Activated MST1 in islets. Human isolated islets from nondiabetic control subjects ($n = 7$) and subjects with T2D ($n = 4$, all with documented fasting plasma glucose >150 mg/dl) (**d**) and from 10-week-old diabetic *db/db* mice ($n = 5$) and their heterozygous littermates (*db/+*, $n = 5$) (**e**). Left, western blots of MST1 and pMST1 and densitometry analyses. Right, double immunostaining for pMST1 (red) and insulin (green) in sections from human isolated islets from nondiabetic control subjects and subjects with T2D and from 6-week-old diabetic *db/db* mice (representative analyses from 10 pancreases from subjects with T2D and >10 pancreases from control subjects and from 7 *db/db* mice and 7 heterozygous controls are shown). Scale bar, 100 μm. (**f**) Western blots of Mst1, clMst1, pMst1, pAkt, pGsk3 and caspase-3 cleavage and densitometry analysis for INS-1E cells transfected with GFP control or Myr-AKT1 expression plasmids exposed to 22.2 mM glucose for 72 h. (**g**) Western blots of Mst1, clMst1, pAkt, pGsk3, pFoxo1 and caspase-3 cleavage and densitometry analysis for INS-1E cells exposed to the PI3K inhibitor LY294002 (LY, 10 μM for 8 h). (**h**) Western blots of clMst1, pAkt, pGsk3, pFoxo1 and caspase-3 cleavage and densitometry analysis for INS-1E cells exposed to the AKT inhibitor triciribine (AKTi, 10 μM for 6 h). (**i**) Western blots of Mst1, pAkt and tAkt for INS-1E cells infected with an adenovirus expressing GFP (Ad-GFP) or MST1 (Ad-MST1) or transfected with shMst1 or shScr control expression plasmids for 48 h, serum-starved for 12 h and then stimulated with insulin. All graphs show densitometry analyses from at least 3 independent experiments normalized to actin or tubulin. All western blots show representative results from at least 3 independent experiments from 3 different donors or mice. Tubulin or actin was used as loading control. Data are expressed as means ± s.e.m. $^{*}P < 0.05$ compared to untreated or nondiabetic control. $^{\#}P < 0.05$ Myr-AKT1 compared to GFP at 22.2 mM glucose.

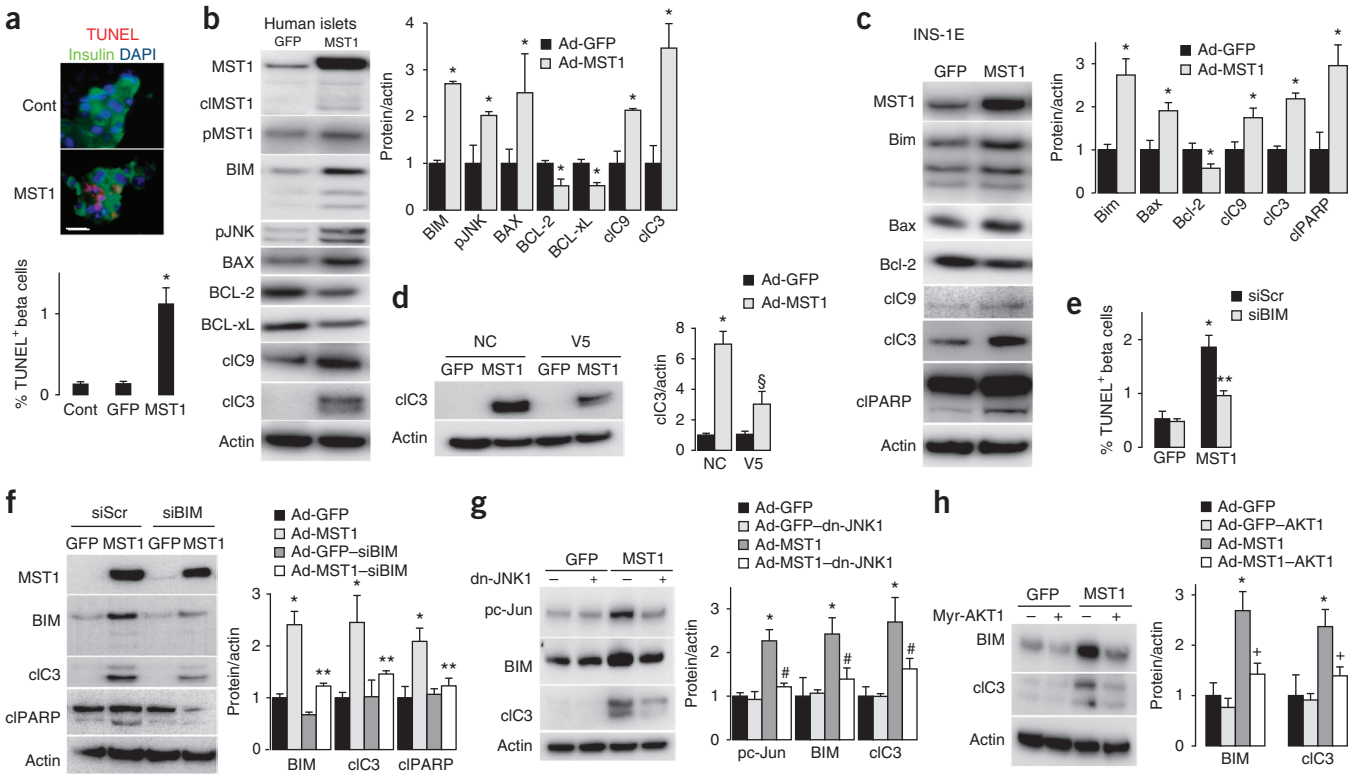

Figure 2 MST1 induces beta cell death. (**a**–**d**) MST1 overexpression in human islets (**a**,**b**) and INS-1E cells (**c**) for 48 h. Triple staining for DAPI (blue), TUNEL (red) and insulin (green) (**a**) TUNEL analysis from an average number of 18,501 insulin-positive beta cells. Scale bar, 100 µm. (**b**,**c**) Adenovirus-mediated upregulation of MST1. Western blots and densitometry analysis of MST1, cleaved MST1, BIM, pJNK, BAX, BCL-2, BCL-xL, cleaved caspase-9 (clC9), cleaved caspase-3 and PARP in human islets (**b**) and INS-1E cells (**c**). (**d**) Western blot and densitometry analysis of caspase-3 cleavage from Ad-GFP– or Ad-MST1–infected human islets exposed to BAX inhibitory peptide V5 or negative control (NC) peptide for 36 h. (**e**,**f**) Human islets transfected with BIM siRNA (siBIM) or control Scr siRNA (siScr) infected with Ad-GFP or Ad-MST1 for 48 h. (**e**) Analysis of cells positive for both TUNEL and insulin out of 10,378 insulin-positive counted beta cells. (**f**) Western blot and densitometry analysis of MST1, BIM and caspase-3 and PARP cleavage. (**g**) Western blot and densitometry analysis of pc-Jun, BIM and caspase-3 cleavage from human islets transfected with GFP or dn-JNK1 expression plasmids and infected with Ad-GFP or Ad-MST1 for 48 h. (**h**) Western blot and densitometry analysis of BIM and caspase-3 cleavage from human islets transfected with GFP or Myr-AKT1 expression plasmids and infected with Ad-GFP or Ad-MST1 for 48 h. All graphs show densitometry analysis from at least 3 independent experiments normalized to actin. All western blots show representative results from at least 3 independent experiments from 3 different donors (human islets). Actin was used as loading control. TUNEL analyses are from 3 independent experiments from 3 different donors. Data are expressed as means ± s.e.m. $^{*}P < 0.05$ MST1 overexpression compared to GFP control, §$P < 0.05$ V5-MST1 compared to MST1, $^{**}P < 0.05$ siBIM-MST1 compared to siScr-MST1, $^{\#}P < 0.05$ dn-JNK–MST1 compared to MST1, $^{+}P < 0.05$ AKT1-MST1 compared to MST1.

both MST1 and Myr-AKT1, which reduced BIM induction and caspase-3 cleavage (**Fig. 2h**), indicating that AKT negatively regulates the downstream target of MST1. These data suggest that MST1 is a critical mediator of beta cell apoptosis through activation of the BIM-dependent intrinsic apoptotic pathway and controlled by AKT and JNK signaling pathways.

MST1 impairs beta cell function by destabilizing PDX1

We hypothesized that MST1 activation may elicit changes in beta cell–specific gene transcription that initiate the process of beta cell failure. Overexpression of MST1 led to a complete loss of glucose-stimulated insulin secretion (GSIS; **Fig. 3a** and **Supplementary Fig. 4a**), which could not be accounted for solely by the induction of apoptosis. Previously, we noted that the critical beta cell transcription factor PDX1, which mediates glucose-induced insulin gene transcription in mature beta cells[16,18], is mislocalized and reduced in diabetes[19]. These changes are subsequently associated with impaired beta cell function and hyperglycemia. Stress-induced kinases such as JNK and glycogen synthase kinase-3 (GSK3) phosphorylate PDX1, antagonizing its activity[33,34], which leads to beta cell failure. Thus, we hypothesized that the drastic reduction in insulin secretion following MST1 overexpression may be mediated by PDX1. PDX1 levels were markedly reduced in response to MST1 overexpression in human islets (**Fig. 3b**) and INS-1E cells (**Supplementary Fig. 4b**). In contrast, MST1 overexpression did not affect the amount of mRNA encoding PDX1 (**Fig. 3b** and **Supplementary Fig. 4b**), suggesting that MST1 may regulate PDX1 at the post-transcriptional level. Analysis of PDX1 target genes demonstrated that overexpression of MST1 significantly downregulated *INS* (*Ins1* or *Ins2* for INS-1E), *SLC2A2* and *GCK* in human islets (**Fig. 3b**) and INS-1E cells (**Supplementary Fig. 4b**). Although SLC2A2 is not the predominant glucose transporter in human beta cells[35], we analyzed its expression to provide comparison to the mouse data.

To gain better insight into the role of MST1 in regulation of insulin secretion, we performed GSIS using two insulin secretagogues: GLP1 and glibenclamide. MST1 overexpression significantly abolished GLP1-enhanced glucose-induced insulin secretion ($P < 0.05$ compared to control condition), whereas glibenclamide-induced insulin secretion was not affected, suggesting that defective insulin secretion may occur at a step upstream of calcium influx (**Supplementary Fig. 4c**).

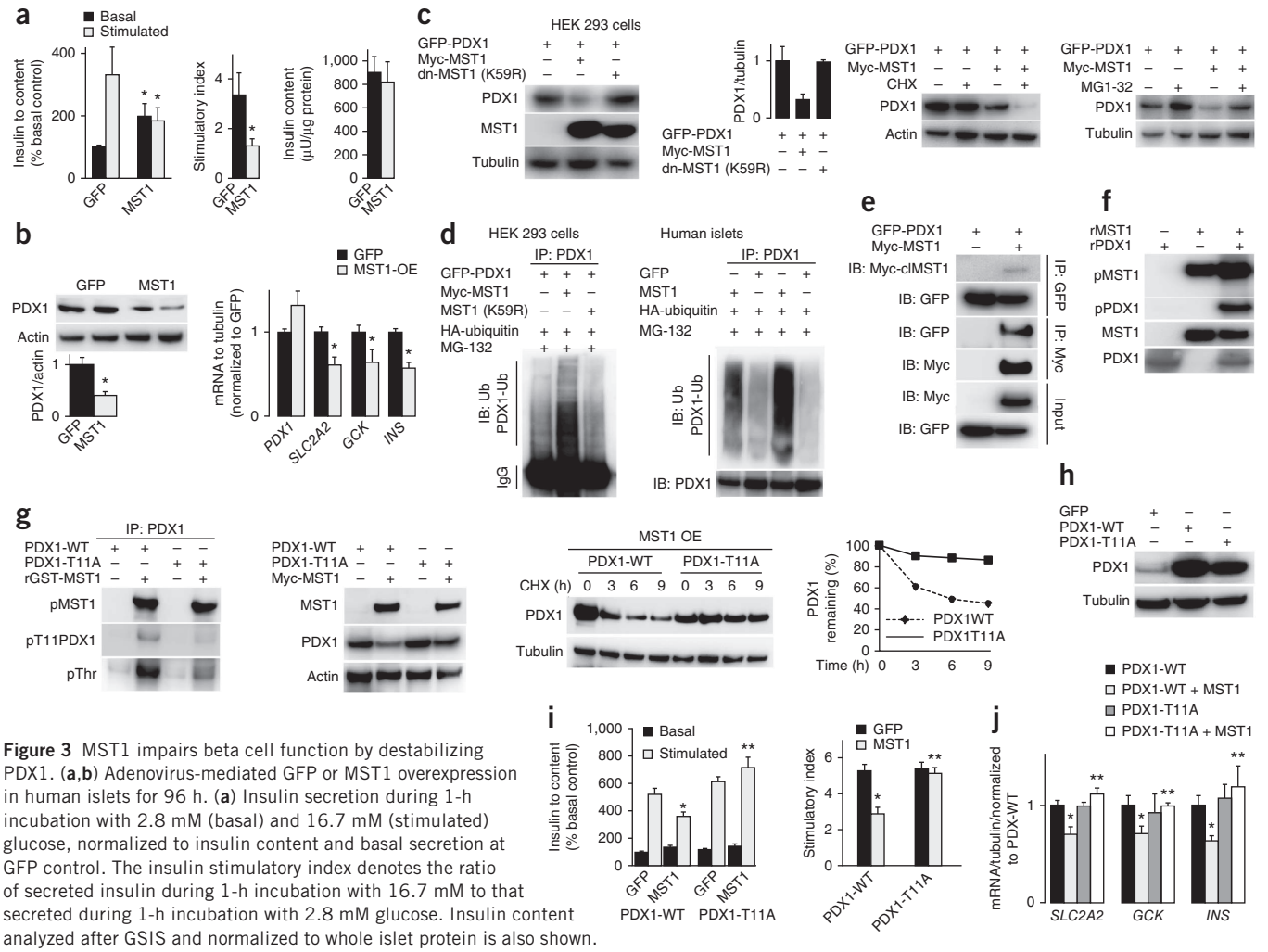

Figure 3 MST1 impairs beta cell function by destabilizing PDX1. (**a**,**b**) Adenovirus-mediated GFP or MST1 overexpression in human islets for 96 h. (**a**) Insulin secretion during 1-h incubation with 2.8 mM (basal) and 16.7 mM (stimulated) glucose, normalized to insulin content and basal secretion at GFP control. The insulin stimulatory index denotes the ratio of secreted insulin during 1-h incubation with 16.7 mM to that secreted during 1-h incubation with 2.8 mM glucose. Insulin content analyzed after GSIS and normalized to whole islet protein is also shown. (**b**) Left, western blot and densitometry analysis of PDX1. Right, RT-PCR analysis of PDX1 target genes *SLC2A2, GCK* and *INS*. (**c**) Western blot and densitometry analysis of PDX1 and MST1 from HEK 293 cells transfected with plasmids encoding Myc-MST1 and GFP-PDX1 with kinase-dead MST1 (dn-MST1, K59R) cotransfected with GFP-PDX1 (left) and western blot of PDX-1 from HEK 293 cells treated with CHX for 8 h at 48 h after transfection, (middle) or treated with the proteasome inhibitor MG-132 for 6 h at 36 h after transfection (right). (**d**) Immunoblotting with ubiquitin-specific antibody after immunoprecipitation with an anti-PDX1 antibody of HEK 293 cells transfected with GFP-PDX1 and hemagglutinin (HA)-ubiquitin (Ub), alone or together with Myc-MST1 or MST1-K59R expression plasmids for 48 h (left) and human islets transfected with HA-ubiquitin and infected with Ad-GFP or Ad-MST1 for 48 h (right; 2 different donors). MG-132 was added during the last 6 h of the experiment. (**e**) Western blot analysis for Myc and GFP with precipitates and input fraction after reciprocal co-immunoprecipitations (using anti-GFP and anti-Myc antibodies) from HEK 293 cells transfected with GFP-PDX1 alone or together with Myc-MST1 for 48 h. (**f**) Western blot of pThr (pan–phosphorylated threonine), MST1 and PDX1 from *in vitro* kinase assay performed with recombinant MST1 (rMST1) and recombinant PDX1 (rPDX1) proteins. (**g**) Left, western blot of pPDX1 (pT11PDX1) and pThr (after immunoprecipitation with anti-PDX1) from HEK 293 cells transfected with PDX1-WT or PDX1-T11A expression plasmids and subjected to an *in vitro* kinase assay using recombinant MST1. Middle, western blot of MST1 and PDX1 from HEK 293 cells transfected with PDX1-WT or PDX1-T11A expression plasmids alone or together with MST1 expression plasmids for 48 h. Right, western blot of PDX1 and densitometry analysis of bands for PDX1-WT or PDX1-T11A cotransfected with MST1 in HEK 293 cells for 36 h and treated with CHX. (**h**) Western blot of PDX1 from human islets transfected with GFP, PDX1-WT or PDX1-T11A expression plasmids. (**i**) Insulin secretion during 1-h incubation with 2.8 mM (basal) and 16.7 mM (stimulated) glucose, normalized to insulin content and basal secretion at control and insulin stimulatory index, which denotes the ratio of secreted insulin during 1-h incubation with 16.7 mM to that secreted at 2.8 mM glucose. (**j**) PDX1 target genes in human islets analyzed by RT-PCR and levels normalized to tubulin and shown as change from PDX1-WT transfected islets from human islets infected with Ad-GFP or Ad-MST1 for 72 h. All western blots show representative results from at least 3 independent experiments from 3 different donors (human islets). Tubulin or actin was used as loading control. RT-PCR (**b**,**j**) and GSIS (**a**,**i**) show pooled results from 3 independent experiments from 3 different donors. Data are expressed as means ± s.e.m. $^{*}P < 0.05$ MST overexpression compared to control, $^{**}P < 0.05$ PDX1-T11A + MST1 compared to PDX1-WT + MST1.

MST1 overexpression had no effect on insulin content (**Fig. 3a** and **Supplementary Fig. 4a**), and thus insulin secretion was normalized on insulin content.

To clarify the mechanism by which MST1 regulates PDX1, we examined the effects of ectopic expression of MST1 and PDX1 in human embryonic kidney (HEK) 293 cells. We found lower PDX1 levels in cells co-overexpressing WT MST1, whereas the kinase-dead MST1-K59R had no effect (**Fig. 3c**). Thus, kinase activity is required for MST1-induced PDX1 degradation. Overexpression of *MST1* also attenuated the transcriptional activity of PDX1 on the rat insulin promoter (RIP), as shown by luciferase assays in PDX1-overexpressing HEK 293 and INS-1E cells (**Supplementary Fig. 4d**).

To discriminate between a transcriptional or translational and a post-translational effect of MST1 on PDX1, we followed the stability of overexpressed PDX1 upon treatment with cycloheximide (CHX), an inhibitor of protein translation. Upon CHX exposure, PDX1 protein levels rapidly decreased when coexpressed with MST1 (**Fig. 3c**), which suggests that MST1 reduced PDX1 protein stability. Consistent with these observations, MST1 overexpression also decreased protein stability of endogenous PDX1 in human islets (**Supplementary Fig. 4e**). In contrast, treatment of PDX1-overexpressing HEK 293 cells with the proteasome inhibitor MG-132 reduced the disappearance of PDX1 (**Fig. 3c**), indicating that MST1 induced activation of the ubiquitin proteasome pathway. Proteasomal degradation of PDX1 has been described before and leads to impaired beta cell function and survival[36].

We next performed *in vivo* ubiquitination assays to determine whether MST1 induces PDX1 ubiquitination. PDX1 cotransfected with MST1, but not with MST1-K59R, was heavily ubiquitinated in HEK 293 cells. We confirmed this in human islets by showing that MST1 overexpression strongly promoted endogenous PDX1 ubiquitination (**Fig. 3d**). Subsequently, we verified a direct interaction between PDX1 and MST1 proteins. Reciprocal co-immunoprecipitations showed the interaction between MST1 and PDX1 in HEK 293 cells cotransfected with GFP-tagged PDX1 and Myc-tagged MST1 (**Fig. 3e**).

We next examined whether a prodiabetic milieu regulates the association between MST1 and PDX1. Notably, both cytokine toxicity and glucotoxicity augment the interaction between MST1 and PDX1 in INS-1E cells (**Supplementary Fig. 4e**). As we observed that PDX1 ubiquitination and degradation required MST1 kinase activity, we tested whether MST1 directly phosphorylates PDX1. *In vitro* kinase assays showed that MST1 efficiently phosphorylated PDX1; these included autoradiography using radiolabeled ^{32}P (**Supplementary Fig. 4f**), as well as nonradioactive kinase assays and western blotting using an antibody specific to pan–phosphorylated threonine (**Fig. 3f**). We confirmed the *in vitro* kinase assays in HEK 293 cells; coexpression of MST1 and PDX1 led to PDX1 phosphorylation (**Supplementary Fig. 4f**). Together, these results establish PDX1 as a substrate for MST1.

We determined the potential MST1-targeted phosphorylation sites on PDX1 theoretically with the NetPhos 2.0 program[37]. This identified six candidate sites within the PDX1 sequence; T11, T126, T152, T155, T214 and T231 (based on the probability that a phosphosite is a substrate of MST1, given as relative score) (**Supplementary Fig. 4g**). These six sites were individually mutated to alanine to generate phosphodeficient constructs as described previously[38]. We subcloned them into pGEX bacterial expression vectors. PDX1-GST fusion proteins with the six different PDX1 mutations were purified from bacteria and used as substrates for MST1 in the kinase assay. With the exception of PDX1-T11A, WT recombinant PDX1 and the other mutants proteins were efficiently phosphorylated at threonine (**Supplementary Fig. 4h**). To confirm this, we transfected all PDX1 mutant plasmids into HEK 293 cells, immunoprecipitated them with a PDX1-specific antibody and incubated them with recombinant MST1 in a kinase assay. MST1 highly phosphorylated PDX1-WT and other mutant proteins, but phosphorylation in the PDX1-T11A mutant was markedly lower (data not shown), indicating that T11 is the major site of phosphorylation by MST1.

In order to confirm T11 as the specific phosphorylation site, we used a phosphospecific antibody against the T11 phosphorylation site in PDX1, which recognized T11 phosphorylation after co-incubation of recombinant PDX1-GST fusion protein with recombinant GST-MST1 (**Supplementary Fig. 4h**). Consistent with this, co-incubation of immunoprecipitated PDX1-WT or PDX1-T11A with recombinant MST1 resulted in robust MST1-induced PDX1-WT phosphorylation at the T11 site (shown by antibody to pT11) and in overall threonine phosphorylation (shown by antibody to pan–phosphorylated threonine); PDX1-T11 phosphorylation was markedly reduced in the PDX1-T11A mutant protein (**Fig. 3g**). We further corroborated this by an *in vivo* kinase assay (**Supplementary Fig. 4h**). Alignment of the amino acid sequences of PDX1 from different species revealed that the T11 site is highly conserved among those species (**Supplementary Fig. 4i**).

If T11 is the specific MST1-induced phosphorylation site of PDX1 and is responsible for beta cell dysfunction, one would expect that mutated PDX1-T11A would reverse beta cell dysfunction. MST1 induced a rapid degradation of exogenous WT PDX1 in the presence of CHX that did not occur in PDX1-T11A mutant–transfected cells (**Fig. 3g**). Furthermore, the half-life of the PDX1-T11A mutant was similar to that of PDX1-WT in the absence of MST1 (data not shown). Consistent with these data, there was less PDX1 ubiquitination in the PDX1-T11A–transfected cells than in those transfected with PDX1-WT (**Supplementary Fig. 4j**).

Because T11 is located within the transactivational domain of PDX1 and to evaluate the functional significance of the T11-dependent ubiquitination and degradation, we assessed transcriptional activity of PDX1. Reduction of PDX1 transcriptional activity occurred only in PDX1-WT– but not in PDX1-T11A–transfected cells (**Supplementary Fig. 4j**). As the T11A mutation of PDX1 prolongs PDX1 stability in the presence of MST1, we asked whether PDX1 stability is directly linked to improved beta cell function. PDX1-T11A mutant overexpression (**Fig. 3h**) normalized MST1-induced impairment in GSIS in human islets (**Fig. 3i**) and INS-1E cells (**Supplementary Fig. 4j**) and restored MST1-induced downregulation of PDX1 target genes (**Fig. 3j** and **Supplementary Fig. 4j**). These findings indicate that MST1-induced PDX1 phosphorylation at T11 leads directly to PDX1 destabilization and impaired beta cell function and suggest that PDX1 is a crucial target of MST1 in the regulation of beta cell function.

MST1 deficiency improves beta cell survival and function

Further analyses aimed to prove whether MST1 not only mediated beta cell death and impaired function *in vitro* but also, when downregulated, allowed for rescue from beta cell failure (**Fig. 4** and **Supplementary Fig. 5**). First, about 80% depletion of MST1 in human islets, achieved with siRNA, protected from cytokine and hydrogen peroxide toxicity as well as glucolipotoxicity; beta cell apoptosis was also inhibited (**Fig. 4a**,**b** and **Supplementary Fig. 5a**). Silencing of *MST1* also significantly reduced BIM upregulation induced by diabetogenic conditions in human islets (**Fig. 4b**,**c** and **Supplementary Fig. 5a**).

Second, beta cell function was greatly improved by *MST1* gene silencing under diabetogenic conditions (**Fig. 4d** and **Supplementary Fig. 5**). Notably, IL/IF- and high glucose + palmitate (HG/Pal)-induced cleavage of caspase-3 and caspase-9 and phosphorylation of H2B was lower in MST1-depleted human islets than in control islets (**Fig. 4b**). *Mst1*$^{-/-}$ islets were largely resistant to IL/IF- and HG/Pal-mediated apoptosis, as determined by TUNEL staining (**Fig. 4e**). In addition to the protective effect of *Mst1* knockout on beta cell survival, *Mst1*$^{-/-}$ islets also showed improved GSIS after long-term culture with IL/IF and HG/Pal (**Fig. 4f** and **Supplementary Fig. 5**). To further support the role of MST1 as a main mediator of apoptosis in beta cells, we generated INS-1E cells stably transfected with vectors carrying *Mst1*-targeting shRNA (sh*Mst1*) or scrambled control shRNA (shScr) and found that Mst1 expression in cells stably expressing sh*Mst1* was about 70% lower than that in cells

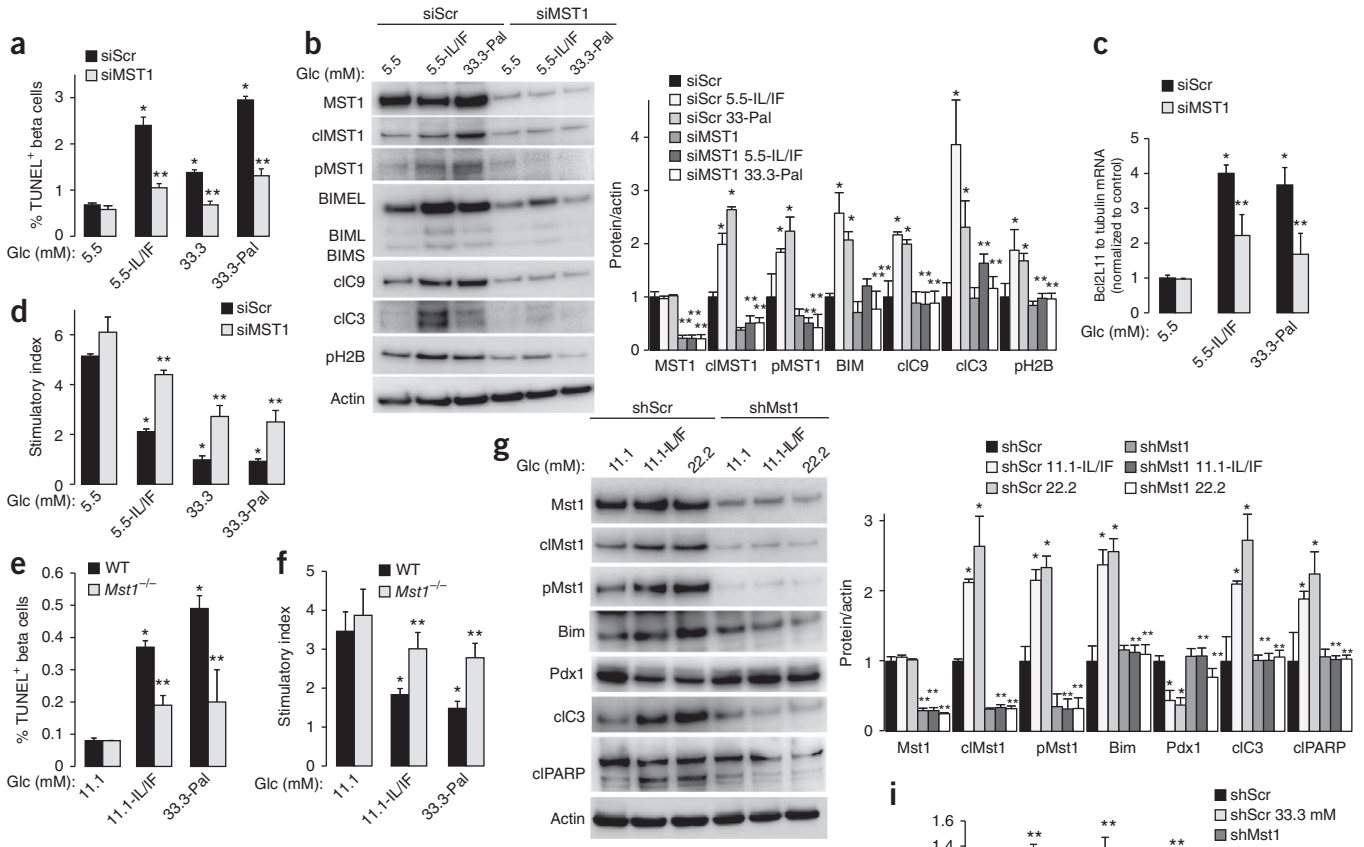

Figure 4 MST1 deficiency improves beta cell survival and function. (**a**–**d**) Analysis of human islets transfected with MST1 siRNA (siMST1) or control siScr and treated with the cytokine mixture IL/IF, 33.3 mM glucose or the mixture of 33.3 mM glucose and 0.5 mM palmitate for 72 h. (**a**) TUNEL-positive beta cells from an average number of 11,390 insulin-positive beta cells for each treatment condition. (**b**) Western blots and densitometry analysis of MST1, pMST1, BIM, pH2B and caspase-9 and caspase-3 cleavage. (**c**) RT-PCR for *BCL2L11* in human islets normalized to tubulin shown as change from siScr control transfected islets. (**d**) Insulin stimulatory index denotes the ratio of secreted insulin during 1-h incubation with 16.7 mM to that secreted during 1-h incubation with 2.8 mM glucose (after the indicated treatments). (**e**) Analysis of TUNEL-positive beta cells from an average number of 24,180 insulin-positive beta cells counted for each treatment condition. (**f**) Insulin stimulatory index denotes the ratio of secreted insulin during 1-h incubation with 16.7 mM to that secreted during 1-h incubation with 2.8 mM glucose from isolated islets from *Mst1*$^{-/-}$ mice and their WT littermates after exposure to the cytokine mixture IL/IF or the mixture of 33.3 mM glucose and 0.5 mM palmitate for 72 h. (**g**–**i**) Western blots and densitometry analysis of Mst1, cIMst1, pMST1, Bim, Pdx1, caspase-3 and PARP cleavage (**g**), insulin stimulatory index (**h**) and RT-PCR analysis of PDX1 target genes *Slc2a2, Gck, Ins1* and *Ins2* normalized to tubulin and shown as change from shScr (**i**) in stable INS-1E clones generated by transfection of vectors for shMst1 and shScr control and treated with the cytokine mixture IL/IF or with 22.2 or 33.3 mM glucose for 72 h. Representative results from 3 independent experiments from 3 different donors (human islets) (**b**,**g**). Actin was used as loading control. TUNEL data (**a**,**e**), GSIS (**d**,**f**,**h**) or RT-PCR (**c**,**i**) show pooled results from 3 independent experiments from 3 different donors (human islets). Data are expressed as means ± s.e.m. $*P < 0.05$ compared to siScr (**a**–**d**), WT (**e**,**f**) or shScr untreated controls (**g**,**h**,**i**); $**P < 0.05$ compared to siScr (**a**–**d**), WT (**e**,**f**) or shScr (**g**–**i**) at the same treatment conditions.

expressing shScr (**Fig. 4g**). We treated INS-1E clones with IL/IF and HG for 72 h. Bim induction, caspase-3 and PARP cleavage in Mst1-depleted cells were significantly lower than that in control cells (**Fig. 4g**). Additionally, *Mst1* silencing also abrogated caspase-3 and PARP cleavage induced by palmitate (**Supplementary Fig. 5b**) and hydrogen peroxide (**Supplementary Fig. 5c**). Cytochrome *c* release was markedly reduced in Mst1-depleted beta cells under diabetogenic conditions (**Supplementary Fig. 5d**,**e**). A second shRNA clone targeting the *Mst1* gene with comparable gene silencing efficiency confirmed the antiapoptotic effect of *Mst1* silencing in INS-1E cells; Mst1 depletion markedly suppressed IL/IF- and HG-induced Bim upregulation and cleavage of caspase-3 and PARP (**Supplementary Fig. 5f**). Confirmation the results of the sh*Mst1* approach, inhibition of endogenous Mst1 activity by overexpression of Mst1-K59R completely inhibited glucose-induced caspase-3 and PARP cleavage in beta cells (**Supplementary Fig. 5g**).

Mst1 deficiency significantly attenuated Pdx1 depletion caused by cytokine or high glucose treatment (**Fig. 4g** and **Supplementary Fig. 5f**), implying that MST1 is indispensable for the reduction in amount of PDX1 induced by a diabetic milieu. Our next objective was to determine whether knockdown of Mst1 expression leads to improvement of GSIS and restoration of Pdx1 target genes in INS-1E cells under diabetogenic conditions. GSIS was significantly improved in Mst1-depleted beta cells (**Fig. 4h** and **Supplementary Fig. 5j**),

whereas levels of Pdx1 target genes, for example, *Slc2a2*, *Gck*, *Ins1* and *Ins2*, were restored in Mst1-depleted INS-1E cells (**Fig. 4i**). These data prove MST1 as determinant for beta cell apoptosis and defective insulin secretion under a diabetic milieu in beta cells *in vitro*.

Mst1 deletion protects from streptozotocin-induced diabetes

As MST1 depletion protected from beta cell apoptosis and restored beta cell function *in vitro*, we hypothesized that Mst1 deficiency may protect against diabetes *in vivo* by promoting beta cell survival and preserving beta cell mass. To test this hypothesis, we used *Mst1*$^{-/-}$ mice. Neither body weight nor food intake differed between *Mst1*$^{-/-}$ mice and their WT (*Mst1*$^{+/+}$) littermates (data not shown). Also, glucose tolerance, insulin tolerance and glucose-induced insulin response did not differ between WT and *Mst1*$^{-/-}$ mice at 2 months of age (**Supplementary Fig. 6a**). However, intraperitoneal (i.p.) glucose tolerance tests (GTTs) and i.p. insulin tolerance tests (ITTs) revealed slight improvement in *Mst1*$^{-/-}$ mice at 6 months of age at 60 min after glucose or insulin injection (**Supplementary Fig. 6b**).

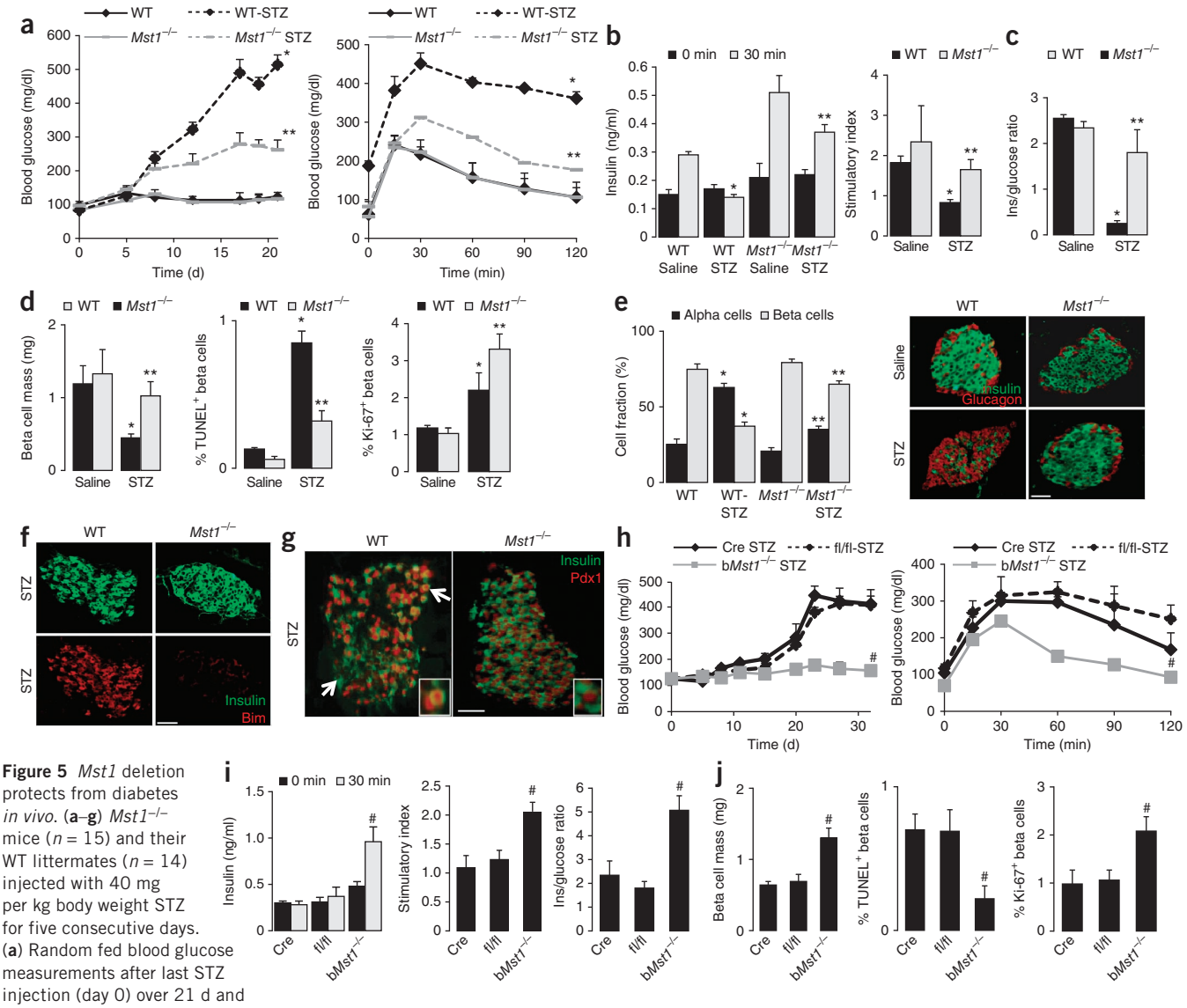

Figure 5 *Mst1* deletion protects from diabetes *in vivo*. (**a**–**g**) *Mst1*$^{-/-}$ mice ($n = 15$) and their WT littermates ($n = 14$) injected with 40 mg per kg body weight STZ for five consecutive days. (**a**) Random fed blood glucose measurements after last STZ injection (day 0) over 21 d and i.p. GTT (ipGTT) performed at day 17. (**b**) Insulin secretion during an i.p. GTT measured before (0 min) and 30 min after glucose injection (left) expressed as ratio of secreted insulin at 30 min to that secreted at 0 min (stimulatory index, right). (**c**) Ratio of secreted insulin and glucose calculated at fed state. (**d**) Beta cell mass and quantitative analyses from triple stainings for TUNEL or Ki-67, insulin and DAPI expressed as percentage of TUNEL- or Ki-67–positive beta cells ± s.e.m. from a mean scored number of 23,121 beta cells for each treatment condition. (**e**) Percentage of alpha cells (stained in red) and beta cells (stained in green) of the whole pancreatic sections from 10 sections spanning the width of the pancreas. Scale bar, 100 µm. (**f**,**g**) Representative double staining for Bim (red, **f**) or Pdx1 (red, **g**) and insulin (green) from MLD-STZ–treated *Mst1*$^{-/-}$ mice and controls killed at day 22. White arrows indicate areas of cytosolic Pdx1 localization and its total absence in WT-STZ–treated mice. Scale bars, 100 µm. (**h**–**j**) b*Mst1*$^{-/-}$ mice with specific deletion in the beta cells using the Cre-*loxP* system ($n = 5$) and RIP-Cre ($n = 3$) and *Mst1*$^{fl/fl}$ controls ($n = 3$) injected with 40 mg per kg body weight STZ for five consecutive days. (**h**) Random fed blood glucose measurements after last STZ injection (day 0) over 32 d and i.p. GTT at day 30. (**i**) Insulin secretion during an i.p. GTT measured before (0 min) and 30 min after glucose injection. Data are expressed as ratio of secreted insulin at 30 min to that secreted at 0 min (stimulatory index). The ratio of secreted insulin and glucose calculated at fed state (right). (**j**) Beta cell mass, TUNEL or Ki-67 analysis, expressed as percentage of TUNEL- or Ki-67–positive beta cells from mice at day 32. Data show means ± s.e.m. $^{*}P < 0.05$ MLD-STZ–treated WT mice compared to saline-injected WT mice, $^{**}P < 0.05$ MLD-STZ–treated *MST1*$^{-/-}$ mice compared to MLD-STZ–treated WT mice. $^{\#}P < 0.05$ MLD-STZ–treated b*Mst*$^{-/-}$ mice compared to MLD-STZ–treated *Mst1*$^{fl/fl}$ or RIP-Cre mice.

We induced diabetes by multiple low-dose (MLD) streptozotocin (STZ) injections in *Mst1*$^{-/-}$ mice and WT controls. Whereas MLD-STZ injection induced progressive hyperglycemia and severely impaired glucose tolerance in WT mice, blood glucose levels were significantly reduced and glucose tolerance was highly improved in *Mst1*$^{-/-}$ mice (**Fig. 5a**). The MLD-STZ treatment led to impaired insulin secretion and a decreased insulin-to-glucose ratio in WT mice, which were significantly restored in *Mst1*$^{-/-}$ mice (**Fig. 5b**,**c**). Islet architecture in MLD-STZ–treated WT mice was disrupted and accompanied by less insulin-positive area, a smaller beta cell fraction, lower islet density, smaller islet size and lower beta cell mass compared to that of non–MLD-STZ–treated mice. In contrast, islet architecture of MLD-STZ–treated *Mst1*$^{-/-}$ mice had a close to normal appearance, and beta cell fraction, islet density and beta cell mass were similar to those in non–MLD-STZ–treated mice (**Fig. 5d**,**e** and **Supplementary Fig. 6c**). Islet size also tended to be higher in MLD-STZ–injected *Mst1*$^{-/-}$ mice than in WT mice, although this effect was not statistically significant (**Supplementary Fig. 6c**).

To elucidate how MST1 deletion may affect beta cell mass, we studied beta cell apoptosis and proliferation. TUNEL staining demonstrated that the rate of apoptosis was dramatically higher in MLD-STZ–treated WT mice than in treated *Mst1*$^{-/-}$ mice; the *Mst1* deletion markedly lowered the rate of apoptosis. Beta cell proliferation was higher in MLD-STZ–treated WT mice compared to untreated WT mice, but treated *Mst1*$^{-/-}$ beta cells showed even higher proliferation, indicative of an improved compensatory capacity (**Fig. 5d** and **Supplementary Fig. 6d**,**e**). No difference in the frequency of proliferating beta cells was observed between islets from *Mst1*$^{-/-}$ mice and those from their WT littermates at basal levels. These results suggest that *Mst1* deletion boosts beta cell mass and islet density predominantly as a result of lower rates of beta cell apoptosis and higher beta cell proliferation in response to diabetogenic stimulation.

To further assess the effect of MLD-STZ, we performed immunohistochemical analyses of insulin and glucagon on pancreatic sections. Islet cells from MLD-STZ–treated WT mice were architecturally distorted, containing significantly fewer insulin-positive cells and proportionally more glucagon-positive cells, which resulted in a higher alpha cell–to–beta cell ratio compared to untreated WT mice (**Fig. 5e**). This is consistent with the previously reported alpha cell hyperplasia in diabetes[39,40]. In contrast, the number of glucagon-positive alpha cells in MLD-STZ–injected *Mst1*$^{-/-}$ islets was not higher and confined to the rim of the islets, suggesting that the architecture of MLD-STZ–injected *Mst1*$^{-/-}$ islets was close to normal (**Fig. 5e**). In line with our *in vitro* results in beta cells, where MST1 acts through changes in BIM, expression of the latter was clearly seen in beta cells in diabetic MLD-STZ–treated WT mice, but not in treated *Mst1*$^{-/-}$ mice (**Fig. 5f**).

We next examined Pdx1 as a beta cell–specific MST1 substrate whose expression is regulated by both its abundance and its subcellular localization in diabetic conditions[19]. Whereas MLD-STZ–treated WT mice showed a reduced nuclear localization of Pdx1 in beta cells, Pdx1 expression was normalized and the prominent nuclear localization important for its functionality reestablished in MLD-STZ–treated *Mst1*$^{-/-}$ mice (**Fig. 5g**). The expression of the Pdx1 target Glut2 in beta cells was largely preserved in the MLD-STZ–treated *Mst1*$^{-/-}$ mice, whereas it was barely detectable in the beta cells of MLD-STZ–treated WT mice (**Supplementary Fig. 6f**). These findings suggest that *Mst1* deletion preserves Pdx1 and Glut2 expression in beta cells and thus preserves the function of beta cells in the MLD-STZ model of diabetes.

To directly assess the protective effect of *Mst1* deletion in MLD-STZ–induced beta cell apoptosis, we treated isolated mouse islets and INS-1E cells with STZ *in vitro* and found that STZ strongly induced phosphorylation of Mst1, Bim expression and ultimately apoptosis, and such apoptotic induction by STZ was attenuated by Mst1 depletion (**Supplementary Fig. 6g**,**h**), consistent with the *in vivo* observations in *Mst1*$^{-/-}$ mice.

To exclude a secondary effect of the *Mst1* deletion on beta cells, we generated mice with beta cell–specific knockout of *Mst1* by the Cre-*loxP* system (hereafter referred to as b*Mst1*$^{-/-}$ mice). These mice contained a null mutation for *Mst1* only in beta cells, as confirmed by western blotting of lysates from isolated islets (**Supplementary Fig. 7a**). b*Mst1*$^{-/-}$ mice were viable, fertile and showed no difference in food intake and body weight (data not shown), glucose tolerance or insulin sensitivity compared to *Mst1*$^{fl/fl}$ mice, which do not express Cre (**Supplementary Fig. 7b**,**c**), or *loxP*-negative mice (RIP-Cre mice; data not shown). To assess whether b*Mst1*$^{-/-}$ mice might also be protected against diabetes, we again used the model of MLD-STZ–induced diabetes. After MLD-STZ treatment, blood glucose levels in *Mst1*$^{fl/fl}$ and RIP-Cre control mice increased gradually (**Fig. 5h**). Whereas both control groups became overtly diabetic, reaching blood glucose levels >400 mg/dl, b*Mst1*$^{-/-}$ mice maintained normal blood glucose levels. *Mst1*$^{fl/fl}$ and RIP-Cre control mice exhibited impaired glucose tolerance; this was notably prevented in b*Mst1*$^{-/-}$ mice (**Fig. 5h**). This protection was accompanied by significant restoration of glucose-induced insulin response and insulin-to-glucose ratio (**Fig. 5i**). Beta cell protection was also confirmed by the considerably higher beta cell mass in the MLD-STZ–treated b*Mst1*$^{-/-}$ mice, resulting from enhanced beta cell survival and proliferation (**Fig. 5j**), compared to *Mst1*$^{fl/fl}$ and RIP-Cre control mice. These data indicate that beta cell–specific disruption of *Mst1* prevented progressive hyperglycemia and improved glucose tolerance in MLD-STZ–treated mice as a result of less apoptosis and restoration of beta cell mass, suggesting that beta cell–specific activation of Mst1 is a key event in the progressive loss of beta cells in diabetes.

Mst1 deletion protects from HFD-induced diabetes

We further confirmed the protective effect of *Mst1* deletion against hyperglycemia and development of diabetes in a mouse model of T2D. We fed b*Mst1*$^{-/-}$ mice and RIP-Cre controls a normal diet (ND) or a HFD for 20 weeks. Mice fed a HFD gained more weight than the ND-fed group. Beta cell–specific disruption of *Mst1* had an effect on neither weight gain nor food intake in both groups (**Supplementary Fig. 7d**,**e**). HFD feeding increased fed and fasted glucose levels (**Fig. 6a**,**b**) and impaired glucose tolerance (**Fig. 6b**) in the HFD-treated RIP-Cre control mice compared to ND-fed mice, whereas HFD-treated b*Mst1*$^{-/-}$ mice showed significantly lower fed and fasted glucose levels as well as improved glucose tolerance (**Fig. 6a**,**b**).

In RIP-Cre mice on a HFD, insulin secretion during i.p. glucose challenge was markedly attenuated compared with that of the ND-fed group. In contrast, HFD-induced impairment in GSIS was dramatically reversed in mice with beta cell–specific deletion of *Mst1* (**Fig. 6c**). For assessing beta cell glucose responsiveness, we isolated islets from all ND- and HFD-fed groups. Whereas GSIS was severely impaired in islets isolated from HFD-treated RIP-Cre mice compared with ND-treated RIP-Cre mice, islets from b*Mst1*$^{-/-}$ mice remained fully responsive to glucose with improved insulin secretion under the HFD (**Fig. 6d**). Consistent with the improved metabolic phenotype of b*Mst1*$^{-/-}$ mice on HFD, b*Mst1*$^{-/-}$ mice had a higher compensatory beta cell mass relative to WT HFD control mice (**Fig. 6e**). The combination of lower rate of beta cell apoptosis and elevated beta cell proliferation (**Fig. 6e**) in b*Mst1*$^{-/-}$ mice on the HFD, which accounts

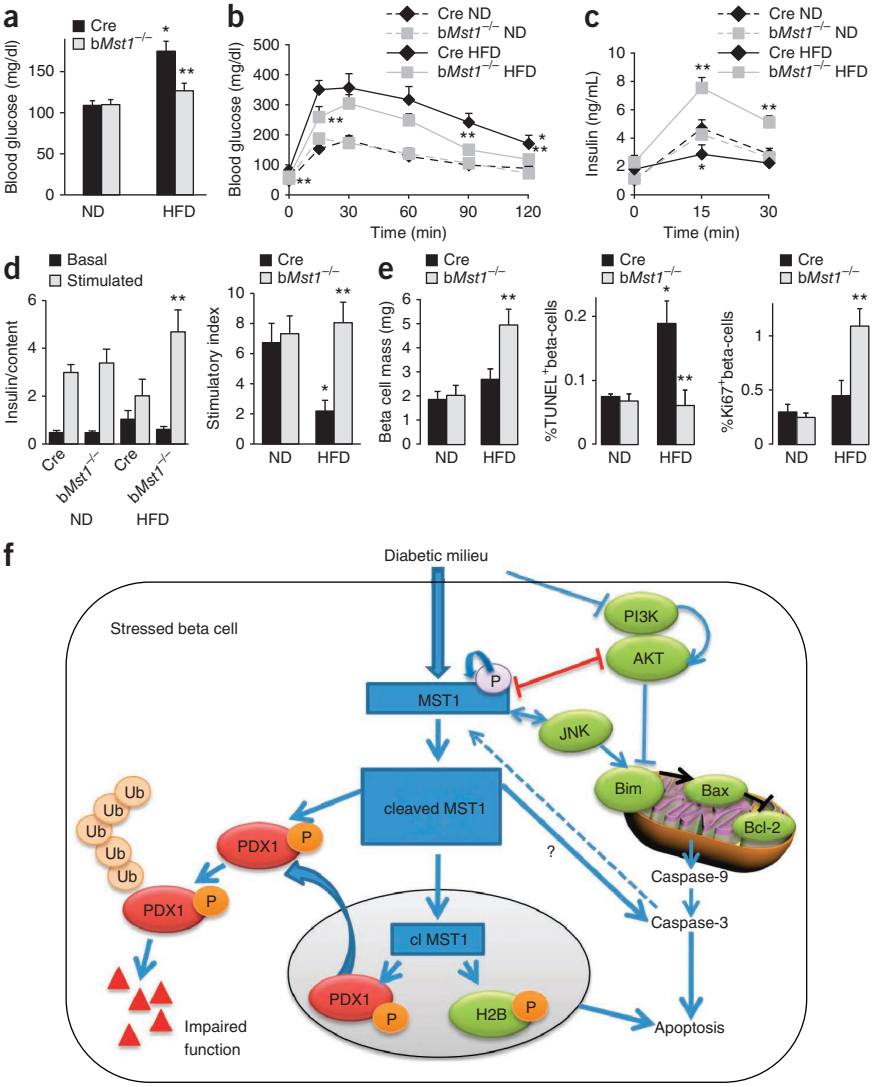

Figure 6 Beta cell–specific disruption of *Mst1* prevents hyperglycemia and HFD-induced diabetes progression. (**a**–**e**) b*Mst1*$^{-/-}$ mice ($n = 12$) and Cre control mice ($n = 12$) fed a ND or a HFD diet for 20 weeks. (**a**–**c**) Random fed blood glucose measurements (**a**), i.p. GTT (**b**) and insulin secretion (**c**) during an i.p. GTT measured before (0 min) and 15 and 30 min after glucose injection. (**d**) Insulin secretion during 1-h incubation with 2.8 mM (basal) and 16.7 mM (stimulated) glucose normalized to insulin content from isolated islets from all 4 treatment groups at week 21, cultured overnight and subjected to an *in vitro* GSIS assay. The insulin stimulatory index denotes the ratio of secreted insulin during 1-h incubation with 16.7 mM to secreted insulin at 2.8 mM glucose. (**e**) Beta cell mass, TUNEL and Ki-67 analysis expressed as percentage of TUNEL- or Ki-67–positive beta cells ± s.e.m. from a mean number of 28,521 scored beta cells for each treatment condition. $^{*}P < 0.05$ HFD-fed Cre mice (Cre HFD) compared to ND-fed Cre mice (Cre ND). $^{**}P < 0.05$ HFD-fed b*Mst1*$^{-/-}$ mice (b*Mst1*$^{-/-}$ HFD) compared to HFD-fed Cre mice (Cre HFD). (**f**) Our view on how diabetic stimuli lead to activation of MST1. Active MST1 triggers cytochrome *c* release and mitochondrial-dependent apoptosis by modulating Bim/Bax/Bcl-2/Bcl-xL through JNK-AKT signaling. Active caspase-9 then triggers cleavage of caspase-3, which triggers the caspase-3–dependent cleavage of MST1 to its constitutively active fragment, which leads to further MST1 activation and processing of caspase-3 by a positive feedback mechanism, and acceleration of beta cell death occurs. Cleaved MST1 translocates to the nucleus and directly phosphorylates PDX1 (we do not exclude the possibility that MST1 targets PDX1 also in cytoplasm) and histone H2B. PDX1 then shuttles to cytosol, where it undergoes ubiquitination and subsequent degradation by proteasome machinery, and beta cell function is impaired. Histone H2B phosphorylation by MST1 also induces chromatin condensation, one of the characteristic features of apoptosis.

for the higher beta cell mass in b*MST1*$^{-/-}$ mice under the HFD, correlates with the improved glucose tolerance and insulin secretion. This is also supported by results from an i.p. ITT: glucose levels were normalized to the basal levels before insulin injection, and b*Mst1*$^{-/-}$ mice and RIP-Cre control mice on HFD showed a similar impairment in insulin sensitivity (**Supplementary Fig. 7f,g**).

To test whether knockdown of MST1 expression could directly rescue beta cells, we transfected islets isolated from 10-week-old obese *db/db* mice and their heterozygous littermates with scrambled control siRNA or *Mst1* siRNA. Whereas Scr siRNA–treated isolated islets from *db/db* mice showed low Pdx1 expression and high caspase-3 cleavage and Bim expression, *Mst1* silencing restored Pdx1, inhibited Bim upregulation and dramatically reduced caspase-3 cleavage (**Supplementary Fig. 8**).

DISCUSSION

Our work shows that MST1 acts as an essential apoptotic molecule in the presence of diabetic stimuli and is a common component in the diverse signaling pathways leading to impaired beta cell survival in diabetes. We identified PDX1 as a beta cell–specific substrate for MST1. PDX1 ubiquitination and subsequent degradation, resulting from inhibitory T11 phosphorylation, is crucial for beta cell dysfunction after MST1 hyperactivation in diabetes (**Fig. 6f**). Deletion of *Mst1* preserves beta cell function and survival providing protection from diabetic insults.

MST1 has a central role in the initiation of cell death[9,41–44]. In line with our data, *Mst1* ablation *in vivo* resulted in resistance to apoptosis induced by tumor necrosis factor-α[45], Fas ligand[46] or IFN-γ[47]. Notably, suppression of endogenous Mst1 by cardiac-specific overexpression of the dominant-negative form of MST1 prevented cardiomyocyte death induced by ischemia-reperfusion[48], which supports the pathophysiological significance of MST1. The diversity of diabetic stimuli by which MST1 is activated in beta cells suggests that this enzyme may be a common component in the many signaling pathways leading to beta cell apoptosis. Although the endogenous molecules that trigger MST1 activation remain unknown, we show that MST1 is highly active in a diabetic environment and induces the mitochondrial-dependent apoptosis pathway in beta cells through targeting BIM, which leads to alterations in BCL-2/BAX or BCL-xL/BAX ratios, cytochrome *c* release, subsequent caspase-9 and caspase-3 cleavage and cell death.

The PI3K-AKT pathway has a critical role in the regulation of beta cell survival. AKT-mediated phosphorylation of multiple substrates positively regulates insulin transcription, insulin secretion and beta cell growth and survival[21,22,49]. Recent studies suggest potential crosstalk between MST1 and AKT[23,24]. MST1 activity is negatively regulated by AKT-mediated phosphorylation at its T120 and T387 residues, which results in inhibition of its cleavage, autophosphorylation, kinase activity and nuclear translocation[23]. On the other hand, MST1 and its cleaved form interact with AKT1 and act as direct AKT1 inhibitors[24]. Our data demonstrate that activation of the PI3K-AKT pathway in beta cells abrogates glucose- and cytokine-induced MST1 activation and beta cell apoptosis, whereas suppression of PI3K-AKT signaling induces MST1 activity and beta cell apoptosis. AKT and MST1 are components of two parallel stress-triggered signaling pathways that functionally antagonize each other. Activated AKT itself downregulates MST1 function in beta cells, indicating the existence of a potential bidirectional crosstalk between these two pathways. Here, we show that MST1 and AKT negatively regulate each other and constitute a stress-sensitive survival pathway. Under acute stress conditions, AKT promoted cell survival by inhibiting MST1, but prolonged stress decreased AKT activity, which allowed for proapoptotic MST1 signaling.

MST1 may affect signal pathways of diabetic stimuli through modulation of transcription factors and gene expression profiles that initiate the process of beta cell failure. In this study, we show that MST1 can physically interact with and phosphorylate PDX1. Targeted disruption of PDX1 in beta cells leads to diabetes, and reducing its expression affects insulin expression and secretion[50]. We have identified the T11 residue of PDX1 as the phosphorylation site used by MST1. Such a kinase-dependent function would be consistent with the comparably low level of PDX1 and high levels of active MST1 in stressed beta cells and pancreases of diabetic mice in our study. PDX1 is restored by deletion of *Mst1* under diabetic conditions. T11 is found in the highly conserved region of PDX1 at the transcription activation domain. T11 phosphorylation of PDX1 by MST1 marks PDX1 for degradation by the proteasome machinery, which would prohibit it from functioning as a transcription factor in the nucleus. In that regard, overexpression of MST1 caused reduction of PDX1 target gene expression and impairment of beta cell function, as assessed by GSIS, whereas mutation of the T11 site allowed PDX1 to be more stabilized and resistant to MST1-induced degradation, restoring PDX1-induced gene expression and improvement of beta cell function. The same site (T11) was previously shown to be targeted by DNA-dependent protein kinase. Consistent with our data, phosphorylation of PDX1 by this kinase results in enhanced PDX1 protein degradation[51]. PDX1 is degraded by the ubiquitin-proteasome pathway; PDX1 C terminal–inhibiting factor-1 (PCIF1) targets PDX1 for ubiquitination and proteasomal degradation by the E3 ubiquitin ligase cullin 3. Ubiquitination of PDX1 regulates its activity, as Pcif1 deficiency normalizes Pdx1 protein levels and improves glucose homeostasis and beta cell function in *Pdx1*$^{+/-}$ mice[36]. Notably, accumulation of polyubiquinated proteins was higher in beta cells of individuals with T2D than in nondiabetic controls[52], highlighting that higher expression of polyubiquinated proteins may contribute to beta cell dysfunction under diabetic conditions.

In mammals, the absolute number of beta cells reflects a dynamic balance between beta cell growth and death. An inadequate expansion of beta cell mass to compensate for the increased insulin demand, followed by the eventual loss of beta cells due to apoptosis, is a hallmark of diabetes[4,53]. This is most apparent in T1D when ongoing autoimmunity causes destruction and consequent loss of beta cells. Through deletion of the MST1-mediated death signal, we have uncovered a deleterious action of MST1 that induces apoptosis in response to diabetic injuries in the immune-mediated beta cell destruction in the MLD-STZ model, a model of beta cell demise that occurs in the absence of insulin resistance. *Mst1* deletion not only prevents MLD-STZ–induced beta cell death but also improves the capacity of beta cells to produce insulin. *Mst1* deletion preserves beta cell mass, improves beta cell function and prevents islet deterioration, as shown by the maintenance of the islet structure, density, size and mass. The observed ability to preserve islet appearance is associated with a protective role for Mst1 deficiency in MLD-STZ–induced beta cell death and in enhancing beta cell proliferation.

Preservation of PDX1 is one mechanism involved in the protection of beta cells by MST1 depletion. This conclusion is strongly supported by our *in vitro* and *in vivo* data; Pdx1 target gene expression is normalized and Glut2 localization is preserved in *Mst1*$^{-/-}$ mice. As both Pdx1 and Glut2 are involved in glucose sensing and GSIS, *Mst1*$^{-/-}$ mice show normal blood glucose levels and high circulating insulin concentrations. STZ enters beta cells via Glut2. It is unlikely that the resistance of *Mst1*$^{-/-}$ mice to MLD-STZ–induced beta cell damage is due to changes in membrane Glut2 expression in beta cells because *Mst1* deletion did not reduce membrane expression of Glut2 in beta cells in mice without STZ treatments.

The high rate of apoptosis in the Mst1-deficient thymocytes further illustrates the cell type–specific variation in the outputs of MST1 signaling. Whereas in thymocytes and T cells deletion of *Mst1* increases the apoptosis rate[54–56], possibly through high levels of reactive oxygen species, Mst1-deficient hepatocytes and microglia exhibit a marked resistance to stress-induced apoptosis[46,47]. Thus, the consequences of Mst1 deficiency need to be established in each cell type and tissue. We used a tissue-specific gene-targeting approach in the current study to provide insights into the biological role of Mst1 in beta cells *in vivo*. It is known that activation and migration of both T cells and macrophages play an important part in islet destruction leading to hyperglycemia in the MLD-STZ model[57]. Infiltrating macrophages and T cells are a major source of the proinflammatory cytokines that promote islet destruction. Thus, the depletion of peripheral T cells in *Mst1*$^{-/-}$ mice[54,55] might be a reason for their protection from MLD-STZ–induced hyperglycemia. We cannot exclude such T cell depletion in our model, but if it occurs, it only has a minor role, as beta cell–specific deletion of *Mst1* in mice completely protected them from hyperglycemia and islet destruction. This shows that *Mst1* ablation in beta cells, but not in other tissues, is a major reason for the protection from MLD-STZ–induced diabetes. Notably, beta cell–specific deletion of *Mst1* in this model led to protection against beta cell apoptosis and diabetes, further underlining the critical role of MST1 in beta cell survival.

The detrimental effects of a long-term HFD on beta cell function and insulin sensitivity leading to glucose intolerance and T2D in mice have been clearly established[58]. As expected, long-term HFD feeding was associated with insulin resistance, glucose intolerance, beta cell dysfunction and loss of compensatory beta cell adaptation. As observed in the MLD-STZ model, in the HFD diabetes model, beta cell–specific *Mst1* deletion results in improved glucose tolerance, insulin secretion and beta cell mass as a result of improved beta cell survival and proliferation, whereas insulin sensitivity is not affected. We have not investigated whether Mst1 is also activated in other organs during diabetes progression, but activated Mst1 has been found in the kidneys of hyperglycemic insulin receptor substrate-2 knockout mice[59] and in epididymal fat pads of HFD-treated mice[60].

Our findings raise the possibility that MST1 hyperactivity is associated with beta cell failure and development of diabetes. Current therapies for the treatment of diabetes mellitus are directed toward alleviating the symptoms of the disease, but there is an urgent medical need for therapies that slow or prevent the loss (rapid in T1D, progressive in T2D) of functional pancreatic beta cell mass. In light of the critical role of MST1 in beta cell failure and initiation of pro-diabetic milieu–induced apoptotic signaling, therapeutic strategies designed to inhibit MST1 activity may both protect beta cells against the effects of autoimmune attack in T1D and preserve beta cell mass and function in T2D.

METHODS

Methods and any associated references are available in the online version of the paper.

Note: Any Supplementary Information and Source Data files are available in the online version of the paper.

ACKNOWLEDGMENTS

This work was supported by the JDRF, the German Research Foundation (Emmy Noether Programm MA4172/1-1), the European Research Council, the German Federal Ministry of Science (Diabetes Competence Network), the European Federation for the Study of Diabetes and University of Bremen Research Funds (all to K.M.). We thank J. Bergemann for excellent technical assistance, G. Dharmadhikari and M. Panse for help with the analyses and G. Rutter and D. Schumann for critical discussion. Human islets were provided through the Juvenile Diabetes Research Foundation award 31-2008-413 (European Consortium for Islet Transplantation Islets for Basic Research Program) and by the Integrated Islet Distribution Program. Human pancreatic sections were obtained from the National Disease Research Interchange, which is supported by the US National Institutes of Health. MST1 and dn-MST1 plasmids and adenoviruses were provided by J. Sadoshima and Y. Maejima (Rutgers New Jersey Medical School), PDX1-WT plasmids and pGEX bacterial expression vector by R. Walther (University of Greifswald), INS-1E cells by C. Wollheim (Lund and Geneva Universities), RIP-Cre mice by P. Herrera (University of Geneva) and A. Mansouri (Max Planck Institute for Biophysical Chemistry), mouse pB.RSV.PDX1-GFP plasmid by I. Leibiger (Karolinska University) and rat insulin-2 promoter plasmid by R. Zinkernagel (University of Zurich). Adenovirus carrying eGFP as a control was provided by A.E. Karlsen (Novo Nordisk A/S).

AUTHOR CONTRIBUTIONS

A.A. conceived of the project, designed all and performed most of the experiments, analyzed the data and wrote the paper. F. Paroni provided experimental and technical support and analyzed data. Z.A., S.K., V.K. and T.Y. performed experiments and analyzed data. T.F. provided mutated PDX1 plasmids, W.T. provided *Mst1*$^{-/-}$ and *Mst1*$^{fl/fl}$ mice and J.K.C., F. Pattou and J.O. isolated human islets. K.M. supervised the project and wrote the paper.

COMPETING FINANCIAL INTERESTS

The authors declare no competing financial interests.

1. Kurrer, M.O., Pakala, S.V., Hanson, H.L. & Katz, J.D. Beta cell apoptosis in T cell–mediated autoimmune diabetes. *Proc. Natl. Acad. Sci. USA* **94**, 213–218 (1997).
2. Mathis, D., Vence, L. & Benoist, C. Beta-cell death during progression to diabetes. *Nature* **414**, 792–798 (2001).
3. Butler, A.E. *et al.* Beta-cell deficit and increased beta-cell apoptosis in humans with type 2 diabetes. *Diabetes* **52**, 102–110 (2003).
4. Rhodes, C.J. Type 2 diabetes—a matter of beta-cell life and death? *Science* **307**, 380–384 (2005).
5. Donath, M.Y., Storling, J., Maedler, K. & Mandrup-Poulsen, T. Inflammatory mediators and islet beta-cell failure: a link between type 1 and type 2 diabetes. *J. Mol. Med.* **81**, 455–470 (2003).
6. The Diabetes Control and Complications Trial Research Group. Effect of intensive therapy on residual beta-cell function in patients with type 1 diabetes in the diabetes control and complications trial. A randomized, controlled trial. *Ann. Intern. Med.* **128**, 517–523 (1998).
7. Lenzen, S., Drinkgern, J. & Tiedge, M. Low antioxidant enzyme gene expression in pancreatic islets compared with various other mouse tissues. *Free Radic. Biol. Med.* **20**, 463–466 (1996).
8. Ling, P., Lu, T.J., Yuan, C.J. & Lai, M.D. Biosignaling of mammalian Ste20-related kinases. *Cell. Signal.* **20**, 1237–1247 (2008).
9. Avruch, J. *et al.* Protein kinases of the Hippo pathway: regulation and substrates. *Semin. Cell Dev. Biol.* **23**, 770–784 (2012).
10. Lee, K.K. *et al.* Proteolytic activation of MST/Krs, STE20-related protein kinase, by caspase during apoptosis. *Oncogene* **16**, 3029–3037 (1998).
11. Kakeya, H., Onose, R. & Osada, H. Caspase-mediated activation of a 36-kDa myelin basic protein kinase during anticancer drug-induced apoptosis. *Cancer Res.* **58**, 4888–4894 (1998).
12. Bi, W. *et al.* c-Jun N-terminal kinase enhances MST1-mediated pro-apoptotic signaling through phosphorylation at serine 82. *J. Biol. Chem.* **285**, 6259–6264 (2010).
13. Cheung, W.L. *et al.* Apoptotic phosphorylation of histone H2B is mediated by mammalian sterile twenty kinase. *Cell* **113**, 507–517 (2003).
14. Jonsson, J., Carlsson, L., Edlund, T. & Edlund, H. Insulin-promoter-factor 1 is required for pancreas development in mice. *Nature* **371**, 606–609 (1994).
15. Stoffers, D.A., Zinkin, N.T., Stanojevic, V., Clarke, W.L. & Habener, J.F. Pancreatic agenesis attributable to a single nucleotide deletion in the human *IPF1* gene coding sequence. *Nat. Genet.* **15**, 106–110 (1997).
16. Johnson, J.D. *et al.* Increased islet apoptosis in *Pdx1*$^{+/-}$ mice. *J. Clin. Invest.* **111**, 1147–1160 (2003).
17. Stoffers, D.A., Ferrer, J., Clarke, W.L. & Habener, J.F. Early-onset type-II diabetes mellitus (MODY4) linked to IPF1. *Nat. Genet.* **17**, 138–139 (1997).
18. Brissova, M. *et al.* Reduction in pancreatic transcription factor PDX-1 impairs glucose-stimulated insulin secretion. *J. Biol. Chem.* **277**, 11225–11232 (2002).
19. Ardestani, A. *et al.* Neutralizing interleukin-1β (IL-1β) induces beta cell survival by maintaining PDX1 protein nuclear localization. *J. Biol. Chem.* **286**, 17144–17155 (2011).
20. Lee, K.K., Ohyama, T., Yajima, N., Tsubuki, S. & Yonehara, S. MST, a physiological caspase substrate, highly sensitizes apoptosis both upstream and downstream of caspase activation. *J. Biol. Chem.* **276**, 19276–19285 (2001).
21. Tuttle, R.L. *et al.* Regulation of pancreatic beta-cell growth and survival by the serine/threonine protein kinase Akt1/PKBα. *Nat. Med.* **7**, 1133–1137 (2001).
22. Bernal-Mizrachi, E., Wen, W., Stahlhut, S., Welling, C.M. & Permutt, M.A. Islet beta cell expression of constitutively active Akt1/PKB α induces striking hypertrophy, hyperplasia, and hyperinsulinemia. *J. Clin. Invest.* **108**, 1631–1638 (2001).
23. Yuan, Z. *et al.* Phosphoinositide 3-kinase/Akt inhibits MST1-mediated pro-apoptotic signaling through phosphorylation of threonine 120. *J. Biol. Chem.* **285**, 3815–3824 (2010).
24. Cinar, B. *et al.* The pro-apoptotic kinase Mst1 and its caspase cleavage products are direct inhibitors of Akt1. *EMBO J.* **26**, 4523–4534 (2007).
25. Trümper, K. *et al.* Integrative mitogenic role of protein kinase B/Akt in beta-cells. *Ann. NY Acad. Sci.* **921**, 242–250 (2000).
26. Matallanas, D. *et al.* RASSF1A elicits apoptosis through an MST2 pathway directing proapoptotic transcription by the p73 tumor suppressor protein. *Mol. Cell* **27**, 962–975 (2007).
27. Valis, K. *et al.* Hippo/Mst1 stimulates transcription of the proapoptotic mediator NOXA in a FoxO1-dependent manner. *Cancer Res.* **71**, 946–954 (2011).
28. Grunnet, L.G. *et al.* Proinflammatory cytokines activate the intrinsic apoptotic pathway in beta-cells. *Diabetes* **58**, 1807–1815 (2009).
29. Opferman, J.T. & Korsmeyer, S.J. Apoptosis in the development and maintenance of the immune system. *Nat. Immunol.* **4**, 410–415 (2003).
30. Yamamoto, S. *et al.* Activation of Mst1 causes dilated cardiomyopathy by stimulating apoptosis without compensatory ventricular myocyte hypertrophy. *J. Clin. Invest.* **111**, 1463–1474 (2003).
31. Lei, K. & Davis, R.J. JNK phosphorylation of Bim-related members of the Bcl2 family induces Bax-dependent apoptosis. *Proc. Natl. Acad. Sci. USA* **100**, 2432–2437 (2003).
32. Rahmani, M. *et al.* The BH3-only protein Bim plays a critical role in leukemia cell death triggered by concomitant inhibition of the PI3K/Akt and MEK/ERK1/2 pathways. *Blood* **114**, 4507–4516 (2009).
33. Humphrey, R.K., Yu, S.M., Flores, L.E. & Jhala, U.S. Glucose regulates steady-state levels of PDX1 via the reciprocal actions of GSK3 and AKT kinases. *J. Biol. Chem.* **285**, 3406–3416 (2010).
34. Kawamori, D. *et al.* The forkhead transcription factor Foxo1 bridges the JNK pathway and the transcription factor PDX-1 through its intracellular translocation. *J. Biol. Chem.* **281**, 1091–1098 (2006).
35. McCulloch, L.J. *et al.* GLUT2 (SLC2A2) is not the principal glucose transporter in human pancreatic beta cells: implications for understanding genetic association signals at this locus. *Mol. Genet. Metab.* **104**, 648–653 (2011).
36. Claiborn, K.C. *et al.* Pcif1 modulates Pdx1 protein stability and pancreatic beta cell function and survival in mice. *J. Clin. Invest.* **120**, 3713–3721 (2010).
37. Miller, M.L. *et al.* Linear motif atlas for phosphorylation-dependent signaling. *Sci. Signal.* **1**, ra2 (2008).
38. Frogne, T., Sylvestersen, K.B., Kubicek, S., Nielsen, M.L. & Hecksher-Sorensen, J. Pdx1 is post-translationally modified *in vivo* and serine 61 is the principal site of phosphorylation. *PLoS ONE* **7**, e35233 (2012).
39. Dunning, B.E. & Gerich, J.E. The role of alpha cell dysregulation in fasting and postprandial hyperglycemia in type 2 diabetes and therapeutic implications. *Endocr. Rev.* **28**, 253–283 (2007).

40. Li, Z., Karlsson, F.A. & Sandler, S. Islet loss and alpha cell expansion in type 1 diabetes induced by multiple low-dose streptozotocin administration in mice. *J. Endocrinol.* **165**, 93–99 (2000).
41. Lin, Y., Khokhlatchev, A., Figeys, D. & Avruch, J. Death-associated protein 4 binds MST1 and augments MST1-induced apoptosis. *J. Biol. Chem.* **277**, 47991–48001 (2002).
42. Del Re, D.P. *et al.* Proapoptotic Rassf1A/Mst1 signaling in cardiac fibroblasts is protective against pressure overload in mice. *J. Clin. Invest.* **120**, 3555–3567 (2010).
43. Graves, J.D., Draves, K.E., Gotoh, Y., Krebs, E.G. & Clark, E.A. Both phosphorylation and caspase-mediated cleavage contribute to regulation of the Ste20-like protein kinase Mst1 during CD95/Fas-induced apoptosis. *J. Biol. Chem.* **276**, 14909–14915 (2001).
44. Graves, J.D. *et al.* Caspase-mediated activation and induction of apoptosis by the mammalian Ste20-like kinase Mst1. *EMBO J.* **17**, 2224–2234 (1998).
45. Song, H. *et al.* Mammalian Mst1 and Mst2 kinases play essential roles in organ size control and tumor suppression. *Proc. Natl. Acad. Sci. USA* **107**, 1431–1436 (2010).
46. Zhou, D. *et al.* Mst1 and Mst2 maintain hepatocyte quiescence and suppress hepatocellular carcinoma development through inactivation of the Yap1 oncogene. *Cancer Cell* **16**, 425–438 (2009).
47. Yun, H.J. *et al.* Daxx mediates activation-induced cell death in microglia by triggering MST1 signalling. *EMBO J.* **30**, 2465–2476 (2011).
48. Odashima, M. *et al.* Inhibition of endogenous Mst1 prevents apoptosis and cardiac dysfunction without affecting cardiac hypertrophy after myocardial infarction. *Circ. Res.* **100**, 1344–1352 (2007).
49. Assmann, A., Ueki, K., Winnay, J.N., Kadowaki, T. & Kulkarni, R.N. Glucose effects on beta-cell growth and survival require activation of insulin receptors and insulin receptor substrate 2. *Mol. Cell. Biol.* **29**, 3219–3228 (2009).
50. Ahlgren, U., Jonsson, J., Jonsson, L., Simu, K. & Edlund, H. beta-cell–specific inactivation of the mouse Ipf1/Pdx1 gene results in loss of the beta-cell phenotype and maturity onset diabetes. *Genes Dev.* **12**, 1763–1768 (1998).
51. Lebrun, P., Montminy, M.R. & Van Obberghen, E. Regulation of the pancreatic duodenal homeobox-1 protein by DNA-dependent protein kinase. *J. Biol. Chem.* **280**, 38203–38210 (2005).
52. Costes, S. *et al.* Beta-cell dysfunctional ERAD/ubiquitin/proteasome system in type 2 diabetes mediated by islet amyloid polypeptide-induced UCH-L1 deficiency. *Diabetes* **60**, 227–238 (2011).
53. Butler, P.C., Meier, J.J., Butler, A.E. & Bhushan, A. The replication of beta cells in normal physiology, in disease and for therapy. *Nat. Clin. Pract. Endocrinol. Metab.* **3**, 758–768 (2007).
54. Choi, J. *et al.* Mst1-FoxO signaling protects naive T lymphocytes from cellular oxidative stress in mice. *PLoS ONE* **4**, e8011 (2009).
55. Dong, Y. *et al.* A cell-intrinsic role for Mst1 in regulating thymocyte egress. *J. Immunol.* **183**, 3865–3872 (2009).
56. Ueda, Y. *et al.* Mst1 regulates integrin-dependent thymocyte trafficking and antigen recognition in the thymus. *Nat. Commun.* **3**, 1098 (2012).
57. Soltani, N. *et al.* GABA exerts protective and regenerative effects on islet beta cells and reverses diabetes. *Proc. Natl. Acad. Sci. USA* **108**, 11692–11697 (2011).
58. Sauter, N.S., Schulthess, F.T., Galasso, R., Castellani, L.W. & Maedler, K. The antiinflammatory cytokine interleukin-1 receptor antagonist protects from high-fat diet–induced hyperglycemia. *Endocrinology* **149**, 2208–2218 (2008).
59. Carew, R.M. *et al.* Deletion of Irs2 causes reduced kidney size in mice: role for inhibition of GSK3β? *BMC Dev. Biol.* **10**, 73 (2010).
60. Kawano, Y. *et al.* Loss of Pdk1-Foxo1 signaling in myeloid cells predisposes to adipose tissue inflammation and insulin resistance. *Diabetes* **61**, 1935–1948 (2012).

ONLINE METHODS

Cell culture, treatment and islet isolation. Human islets were isolated from twenty pancreases of healthy organ donors and from five with T2D at the University of Illinois at Chicago or Lille University and cultured on extracellular matrix (ECM)-coated dishes (Novamed, Jerusalem, Israel) as described previously[61]. Informed consent was obtained from all subjects. Islet purity was greater than 95% as judged by dithizone staining (if this degree of purity was not achieved by routine isolation, islets were handpicked). Ethical approval for the use of human islets had been granted by the Ethics Committee of the University of Bremen. Islets from *Mst1*$^{-/-}$ mice and their WT littermates were isolated as described previously[61]. Pancreases were perifused with a Liberase TM (#05401119001, Roche, Mannheim, Germany) solution according to the manufacturer's instructions and digested at 37 °C, followed by washing and handpicking. The clonal rat beta cell line INS-1E was provided by C. Wollheim. Human islets were cultured in complete CMRL-1066 (Invitrogen) medium at 5.5 mM glucose, mouse islets and INS-1E cells were cultured in complete RPMI-1640 medium at 11.1 mM glucose and HEK 293 cells were cultured in DMEM. All media included glutamate, 1% penicillin-streptomycin and 10% FBS (all from PAA). INS-1E medium was supplemented with 10 mM HEPES, 1 mM sodium pyruvate and 50 μM β-mercaptoethanol. Islets and INS-1E cells were exposed to complex diabetogenic conditions: 22.2 or 33.3 mM glucose, 0.5 mM palmitic acid or the mixture of 2 ng/ml recombinant human IL-1β (R&D Systems, Minneapolis, MN) plus 1,000 U/ml recombinant human IFN-γ (PeproTech) for 72 h, 100 μM H_2O_2 for 6 h, 1 mM streptozotocin (STZ) for 8 h or 1 mM thapsigargin for 6 h (all Sigma). In some experiments, cells were additionally cultured with 10–25 μM JNK-selective inhibitor SP600125, 10 μM PI3K-selective inhibitor LY294002, 10 or 20 μM AKT inhibitor V, triciribine, a selective AKT1/2/3 inhibitor, 50 μM pancaspase inhibitor Z-VAD (OMe)-fmk, 100 μM Bax-inhibiting peptide V5 or Bax-inhibiting peptide, negative control, 20 μM InSolution MG-132, proteasome inhibitor (all Calbiochem), 100 nM glucagon like-peptide 1 (GLP1), 100 nM recombinant human insulin and 50 μg/ml cycloheximide (CHX) and 1 μM glibenclamide (all Sigma). Palmitic acid was dissolved as described previously[62].

Mice. For MLD-STZ experiments, 8- to 10-week old *Mst1*$^{-/-}$ mice on a 129/sv genetic background[55] and their *Mst1*$^{+/+}$ WT littermates were i.p. injected with STZ (40 mg per kg body weight; Sigma) freshly dissolved in 50 mM sodium citrate buffer (pH 4.5) or citrate buffer as control for five consecutive days (referred to as multiple low-dose (MLD)-STZ). To create beta cell–specific *Mst1*$^{-/-}$ mice, mice harboring exon 4 of the *Mst1* gene flanked by *loxP* sites (*Mst1*$^{fl/fl}$)[55] were crossed with mice expressing Cre under the rat insulin-2 promoter (B6;D2-Tg(Ins-Cre)23Herr: RIP-Cre[63], provided by P. Herrera, University of Geneva and A. Mansouri, Max Planck Institute for Biophysical Chemistry). RIP-Cre-*Mst1*$^{fl/-}$ mice were intercrossed to generate RIP-Cre-*Mst1*$^{fl/fl}$. Mice were MLD-STZ injected as described above. For the high-fat diet (HFD) experiments, 8-week-old RIP-Cre-*Mst1*$^{fl/fl}$ (b*Mst1*$^{-/-}$) mice and their RIP-Cre littermates were fed a normal diet (ND, Harlan Teklad Rodent Diet 8604, containing 12.2, 57.6 and 30.2% calories from fat, carbohydrate and protein, respectively) or a high-fat, high-sucrose diet (HFD, Surwit Research Diets, New Brunswick, NJ, containing 58, 26 and 16% calories from fat, carbohydrate and protein, respectively[58,64]) for 20 weeks. For both models, random blood was obtained from the tail vein of nonfasted mice, and glucose was measured using a Glucometer (Freestyle; TheraSense, Alameda, CA). Mice were killed at the end of experiment, and pancreases were isolated. Throughout the whole study, food consumption and body weight were measured weekly. Only male mice were used in the experiments. All animals were housed in a temperature-controlled room with a 12-h light-dark cycle and were allowed free access to food and water in agreement with US National Institutes of Health animal care guidelines and the German animal protection law and approved by the Bremen Senate.

Intraperitoneal glucose and ITTs and measurement of insulin release. For i.p. GTTs, mice were fasted 12 h overnight and injected i.p. with glucose (40%; B. Braun, Melsungen, Germany) at a dose of 1 g per kg body weight. Blood samples were obtained at time points 0, 15, 30, 60, 90 and 120 min for glucose measurements using a glucometer and at time points 0, 15 and 30 min for measurement of serum insulin levels. For i.p. ITTs, mice were injected with 0.75 U per kg body weight recombinant human insulin (Novolin, Novo Nordisk) after a 5-h fast, and glucose concentration was determined with the glucometer. Insulin secretion was measured before (0 min) and after (15 and 30 min) i.p. injection of glucose (2 g per kg body weight) and measured using ultrasensitive mouse Elisa kit (ALPCO Diagnostics, Salem, NH).

Plasmids. pCMV-Myc-MST1 and kinase-dead pCMV-MST1-K59R (dn-MST1) was provided by J. Sadoshima and Y. Maejima (Rutgers New Jersey Medical School)[30]. Mouse pB.RSV.PDX1-GFP plasmid was provided by I. Leibiger (Karolinska University, Stockholm). pcDNA3 Myr-HA AKT1, pCDNA3 HA-ubiquitin and pCDNA3 Jnk1a1 (apf) (dn-JNK) plasmids were obtained from Addgene (Cambridge, MA). Mouse PDX1 mutants (T11, T126, T152, T155, T214 and T231) in the pCGIG5 vector were generated by site-directed mutagenesis as described previously[38]. All mutations were verified by sequencing. To make bacterial expression plasmids for PDX1 mutants, the complete mouse PDX1 coding sequence (WT and mutants) has been amplified by PCR using a specific set of primers from pCGIG5 plasmids and cloned into a pGEX-6P-1 bacterial expression vector (provided by R. Walther, University of Greifswald). The rat insulin–driven luciferase vector (RIP-luc) was constructed by subcloning a 700–base pair (bp) fragment containing 660 bp of the rat insulin-2 promoter (provided by R. Zinkernagel, University of Zurich) into a pMCS-Green-*Renilla*-Luc vector (Thermo Scientific). pCMV-Red Firefly Luc vector was obtained from Thermo Scientific.

Transfections. To knock down MST1 expression in human islets, SMARTpool technology from Dharmacon was used. A mix of ON-TARGETplus siRNAs directed against human MST1 sequences UAAAGAGACCGGCCAGAUU, GAUGGGCACUGUCCGAGUA, GCCCUCAUGUAGUCAAAUA and CCA GAGCUAUGGUCAGAUA and mouse Mst1 sequences GAUGGGCACUG UCCGAGUA, UGACAGCCCUCACGUAGUC, GCAGGUCAACUUACAG AUA and CUACAGCACCCGUUUGUUA. (100 nM, Dharmacon) was transiently transfected into human and mouse islets and efficiently reduced MST1 levels. An ON-TARGETplus nontargeting siRNA pool from Dharmacon served as a control. To knock down BIM and caspase-3 expression in human islets, siRNAs targeting human BIM (SignalSilence Bim SiRNA I, Cell Signaling) and caspase-3 (NEB) were used. GFP, MST1, dn-MST1 (K59R), dn-JNK1 and Myr-AKT1 plasmids were used to overexpress these proteins in human islets and INS-1E cells.

An adapted improved protocol to achieve silencing and overexpression in human islets was developed[19,65]. Islets were partially dispersed with accutase (PAA) to break islets into smaller cell aggregates to increase transfection efficiency and cultured on ECM dishes for at least 2 d. Isolated islets and INS-1E cells were exposed to transfection Ca^{2+}-KRH medium (KCl 4.74 mM, KH_2PO_4 1.19 mM, $MgCl_2$•$6H_2O$ 1.19 mM, NaCl 119 mM, $CaCl_2$ 2.54 mM, $NaHCO_3$ 25 mM and HEPES 10 mM). After 1-h incubation, lipoplexes (Lipofectamine 2000, Invitrogen)/siRNA ratio 1:20 pmol or –lipoplexes/DNA ratio 2.5:1) were added to transfect the islets and INS-1E cells. After an additional 6-h incubation, CMRL-1066 or RPMI-1640 medium containing 20% FCS and L-glutamine were added to the transfected islets or INS-1E cells. Efficient transfection was evaluated based on fluorescein-labeled siRNA (NEB) or eGFP-positive cells analyzed by fluorescent or confocal microscopy. HEK 293 cells were transiently transfected using Opti-MEM medium and Lipofectamine (Invitrogen) according to the manufacturer's instructions.

Glucose-stimulated insulin secretion. For acute insulin release in response to glucose, primary human and mouse islets and INS-1E cells were washed and preincubated (30 min) in Krebs-Ringer bicarbonate buffer (KRB) containing 2.8 mM glucose and 0.5% BSA. KRB was then replaced by KRB 2.8 mM glucose for 1 h (basal), followed by an additional 1 h in KRB 16.7 mM glucose with or without 100 nM GLP1 or 1 μM glibenclamide. Insulin content was extracted with 0.18N HCl in 70% ethanol. Insulin was determined using human and mouse insulin ELISA (ALPCO Diagnostics, Salem, NH). Secreted insulin was normalized to insulin content.

Immunohistochemistry. Pancreatic tissues were processed as previously described[66]. In brief, mouse pancreases were dissected and fixed in 4%

doi:10.1038/nm.3482

formaldehyde at 4 °C for 12 h before embedding in paraffin. Human and mouse 4-μm sections were deparaffinized, rehydrated and incubated overnight at 4 °C with anti-insulin (A0546, 1:50), anti-glucagon (A0565, 1:50) and rat anti–mouse Ki-67 (M7249, 1:50) antibodies from Dako, anti-pMST1 (3681, 1:100) and anti-Bim (2933, 1:100) antibodies from Cell Signaling Technology (CST), anti-PDX1 antibody (47267, 1:1,200) from Abcam and anti-Glut2 antibody (07-1402, 1:100) from Chemicon, followed by FITC- or Cy3-conjugated secondary antibodies (Jackson ImmunoResearch Laboratories, 1:100). Slides were mounted with Vectashield with DAPI (Vector Labs). For mouse sections or primary islets cultured on ECM dishes, beta cell apoptosis was analyzed by the TUNEL technique according to the manufacturer's instructions (*In situ* Cell Death Detection Kit, TMR red; Roche) and double stained for insulin. Fluorescence was analyzed using a Nikon MEA53200 (Nikon, Dusseldorf, Germany) microscope, and images were acquired using NIS-Elements software (Nikon).

Morphometric analysis. For morphometric data, ten sections (spanning the width of the pancreas) per mouse were analyzed. Pancreatic tissue area and insulin-positive area were determined by computer-assisted measurements using a Nikon MEA53200 (Nikon, Dusseldorf, Germany) microscope, and images were acquired using NIS-Elements software (Nikon). The number of islets (defined as insulin-positive aggregates at least 25 μm in diameter) was scored and used to calculate islet density (number of islets per square centimeter of tissue), mean islet size (the ratio of the total insulin-positive area to the total islet number on the sections). Mean percentage beta cell fraction per pancreas was calculated as the ratio of insulin-positive to whole pancreatic tissue area. Beta cell mass was obtained by multiplying the beta cell fraction by the weight of the pancreas. Morphometric beta cell and islet characterizations are results from analyses of at least 100 islets per mouse.

Western blot analysis. At the end of the incubation periods, islets and INS-1E cells were washed in ice-cold PBS and lysed in lysis buffer containing 20 mM Tris acetate, 0.27 M sucrose, 1 mM EDTA, 1 mM EGTA, 50 mM NaF, 1% Triton X-100, 5 mM sodium pyrophosphate and 10 mM β-glycerophosphate. Prior to use, the lysis buffer was supplemented with Protease and Phosphatase Inhibitors (Pierce, Rockford, IL, USA). Protein concentrations were determined with the BCA protein assay (Pierce). Equivalent amounts of protein from each treatment group were run on a NuPAGE 4–12% Bis-Tris gel (Invitrogen) and electrically transferred onto PVDF membranes. After 1-h blocking at room temperature using 5% milk (CST), membranes were incubated overnight at 4 °C with the following antibodies: rabbit anti-MST1 (3682), rabbit anti-pMST1 (3681), rabbit anti-ubiquitin (3933), rabbit anti-Bim (2933), rabbit anti-AKT (9272), rabbit anti-pAKT (Ser437) (4058), rabbit anti-Bax (2772), rabbit anti–Bcl-2 (2870), rabbit anti–Bcl-xL (2764), rabbit anti-Bad (9239), rabbit anti-pBad (5284), rabbit anti-PUMA (4976), rabbit anti-Bak (6947), rabbit anti-Mcl1 (4572), rabbit anti-pan–phosphorylated threonine (9381), mouse monoclonal anti-pan–phosphorylated threonine (9386), rabbit anti-pGSK-3 (9336), rabbit anti-pFOXO1 (9461), mouse anti-Myc (2276), rabbit anti–cleaved caspase-3 (9664), rabbit anti–cleaved caspase-9 (rat specific; 9507), rabbit anti–cleaved caspase-9 (human specific; 9505), rabbit anti–cytochrome *c* (4272), rabbit anti–cytochrome oxidase (4850), rabbit anti-pJNK (T183/Y185) (9251), rabbit anti–c-Jun (S63) (9261), rabbit anti-PARP (9542), rabbit anti-tubulin (2146), rabbit anti–glyceraldehyde 3-phosphate dehydrogenase (2118) and rabbit anti–β-actin (4967) all from CST); rabbit anti-pMST1 (79199), rabbit anti-GFP (290), mouse anti-NOXA (13654) and rabbit anti-PDX1 (47267) all from Abcam; rabbit anti-pH2B (07-191) from Millipore and rabbit anti-pPDX1 (T11) (PA5-13046) from Thermo Scientific, followed by horseradish-peroxidase–linked anti-rabbit or anti-mouse IgG (Jackson). All primary antibodies were used at 1:1,000 dilution in Tris-buffered saline plus Tween-20 (TBS-T) containing 5% BSA, except for the antibody to PDX1 (1:6,000). Membrane was developed using a chemiluminescence assay system (Pierce) and analyzed using DocITLS image acquisition 6.6a (UVP BioImaging Systems, Upland, CA, USA).

Immunoprecipitation. For immunoprecipitation, cells were washed with PBS and lysed in cold buffer containing 20 mM Tris-HCl (pH 7.5), 150 mM NaCl, 0.27 M sucrose, 1 mM EDTA, 1 mM EGTA, 50 mM NaF, 1% NP-40, 5 mM sodium pyrophosphate and 10 mM β-glycerophosphate supplemented with proteinase and phosphatase inhibitors for 30 min on ice. Lysates were centrifuged at 12,000*g* for 15 min at 4 °C before immunoprecipitation. Immunoprecipitations were carried out with incubating 0.5–1 mg of total lysate with rabbit anti-PDX1 (1:500; Abcam), rabbit anti-MST1 (1:50; CST), mouse anti-Myc (1:1,000; CST) and rabbit anti-GFP (1:1,000; Abcam) antibodies on a rotator at 4 °C overnight. Immunocomplexes were then captured with Protein A Agarose Fast Flow (Millipore) by rotation at 4 °C for 4 h. After five washes with cold lysis buffer, the immunoprecipitates were used for kinase assays or resuspended in sample buffer and separated by NuPAGE 4–12% Bis-Tris gels (Invitrogen).

***In vitro* kinase assay.** Purified human active MST1 without GST-tag (Upstate Biotechnology) or with GST-tag (Abcam) was incubated with ^{32}P-ATP (2 μCi, PerkinElmer Life Sciences), ATP (100 μM) and 1 mM dithiothreitol in a kinase buffer containing 40 mM HEPES (pH 7.4), 20 mM $MgCl_2$, 1 mM EDTA and 1 μg of purified recombinant human PDX1 (Abcam) or bacterially purified PDX1-GST (WT and mutants) as substrates. After incubation at 30 °C for 30 min, the reaction was stopped by adding loading buffer and proteins were separated on NuPAGE gels and phosphorylation levels visualized either by autoradiography or specific antibody for pPDX1 (T11) or pThr. The total PDX1 was detected with anti-PDX1 antibody.

***In vivo* kinase assay.** HEK 293 cells were transiently transfected with PDX1 and MST1 expression plasmids. Next, cell lysates were subjected to immunoprecipitation with anti-PDX1 antibody. The immunoprecipitates were separated by NuPAGE Bis-Tris gels and transferred to PVDF membranes and subsequently subjected to analyses of phosphorylation levels by pan–phosphorylated threonine antibody, which binds to threonine phosphorylated sites in a manner largely independent of the surrounding amino acid sequence or pan–phosphorylated serine antibody, which recognizes serine-phosphorylated proteins.

***In vivo* ubiquitination.** HEK 293 cells were cultured in 10-cm cell culture dishes and transfected with HA-ubiquitin and PDX1 and MST1 expression plasmids for 48 h. For ubiquitination in human islets, 5,000 islets per condition were transfected with ubiquitin plasmid. After 24 h, islets were infected with Ad-GFP or Ad-MST1 for 6 h and kept for another 48 h. HEK 293 cells and islets were exposed to 20 μM MG-132 for the last 6 h of the experiment. Lysates were immunoprecipitated with PDX1-specific antibody overnight at 4 °C. Immunocomplexes were then captured with Protein A Agarose by rotation at 4 °C for 4 h. After extensive washing, immunoprecipitates were boiled in sample buffer and proteins subjected to western blotting with ubiquitin-specific antibody.

Protein degradation analysis. HEK 293 cells were transfected with PDX1 alone or together with MST1 expression plasmids. Human islets were infected with Ad-GFP (control) or Ad-MST1. At 48 h after transfection or infection, cells were treated with 50 μg/ml translation initiation inhibitor CHX, which was added to the medium at the times indicated, and the lysates were subjected to western blotting.

RNA extraction and RT-PCR analysis. Total RNA was isolated from cultured human islets and INS-1E cells using TRIzol (Invitrogen), and RT-PCR was performed as described previously[67]. For analysis, we used the Applied Biosystems StepOne Real-Time PCR system (Applied Biosystems, CA, USA) with TaqMan(R) Fast Universal PCR Master Mix for TaqMan assays (Applied Biosystems). TaqMan(R) Gene Expression Assays were used for *PDX1* (Hs00426216_m1), *SLC2A2* (Hs01096905_m1), *GCK* (Hs01564555_m1), *INS* (Hs02741908_m1), *PPIA* (Hs99999904_m1), *BCL2L11* (Hs01083836_m1) and *TUBULIN* (Hs00362387_m1) for human and *Pdx1* (Rn00755591_m1), *Slc2a2* (Rn00563565_m1), *Gck* (Rn00688285_m1), *Ins1* (Rn02121433_g1), *Ins2* (Rn01774648_g1), *Ppia* (Rn00690933_m1) and *Tuba1a* (Rn01532518_g1) for rat.

Luciferase reporter assay. The transcriptional activity of the PDX1 at promoter level was evaluated using rat insulin-2–*Renilla* luciferase (Ins2–luc *Renilla*) reporter gene. HEK 293 cells were transfected with Ins2–luc *Renilla*,

pCMV-firefly, PDX1-WT or PDX1-T11A, alone or together with Myc-MST1 expression plasmids for 48 h. INS-1E cells transfected with Ins2-luc *Renilla* and pCMV-firefly plasmids and were infected with Ad-GFP or Ad-MST1 for 48 h. Luciferase activity was determined using the *Renilla* Firefly Luciferase Dual Assay Kit according to the manufacturer's instructions (Pierce). pCMV-firefly was used as transfection control.

Adenovirus infection. Isolated human islets and INS-1E cells were infected with adenovirus carrying eGFP as a control (provided by A.E. Karlsen, Novo Nordisk A/S, Denmark) or MST1 (Ad-MST1, provided by J. Sadoshima) at a multiplicity of infection (MOI) of 20 (for INS-1E) or 100 (for human islets) for 4 h. Adenovirus was subsequently washed off with PBS and replaced by fresh medium with 10% FBS, and GSIS or RNA and protein isolation performed after 48 or 72 h after infection.

Purification of PDX1-GST recombinant proteins. Expression and induction of recombinant GST proteins were performed as described previously[68]. *Escherichia coli* BL21 cells with various GST-fusion expression plasmids were cultured at 37 °C, and expression of recombinant proteins was induced by 0.1 mM final concentration of isopropyl-β-D-thiogalactoside (IPTG; Sigma) for 2.5 h. Cells were lysed using B-PER bacterial protein extraction reagent (Pierce) and purified using Glutathione Spin Columns (Pierce).

Cytochrome *c* release. Cytochrome *c* release was performed by digitonin-based subcellular fractionation technique[69]. Briefly, INS-1E cells were digitonin-permeabilized for 5 min on ice after resuspension of the cell pellet in 200 µl of cytosolic extraction buffer (250 mM sucrose, 70 mM KCl, 137 mM NaCl, 4.3 mM Na_2HPO_4 and 1.4 mM KH_2PO_4 (pH 7.2) with 300 µg/ml digitonin (Sigma). Cells were then centrifuged at 1,000*g* for 5 min at 4 °C. Supernatants (cytosolic fractions) were collected and pellets solubilized in the same volume of mitochondrial lysis buffer (50 mM Tris (pH 7.4), 150 mM NaCl, 2 mM EDTA, 2 mM EGTA, 0.2% Triton X-100 and 0.3% NP-40), followed by centrifugation at 10,000*g* for 10 min at 4 C. After centrifugation, supernatants, which are the heavy membrane fractions enriched for mitochondria, as well as cytosolic fractions were subjected to western blot analysis.

Generation of stably expressed shRNAMST1 INS1-E cell line. To knock down MST1 expression in INS-1E cells, two different lentiviral shRNA targeting MST1 or control shRNA vectors (pGIPZ collection, Open Biosystems, Huntsville, AL) were transfected into INS-1E cells, and stable clones were generated by selection with puromycin (1 to 2.5 µg/ml). Positive clonal cell lines were identified by immunoblotting using antibody directed against MST1. After selection, INS-1E lines were maintained in culture medium containing 1.5 µg/ml puromycin.

Statistical analyses. Samples were evaluated in a randomized manner by five investigators (A.A., V.K., S.K., T.Y. and Z.A.) who were blinded to the treatment conditions. To perform statistical analysis, at least 3 independent experiments from 3 different organ donors were performed for human islets, at least 3 independent experiments were performed for mouse islets and cell lines and at least 3 independent tissue samples or mice were included in the analyses, as reported in all figure legends. No statistical method was used to predetermine sample size. Data are presented as means ± s.e.m. Mean differences were determined by Student's *t*-tests. To account for multiplicity in the treated cells *in vitro* and in mice *in vivo*, a Bonferroni correction was used.

61. Schulthess, F.T. *et al.* CXCL10 impairs beta cell function and viability in diabetes through TLR4 signaling. *Cell Metab.* **9**, 125–139 (2009).
62. Maedler, K. *et al.* Distinct effects of saturated and monounsaturated fatty acids on beta-cell turnover and function. *Diabetes* **50**, 69–76 (2001).
63. Herrera, P.L. Adult insulin- and glucagon-producing cells differentiate from two independent cell lineages. *Development* **127**, 2317–2322 (2000).
64. Surwit, R.S., Kuhn, C.M., Cochrane, C., McCubbin, J.A. & Feinglos, M.N. Diet-induced type II diabetes in C57BL/6J mice. *Diabetes* **37**, 1163–1167 (1988).
65. Kang, H.C. & Bae, Y.H. Transfection of rat pancreatic islet tissue by polymeric gene vectors. *Diabetes Technol. Ther.* **11**, 443–449 (2009).
66. Shu, L. *et al.* Transcription factor 7-like 2 regulates beta-cell survival and function in human pancreatic islets. *Diabetes* **57**, 645–653 (2008).
67. Shu, L. *et al.* TCF7L2 promotes beta cell regeneration in human and mouse pancreas. *Diabetologia* **55**, 3296–3307 (2012).
68. Tolia, N.H. & Joshua-Tor, L. Strategies for protein coexpression in *Escherichia coli*. *Nat. Methods* **3**, 55–64 (2006).
69. Arnoult, D. Apoptosis-associated mitochondrial outer membrane permeabilization assays. *Methods* **44**, 229–234 (2008).

doi:10.1038/nm.3482

Supplementary information

MST1 is a novel regulator of apoptosis in pancreatic beta-cells

Nature Medicine: doi:10.1038/nm.3482

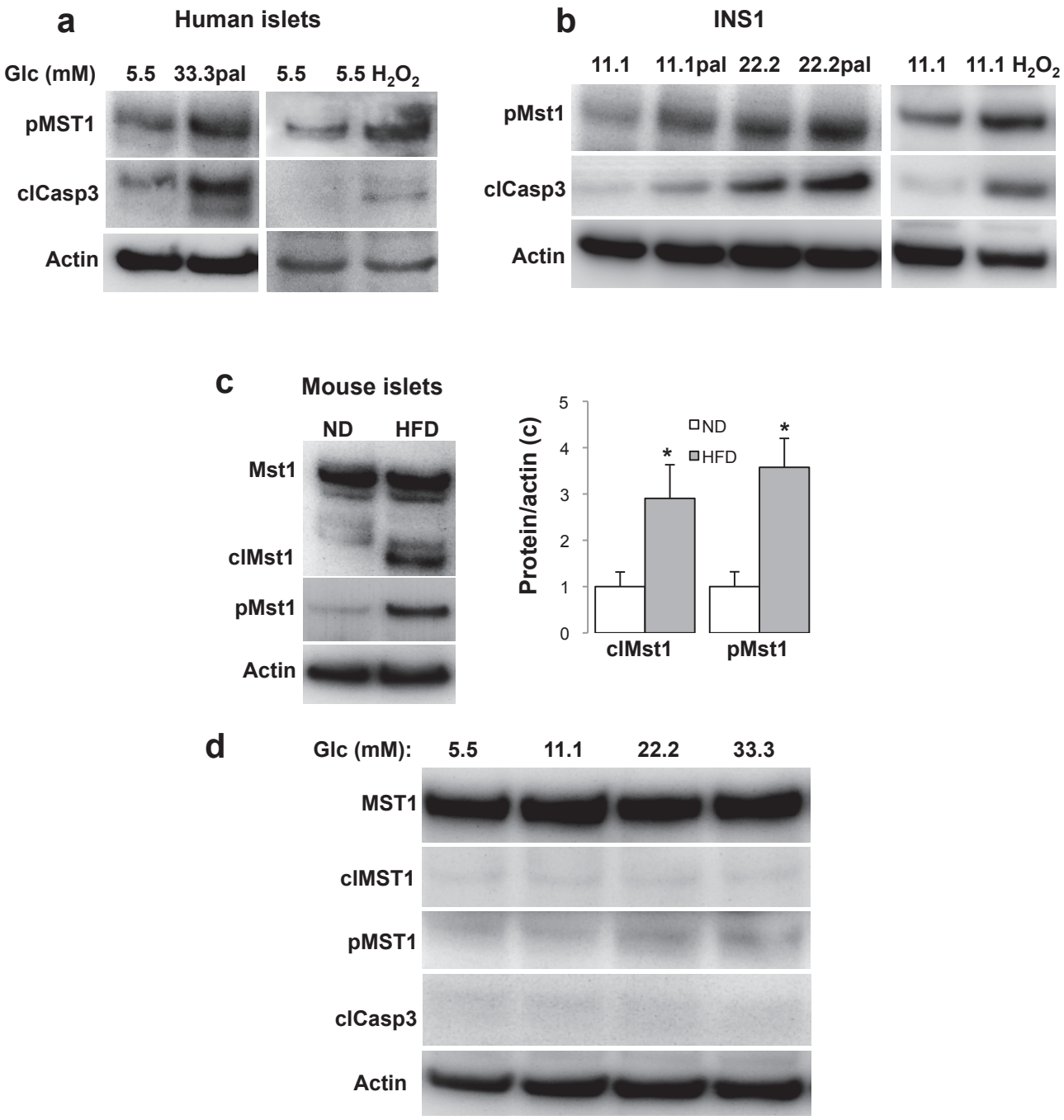

Supplementary Figure 1. Diabetogenic conditions induce MST1 activation and JNK and caspase-3 are responsible for stress-induced MST1 cleavage and apoptosis.
(a) Human islets and **(b)** INS-1E cells exposed to diabetogenic conditions (22.2 or 33.3 mM glucose, 0.5 mM palmitate or the mixture of 22.2 or 33.3 mM glucose and 0.5 mM palmitate (33.3Pal) for 72h (human islets) and 24h (INS-1E cells) or 100 μM H_2O_2 for 6h). **(c)** Isolated islets from normal diet (ND) (n=3) or high fat/high sucrose (HFD)-fed (n=3) mice treated for 16 weeks. Right panel shows densitometry analysis normalized to actin from 3 mice per condition. Western blots show representative results from 3 independent experiments from 3 different donors or mice. **(d)** Short term culture of human islets with high glucose does not induce MST1 activation and apoptosis. Human islets exposed to different concentration of high glucose (11.1, 22.2 and 33.3 mM) for 24h. MST1, pMST1 and caspase-3 cleavage were analyzed by western blotting. Western blots show representative results from 2 independent experiments from 2 different donors. Actin was used as loading control. *p<0.05 compared to ND.

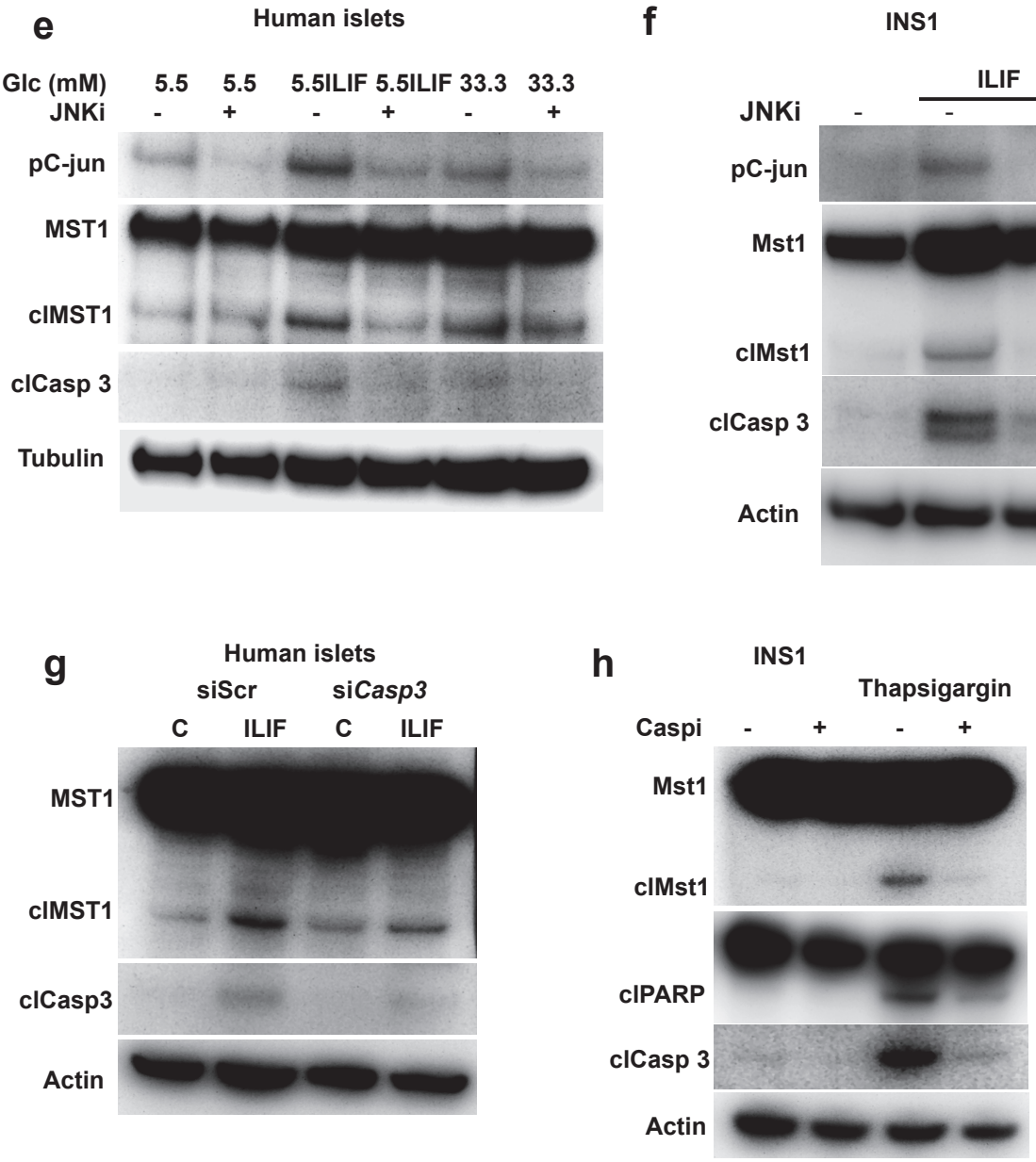

Supplementary Figure 1. (continued)
(e,f) Human islets and INS-1E were pretreated with JNK selective inhibitor, SP600125 (25 μM for human islets, 10 μM for INS-1E cells) or vehicle control for 1h and then exposed to diabetogenic conditions (33.3 mM glucose or IL-1β/IFNγ) for 72h. **(g)** Human islets transfected with caspase-3 siRNA or control siScr and treated with IL/IF for 72h. **(h)** INS-1E cells were pretreated with pan-caspase inhibitor z-DEVD-fmk (50 μM; Caspi) or vehicle control for 1h and then exposed to ER-stress inducer thapsigargin (1 μM) for 6h. MST1, pC-Jun, caspase-3 and PARP cleavage were analyzed by western blotting. All western blots show representative results from 2 independent experiments from 2 donors (human islets). Tubulin/Actin was used as loading control.

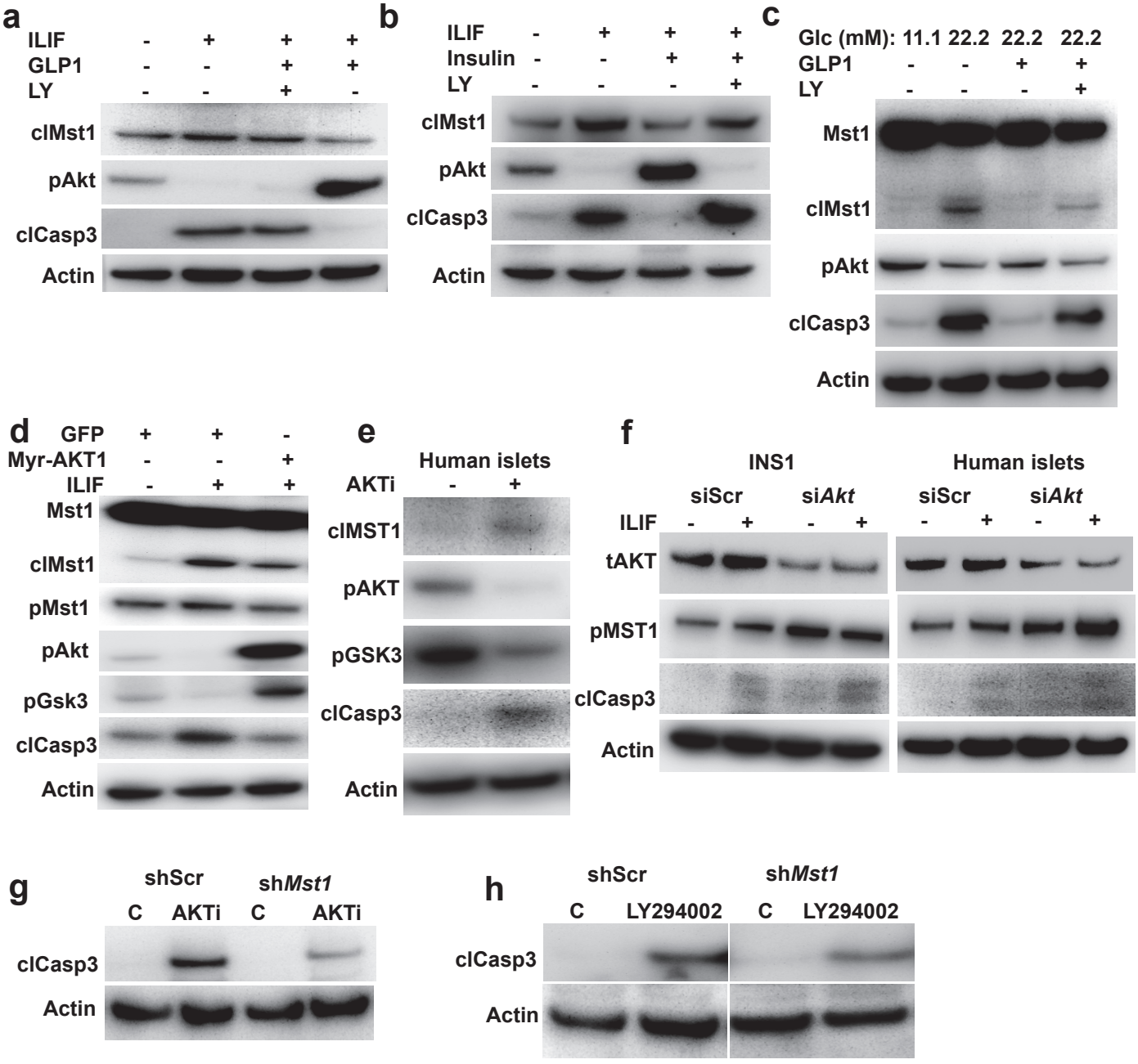

Supplementary Figure 2. MST1-AKT crosstalk.
AKT suppresses MST1 activation and β-cell apoptosis. **(a-c)** INS-1E cells pretreated with **(a,c)** GLP1 (100 nM) or **(b)** insulin (100 nM) with or without PI3K inhibitor LY294002 (10μM) for 1h were exposed to diabetogenic conditions (**a,b**: IL-1β/IFNγ or **c**: 22.2 mM glucose) for 72 h. **(d)** INS-1E cells transfected with GFP control or Myr-AKT1 expression-plasmids and exposed to IL-1β/IFNγ for 72 h. AKT inhibition induces MST1 activation and β-cell apoptosis. **(e)** AKT was inhibited in human islets by exposure to AKT inhibitor Triciribine (20 μM for 24h). **(f)** Human islets and INS-1E cells were transfected with siRNA against Akt1/2/3 and siScr control and treated with IL/IF for 72h. **(g,h)** Stable INS-1E sh*Mst1* and shScr clones were treated with AKT inhibitor (**g**; 10 μM for 6h) or LY294002 (**h**; 10 μM for 8h). MST1, pMST1, tAKT, pAKT, pGSK3 and caspase-3 cleavage were analyzed by western blotting. All western blots show representative results from 2 independent experiments from 2 donors (human islets). Actin was used as loading control.

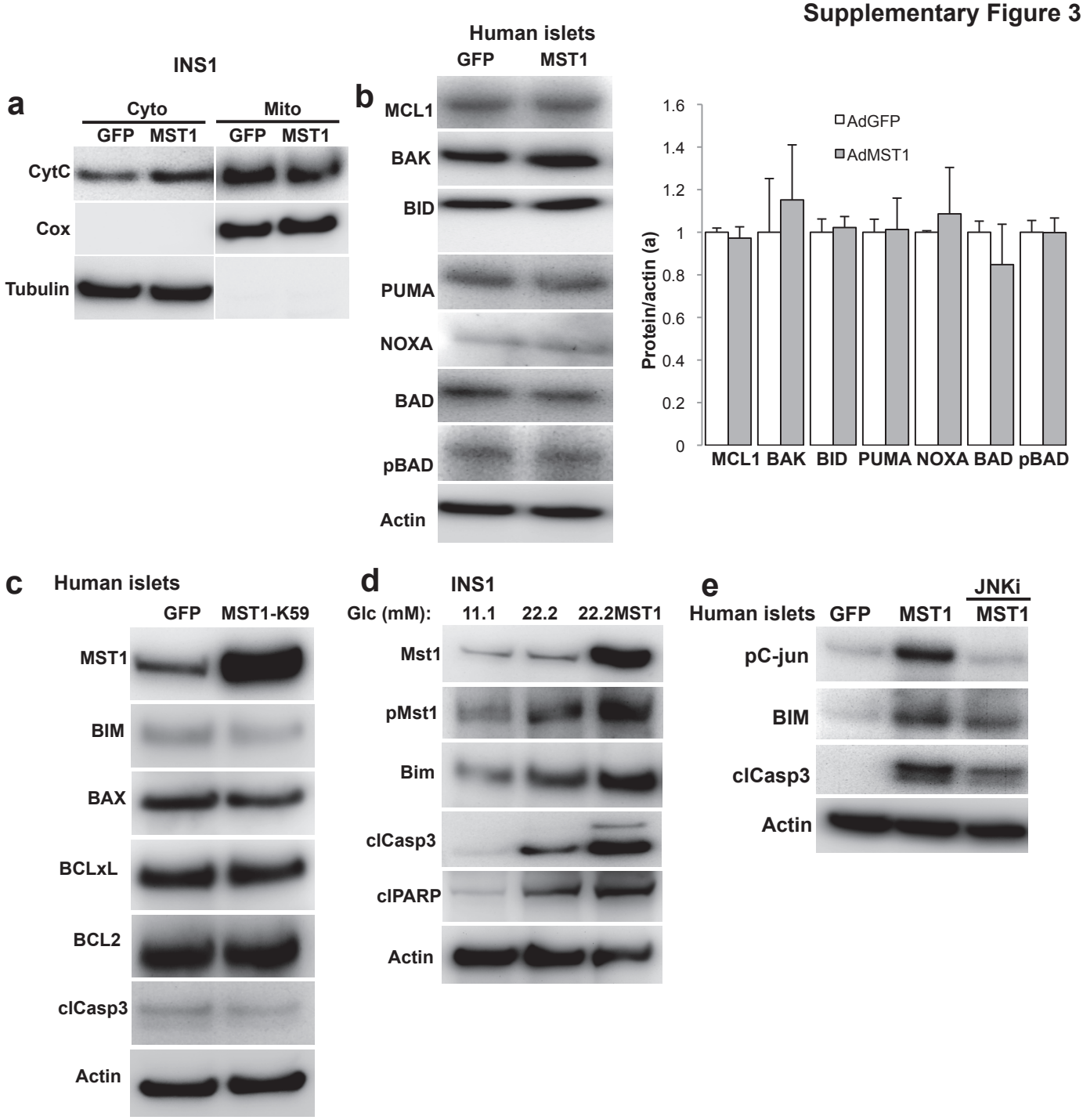

Supplementary Figure 3. MST1 induces beta-cell apoptosis through the mitochondrial apoptotic pathway.

INS-1E cells **(a,d)** and human islets **(b,c,e)** were infected with Ad-GFP or Ad-MST1 or Ad-MST1 (K59). **(a)** Cytochrome c release in INS-1E cells. COX was used to confirm a clean mitochondrial fraction. **(b)** Analysis of the mitochondrial pathway of cell death in Ad-MST1 infected human islets. Right panel shows densitometry analysis from western blots from 3 independent experiments normalized to actin. **(c)** Overexpression of kinase-dead form of MST1 (MST1-K59) does not alter mitochondrial apoptotic pathway nor induces apoptosis. Human islets were infected by Ad-GFP or Ad-MST1 (K59) for 48h. **(d)** INS-1E cells were infected and exposed to 22.2 mM glucose for 48h. **(e)** JNK mediates MST1-induced Bim induction and apoptosis. Human islets were pretreated with JNK selective inhibitor, SP600125 (25 μM) or vehicle control for 1h and infected by Ad-GFP or Ad-MST1 for 48h. MST1, pMST1, BIM, p-c-jun, BAX, BCLxL, BCL2, MCL1, BAK, BID, PUMA, NOXA, BAD, pBAD and caspase-3 and PARP cleavage were analyzed by western blotting. All western blot shows representative results from 3 independent experiments from 3 different donors. Actin/ tubulin was used as loading control.

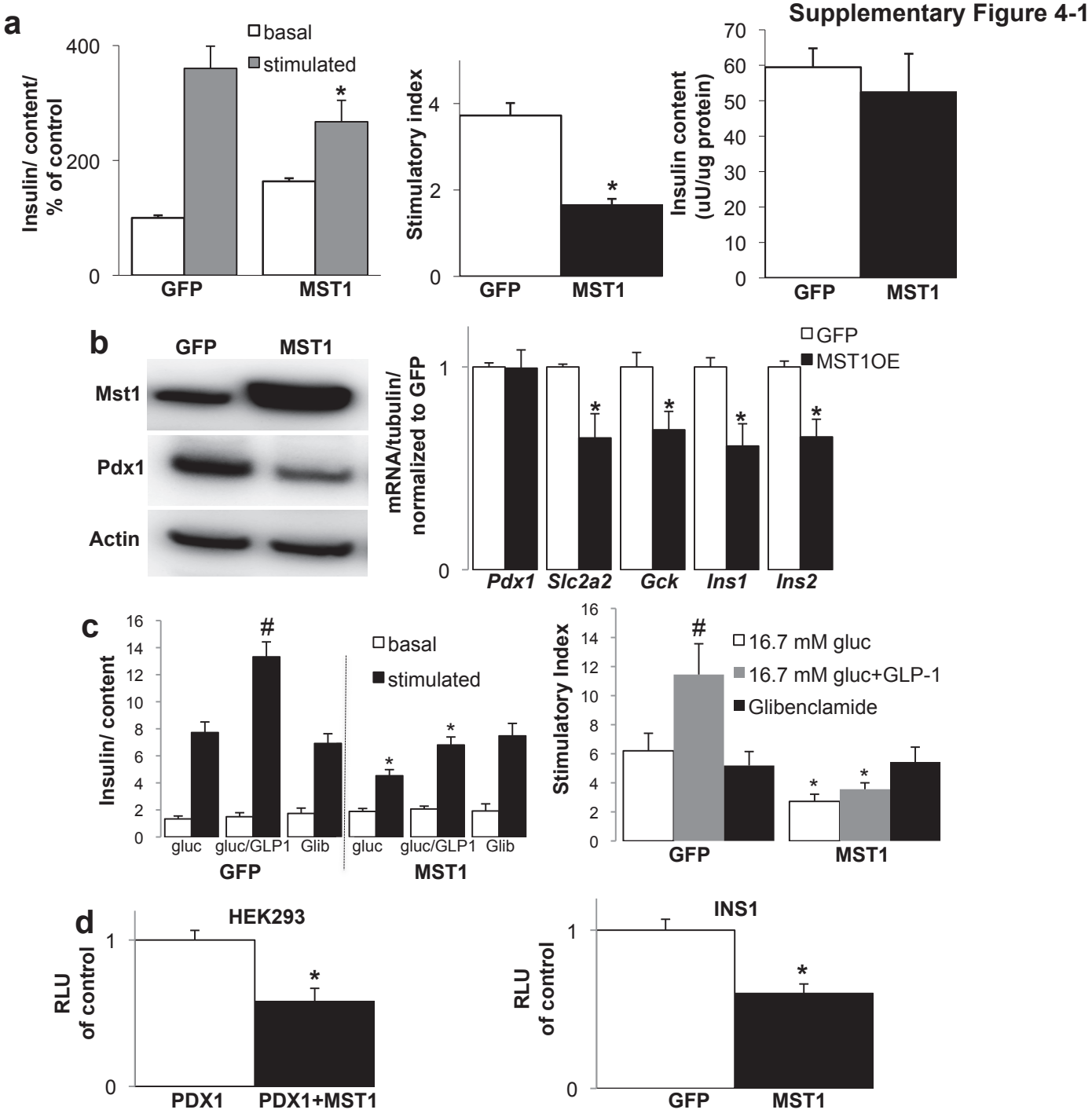

Supplementary Figure 4. MST1 impairs beta-cell function through PDX1 degradation by phosphorylation of PDX1 on T11 site. (a,b) INS-1E cells were infected with Ad-GFP or Ad-MST1 for 96h. **(a)** Insulin secretion during 1h-incubation with 2.8 mM (basal) and 16.7 mM (stimulated) glucose, insulin stimulatory index denotes the ratio of secreted insulin during 1h-incubation with 16.7 mM and 2.8 mM glucose, insulin content was analyzed after the GSIS. **(b)** Mst1 and Pdx1 were analyzed by western blotting and Pdx1 target genes including *Slc2a2, Gck, Ins1* and *Ins2* were analyzed by RT-PCR in INS-1E cells. **(c)** Human islets were infected with Ad-GFP or Ad-MST1 for 96h. Insulin secretion during 1h-incubation with 2.8 mM (basal), 16.7 mM (stimulated), 16.7 mM glucose plus GLP-1 (100nM) and 2.8 mM glucose plus glibenclamide (1uM) and Insulin stimulatory index **(d)** Luciferase reporter assay. HEK293 cells were transfected with PDX1, Ins2-Luc renilla and pCMV-firefly plasmids alone or together with MST1 for 48h (left panel). INS-1E cells transfected with Ins2-Luc renila and pCMV-firefly plasmids and infected with Ad-GFP or Ad-MST1 for 48h (right panel). Data are expressed as RLU (renilla/firefly) normalized to controls. The western blot **(b)** shows representative results from 3 independent experiments. Actin was used as loading control. All other results are shown as means ±SE from 3 independent experiments from 3 independent donors. *p<0.05 MST1-OE compared to GFP-transfected or infected control, same treatment, # p<0.05 GLP-1-treated compared to untreated GFP-infected control.

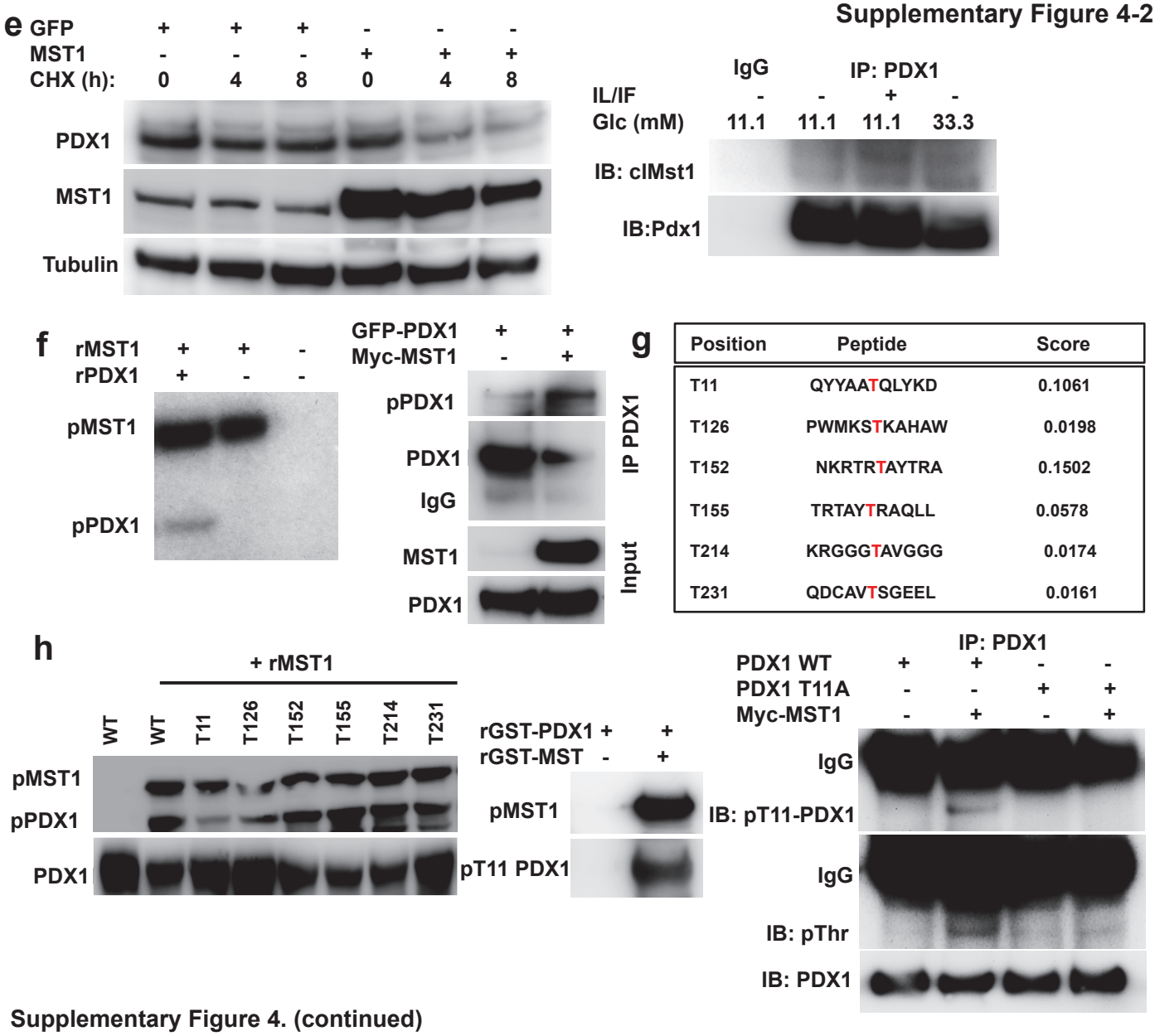

Supplementary Figure 4. (continued)

(e) MST1 destabilizes PDX1 protein in human islets. Human islets were infected with Ad-GFP or Ad-MST1. 48 h after infection, islets were treated with 50 μg/ml cycloheximide (CHX) for different time points (left panel). A diabetogenic milieu increases the PDX1-MST1 interaction. INS-1E cells exposed to 11.1 mM glucose control with or without IL/IF or 33.3 mM glucose for 72 h. Lysates were immunoprecipitated with PDX1 and IgG control antibodies, followed by immunoblotting for Mst1 and Pdx1 (right panel). Representative results from 3 (left panel) or 2 (right panel) independent experiments are shown. **(f)** MST1 phosphorylates PDX1 *in vitro* and *in vivo*. Purified human recombinant MST1 and PDX1 proteins were incubated with ^{32}P-labeled ATP for 30 min at 30°C. Reactions were analyzed by NuPAGE followed by autoradiography (left panel). Lysates of HEK293 cells transfected with GFP-PDX1 alone or together with Myc-MST1 expression plasmids were immunoprecipitated with PDX1 antibody. IP and input fractions were analyzed by NuPAGE followed by western blotting using pan-phospho threonine specific, PDX1 and MST1 antibodies (left panel). **(g)** Potential theoretical PDX1 phosphorylation sites by MST1 were predicted by Netphos 2.0 program. **(h)** The six candidate sites of phosphorylation by MST1 were individually mutated to alanine to generate phospho-deficient mutants. *In vitro* kinase assay was performed by incubating recombinant PDX1-GST fusion proteins including different mutants of PDX1 (purified from bacteria) and GST-MST1. Reaction was analyzed by NuPAGE followed by western blotting using pan-phospho threonine specific and PDX1 antibodies (left panel). Western blot analysis of *in vitro* kinase reaction using phospho-specific antibody generated against phosphorylated T11 form of PDX1 (pT11-PDX1) (middle panel). *In vivo* kinase assay. Lysates of HEK293 cells transfected with PDX1-WT or PDX1-T11A alone or together with Myc-MST1 expressing plasmids, were immunoprecipitated with PDX1 antibody. IP reaction was analyzed by NuPAGE followed by western blotting using pan-phospho threonine, pT11-PDX1 and PDX1 antibodies (right panel). Representative results from 3 independent experiments are shown.

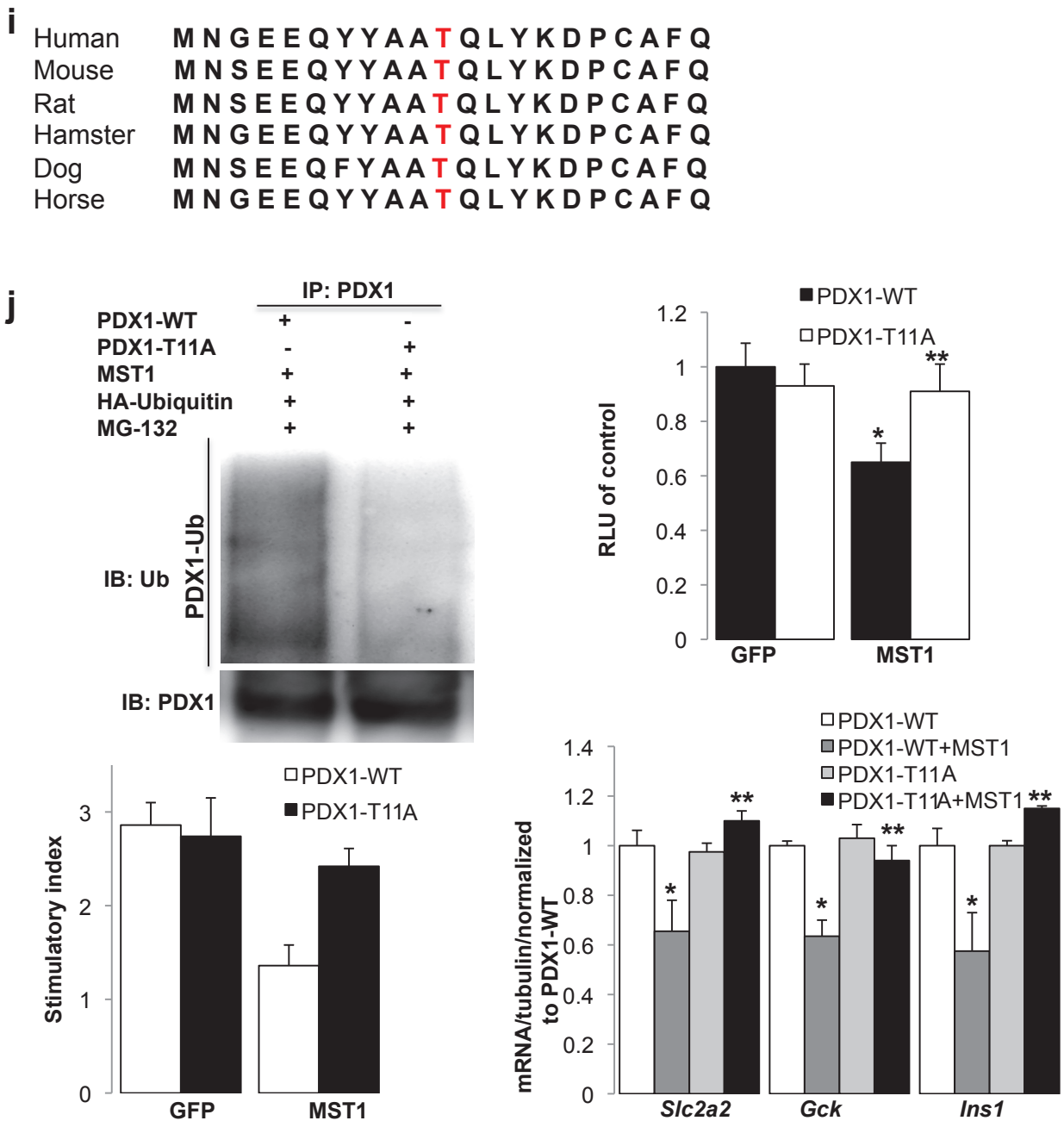

Supplementary Figure 4. (continued)

(i) Alignment of the conserved phosphorylation site in PDX1 (T11, red) from different species. **(j)** *In vivo* ubiquitination assay. HEK293 cells were transfected with PDX1-WT or PDX1-T11A together with Myc-MST1 and HA-ubiquitin expression plasmids for 48h and MG-132 was added during the last 6h of the experiment. Lysates were immunoprecipitated by PDX1 antibody followed by immunoblotting with ubiquitin antibody to detect ubiquitinated PDX1 (upper left panel). Luciferase reporter assay. HEK293 cells were transfected with Ins2-Luc renila, pCMV-firefly, PDX1-WT or PDX1-T11A, alone or together with Myc-MST1 expressing plasmids for 48h. The data expressed as RLU (renilla/firefly) normalized to the PDX1-WT (upper right panel). INS-1E were transfected with PDX1-WT or PDX1-T11A expression-plasmids and infected with Ad-GFP or Ad-MST1 for 72 h (lower panels). Basal (2.8 mM glucose) and stimulated (16.7 mM glucose) insulin secretion was measured during 1h incubation, insulin stimulatory index denotes the ratio of secreted insulin during 1h-incubation with 16.7 mM and 1h-incubation with 2.8 mM glucose (lower left panel). PDX1 target genes in INS-1E cells analyzed by RT-PCR and levels normalized to tubulin shown as change from PDX1-WT transfected INS-1E cells (lower right panel). Representative results in left panels are from 2 independent experiments, results in right panels are shown as means ±SE from 3 independent experiments. *p<0.05 compared to control. **p<0.05 compared to PDX1-WT-MST1.

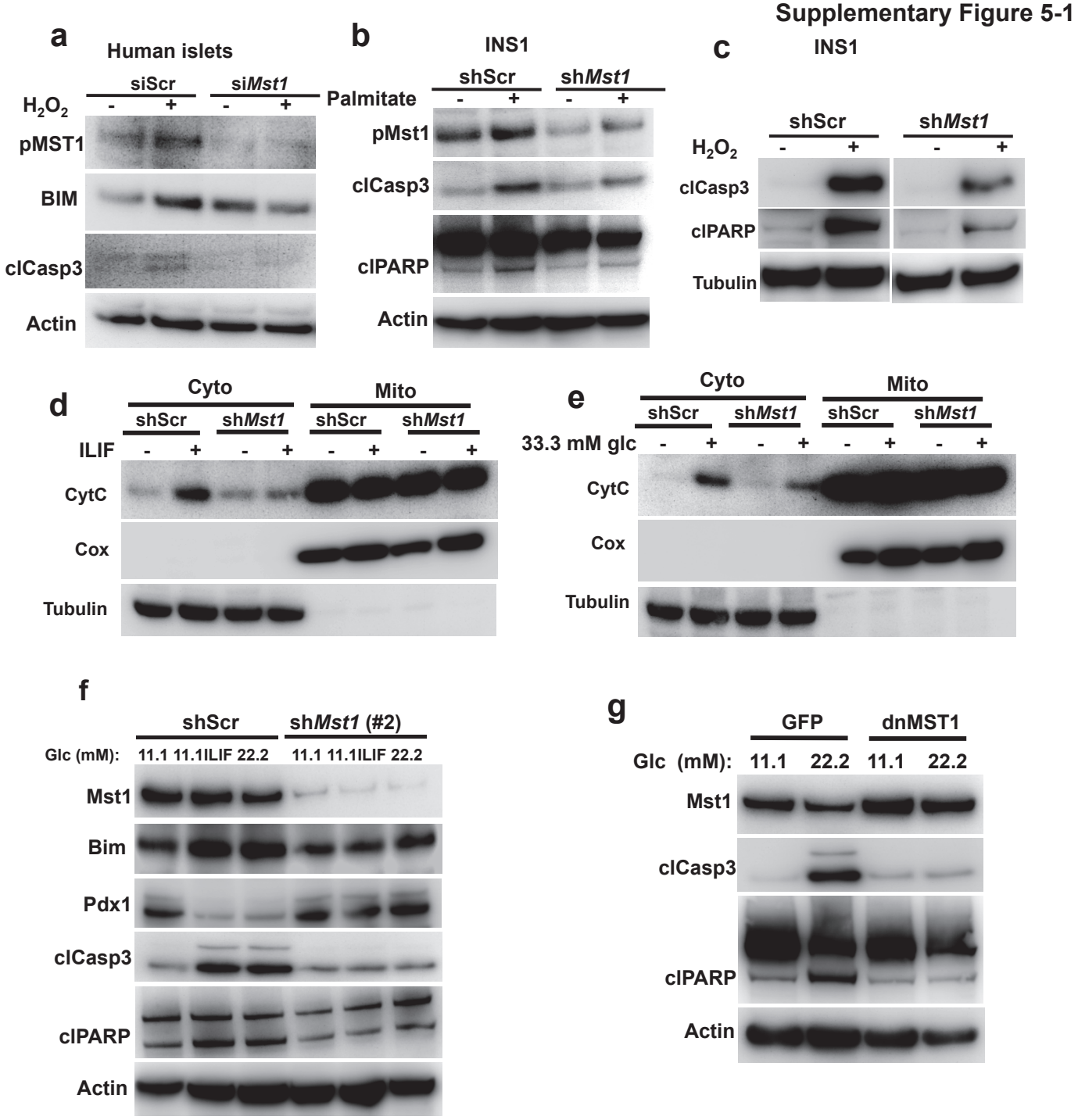

Supplementary Figure 5. MST1 inhibition improves beta-cell survival and function under diabetogenic conditions *in vitro*.

(a) Human islets transfected with MST1 siRNA (smart pool, mixture of 4 siRNA) or control siScr were treated with H_2O_2 for 6h. **(b-e)** Stable INS-1E sh*Mst1* and shScr clones were treated with diabetogenic conditions (**b**: 0.5 mM palmitate for 72h, **c**: 100 µM H_2O_2 for 6h, **d**: cytokine mix IL-1β/IFNγ for 72h or **e**: 33.3 mM glucose). **(d,e)** Cytochrome c release from mitochondria to cytosol was analyzed. **(f)** Stable INS-1E clones were generated by transfection of vectors for sh*Mst1* (clone#2) and shScr control and treated with the cytokines mixture IL/IF or 22.2 mM glucose for 72 hours. **(g)** INS-1E cells were transfected with GFP control or dn-MST1 (K59) plasmids and treated with 22.2 mM glucose for 48h. pMST1, BIM, CytC, Cox, PDX1 and caspase-3 and PARP cleavage were analyzed by western blotting. Western blots show representative results from 3 independent experiments from 3 different donors (human islets). Tubulin/Actin was used as loading control.

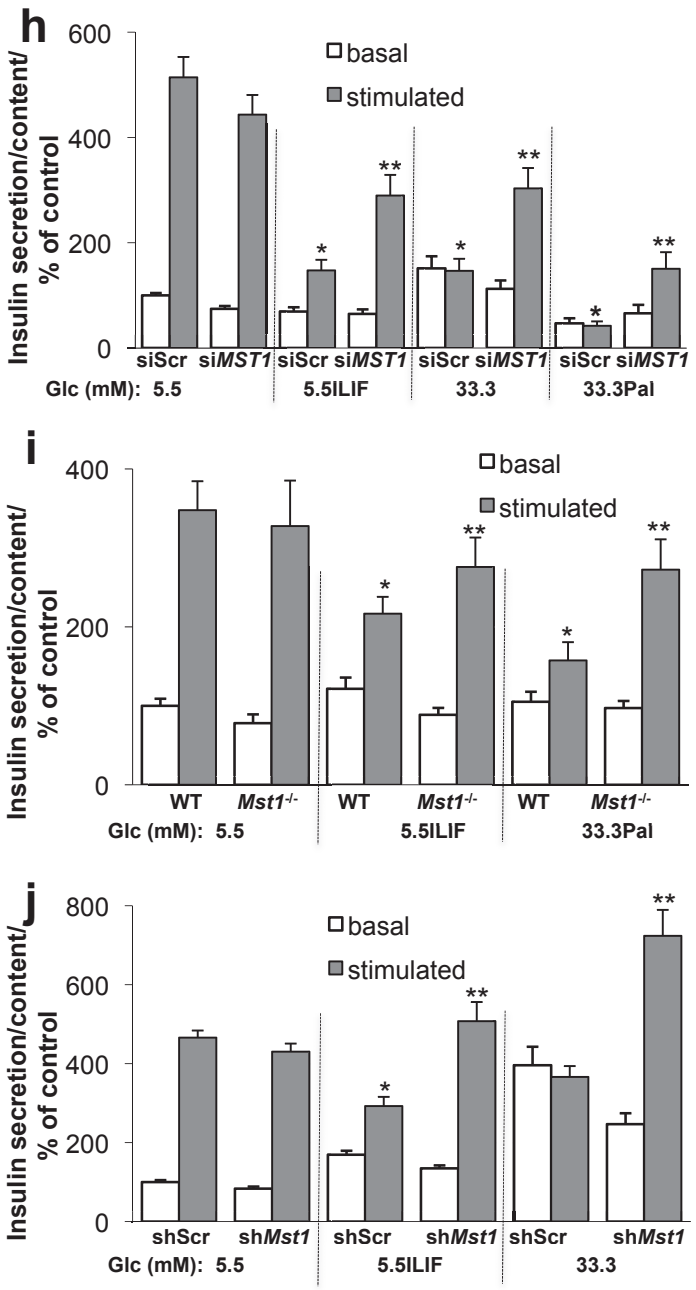

Supplementary Figure 5. (continued)
(h-j) Glucose stimulated insulin secretion (GSIS) during 1h-incubation with 2.8 mM and 16.7 mM glucose, respectively, normalized to insulin content and expressed as % of control basal insulin secretion in **(h)** human islets transfected with siMST1 or siScr, in **(i)** isolated islets from WT and *Mst1*$^{-/-}$ mice or in **(j)** sh*Mst1*-infected INS-1E cells exposed to IL-1β/IFNγ or 33.3 mM glucose for 72 hours. GSIS show pooled results from 3 independent experiments (h-j) from 3 donors (h). *p<0.05 to stimulated untreated control conditions, **p<0.05 to stimulated conditions at sh/siScr/WT control at the same treatment conditions. Respective calculated stimulatory indices are shown for (h) in Fig. 4d, for (i) in Figure 4f and for (j) in Figure 4h.

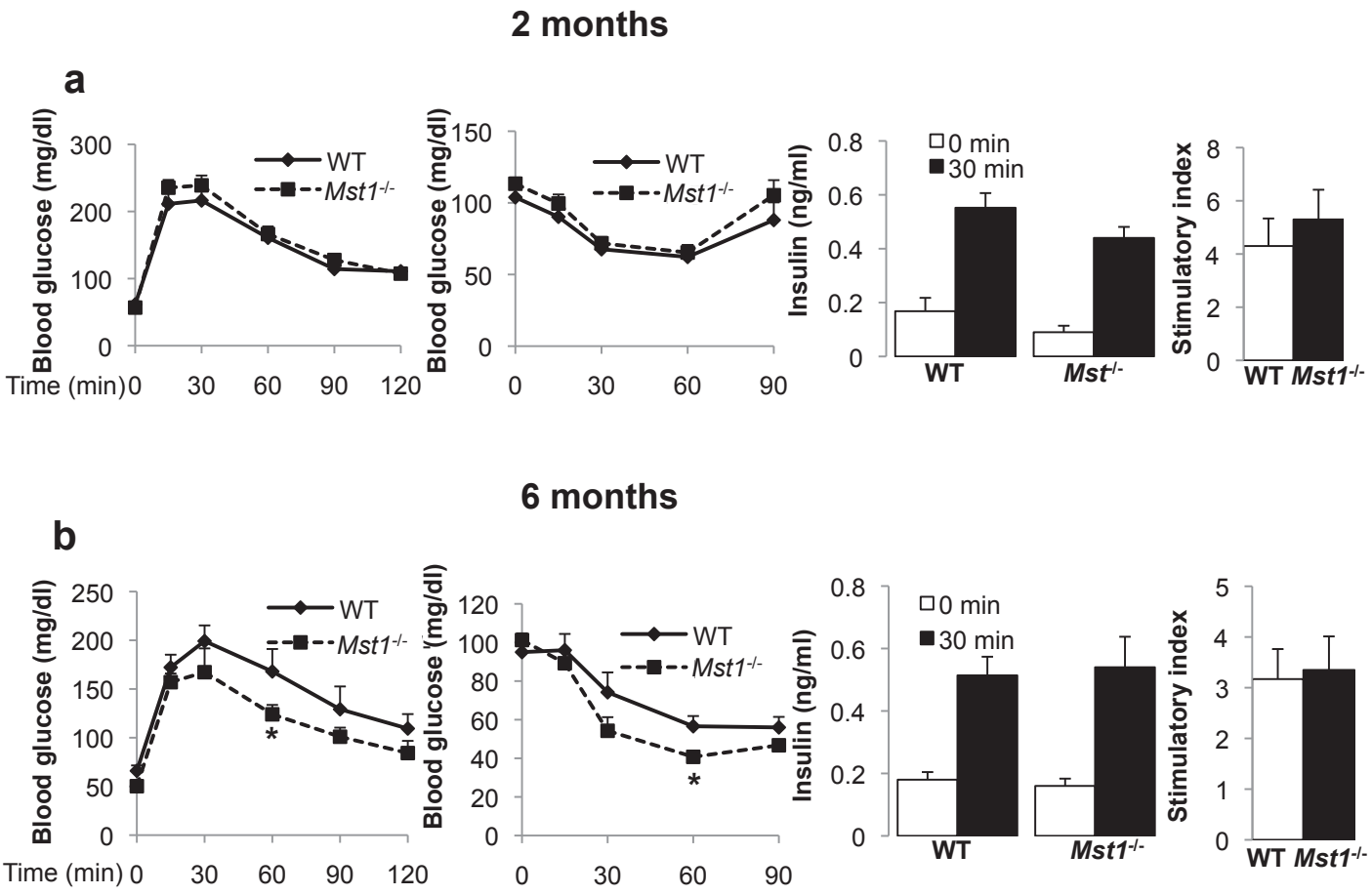

Supplementary Figure 6. ***Mst1*** **deletion has no effect on glycemia nor insulin secretion at normal conditions and protects from STZ-induced diabetes.**
2 month- (**a**; n=9) and 6 month-old (**b**; n=5) *Mst1*$^{-/-}$ mice and their littermates (n=5) were examined. Intraperitoneal glucose tolerance tests (ipGTT) with 1 g/kg BW glucose (left panel). Intraperitoneal insulin tolerance tests (ipITT) with 0.75IU/kg BW insulin (middle panel). Insulin secretion during an ipGTT measured before (0 min) and 30 min after glucose injection and data are expressed as ratio of secreted insulin at 30 min/0 min (stimulatory index) (right panel). *p<0.05 *Mst1*$^{-/-}$ compared to WT.

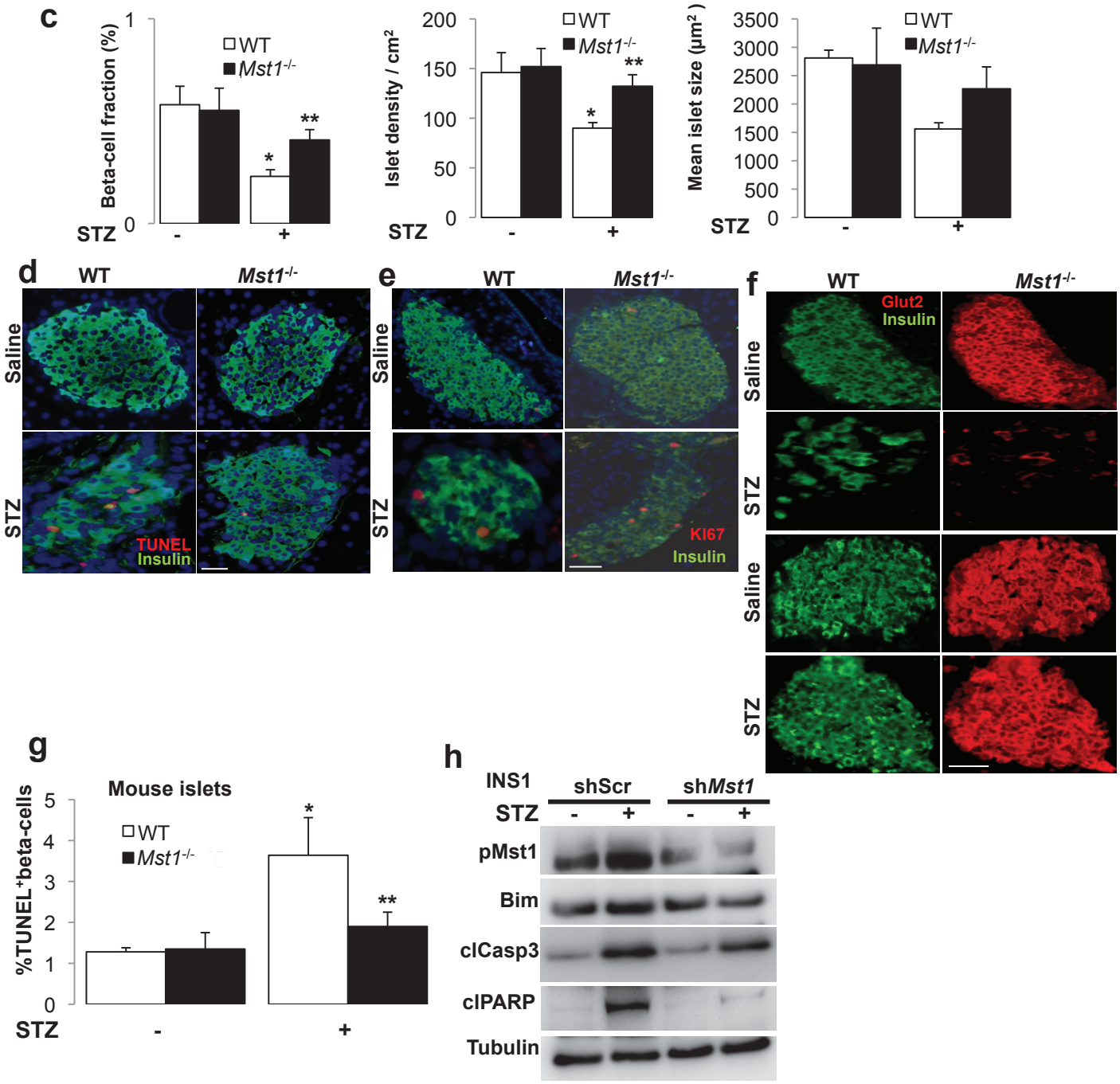

Supplementary Figure 6. (continued)

(c-f) *Mst1*$^{-/-}$ mice (n=15) and their WT littermates (n=14) were injected with 40 mg/kg streptozotocin or citrate buffer for 5 consecutive days and sacrificed at day 22. **(c)** 10 fixed, paraffin embedded pancreas sections per mouse spanning the width of the pancreas were stained for insulin, the percentage of beta-cells of the whole pancreas, islet density/cm^2 pancreas and mean islet size analyzed using NIS-elements microscopic analysis software. **(d-e)** Triple staining for TUNEL **(d)** or Ki67 **(e)** in red, insulin in green and DAPI in blue performed on pancreatic section from different mice groups. **(f)** Representative double-staining for Glut2 (red) and insulin (green) is shown from the different groups. **(g,h)** MST1 deficiency rescued from STZ-induced apoptosis *in vitro*. Cells were exposed to 1mM STZ for 6h. **(g)** Beta-cell apoptosis was analyzed in isolated islets from *Mst1*$^{-/-}$ and control mice by double staining of TUNEL and insulin. Results are expressed as percentage of TUNEL-positive beta-cells ±SE from 3 independent experiments. The mean number of beta-cells scored was 6776 for each treatment condition. **(h)** Stable INS-1E sh*Mst1* and shScr clones; pMst1, Bim, caspase-3 and PARP cleavage were analyzed by western blotting. Western blot shows representative results from 3 independent experiments. Tubulin was used as loading control. *p<0.05 STZ treated compared to vehicle treated control, **p<0.05 *Mst1*$^{-/-}$ compared to WT at same treatment. Scale bar: 100 µM

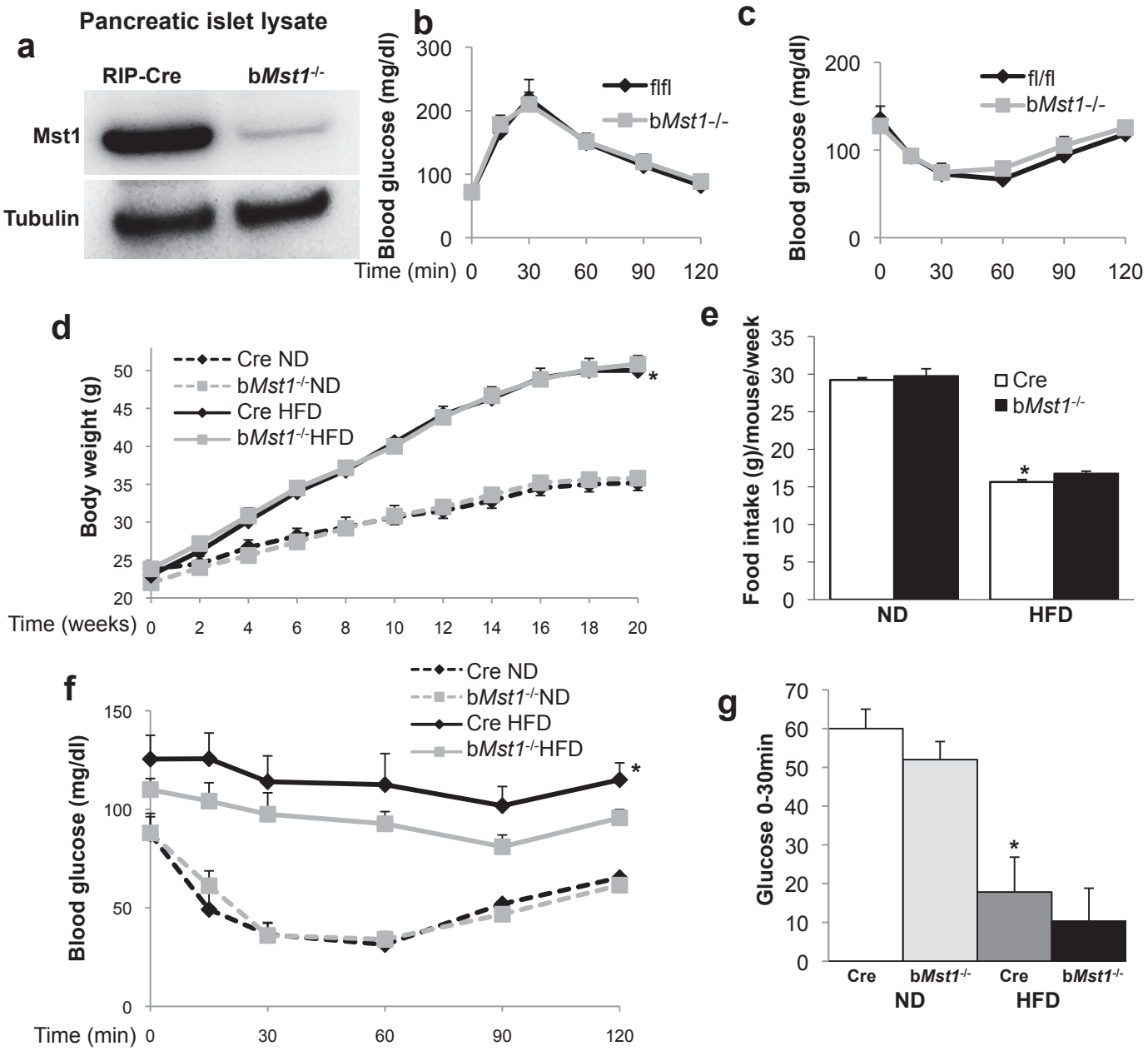

Supplementary Figure 7. Characterization of β-cell specific *Mst1* knockout mice.
(a-c) 2 month-old (n=8) b*Mst1*$^{-/-}$ mice with specific deletion in the beta-cells using the Cre-Lox system and fl/fl controls (n=6) were examined. **(a)** Western blot analysis of protein lysates from the islets of b*Mst1*$^{-/-}$ and Rip-Cre control mice. **(b)** Intraperitoneal glucose tolerance test (ipGTT) with 1 g/kg BW glucose. **(c)** Intraperitoneal insulin tolerance test (ipITT) with 0.75IU/kg BW insulin. **(d-g)** beta-cell specific disruption of *Mst1* has no effect on gain weight, food intake and insulin sensitivity on mice under high-fat diet (HFD). b*Mst1*$^{-/-}$ mice (n=12) and their Rip-Cre controls (n=12) were fed a normal (ND) or a high fat/-high sucrose diet (HFD) for 20 weeks. **(d,e)** Body weight/mouse and average weekly food intake/mouse. **(f,g)** Intraperitoneal insulin tolerance tests (ipITT) with 0.75IU/kg BW insulin, **(g)** the difference of the highest (0 min) and lowest (30 min) glucose concentration was calculated. Data show mean ± SE. *p<0.05 Cre HFD compared to Cre ND.

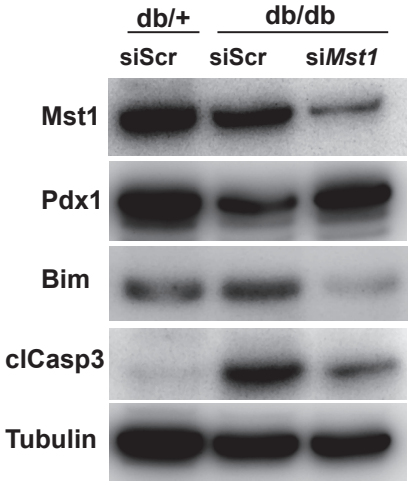

Supplementary Figure 8. Mst1 silencing rescued db/db islets from apoptosis through PDX1 restoration and Bim suppression.
Islets were isolated from diabetic 10-week old db/db mice and their heterozygous non-diabetic littermate controls (db/+) and transfected with siScr control and siMST1. Mst1, Pdx1, Bim and caspase-3 cleavage were analyzed by western blotting. Tubulin was used as loading control. Results are from 3 mice/genotype.

Supplementary information

MST1 is a novel regulator of apoptosis in pancreatic beta-cells

Nature Medicine: doi:10.1038/nm.3482

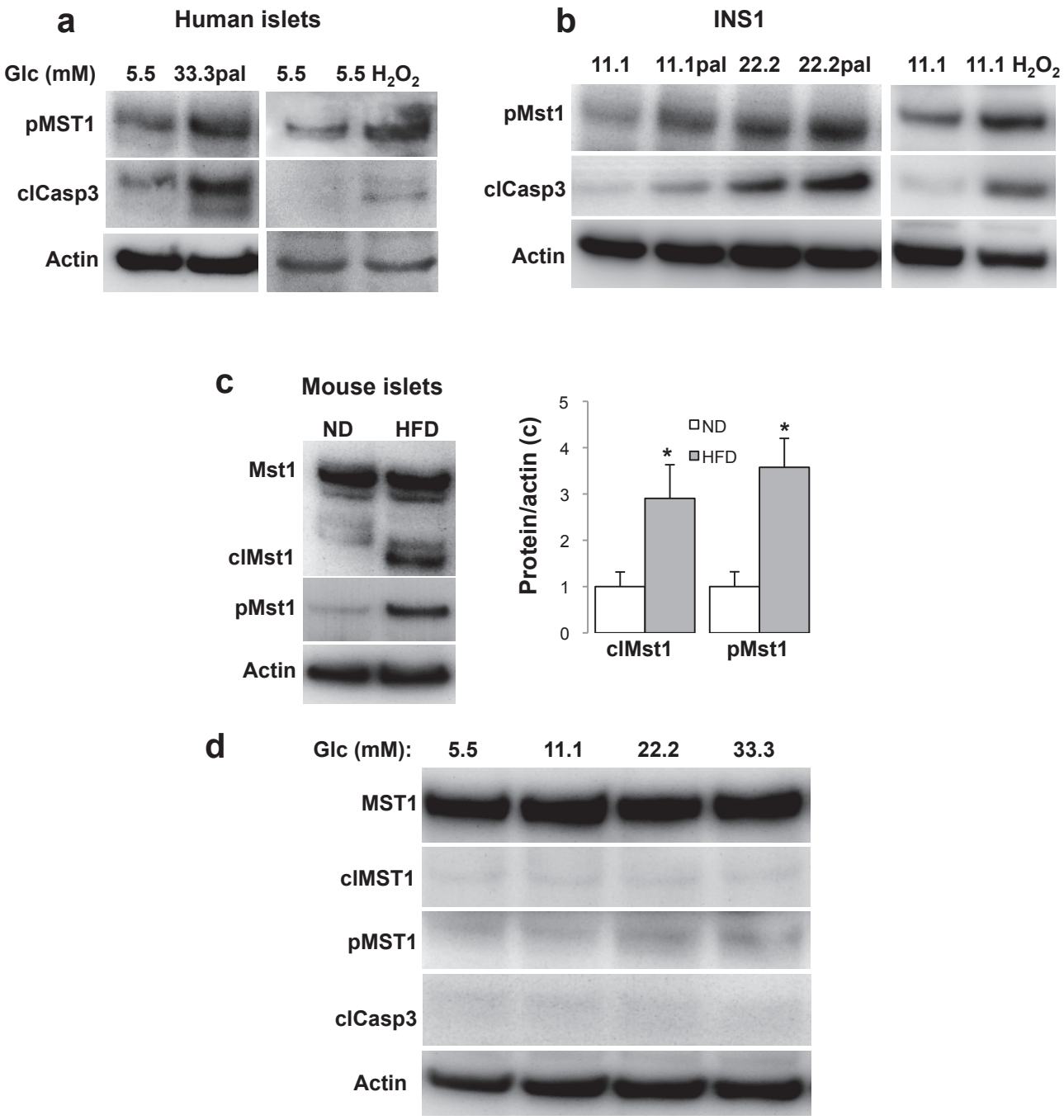

Supplementary Figure 1. Diabetogenic conditions induce MST1 activation and JNK and caspase-3 are responsible for stress-induced MST1 cleavage and apoptosis.
(a) Human islets and **(b)** INS-1E cells exposed to diabetogenic conditions (22.2 or 33.3 mM glucose, 0.5 mM palmitate or the mixture of 22.2 or 33.3 mM glucose and 0.5 mM palmitate (33.3Pal) for 72h (human islets) and 24h (INS-1E cells) or 100 μM H_2O_2 for 6h). **(c)** Isolated islets from normal diet (ND) (n=3) or high fat/high sucrose (HFD)-fed (n=3) mice treated for 16 weeks. Right panel shows densitometry analysis normalized to actin from 3 mice per condition. Western blots show representative results from 3 independent experiments from 3 different donors or mice. **(d)** Short term culture of human islets with high glucose does not induce MST1 activation and apoptosis. Human islets exposed to different concentration of high glucose (11.1, 22.2 and 33.3 mM) for 24h. MST1, pMST1 and caspase-3 cleavage were analyzed by western blotting. Western blots show representative results from 2 independent experiments from 2 different donors. Actin was used as loading control. *p<0.05 compared to ND.

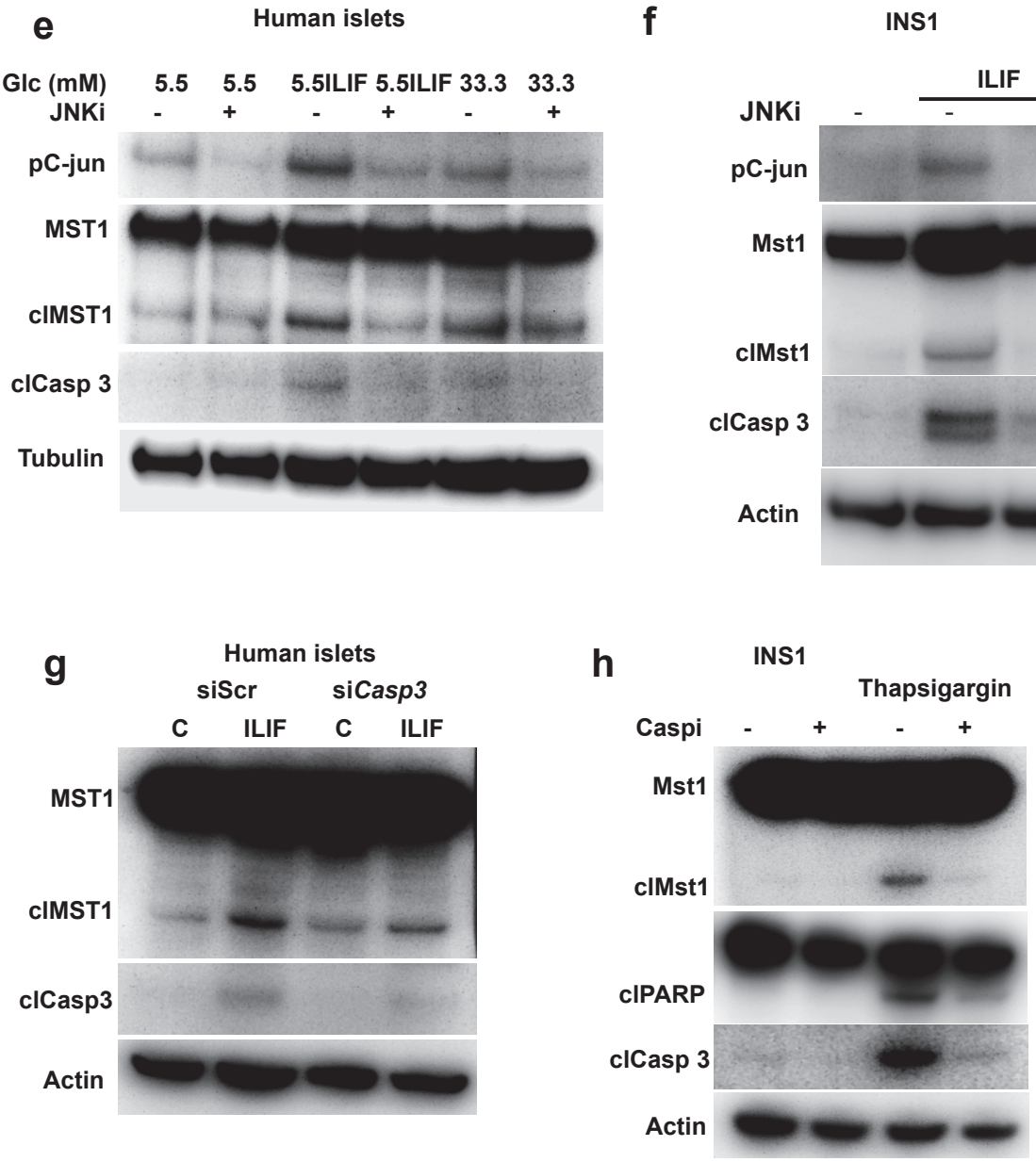

Supplementary Figure 1. (continued)
(e,f) Human islets and INS-1E were pretreated with JNK selective inhibitor, SP600125 (25 μM for human islets, 10 μM for INS-1E cells) or vehicle control for 1h and then exposed to diabetogenic conditions (33.3 mM glucose or IL-1β/IFNγ) for 72h. **(g)** Human islets transfected with caspase-3 siRNA or control siScr and treated with IL/IF for 72h. **(h)** INS-1E cells were pretreated with pan-caspase inhibitor z-DEVD-fmk (50 μM; Caspi) or vehicle control for 1h and then exposed to ER-stress inducer thapsigargin (1 μM) for 6h. MST1, pC-Jun, caspase-3 and PARP cleavage were analyzed by western blotting. All western blots show representative results from 2 independent experiments from 2 donors (human islets). Tubulin/Actin was used as loading control.

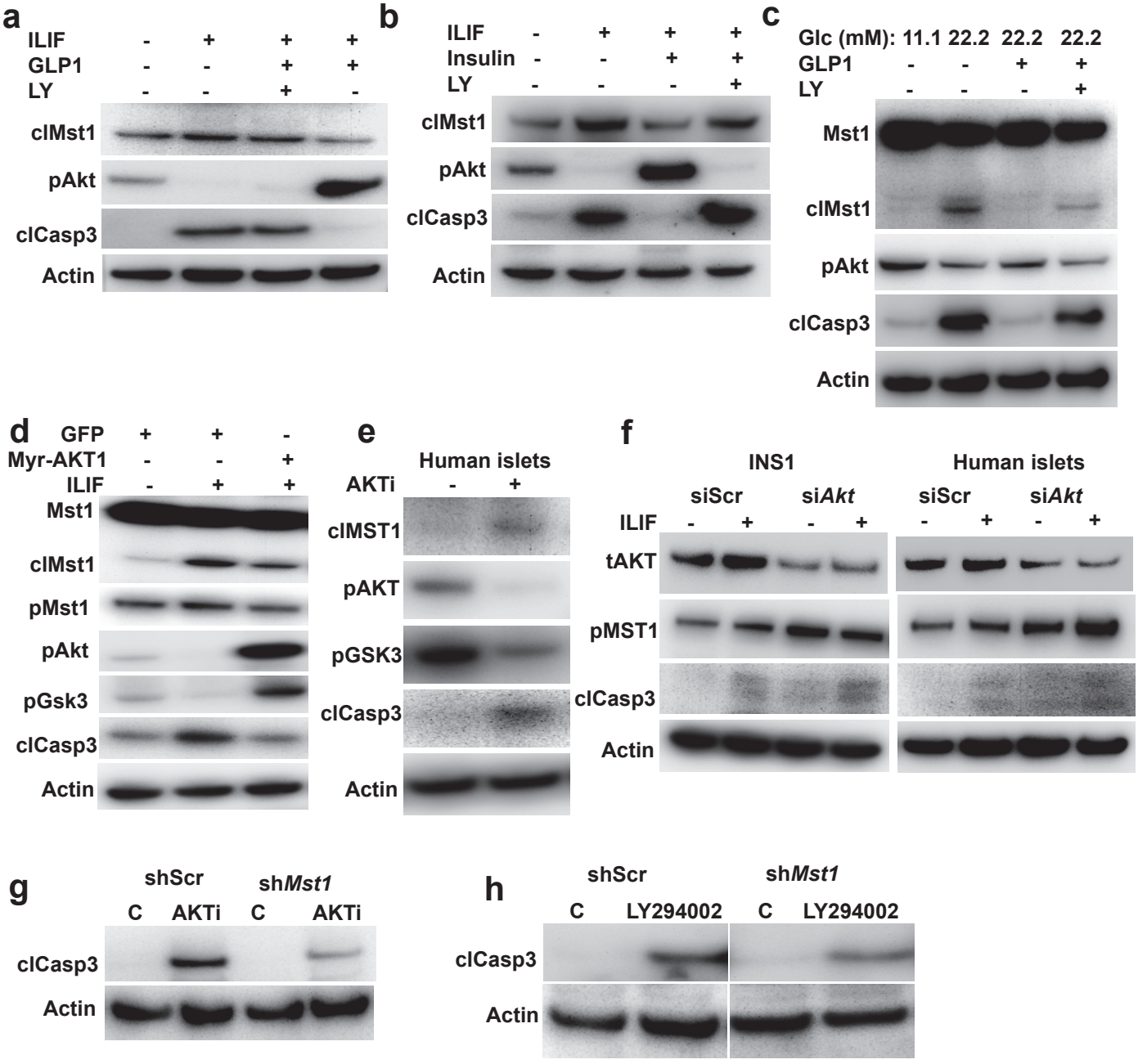

Supplementary Figure 2. MST1-AKT crosstalk.
AKT suppresses MST1 activation and β-cell apoptosis. **(a-c)** INS-1E cells pretreated with **(a,c)** GLP1 (100 nM) or **(b)** insulin (100 nM) with or without PI3K inhibitor LY294002 (10μM) for 1h were exposed to diabetogenic conditions (**a,b**: IL-1β/IFNγ or **c**: 22.2 mM glucose) for 72 h. **(d)** INS-1E cells transfected with GFP control or Myr-AKT1 expression-plasmids and exposed to IL-1β/IFNγ for 72 h. AKT inhibition induces MST1 activation and β-cell apoptosis. **(e)** AKT was inhibited in human islets by exposure to AKT inhibitor Triciribine (20 μM for 24h). **(f)** Human islets and INS-1E cells were transfected with siRNA against Akt1/2/3 and siScr control and treated with IL/IF for 72h. **(g,h)** Stable INS-1E sh*Mst1* and shScr clones were treated with AKT inhibitor (**g**; 10 μM for 6h) or LY294002 (**h**; 10 μM for 8h). MST1, pMST1, tAKT, pAKT, pGSK3 and caspase-3 cleavage were analyzed by western blotting. All western blots show representative results from 2 independent experiments from 2 donors (human islets). Actin was used as loading control.

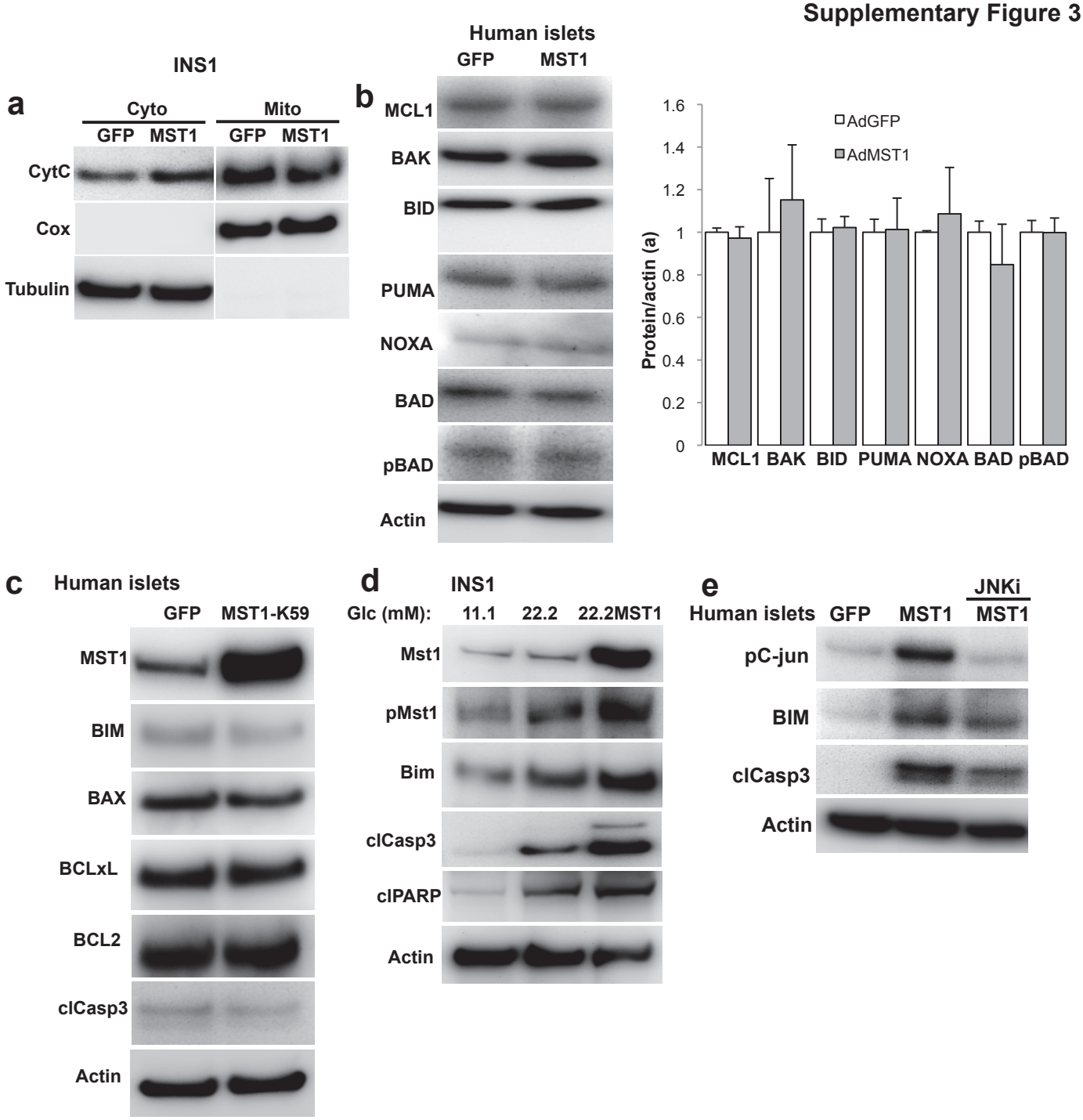

Supplementary Figure 3. MST1 induces beta-cell apoptosis through the mitochondrial apoptotic pathway.

INS-1E cells **(a,d)** and human islets **(b,c,e)** were infected with Ad-GFP or Ad-MST1 or Ad-MST1 (K59). **(a)** Cytochrome c release in INS-1E cells. COX was used to confirm a clean mitochondrial fraction. **(b)** Analysis of the mitochondrial pathway of cell death in Ad-MST1 infected human islets. Right panel shows densitometry analysis from western blots from 3 independent experiments normalized to actin. **(c)** Overexpression of kinase-dead form of MST1 (MST1-K59) does not alter mitochondrial apoptotic pathway nor induces apoptosis. Human islets were infected by Ad-GFP or Ad-MST1 (K59) for 48h. **(d)** INS-1E cells were infected and exposed to 22.2 mM glucose for 48h. **(e)** JNK mediates MST1-induced Bim induction and apoptosis. Human islets were pretreated with JNK selective inhibitor, SP600125 (25 μM) or vehicle control for 1h and infected by Ad-GFP or Ad-MST1 for 48h. MST1, pMST1, BIM, p-c-jun, BAX, BCLxL, BCL2, MCL1, BAK, BID, PUMA, NOXA, BAD, pBAD and caspase-3 and PARP cleavage were analyzed by western blotting. All western blot shows representative results from 3 independent experiments from 3 different donors. Actin/ tubulin was used as loading control.

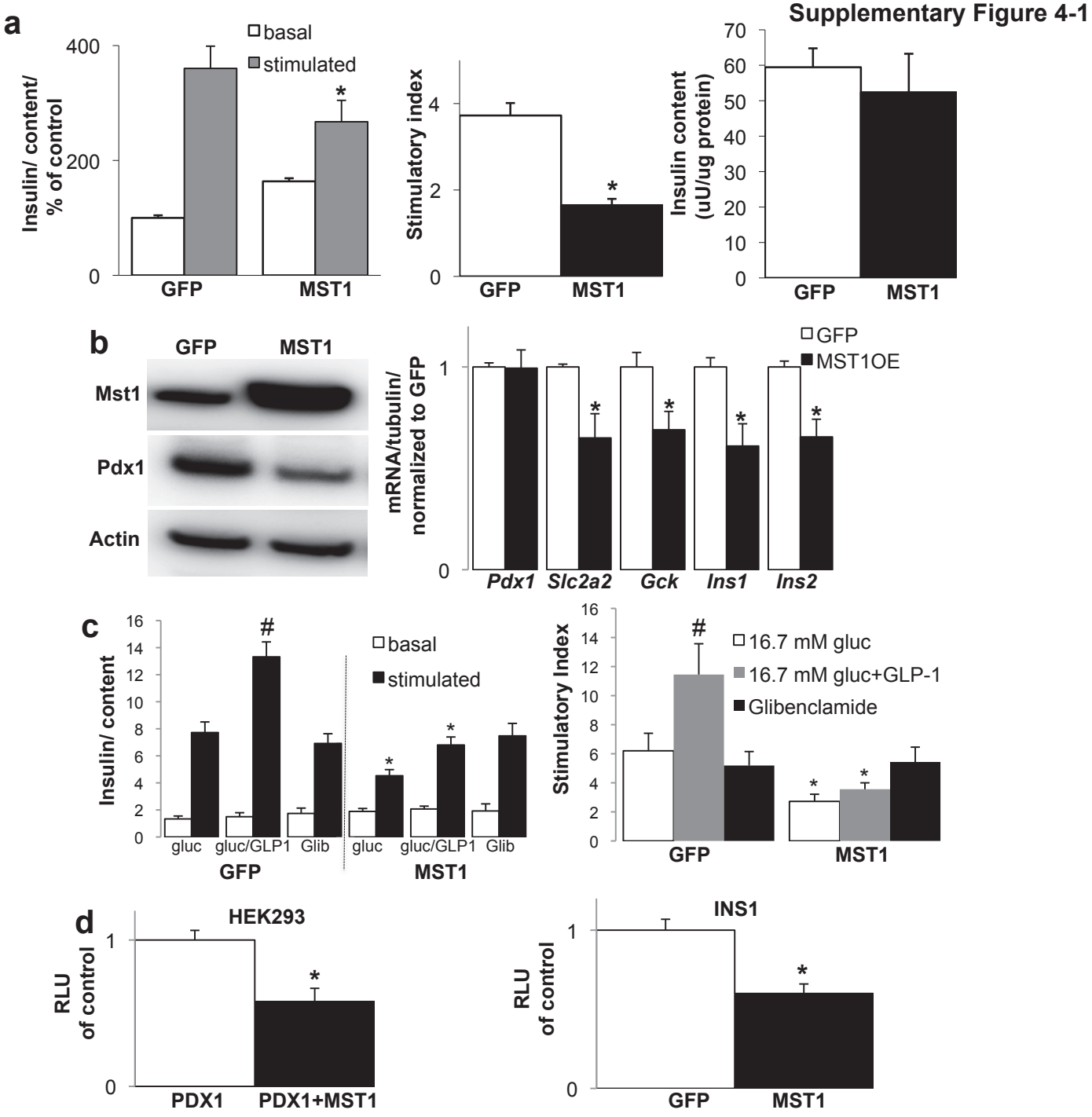

Supplementary Figure 4. MST1 impairs beta-cell function through PDX1 degradation by phosphorylation of PDX1 on T11 site. (a,b) INS-1E cells were infected with Ad-GFP or Ad-MST1 for 96h. **(a)** Insulin secretion during 1h-incubation with 2.8 mM (basal) and 16.7 mM (stimulated) glucose, insulin stimulatory index denotes the ratio of secreted insulin during 1h-incubation with 16.7 mM and 2.8 mM glucose, insulin content was analyzed after the GSIS. **(b)** Mst1 and Pdx1 were analyzed by western blotting and Pdx1 target genes including *Slc2a2, Gck, Ins1* and *Ins2* were analyzed by RT-PCR in INS-1E cells. **(c)** Human islets were infected with Ad-GFP or Ad-MST1 for 96h. Insulin secretion during 1h-incubation with 2.8 mM (basal), 16.7 mM (stimulated), 16.7 mM glucose plus GLP-1 (100nM) and 2.8 mM glucose plus glibenclamide (1uM) and Insulin stimulatory index **(d)** Luciferase reporter assay. HEK293 cells were transfected with PDX1, Ins2-Luc renilla and pCMV-firefly plasmids alone or together with MST1 for 48h (left panel). INS-1E cells transfected with Ins2-Luc renila and pCMV-firefly plasmids and infected with Ad-GFP or Ad-MST1 for 48h (right panel). Data are expressed as RLU (renilla/firefly) normalized to controls. The western blot **(b)** shows representative results from 3 independent experiments. Actin was used as loading control. All other results are shown as means ±SE from 3 independent experiments from 3 independent donors. *p<0.05 MST1-OE compared to GFP-transfected or infected control, same treatment, # p<0.05 GLP-1-treated compared to untreated GFP-infected control.

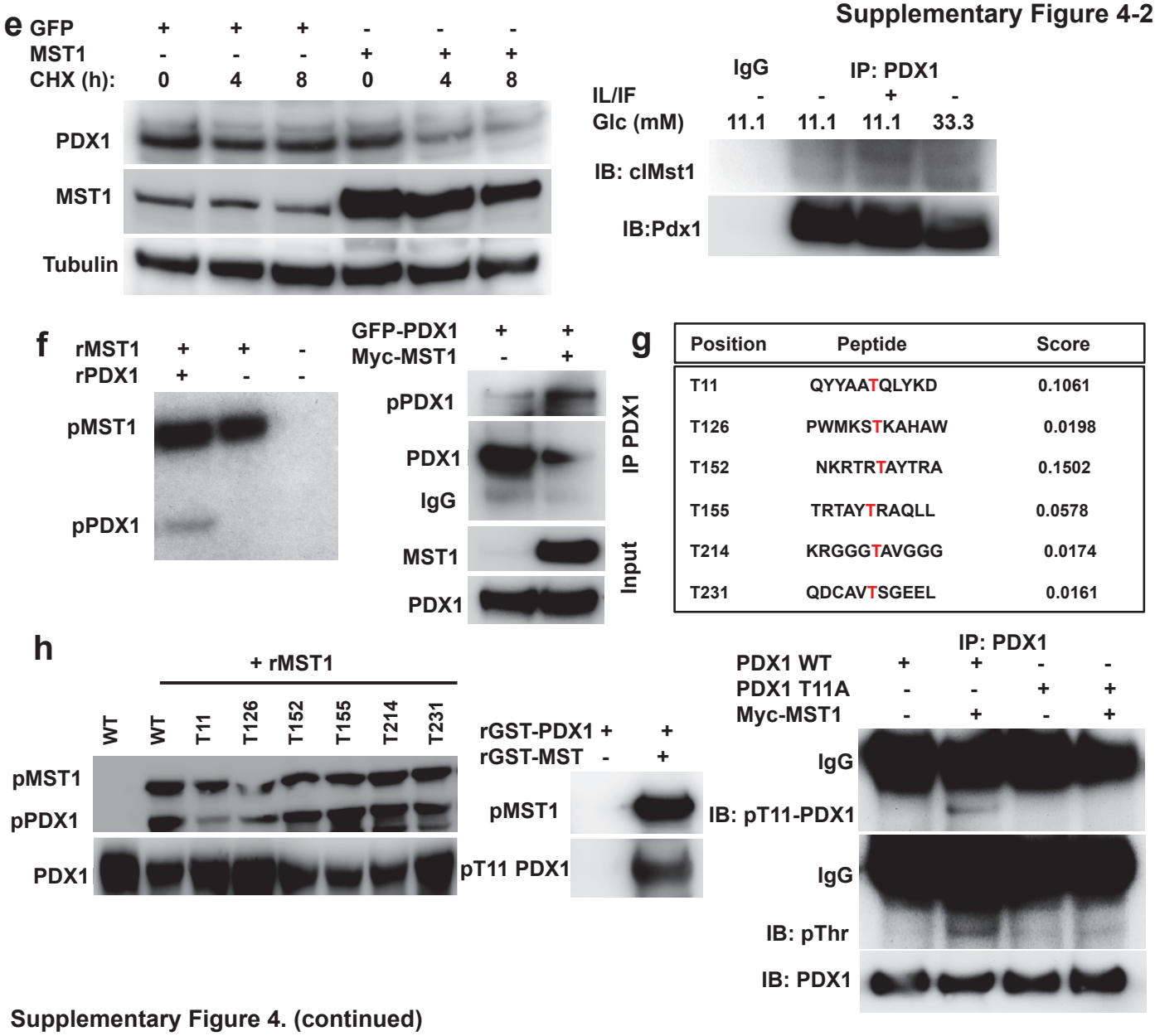

Supplementary Figure 4. (continued)

(e) MST1 destabilizes PDX1 protein in human islets. Human islets were infected with Ad-GFP or Ad-MST1. 48 h after infection, islets were treated with 50 μg/ml cycloheximide (CHX) for different time points (left panel). A diabetogenic milieu increases the PDX1-MST1 interaction. INS-1E cells exposed to 11.1 mM glucose control with or without IL/IF or 33.3 mM glucose for 72 h. Lysates were immunoprecipitated with PDX1 and IgG control antibodies, followed by immunoblotting for Mst1 and Pdx1 (right panel). Representative results from 3 (left panel) or 2 (right panel) independent experiments are shown. **(f)** MST1 phosphorylates PDX1 *in vitro* and *in vivo*. Purified human recombinant MST1 and PDX1 proteins were incubated with ^{32}P-labeled ATP for 30 min at 30°C. Reactions were analyzed by NuPAGE followed by autoradiography (left panel). Lysates of HEK293 cells transfected with GFP-PDX1 alone or together with Myc-MST1 expression plasmids were immunoprecipitated with PDX1 antibody. IP and input fractions were analyzed by NuPAGE followed by western blotting using pan-phospho threonine specific, PDX1 and MST1 antibodies (left panel). **(g)** Potential theoretical PDX1 phosphorylation sites by MST1 were predicted by Netphos 2.0 program. **(h)** The six candidate sites of phosphorylation by MST1 were individually mutated to alanine to generate phospho-deficient mutants. *In vitro* kinase assay was performed by incubating recombinant PDX1-GST fusion proteins including different mutants of PDX1 (purified from bacteria) and GST-MST1. Reaction was analyzed by NuPAGE followed by western blotting using pan-phospho threonine specific and PDX1 antibodies (left panel). Western blot analysis of *in vitro* kinase reaction using phospho-specific antibody generated against phosphorylated T11 form of PDX1 (pT11-PDX1) (middle panel). *In vivo* kinase assay. Lysates of HEK293 cells transfected with PDX1-WT or PDX1-T11A alone or together with Myc-MST1 expressing plasmids, were immunoprecipitated with PDX1 antibody. IP reaction was analyzed by NuPAGE followed by western blotting using pan-phospho threonine, pT11-PDX1 and PDX1 antibodies (right panel). Representative results from 3 independent experiments are shown.

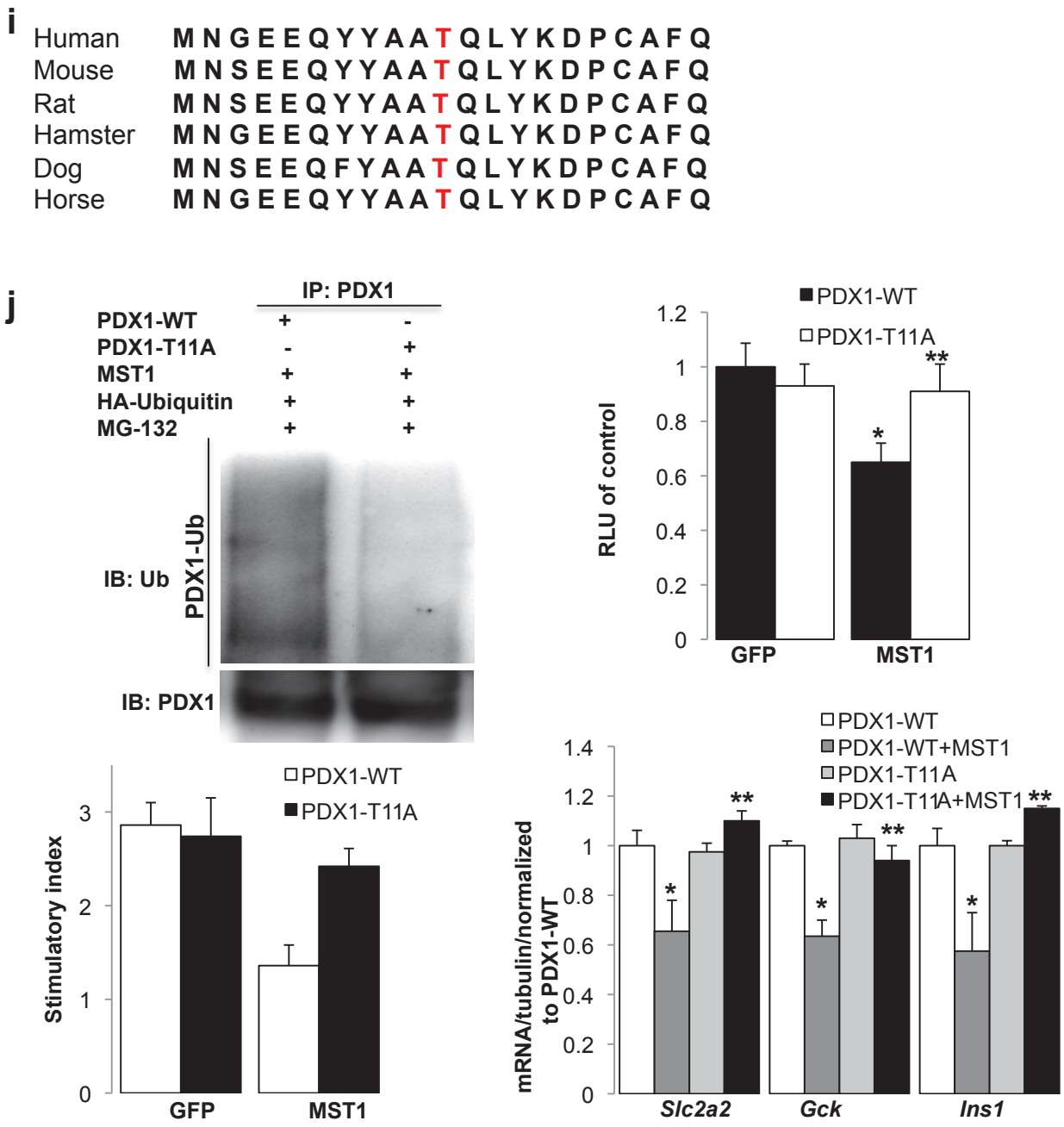

Supplementary Figure 4. (continued)

(i) Alignment of the conserved phosphorylation site in PDX1 (T11, red) from different species. **(j)** *In vivo* ubiquitination assay. HEK293 cells were transfected with PDX1-WT or PDX1-T11A together with Myc-MST1 and HA-ubiquitin expression plasmids for 48h and MG-132 was added during the last 6h of the experiment. Lysates were immunoprecipitated by PDX1 antibody followed by immunoblotting with ubiquitin antibody to detect ubiquitinated PDX1 (upper left panel). Luciferase reporter assay. HEK293 cells were transfected with Ins2-Luc renila, pCMV-firefly, PDX1-WT or PDX1-T11A, alone or together with Myc-MST1 expressing plasmids for 48h. The data expressed as RLU (renilla/firefly) normalized to the PDX1-WT (upper right panel). INS-1E were transfected with PDX1-WT or PDX1-T11A expression-plasmids and infected with Ad-GFP or Ad-MST1 for 72 h (lower panels). Basal (2.8 mM glucose) and stimulated (16.7 mM glucose) insulin secretion was measured during 1h incubation, insulin stimulatory index denotes the ratio of secreted insulin during 1h-incubation with 16.7 mM and 1h-incubation with 2.8 mM glucose (lower left panel). PDX1 target genes in INS-1E cells analyzed by RT-PCR and levels normalized to tubulin shown as change from PDX1-WT transfected INS-1E cells (lower right panel). Representative results in left panels are from 2 independent experiments, results in right panels are shown as means ±SE from 3 independent experiments. *p<0.05 compared to control. **p<0.05 compared to PDX1-WT-MST1.

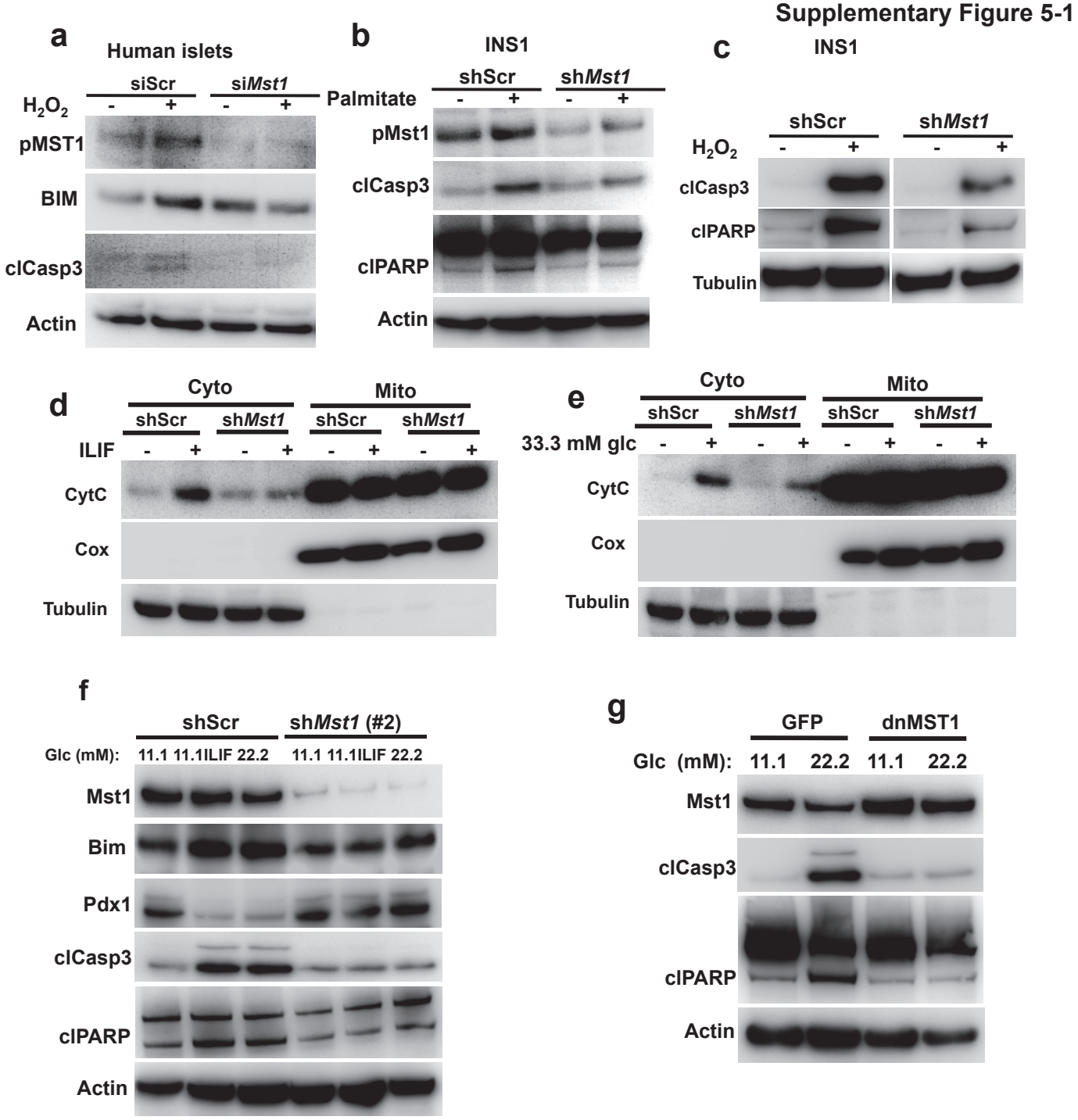

Supplementary Figure 5. MST1 inhibition improves beta-cell survival and function under diabetogenic conditions *in vitro*.

(a) Human islets transfected with MST1 siRNA (smart pool, mixture of 4 siRNA) or control siScr were treated with H_2O_2 for 6h. **(b-e)** Stable INS-1E sh*Mst1* and shScr clones were treated with diabetogenic conditions (**b**: 0.5 mM palmitate for 72h, **c**: 100 µM H_2O_2 for 6h, **d**: cytokine mix IL-1β/IFNγ for 72h or **e**: 33.3 mM glucose). **(d,e)** Cytochrome c release from mitochondria to cytosol was analyzed. **(f)** Stable INS-1E clones were generated by transfection of vectors for sh*Mst1* (clone#2) and shScr control and treated with the cytokines mixture IL/IF or 22.2 mM glucose for 72 hours. **(g)** INS-1E cells were transfected with GFP control or dn-MST1 (K59) plasmids and treated with 22.2 mM glucose for 48h. pMST1, BIM, CytC, Cox, PDX1 and caspase-3 and PARP cleavage were analyzed by western blotting. Western blots show representative results from 3 independent experiments from 3 different donors (human islets). Tubulin/Actin was used as loading control.

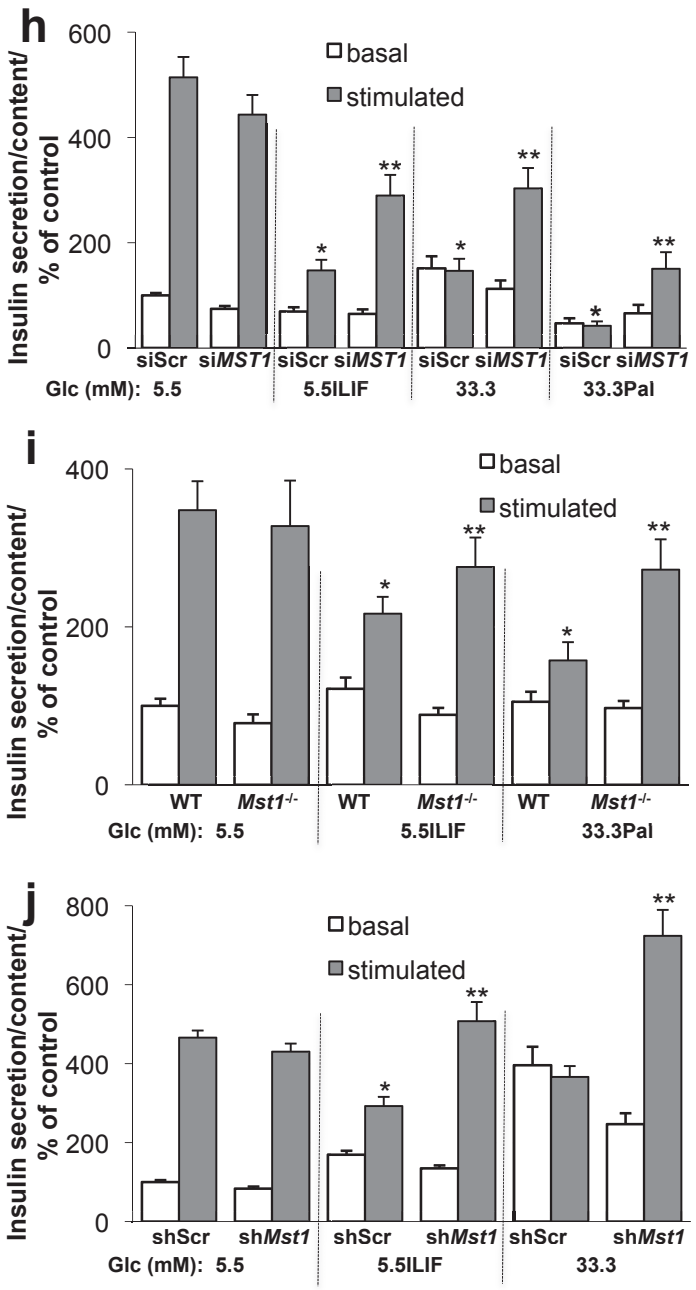

Supplementary Figure 5. (continued)
(h-j) Glucose stimulated insulin secretion (GSIS) during 1h-incubation with 2.8 mM and 16.7 mM glucose, respectively, normalized to insulin content and expressed as % of control basal insulin secretion in **(h)** human islets transfected with siMST1 or siScr, in **(i)** isolated islets from WT and *Mst1*$^{-/-}$ mice or in **(j)** sh*Mst1*-infected INS-1E cells exposed to IL-1β/IFNγ or 33.3 mM glucose for 72 hours. GSIS show pooled results from 3 independent experiments (h-j) from 3 donors (h). *p<0.05 to stimulated untreated control conditions, **p<0.05 to stimulated conditions at sh/siScr/WT control at the same treatment conditions. Respective calculated stimulatory indices are shown for (h) in Fig. 4d, for (i) in Figure 4f and for (j) in Figure 4h.

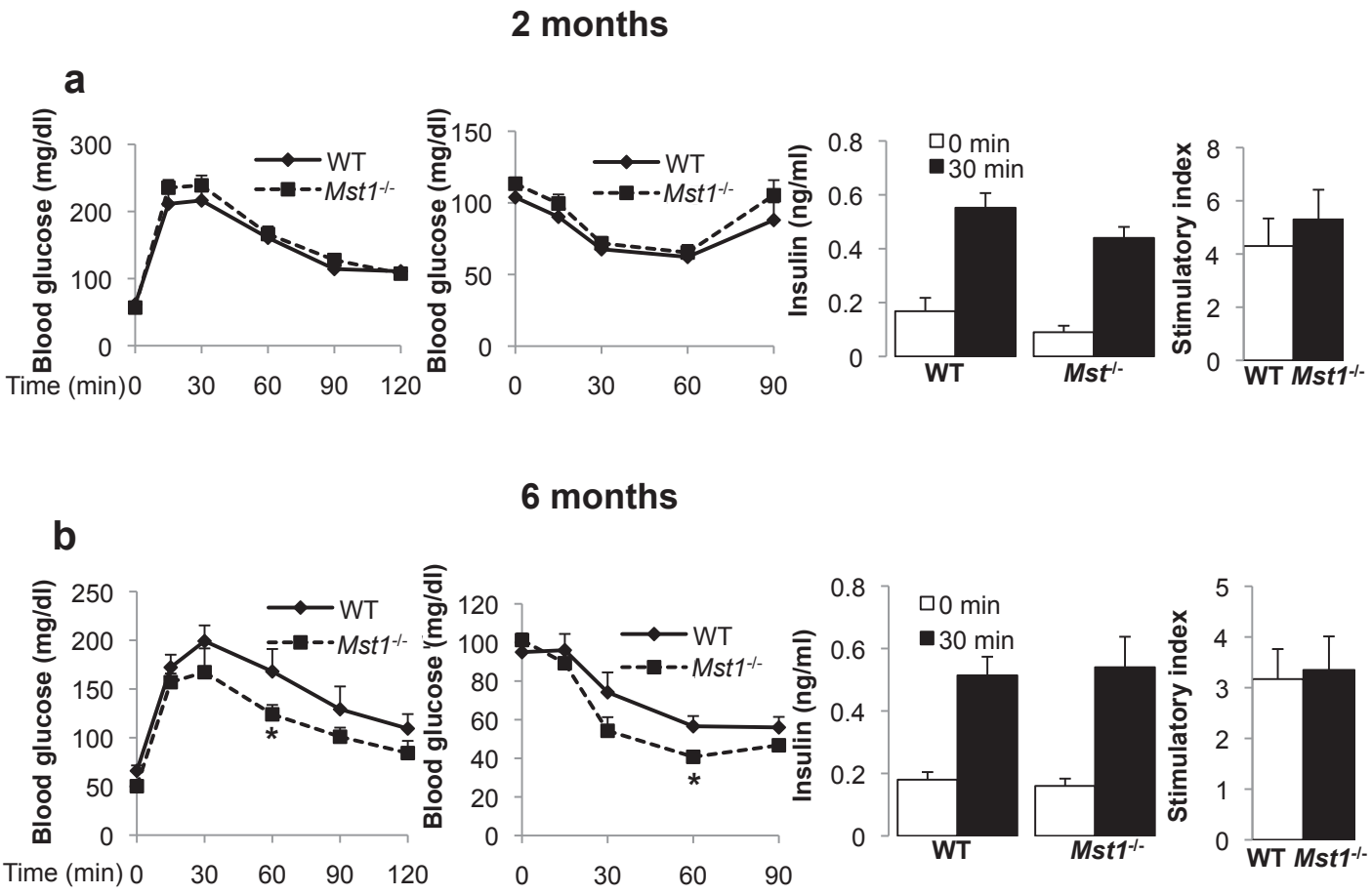

Supplementary Figure 6. ***Mst1*** **deletion has no effect on glycemia nor insulin secretion at normal conditions and protects from STZ-induced diabetes.**
2 month- (**a**; n=9) and 6 month-old (**b**; n=5) *Mst1*$^{-/-}$ mice and their littermates (n=5) were examined. Intraperitoneal glucose tolerance tests (ipGTT) with 1 g/kg BW glucose (left panel). Intraperitoneal insulin tolerance tests (ipITT) with 0.75IU/kg BW insulin (middle panel). Insulin secretion during an ipGTT measured before (0 min) and 30 min after glucose injection and data are expressed as ratio of secreted insulin at 30 min/0 min (stimulatory index) (right panel). *p<0.05 *Mst1*$^{-/-}$ compared to WT.

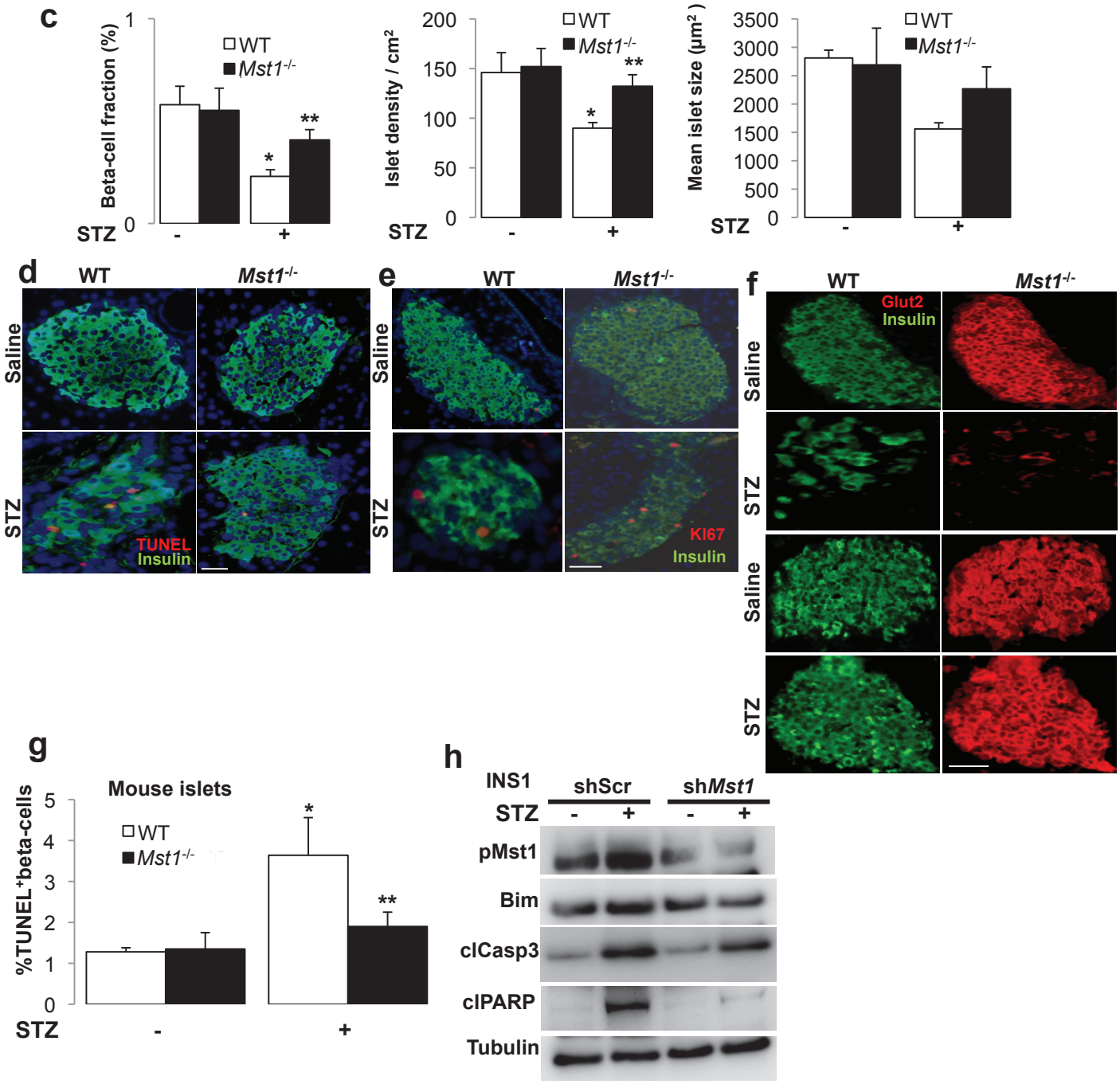

Supplementary Figure 6. (continued)

(c-f) *Mst1*$^{-/-}$ mice (n=15) and their WT littermates (n=14) were injected with 40 mg/kg streptozotocin or citrate buffer for 5 consecutive days and sacrificed at day 22. **(c)** 10 fixed, paraffin embedded pancreas sections per mouse spanning the width of the pancreas were stained for insulin, the percentage of beta-cells of the whole pancreas, islet density/cm^2 pancreas and mean islet size analyzed using NIS-elements microscopic analysis software. **(d-e)** Triple staining for TUNEL **(d)** or Ki67 **(e)** in red, insulin in green and DAPI in blue performed on pancreatic section from different mice groups. **(f)** Representative double-staining for Glut2 (red) and insulin (green) is shown from the different groups. **(g,h)** MST1 deficiency rescued from STZ-induced apoptosis *in vitro*. Cells were exposed to 1mM STZ for 6h. **(g)** Beta-cell apoptosis was analyzed in isolated islets from *Mst1*$^{-/-}$ and control mice by double staining of TUNEL and insulin. Results are expressed as percentage of TUNEL-positive beta-cells ±SE from 3 independent experiments. The mean number of beta-cells scored was 6776 for each treatment condition. **(h)** Stable INS-1E sh*Mst1* and shScr clones; pMst1, Bim, caspase-3 and PARP cleavage were analyzed by western blotting. Western blot shows representative results from 3 independent experiments. Tubulin was used as loading control. *p<0.05 STZ treated compared to vehicle treated control, **p<0.05 *Mst1*$^{-/-}$ compared to WT at same treatment. Scale bar: 100 µM

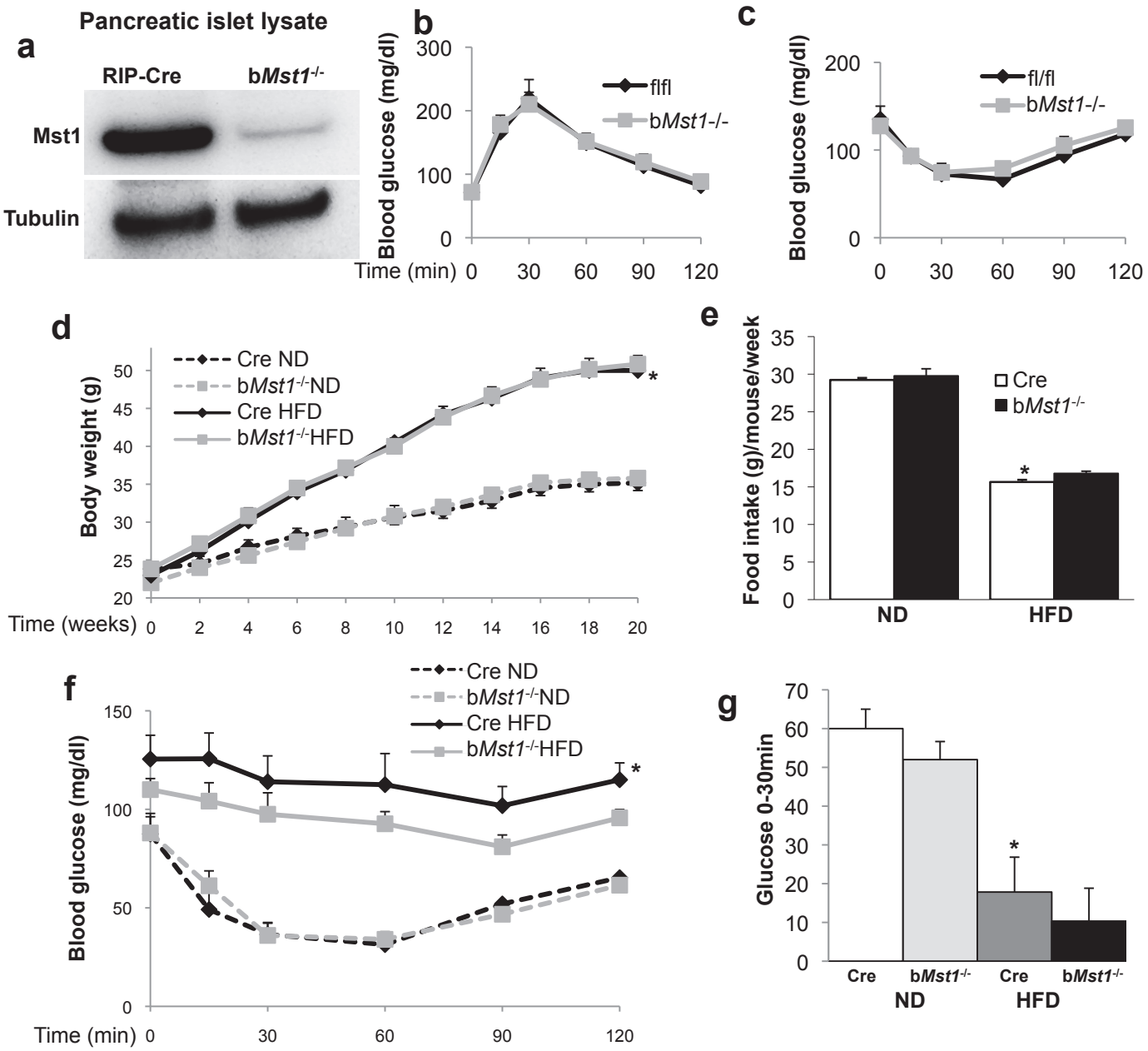

Supplementary Figure 7. Characterization of β-cell specific *Mst1* knockout mice.
(a-c) 2 month-old (n=8) b*Mst1*$^{-/-}$ mice with specific deletion in the beta-cells using the Cre-Lox system and fl/fl controls (n=6) were examined. **(a)** Western blot analysis of protein lysates from the islets of b*Mst1*$^{-/-}$ and Rip-Cre control mice. **(b)** Intraperitoneal glucose tolerance test (ipGTT) with 1 g/kg BW glucose. **(c)** Intraperitoneal insulin tolerance test (ipITT) with 0.75IU/kg BW insulin. **(d-g)** beta-cell specific disruption of *Mst1* has no effect on gain weight, food intake and insulin sensitivity on mice under high-fat diet (HFD). b*Mst1*$^{-/-}$ mice (n=12) and their Rip-Cre controls (n=12) were fed a normal (ND) or a high fat/-high sucrose diet (HFD) for 20 weeks. **(d,e)** Body weight/mouse and average weekly food intake/mouse. **(f,g)** Intraperitoneal insulin tolerance tests (ipITT) with 0.75IU/kg BW insulin, **(g)** the difference of the highest (0 min) and lowest (30 min) glucose concentration was calculated. Data show mean ± SE. *p<0.05 Cre HFD compared to Cre ND.

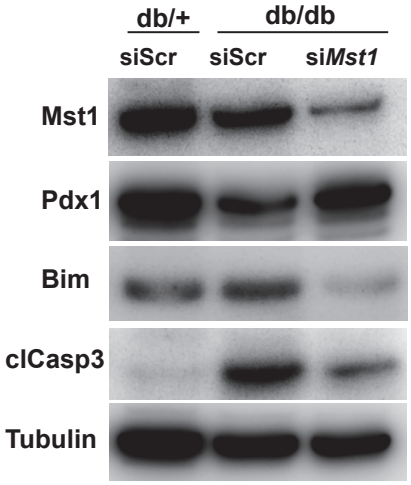

Supplementary Figure 8. Mst1 silencing rescued db/db islets from apoptosis through PDX1 restoration and Bim suppression.
Islets were isolated from diabetic 10-week old db/db mice and their heterozygous non-diabetic littermate controls (db/+) and transfected with siScr control and siMST1. Mst1, Pdx1, Bim and caspase-3 cleavage were analyzed by western blotting. Tubulin was used as loading control. Results are from 3 mice/genotype.

Anke Meyer,[1] Katharina Stolz,[1] Wolfgang Dreher,[2] Jennifer Bergemann,[1] Vani Holebasavanahalli Thimmashetty,[2] Navina Lueschen,[1] Zahra Azizi,[1] Vrushali Khobragade,[1] Kathrin Maedler,[1] and Ekkehard Kuestermann[2]

Manganese-Mediated MRI Signals Correlate With Functional β-Cell Mass During Diabetes Progression

DOI: 10.2337/db14-0864

Diabetes diagnostic therapy and research would strongly benefit from noninvasive accurate imaging of the functional β-cells in the pancreas. Here, we developed an analysis of functional β-cell mass (BCM) by measuring manganese (Mn^{2+}) uptake kinetics into glucose-stimulated β-cells by T1-weighted in vivo Mn^{2+}-mediated MRI (MnMRI) in C57Bl/6J mice. Weekly MRI analysis during the diabetes progression in mice fed a high-fat/high-sucrose diet (HFD) showed increased Mn^{2+}-signals in the pancreas of the HFD-fed mice during the compensation phase, when glucose tolerance and glucose-stimulated insulin secretion (GSIS) were improved and BCM was increased compared with normal diet–fed mice. The increased signal was only transient; from the 4th week on, MRI signals decreased significantly in the HFD group, and the reduced MRI signal in HFD mice persisted over the whole 12-week experimental period, which again correlated with both impaired glucose tolerance and GSIS, although BCM remained unchanged. Rapid and significantly decreased MRI signals were confirmed in diabetic mice after streptozotocin (STZ) injection. No long-term effects of Mn^{2+} on glucose tolerance were observed. Our optimized MnMRI protocol fulfills the requirements of noninvasive MRI analysis and detects already small changes in the functional BCM.

Both type 1 and type 2 diabetes are characterized by a loss and/or dysfunction of β-cells (1–5). As long as physiological insulin secretion is maintained by the β-cell, treatment toward the preservation of normoglycemia is easier to achieve. Thus, it is important to detect β-cell failure at a very early stage of the disease or even during the β-cell compensation phase. β-Cell compensation to maintain normoglycemia can be achieved in two ways: by increasing mass or increasing function (or both). Functional β-cell compensation can occur until up to a 65% β-cell loss; only at further β-cell mass (BCM) reduction was insulin secretion found to decline in patients (6). This analysis from autopsy pancreases highlights that the absolute BCM measure in an individual may not provide sufficient information on the status of diabetes progression and that the analysis of the functional BCM is essential for the evaluation of the diabetes risk.

Today, monitoring of functional BCM is achieved by measuring insulin and C-peptide secretion during a glucose as well as arginine tolerance test (7–9). Retrospective studies using human pancreata from autopsy show a strong correlation of fasting blood glucose levels with BCM and a reduction in BCM already before the diagnosis in subjects with impaired fasting glucose levels (1,10). The ideal time of diagnosis is the onset of diabetes at a stage when the functional BCM has just changed.

The noninvasive measurement of functional BCM has enormous potential for diagnostics but is rather challenging to achieve, partly because a ligand for specific β-cell labeling is currently not available (11–14). It is not possible to measure the actual mass of functional β-cells in vivo (15). MRI using manganese (Mn^{2+}) shows such monitoring of β-cell functionality in cell culture (16). Similar to Ca^{2+}, Mn^{2+} is taken up by glucose-activated β-cells, resulting in a robust signal increase in glucose-stimulated rodent β-cell lines and in islets (16,17). The uptake of Mn^{2+} is controlled by voltage-gated Ca^{2+} channels (18), and Mn^{2+} accumulates in the cytoplasm, primarily in the perinuclear region (19). Mn^{2+} uptake is glucose dependent and can be

[1]Centre for Biomolecular Interactions Bremen, University of Bremen, Bremen, Germany
[2]In-vivo-MR, University of Bremen, Bremen, Germany
Corresponding author: Kathrin Maedler, kmaedler@uni-bremen.de.

Received 30 May 2014 and accepted 13 January 2015.

This article contains Supplementary Data online at http://diabetes.diabetesjournals.org/lookup/suppl/doi:10.2337/db14-0864/-/DC1.

K.M. and E.K. contributed equally to this study.

used in vivo to assess the functionality of both grafted and endogenous pancreatic islets. Mn^{2+} behaves like calcium and will therefore enter metabolically active β-cells (16). $MnCl_2$-enhanced signals also reflect functional β-cells in vivo; pancreatic MRI signals of mice with streptozotocin (STZ)-induced diabetes were decreased in the case of both high- and low-dose STZ compared with nondiabetic control animals (20) and in BDC2.5 T-cell receptor transgenic nonobese diabetic mice even before the diabetes onset could be measured in the blood (21). Individual islets can be detected by MRI in $MnCl_2$-injected exteriorized pancreases, exactly correlating with immunohistochemistry performed in parallel (22).

First correlations could be made in humans by a single mangafodipir infusion; MRI data analysis could clearly and significantly distinguish between people without diabetes and patients with type 2 diabetes without differences in MRI signals in other tissues (23).

Mn^{2+} can be used not only in vitro to characterize isolated islet potency but also, more importantly, in vivo to assess the functionality of both grafted and endogenous pancreatic islets (16,24), since Mn^{2+} is also an excellent MRI agent owing to its effect on the longitudinal relaxation (T1) and was used as one of the first MRI contrast agents (25).

As with other contrast agents, Mn^{2+} has limitations mainly linked to its lack of cell specificity and its potential cytotoxicity. Chronic exposure to high concentrations of Mn^{2+} lead to extrapyramidal dysfunction resembling the dystonic movements associated with Parkinson disease, called manganism (26–28). Based on previous studies in mice, 20–35 mg/kg doses $MnCl_2$ were used for pancreas MRI in rodents (20,22). Although LD_{50} levels of 38 mg/kg i.v. injections in mice were reported (29), concentrations up to 175 mg/kg were injected to reach a sufficient Mn^{2+} concentration in the brain (30), which also led to systemic toxicity such as loss of temperature regulation, and Mn^{2+}-based signals changes in the brain were still measured for >4 days after Mn^{2+} infusion (30).

The present study aimed at developing a strategy to monitor the functional BCM by measuring Mn^{2+} uptake into β-cells by T1-weighted contrast in vivo Mn^{2+}-mediated MRI (MnMRI). By analyzing the Mn^{2+}-dependent MRI signal kinetics, we were able to identify early changes of functional BCM during β-cell compensation and failure in two diabetic mouse models in vivo.

RESEARCH DESIGN AND METHODS

Animals

C57Bl/6J mice were fed a high-fat/high-sucrose diet (HFD) ("Surwit" [31]) for 12 weeks as previously described (32) or injected with one single high dose of STZ (150 mg/kg i.p.) freshly dissolved in 0.1 mol/L citrate buffer (pH 4.5) (33). All animals were housed in a temperature-controlled room with a 12-h light, 12-h dark cycle and were allowed free access to food and water in compliance with Section 8 of the German animal protection law, the Guide for the Care and Use of Laboratory Animals, and the Bremen Senate in agreement with the National Institutes of Health Animal Care Guidelines (34). Blood glucose (measured with a glucometer) and weight were monitored during the experiments.

Intraperitoneal Glucose Tolerance Test

Glucose tolerance was monitored by intraperitoneal glucose tolerance tests (ipGTTs) in mice. For ipGTTs, mice were fasted 12 h overnight and injected with glucose (40%; B. Braun, Melsungen, Germany) at a dose of 1 g/kg body wt i.p. Blood samples were obtained at time points 0, 15, 30, 60, 90, and 120 min for glucose measurements using a glucometer. For detection of the effect of Mn^{2+} on glucose tolerance, 25 mg/kg $MnCl_2$ or vehicle control was injected once weekly in two consecutive experiments and ipGTT measured before and immediately after injection and at days 1 and 3.

Glucose-Stimulated Insulin Secretion

In Vivo Glucose-Stimulated Insulin Secretion

At time points 0 and 30 min after 2 g/kg body wt i.p. glucose injection, blood samples were collected for measurement of serum insulin levels. Insulin was determined with a mouse insulin ELISA kit (ALPCO Diagnostics, Salem, NH).

In Vitro Glucose-Stimulated Insulin Secretion

After the serial Mn^{2+} injections and MRI measurements, pancreata of normal diet (ND) and HFD animals were perfused with a Liberase TM (cat. no. 05401119001; Roche, Mannheim, Germany) solution according to the manufacturer's instructions and digested at 37°C, followed by washing and gradient purification of the islets using a 50:50 mixture of Histopaque1077 and -1119 (Sigma-Aldrich, Munich, Germany) as previously described (35,36). For acute insulin release in response to glucose, islets were washed and preincubated (30 min) in Krebs-Ringer bicarbonate buffer (KRBB) containing 2.8 mmol/L glucose and 0.5% BSA. The KRBB was then replaced by KRBB containing 2.8 mmol/L glucose for 1 h (basal), followed by an additional 1 h incubation in KRBB containing 16.7 mmol/L glucose (stimulated). Stimulatory index was calculated as stimulated divided by basal secretion.

Morphometric and β-Cell Mass Analysis

Pancreatic tissues were processed as previously described (32,37). Mouse pancreata were dissected and fixed in 4% formaldehyde at 4°C for 12 h before embedding in paraffin. For Ki67 and insulin staining, 2-μm sections were deparaffinized, rehydrated, and incubated overnight at 4°C with anti-Ki67 and the next day with anti-insulin (both Dako, Hamburg, Germany), followed by fluorescein isothiocyanate– or Cy3-conjugated secondary antibodies (Jackson ImmunoResearch Laboratories, West Grove, PA). Slides were mounted with glycerol gelatin (Sigma) or with Vectashield with DAPI (Vector Laboratories). For BCM measurement, 10 sections (spanning the width of the pancreas) per mouse were analyzed. Pancreatic

tissue area and insulin-positive area as well as nuclear size and nuclear distance were determined by computer-assisted measurements using a Nikon MEA53200 microscope (Nikon GmbH, Düsseldorf, Germany), and images were acquired using NIS-Elements software (Nikon). BCM was obtained by multiplying the ratio of insulin-positive tissue area to whole pancreatic tissue area by the weight of the pancreas as previously described (32).

MRI

For MnMRI, mice were fasted overnight and anesthetized with 1.0–2.0% isoflurane in 250 mL/min O_2, received a tail vein catheter, and were positioned in supine position on a warmed animal bed. Breathing was monitored with a pressure sensor at the chest. Just before positioning inside the magnet, mice received 2 g/kg glucose i.p., and two to four baseline images were acquired before $MnCl_2$ (8 mg/kg i.v.) was injected via a tail vein catheter. (For protocol, see Fig. 1*A*.) The experiments were performed on a 7 Tesla MR system (BioSpec 70/20 USR with AVIII; Bruker, Ettlingen, Germany) using a quadrature volume coil (72-mm inner diameter) for both radiofrequency transmission and signal reception. The scan repetition time was at least 6 s to ensure full relaxation and thus to avoid any breathing rate–dependent T1

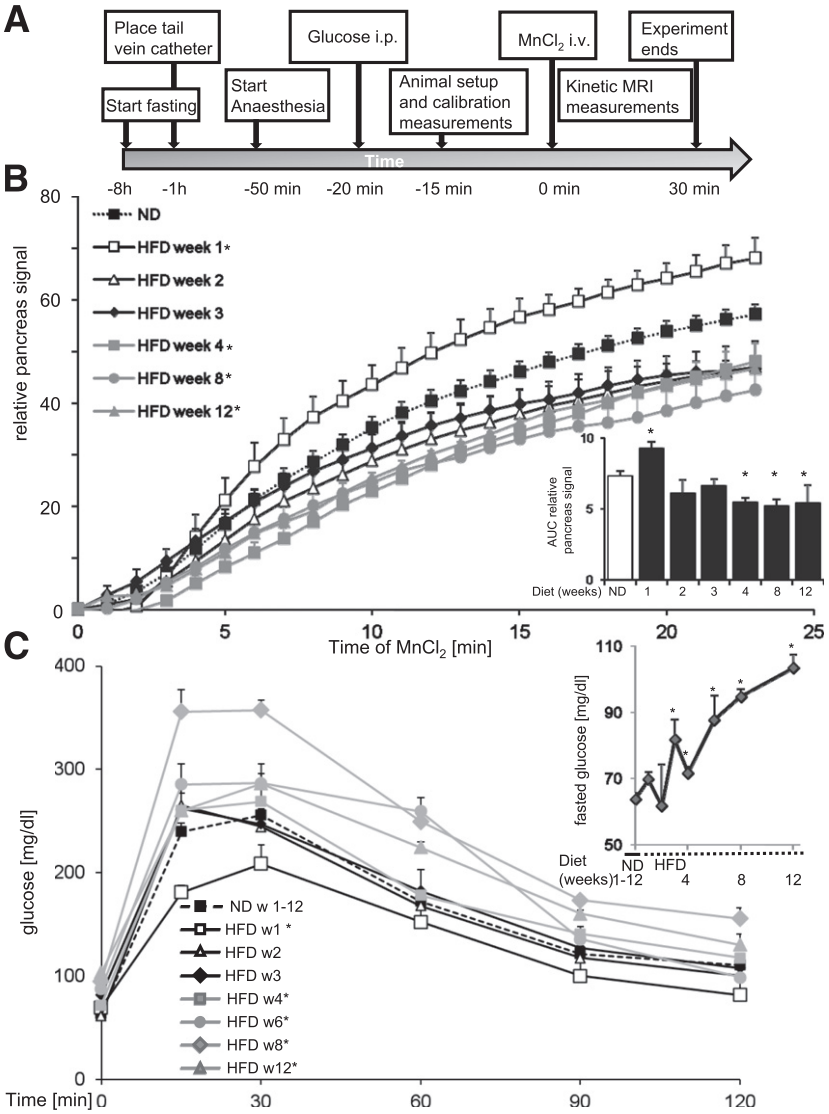

Figure 1—MRI measurements during HFD feeding of C57Bl/6J mice. *A*: Experimental work flow of the MnMRI measurement. *B*: Relative pancreas signals by MnMRI normalized to final liver signals after 23 min of $MnCl_2$ injection from age-matched ND (n = 19) and HFD mice over 12 weeks (n = 3, 6, 4, 3, 3, and 3 for HFD at 1, 2, 3, 4, 8, and 12 weeks, respectively; all mice 12 weeks old at the beginning of the feeding and analysis). Reported signal intensities reflect the signal changes after subtraction of the mean baseline signal taken from the first three to four images prior to intravenous Mn^{2+} injection. Before averaging of individual time courses, data were linearly interpolated and regridded to 1-min intervals referenced to t = 0 for Mn^{2+} injection. AUC integrations are done for the time interval of 0–23 min. *C*: ipGTT and fasting glucose levels (insert) from age-matched ND (n = 33) and HFD mice over 12 weeks (n = 3 for each data point at 1, 2, 3, 4, 8, and 12 weeks). w, week. *P < 0.05 compared with ND control.

effects (38). Time course experiments were acquired using a 3D Snapshot-FLASH sequence with inversion recovery preparation (39) with the following parameters: time of inversion (TI) = 700 ms, FLASH-type signal readout: echo time = 0.9 ms (thus insensitive to T2 relaxation), repetition time = 1.98 ms, excitation pulse = 10°, bandwidth = 500 kHz, matrix = 192 × 96 × 16, field of view = 70 × 35 × 16 mm, nominal image resolution = 365 × 365 × 1,000 μm, centric phase encoding, time of acquisition = 190 ms (38,40). For reference purposes, one proton-density image was acquired using the same 3D Snapshot-FLASH method but omitting the inversion preparation. During the experiments, all measurement parameters were kept constant (personnel, injection system, Mn^{2+} charge, narcotic setup).

Image Analysis

After standard image reconstruction on the Bruker system, the image data were converted from the Bruker to standard NIfTI data format using a home-written software (coded in Matlab 2008b, using "Tools for NIfTI and ANALYZE image" by Jimmy Chen, Matlab File Exchange [http://www.mathworks.de/matlabcentral/fileexchange/8797-tools-for-nifti-and-analyze-image]). These three-dimensional data sets were then subjected to a rigid body motion correction and concatenated to a single four-dimensional data set using SPM8 (Wellcome Department of Imaging Neuroscience, University College London [http://www.fil.ion.ucl.ac.uk/spm/]) for further analysis. The time course data of pancreatic and hepatic tissues were derived from manually drawn regions of interest (ROIs) (38,40). A reduction in breathing rate was often observed directly after bolus $MnCl_2$ administration, which normalized after ~3–5 min. ROIs were chosen after Mn^{2+} application. An organ-specific differentiation of MRI signals in the mouse abdomen is feasible, since each organ in the abdomen can be discriminated owing to their time- and signal amplitude–dependent response to the Mn^{2+} application. In the HFD studies, MRI signals were normalized to the 23-min liver signal in order to see the pancreas-specific kinetics. In the STZ studies, pancreatic MRI signals were normalized to the maximal signal of the corresponding ROI (proton-density image) because of the hepatic fibrosis induced by STZ injection.

Statistical Analysis

Stainings/MRI sets were evaluated in a randomized manner independently by the investigators (A.M., K.S., N.L., Z.A., V.K., and E.K.). The results presented are means ± SEM). The significance of difference between individual experiments was tested by Student *t* test. Significance was set at $P < 0.05$.

RESULTS

MRI Signals Correlate With β-Cell Compensation and Failure During 12 Weeks of HFD Feeding

For monitoring of β-cell function and mass during diabetes progression in the HFD mouse model, MnMRI (Figs. 1*A* and *B* and 2) together with ipGTT, insulin secretion during the ipGTT, and BCM (Figs. 1*C* and 3*A–C*) was analyzed. Figure 1*A* shows the experimental setting of the MnMRI measurements in the mice. Glucose was delivered intraperitoneally 25 min before intravenous $MnCl_2$ application to allow glucose-dependent Mn^{2+} uptake into the β-cells.

After Mn^{2+} injection, the signal increased in T1-weighted magnetic resonance images in a diet- and time-dependent manner (Fig. 1*B*); a time course of MnMRI revealed enlarged MRI signals after 1 week of HFD compared with in ND control mice. The increased signal was only transient, and decreased signals were measured with prolonged diet already after 2 weeks of the HFD. From the 4th week on, MRI signals decreased significantly in the HFD group, compared with ND mice, which had stable MRI signals during the course of the experiment. Such reduced MRI signals in HFD mice persisted over the whole 12-week experimental period, which is also reflected by the area-under-the-curve (AUC) calculation (Fig. 1*B*) of the MRI kinetics as well as by the continued MRI signal change from one single representative mouse over the 12 weeks of HFD (Supplementary Fig. 1*A*).

In order to compensate for inevitable variations of Mn^{2+} delivery to the tissues, we normalized pancreatic MRI signals to those of the liver. Reported signal intensities reflect the signal changes after subtraction of the mean baseline signal taken from the first three to four images prior to intravenous Mn^{2+} injection (Fig. 2). Before averaging of individual time courses, data were linearly interpolated and regridded to 1-min intervals referenced to $t = 0$ for Mn^{2+} injection.

Progressive Decline of Glucose Tolerance and β-Cell Function During 12 Weeks of HFD

The MnMRI signals in the HFD mice correlated well with both glucose tolerance and insulin secretion during the

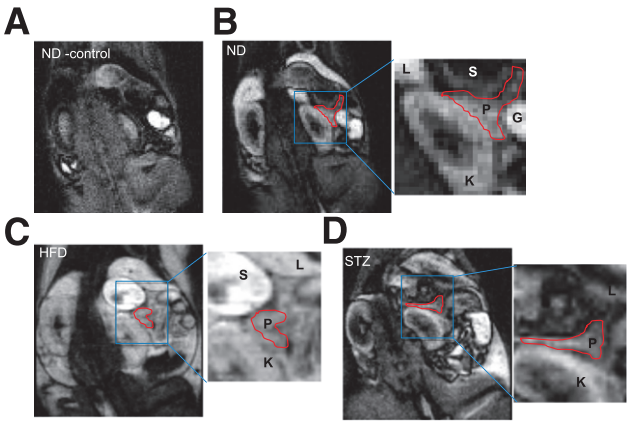

Figure 2—$Mn2^{+}$-based signals in the mouse abdomen. Representative ND MnMRI images and enlarged pancreas regions (right) from ND control mice before (*A*) and after (*B*) $MnCl_2$ injection and from HFD (*C*) and STZ (*D*) mice after $MnCl_2$ injection. G, gut; K, kidney; L, liver; P, pancreas; S, stomach. (A high-quality color representation of this figure is available in the online issue.)

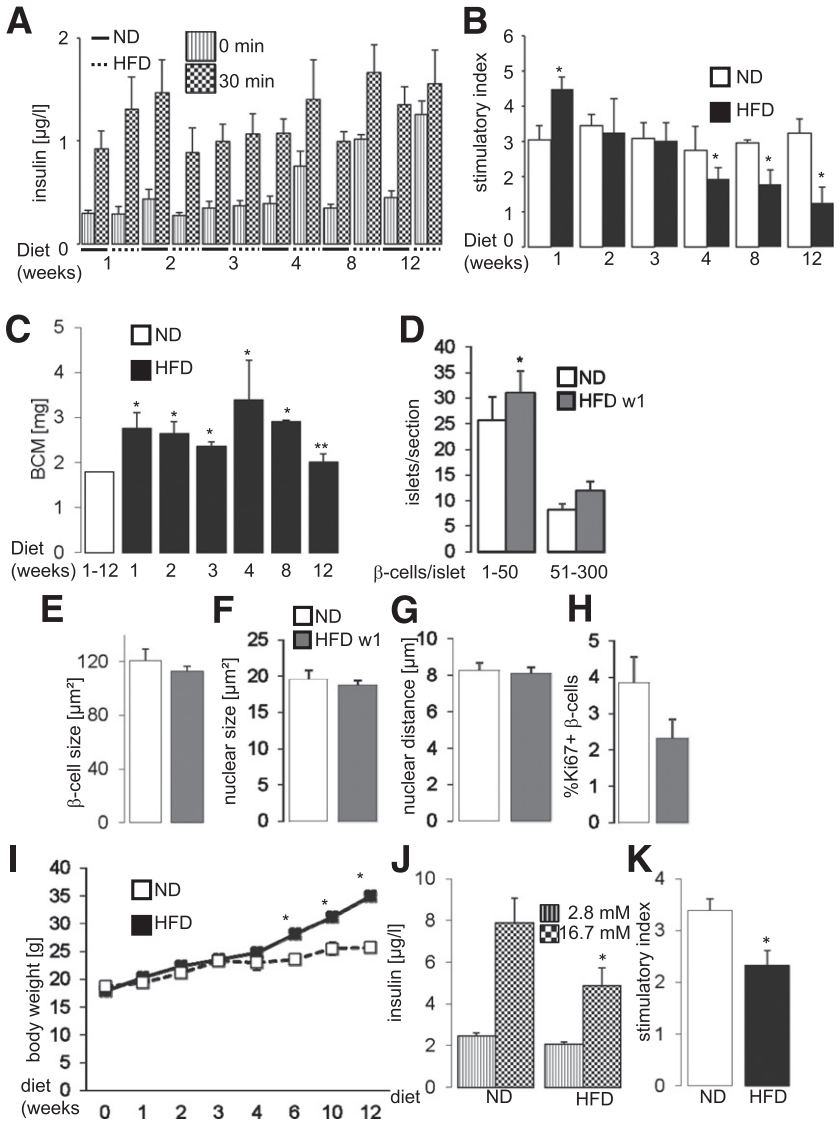

Figure 3—Progressive decline of glucose tolerance and β-cell function during 12 weeks of HFD. In vivo GSIS during the ipGTT (*A* and *B*) and β-cell mass (*C*) from ND and HFD mice fed over 12 weeks (n = 14 for ND; n = 3, 3, 3, 8, 8, and 8 for HFD at 1, 2, 3, 4, 8, and 12 weeks, respectively). *D*: Islet density was analyzed by counting all islets/section from ND and HFD mice and presenting them in two size groups with 1–50 and 51–300 β-cells/islet. *E*: Mean β-cell size was approximated by dividing total insulin-positive area by number of β-cells. Mean β-cell nuclear size (*F*), nuclear distance (*G*), and β-cell proliferation by double staining for Ki67 and insulin (*H*) were analyzed in a mean number of 155 islets/mouse from three mice/group. *I*: Mouse weight over the course of the diet. *J* and *K*: In vitro GSIS from isolated islets from $MnCl_2$-injected ND and HFD mice at the end of the 16-week experiment. Insulin secretion during 1-h incubation with 2.8 mmol/L (basal) and 16.7 mmol/L (stimulated) glucose. *K*: The insulin stimulatory index denotes the ratio of secreted insulin during 1-h incubation with 16.7 mmol/L and 2.8 mmol/L glucose, respectively. *P < 0.05 compared with ND control; **P < 0.05 compared with 8-week HFD data set.

course of HFD feeding (Figs. 1 and 3; Supplementary Fig. 1*A*). At 1 week after HFD, when MRI signals were increased, glucose tolerance was improved (Fig. 1*C*), together with increased glucose-stimulated insulin secretion (GSIS) (Fig. 3*A* and *B*), which confirms that the increased glucose-stimulated MnMRI signals indeed reflect the improved β-cell function. HFD feeding significantly impaired glucose tolerance and insulin secretion, with significantly higher glucose levels during the glucose tolerance test and higher fasting glucose (Fig. 1*C*) and reduced GSIS (Fig. 3*A* and *B*) after 4 weeks—the same time point when pancreatic MnMRI signals were reduced—compared with ND mice.

In contrast to the functional changes, BCM remained in the compensatory phase during the first 8 weeks of the HFD. Already after 1 week of HFD, BCM was 1.5-fold increased, while BCM was unchanged in ND controls during the 12 weeks (Fig. 3*C*). Again, the compensatory increase in BCM already after 1 week correlated with the improved function and the increased MRI signal. We did not expect such a fast mass adaptation and therefore analyzed single β-cell and islet size in detail. We observed

a significant increase in smaller islets consisting of 1–50 β-cells throughout the pancreas in the HFD mice for 1 week, compared with ND, while larger islets did not significantly increase (Fig. 3*D*). β-Cell size (Fig. 3*E*), β-cell nuclear size (Fig. 3*F*), and nuclear distance (Fig. 3*G*) as well as Ki67$^+$ β-cells (Fig. 3*H*) were similar in ND and HFD.

In contrast, from 4 weeks on, glucose tolerance and insulin secretion were impaired by the HFD, and MRI signals were reduced and BCM remained increased up to 8 weeks of diet, showing that the functional BCM and not the BCM alone is monitored by MnMRI. A drop in BCM back to the ND level was observed at 12 weeks (Fig. 3*C*); also here, glucose tolerance test (Fig. 1*C*) and GSIS (Fig. 3*A* and *B*) were lower than in control mice.

All mice fed with the HFD gained weight significantly after 6 weeks of feeding (1.4-fold increase compared with ND) (Fig. 3*I*). At the end of the experiments, in vitro GSIS was performed on isolated islets from the $MnCl_2$-injected mice under the ND and HFD (Fig. 3*J* and *K*). In line with our previous data (32,34), HFD significantly reduced GSIS compared with ND controls.

STZ-Induced β-Cell Destruction Correlates With the MnMRI Signal

A second model was tested for the MnMRI analysis of functional BCM. Three-month-old male C57Bl/6 mice were injected with a single dose of 150 mg/kg STZ or vehicle. On day 14, mice were analyzed by MRI (Fig. 4*A–C*; Supplementary Fig. 1*C*) and killed on the next day for BCM measurement (Fig. 4*E*). MRI signals were clearly reduced in the STZ mice (Fig. 4*A*), which was confirmed by the AUC analysis (Fig. 4*B*) (26% reduction). No changes in Mn^{2+} cellular uptake occurred during the first 10 min of $MnCl_2$ injection, although the majority of the β-cells were destroyed. But during the second phase of Mn^{2+} uptake from 10 to 30 min, we observed a 43% induction of the MRI signal in the control mice, while we could only detect a 9% signal enhancement in the STZ mice (Fig. 4*C*). Such 79% reduction of Mn^{2+} uptake also correlates with 73% loss in BCM in the STZ mice (Fig. 4*D*).

For each mouse, the relative pancreas signal at 30 min after bolus $MnCl_2$ infusion was monitored separately before and after STZ injection and its decrease differed between 30 and 75% (Supplementary Fig. 1*A*). In line with the MRI data, STZ increased glucose levels to >400 mg/dL after 14 days (Fig. 4*E*). In contrast to HFD feeding, where liver signals remained unchanged among the treatment groups, liver MRI signals were reduced in the STZ mice (Supplementary Fig. 1*B* and *C*). Pancreas MRI results were normalized to the maximal signal of the respective corresponding ROI (100%) (proton-density image).

No Long-term Effect of Mn^{2+} on Glucose Tolerance

For exclusion of a direct long-term effect of Mn^{2+} on glucose tolerance during the experiments, 25 mg/kg $MnCl_2$ or vehicle control was injected once weekly over 2 weeks and ipGTTs were performed immediately after the $MnCl_2$ injection (Fig. 5*A* and *C*) and 2 days later (Fig. 5*B* and *D*). After the 1st $MnCl_2$ injection, glucose concentrations were slightly increased at 15 and 60 min during the ipGTT (Fig. 5*A*)—an effect that disappeared after 2 days (Fig. 5*B*). Seven days after the first dose, mice

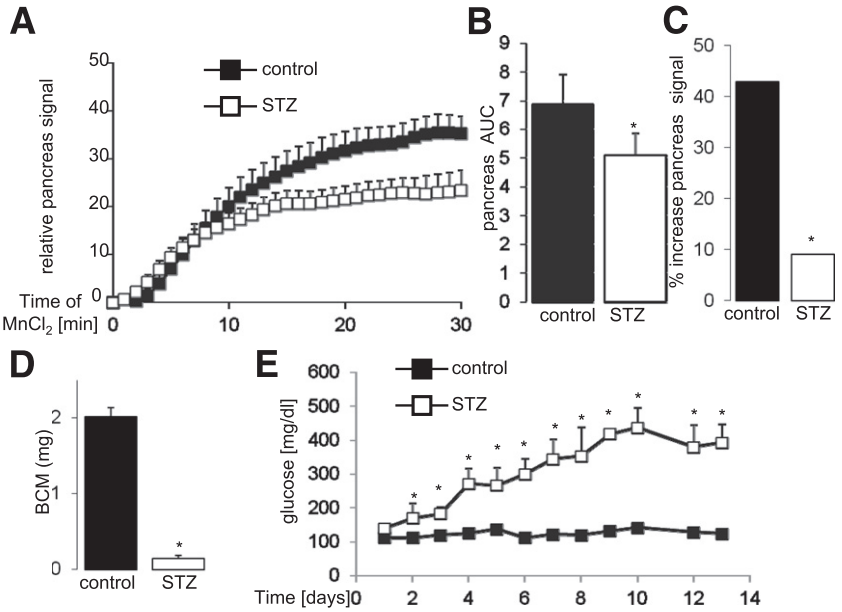

Figure 4—STZ-induced β-cell destruction correlates with the MnMRI signal. *A–C*: MRI analysis in C57Bl/6 mice injected with one single dose of 150 mg/kg STZ (n = 5) or control (n = 5). (*A*) MRI signals were normalized to the maximal signal of the corresponding ROI, the proton-density image during 30 min after $MnCl_2$ injection at day 14 after STZ treatment. *B* and *C*: AUC integrations are shown for the time interval of 0–23 min for the total measurement time (*B*) and for the second phase of Mn^{2+} uptake from 10 to 30 min (*C*). *D* and *E*: β-Cell mass analysis of isolated fixed pancreases at the end of the study (*D*) and random blood glucose levels during the 14 days of the experiment (*E*). *P < 0.05 compared with control.

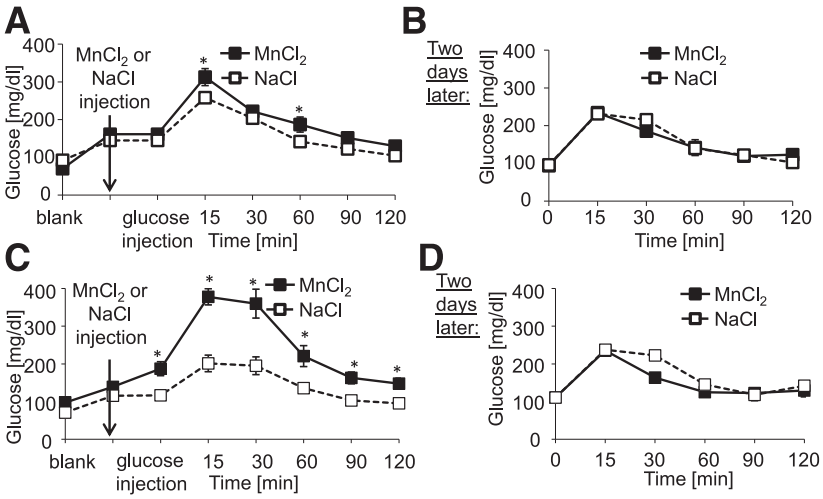

Figure 5—No long-term effect of Mn^{2+} on glucose tolerance. ipGTT with 1 g/kg glucose after the first injection (*A* and *B*) of 25 mg/kg $MnCl_2$ (n = 5) or solvent (NaCl) (n = 5) or the second injection (*C* and *D*) 1 week later in two independent experiments in normal diet fed C57Bl6/J mice. IpGTT was performed either directly after $MnCl_2$ injection (*A* and *C*) or 2 days later (*B* and *D*). *P < 0.05 compared with control.

received a second $MnCl_2$ injection, which showed again an impaired glucose tolerance (Fig. 5*C*), but this effect also washed off 2 days later (Fig. 5*D*). The results show that multiple $MnCl_2$ injections also had no long-term effects on glucose tolerance. We further monitored a possible Mn^{2+} accumulation in the brain but could not detect any MRI signal changes (Supplementary Fig. 1*E*).

DISCUSSION

In this study, we established in vivo imaging of functional BCM and show a strong correlation of MnMRI signals with a functional BCM during β-cell compensation as well as β-cell failure. Importantly, a sole association of MnMRI signals with conventionally determined BCM measurements was not observed; rather, MnMRI data displayed the functional BCM. This can be assumed from MnMRI comparisons with ipGTT, GSIS, and BCM during diabetes progression, when changes in glucose metabolism occur, and subsequently, the glucose-dependent uptake of Mn^{2+} is affected in parallel resulting in enhanced MnMRI signals as long as β-cells compensate successfully for the higher demand of insulin during HFD feeding and display adequate GSIS, which normalize glucose levels. In contrast, when GSIS was impaired and glucose levels rose, MnMRI levels were reduced in the HFD mice, even when a higher BCM was still present and declined further with more severe loss of β-cell function. In the STZ model, a more severe model of β-cell loss where loss of function together with a reduction of BCM occurred rapidly after high-dose STZ injection, MnMRI signals were significantly reduced. Initially, we expected that the MRI signals would change linearly and proportional to the BCM, but in none of the tested models did such linearity occur. Definitely, the BCM method is still the most accurate but invasive method to quantify insulin-producing cells. Our aim was to present a noninvasive alternative to the classical BCM measurement, which also allows studying BCM changes longitudinally, but this method has its limitations with respect to absolute accuracy, and we could not reach sensitivity to a single islet level.

While glucose dependent cellular Mn^{2+} uptake correlated with insulin secretion, we still observed glucose stimulated MnMRI signals after 12 weeks of HFD feeding, which were naturally reduced when compared with the ND group, but in contrast, glucose stimulated insulin secretion did not occur at all after 12 weeks. It is obvious, that basal insulin secretion raises in response to the insulin resistance, especially when free fatty acid levels are chronically elevated (32) and cause a chronic and glucose independent insulin secretion from the β-cells (41,42). In contrast, Mn^{2+} uptake is not elevated under physiological glucose concentrations at insulin resistance.

We could already see β-cell mass compensation after 1 week, a short time of the diet, together with improved function when basal insulin secretion was not increased yet. While improved function was only seen at week 1, it remained stable until week 4. After longer feeding times, basal insulin secretion was highly increased, as shown before, while GSIS is blunted in HFD mice (43), which resulted in an impaired stimulatory index.

It appears that there are different mechanisms of β-cell adaptation at young and old age as well as in the response to HFD feeding. While β-cell proliferation measured by BrdU incorporation is 10 times higher in 2-week-old than in 4-month-old mice, it is also increased after 2 weeks of HFD feeding but not after 14 weeks (43). This indicates that β-cells can proliferate at a young age (44), but at older age, β-cell compensation is unlikely to be mediated by proliferation. β-Cell hypertrophy is another mechanism reported for β-cell compensation (45). Here,

we started the HFD feeding at the age of 12 weeks and observed rapid adaptation in BCM already after 1 week of HFD, which could not be explained by increased proliferation or hypertrophy and was, rather, the result of an increased number of islets in the HFD (Fig. 3*D* and *H*). This possibility needs to be further investigated to avoid misinterpretation, as this was not the focus of our current study.

MRI kinetics display a rapid signal increase within 5 min after $MnCl_2$ injection. AUC analyses were used to calculate the signal differences during the 30 min of analysis and showed clear differences in signal intensities of the region of the pancreas, irrespective of normalization to liver signals or proton-density image. For exclusion of a general and unspecific uptake of $MnCl_2$, signals were measured in muscle during 30 min in response to $MnCl_2$; only a negligible signal decrease was observed, which was expected owing to lack of calcium uptake in the nonactive skeletal muscle (46).

In the HFD experiments, we normalized pancreatic to hepatic signal, since with its high blood flow, intravenously injected $MnCl_2$ quickly accumulates in the liver. This makes the normalization to the liver the best option. Although this is still not optimal because changes in the liver signal occurred in the different mice, so liver signals were individual and could not be correlated with any measure: neither to the selected liver ROI nor to the week of feeding in the two different ND and HFD groups.

During obesity and diabetes progression, liver and pancreas tissue accumulated fat droplets after a time period of 12 weeks, which prevented accurate measurement of the ROIs and was therefore excluded from the study. After week 12, it was not possible to mark pancreatic ROIs without the risk of including the fat signals or voxels, which are influenced by the partial volume effect in all mice and would inhibit accurate data analysis under the established experimental conditions during a longitudinal study.

In STZ experiments, the liver is highly affected by alkylation; a significant reduction of the MnMRI signal intensity in the liver was measured and shown in contrast to findings by Antkowiak et al. (20), where no liver signal changes were assumed. At the end, both our study and that by Antkowiak et al. study show an STZ-based MRI signal reduction under glucose stimulation. Hepatic damage evaluated by increased expression of alanine aminotransferase and morphologic analysis shows large necrotic areas in the liver in STZ-injected rats (47). We suspect that the STZ uptake via GLUT2 transporter of the liver is the reason for hepatic damage (48). Therefore, an alternative MnMRI signal normalization strategy in the pancreas was chosen in the STZ experiments. Signals were referenced to the maximal signal of the corresponding ROI in the proton-density image. Proton-density images were acquired without the inversion recovery pulse to see the maximal signal of the ROI, arising from all protons in the ROI (100%), which is constant over the course of measurement.

It has to be pointed out that with the described method, it is not possible to visualize individual islets, which form clusters of roughly 40–300 μm in diameter (49–51). In theory, the partial volume effect is especially strong when imaging the small β-cell organelles by MnMRI because small single spots appear much brighter in smaller measured voxels. Nevertheless, those small structures fall far below the achievable actual spatial resolution of the MnMRI, especially with our kinetic approach, which is limited to measure time and thus resolution. With increased measuring time, individual islets of Langerhans could be detected by ex vivo MnMRI (22), but even ex vivo, an accurate determination of the islet volume is not possible. The goal of the current study was to detect not individual islets but the correlation of MnMRI signals with β-cell function and mass during β-cell compensation and diabetes progression. Therefore, we set up serial measurements enabling the differentiation between kinetics and final signal amplitude.

Mn^{2+} kinetics follows the glucose-induced Ca^{2+} entry in a better way than a single time point. This can especially be observed by the differences in the HFD and STZ models; while a significant Mn^{2+}-signal decrease in the pancreas was already observed after 5 min in the HFD mice, it occurred only after 10 min in the STZ model. Nevertheless, in our setting of 30-min Mn^{2+} kinetic measurement at 50 min after glucose, a clear plateau phase was not reached yet, while a plateau phase was already reported 15 min after glucose and Mn^{2+} injection (20) and a maximal signal was observed at 1 h (52), which is in accordance with our studies.

We decided on the 30-min experimental setting after Mn^{2+} and 20–50 min after glucose because we did not expect large changes in β-cell Ca^{2+}-channel activity at 50 min after glucose injection. In this longitudinal study, we kept the experimental settings constant for the animals' welfare, which also allowed shorter anesthesia duration for the mice.

One risk under Mn^{2+} exposure is the development of detrimental side effects (manganism), which occur at higher and chronic doses of $MnCl_2$ (LD_{50} 38 mg/kg) (29,53), while in our study, 8 mg/kg was used for the MRI measures in one single bolus injection. No Mn^{2+} enhancement was detectable in the brain, which would be necessary to develop the diseases described. Also, serial Mn^{2+} injections did not lead to a magnetic resonance–detectable accumulation of Mn^{2+} in the brain. A high Mn^{2+} accumulation in a small number of cells cannot be ruled out if their volume is much smaller than the voxel volume of the image taken in these experiments.

Although Mn^{2+} caused a static impairment of glucose tolerance in mice, glucose homeostasis was not durably affected by Mn^{2+} injections.

Other endocrine as well as acinar cells in the pancreas express calcium channels; we consider the glucose-stimulated Mn^{2+} uptake to be rather specific for β-cells, but further in vitro studies on a single cell level are necessary to prove this.

α-Cells carry ATP-sensitive K^+ channels (K_{ATP}) similar to β-cells (54) as well as Ca^{2+}-channels (55,56). K_{ATP} channels play similar roles in both cell types; the difference is that the K_{ATP} channel activity in α-cells is very low. Glucose would lead to closure of the channels and membrane depolarization; however, membrane depolarization in α-cells results in lower Ca^{2+} entry versus in β-cells (57,58). The paracrine effect of insulin on the α-cells does not involve electrical activity, and α-cells are rather electrically active at hypoglycemia (below 5 mmol/L glucose).

Somatostatin-releasing δ-cells are the 3rd largest cell population in islets and also express voltage-gated L-type Ca^{2+}-channels. While increase of glucose results in the stimulation of somatostatin secretion, it had no effects on intracellular Ca^{2+} levels (59), membrane potential, or electrical activity (60) in in vitro studies. Therefore, we also do not expect large amounts of Mn^{2+} entry into δ-cells in response to glucose.

Amylase secretion by acinar cells is also regulated by Ca^{2+}-channels, and Mn^{2+} was shown to increase Amylase secretion in vitro in Ca^{2+}- and Mg^{2+}-free solution; in contrast, under physiological conditions, Mn^{2+} does not induce amylase increase and thus is not expected to give a signal in acinar cells (61); acinar cells show a robust mangafodipir-MRI signal at low glucose (62). By monitoring the difference in the MRI signal from low to high glucose in the mice, we expect a rather β-cell–specific change, as shown previously (52).

Measurements of functional BCM remain a challenge owing to the small size of pancreatic islets, their poor contrast compared with the surrounding tissues, and their position in the body. However, the present study has proven that noninvasive MRI is a reliable tool to detect small changes in the functionality of β-cells in vivo and exhibits the potential for early noninvasive detection of changes in functional BCM. Our approach carries further potential for multifaceted longitudinal studies to monitor functional BCM adaptation during diabetes progression as well as for the evaluation of therapies for diabetes as an alternative to classical BCM analysis. The optimized protocol of T1-weighted MRI of the mouse abdomen fulfills the requirements of least invasive MR imaging.

Acknowledgments. The authors thank Benjamin Pawlik and Amod Godbole (University of Bremen) for help with the MRI analysis and the Maedler laboratory, especially Amin Ardestani and Federico Paroni (University of Bremen), for helpful suggestions.

Funding. This work was supported by the FP7 program In Vivo Imaging of Beta cell Receptors by Applied Nano Technology (VIBRANT; FP7-228933-2), the European Research Council, the Diabetes Competence Network supported by the German Federal Ministry of Science, and University of Bremen research funds.

Duality of Interest. No potential conflicts of interest relevant to this article were reported.

Authors Contributions. A.M., K.M., and E.K. designed, performed, and analyzed research. K.S., W.D., J.B., V.H.T., N.L., Z.A., and V.K. performed experiments. A.M., K.M., and E.K. wrote the manuscript. K.M. is the guarantor of this work and, as such, had full access to all the data in the study and takes responsibility for the integrity of the data and the accuracy of the data analysis.

References

1. Butler AE, Janson J, Bonner-Weir S, Ritzel R, Rizza RA, Butler PC. Beta-cell deficit and increased beta-cell apoptosis in humans with type 2 diabetes. Diabetes 2003;52:102–110
2. Kurrer MO, Pakala SV, Hanson HL, Katz JD. Beta cell apoptosis in T cell-mediated autoimmune diabetes. Proc Natl Acad Sci U S A 1997;94:213–218
3. Mathis D, Vence L, Benoist C. beta-Cell death during progression to diabetes. Nature 2001;414:792–798
4. Nolan CJ, Prentki M. The islet beta-cell: fuel responsive and vulnerable. Trends Endocrinol Metab 2008;19:285–291
5. Rhodes CJ. Type 2 diabetes-a matter of beta-cell life and death? Science 2005;307:380–384
6. Meier JJ, Breuer TG, Bonadonna RC, et al. Pancreatic diabetes manifests when beta cell area declines by approximately 65% in humans. Diabetologia 2012;55:1346–1354
7. Polonsky KS, Rubenstein AH. C-peptide as a measure of the secretion and hepatic extraction of insulin. Pitfalls and limitations. Diabetes 1984;33:486–494
8. Sjostrand M, Carlson K, Arnqvist HJ, et al. Assessment of beta-cell function in young patients with type 2 diabetes: arginine-stimulated insulin secretion may reflect beta-cell reserve. J Intern Med 2014;275:39–48
9. Palmer JP, Fleming GA, Greenbaum CJ, et al. C-peptide is the appropriate outcome measure for type 1 diabetes clinical trials to preserve beta-cell function: report of an ADA workshop, 21-22 October 2001. Diabetes 2004;53:250–264
10. Ritzel RA, Butler AE, Rizza RA, Veldhuis JD, Butler PC. Relationship between beta-cell mass and fasting blood glucose concentration in humans. Diabetes Care 2006;29:717–718
11. Malaisse WJ, Maedler K. Imaging of the β-cells of the islets of Langerhans. Diabetes Res Clin Pract 2012;98:11–18
12. Gotthardt M. A therapeutic insight in beta-cell imaging? Diabetes 2011;60:381–382
13. Wang P, Yoo B, Yang J, et al. GLP-1R-targeting magnetic nanoparticles for pancreatic islet imaging. Diabetes 2014;63:1465–1474
14. Andralojc K, Srinivas M, Brom M, et al. Obstacles on the way to the clinical visualisation of beta cells: looking for the Aeneas of molecular imaging to navigate between Scylla and Charybdis. Diabetologia 2012;55:1247–1257
15. Leibiger IB, Caicedo A, Berggren PO. Non-invasive in vivo imaging of pancreatic β-cell function and survival - a perspective. Acta Physiol (Oxf) 2012;204:178–185
16. Gimi B, Leoni L, Oberholzer J, et al. Functional MR microimaging of pancreatic beta-cell activation. Cell Transplant 2006;15:195–203
17. Nagata M, Kagawa T, Koutou D, Matsushita T, Yamazaki Y, Murase K. Measurement of manganese content in various organs in rats with or without glucose stimulation. Radiological Phys Technol 2011;4:7–12
18. Leoni L, Serai SD, Haque ME, Magin RL, Roman BB. Functional MRI characterization of isolated human islet activation. NMR Biomed 2010;23:1158–1165
19. Leoni L, Dhyani A, La Riviere P, Vogt S, Lai B, Roman BB. β-Cell subcellular localization of glucose-stimulated Mn uptake by X-ray fluorescence microscopy: implications for pancreatic MRI. Contrast Media Mol Imaging 2011;6:474–481
20. Antkowiak PF, Tersey SA, Carter JD, et al. Noninvasive assessment of pancreatic beta-cell function in vivo with manganese-enhanced magnetic resonance imaging. Am J Physiol Endocrinol Metab 2009;296:E573–E578
21. Antkowiak PF, Stevens BK, Nunemaker CS, McDuffie M, Epstein FH. Manganese-enhanced magnetic resonance imaging detects declining pancreatic β-cell mass in a cyclophosphamide-accelerated mouse model of type 1 diabetes. Diabetes 2013;62:44–48
22. Lamprianou S, Immonen R, Nabuurs C, et al. High-resolution magnetic resonance imaging quantitatively detects individual pancreatic islets. Diabetes 2011;60:2853–2860

23. Botsikas D, Terraz S, Vinet L, et al. Pancreatic magnetic resonance imaging after manganese injection distinguishes type 2 diabetic and normoglycemic patients. Islets 2012;4:243–248
24. Leoni L, Roman BB. MR imaging of pancreatic islets: tracking isolation, transplantation and function. Curr Pharm Des 2010;16:1582–1594
25. Mendonça-Dias MH, Gaggelli E, Lauterbur PC. Paramagnetic contrast agents in nuclear magnetic resonance medical imaging. Semin Nucl Med 1983; 13:364–376
26. Gorell JM, Johnson CC, Rybicki BA, et al. Occupational exposure to manganese, copper, lead, iron, mercury and zinc and the risk of Parkinson's disease. Neurotoxicology 1999;20:239–247
27. Olanow CW. Manganese-induced parkinsonism and Parkinson's disease. Ann N Y Acad Sci 2004;1012:209–223
28. Roth JA, Garrick MD. Iron interactions and other biological reactions mediating the physiological and toxic actions of manganese. Biochem Pharmacol 2003;66:1–13
29. Silva AC, Lee JH, Aoki I, Koretsky AP. Manganese-enhanced magnetic resonance imaging (MEMRI): methodological and practical considerations. NMR Biomed 2004;17:532–543
30. Lee JH, Silva AC, Merkle H, Koretsky AP. Manganese-enhanced magnetic resonance imaging of mouse brain after systemic administration of MnCl2: dose-dependent and temporal evolution of T1 contrast. Magn Reson Med 2005;53: 640–648
31. Surwit RS, Kuhn CM, Cochrane C, McCubbin JA, Feinglos MN. Diet-induced type II diabetes in C57BL/6J mice. Diabetes 1988;37:1163–1167
32. Sauter NS, Schulthess FT, Galasso R, Castellani LW, Maedler K. The anti-inflammatory cytokine interleukin-1 receptor antagonist protects from high-fat diet-induced hyperglycemia. Endocrinology 2008;149:2208–2218
33. Wang Z, Dohle C, Friemann J, Green BS, Gleichmann H. Prevention of high- and low-dose STZ-induced diabetes with D-glucose and 5-thio-D-glucose. Diabetes 1993;42:420–428
34. Owyang AM, Maedler K, Gross L, et al. XOMA 052, an anti-IL-1beta monoclonal antibody, improves glucose control and beta-cell function in the diet-induced obesity mouse model. Endocrinology 2010;151:2515–2527
35. Ardestani A, Paroni F, Azizi Z, et al. MST1 is a key regulator of beta cell apoptosis and dysfunction in diabetes. Nat Med 2014;20:385–397
36. Schulthess FT, Paroni F, Sauter NS, et al. CXCL10 impairs beta cell function and viability in diabetes through TLR4 signaling. Cell Metab 2009;9:125–139
37. Shu L, Sauter NS, Schulthess FT, Matveyenko AV, Oberholzer J, Maedler K. Transcription factor 7-like 2 regulates beta-cell survival and function in human pancreatic islets. Diabetes 2008;57:645–653
38. Kustermann E, Meyer A, Godbole A, Dreher W, Maedler K. (2011) Investigating the Pancreatic Function: Robust 3D MR imaging of Mouse Abdomen. In: 19th Annual Meeting & Exhibition International Society for Magnetic Resonance in Medicine, Montreal, Canada
39. Haase A, Matthaei D, Bartkowski R, Dühmke E, Leibfritz D. Inversion recovery snapshot FLASH MR imaging. J Comput Assist Tomogr 1989;13:1036–1040
40. Meyer A, Kuestermann E, Stolz K, Bergemann J, Dreher W, Maedler K. Non-invasive in-vivo analysis of beta cell function and mass by MRI. Diabetologia 2012;55:210
41. Crespin SR, Greenough WB 3rd, Steinberg D. Stimulation of insulin secretion by infusion of free fatty acids. J Clin Invest 1969;48:1934–1943
42. Wiederkehr A, Wollheim CB. Minireview: implication of mitochondria in insulin secretion and action. Endocrinology 2006;147:2643–2649
43. Roat R, Rao V, Doliba NM, et al. Alterations of pancreatic islet structure, metabolism and gene expression in diet-induced obese C57BL/6J mice. PLoS ONE 2014;9:e86815
44. Maedler K, Schumann DM, Schulthess F, et al. Aging correlates with decreased beta-cell proliferative capacity and enhanced sensitivity to apoptosis: a potential role for Fas and pancreatic duodenal homeobox-1. Diabetes 2006;55: 2455–2462
45. Sachdeva MM, Claiborn KC, Khoo C, et al. Pdx1 (MODY4) regulates pancreatic beta cell susceptibility to ER stress. Proc Natl Acad Sci U S A 2009;106: 19090–19095
46. Berchtold MW, Brinkmeier H, Müntener M. Calcium ion in skeletal muscle: its crucial role for muscle function, plasticity, and disease. Physiol Rev 2000;80: 1215–1265
47. Simões C, Domingues P, Ferreira R, et al. Remodeling of liver phospholipidomic profile in streptozotocin-induced diabetic rats. Arch Biochem Biophys 2013;538:95–102
48. Ogawa A, Kurita K, Ikezawa Y, et al. Functional localization of glucose transporter 2 in rat liver. J Histochem Cytochem 1996;44:1231–1236
49. Bosco D, Armanet M, Morel P, et al. Unique arrangement of alpha- and beta-cells in human islets of Langerhans. Diabetes 2010;59:1202–1210
50. Carter JD, Dula SB, Corbin KL, Wu R, Nunemaker CS. A practical guide to rodent islet isolation and assessment. Biol Proced Online 2009;11:3–31
51. Jo J, Hara M, Ahlgren U, Sorenson R, Periwal V. Mathematical models of pancreatic islet size distributions. Islets 2012;4:10–19
52. Antkowiak PF, Vandsburger MH, Epstein FH. Quantitative pancreatic β cell MRI using manganese-enhanced Look-Locker imaging and two-site water exchange analysis. Magn Reson Med 2012;67:1730–1739
53. Boretius S, Frahm J. Manganese-enhanced magnetic resonance imaging. Methods Mol Biol 2011;771:531–568
54. Bokvist K, Olsen HL, Høy M, et al. Characterisation of sulphonylurea and ATP-regulated K+ channels in rat pancreatic A-cells. Pflugers Arch 1999;438: 428–436
55. De Marinis YZ, Salehi A, Ward CE, et al. GLP-1 inhibits and adrenaline stimulates glucagon release by differential modulation of N- and L-type Ca2+ channel-dependent exocytosis. Cell Metab 2010;11:543–553
56. Gromada J, Bokvist K, Ding WG, et al. Adrenaline stimulates glucagon secretion in pancreatic A-cells by increasing the Ca2+ current and the number of granules close to the L-type Ca2+ channels. J Gen Physiol 1997;110:217–228
57. Rorsman P, Salehi SA, Abdulkader F, Braun M, MacDonald PE. K(ATP)-channels and glucose-regulated glucagon secretion. Trends Endocrinol Metab 2008;19:277–284
58. Rorsman P, Braun M, Zhang Q. Regulation of calcium in pancreatic α- and β-cells in health and disease. Cell Calcium 2012;51:300–308
59. Berts A, Liu YJ, Gylfe E, Hellman B. Oscillatory Ca2+ signaling in somatostatin-producing cells from the human pancreas. Metabolism 1997; 46:366–369
60. Braun M, Ramracheya R, Amisten S, et al. Somatostatin release, electrical activity, membrane currents and exocytosis in human pancreatic delta cells. Diabetologia 2009;52:1566–1578
61. Petersen OH, Ueda N. Pancreatic acinar cells: the role of calcium in stimulus-secretion coupling. J Physiol 1976;254:583–606
62. Sahani D, Prasad SR, Maher M, Warshaw AL, Hahn PF, Saini S. Functioning acinar cell pancreatic carcinoma: diagnosis on mangafodipir trisodium (Mn-DPDP)-enhanced MRI. J Comput Assist Tomogr 2002;26:126–128

SUPPLEMENTARY DATA

Supplementary Figure 1.

A) Individual MRI signal development of one mouse during the course of the high fat diet feeding and **B)** Individual STZ MRI signal changes at 30 min post bolus MnCl2 injection. **(C)** MRI Signal development of the liver in C57Bl/6 mice injected with one single dose of 150 mg/kg STZ or control (n=5/group). MRI signals were normalized to the maximal signal of the corresponding ROI, the proton density image during 30 min after MnCl2 injection at day 14 after STZ treatment. **(D)** Area-under-the-curve (AUC) integrations are done for the time interval of 0-30 min. * $p<0.05$ to control.
(E) MRI measurement of the cortex of the mouse brain. During a test period of 15 days and three independent experiments, no accumulation of manganese could be observed in the cortex as well as in other brain areas (not shown). Manually drawn ROIs of the same animal are presented with comparable MRI calibrations and Mn2+-uptake kinetics.

SUPPLEMENTARY DATA

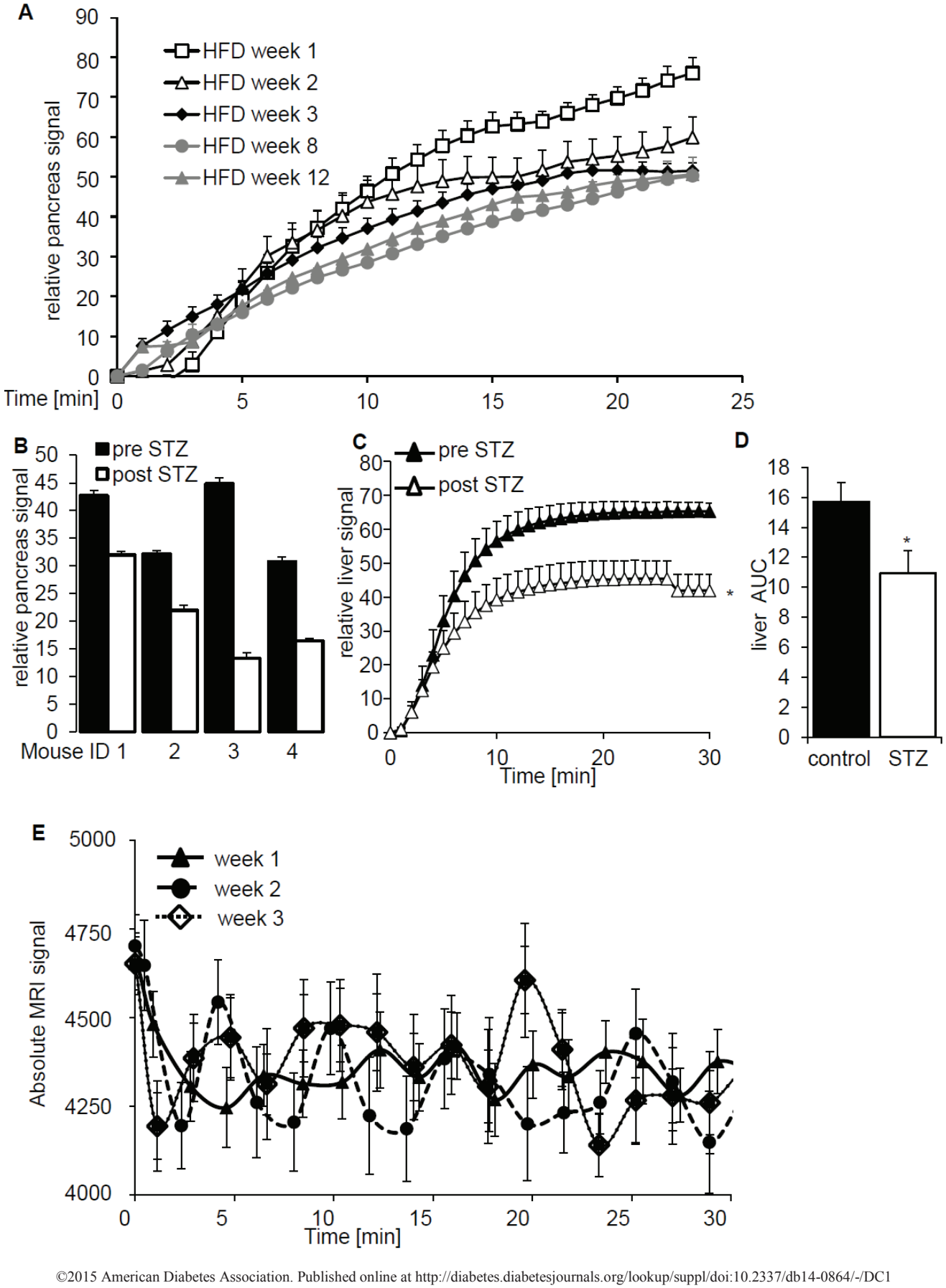

Bioanalytical Chemistry

DOI: 10.1002/anie.201407808

Indicator Displacement Assays Inside Live Cells**

*Amir Norouzy, Zahra Azizi, and Werner M. Nau**

Abstract: *The macrocycle p-sulfonatocalix[4]arene (CX4) and the fluorescent dye lucigenin (LCG) form a stable host–guest complex, in which the dye fluorescence is quenched. Incubation of live V79 and CHO cells with the CX4/LCG chemosensing ensemble resulted in its spontaneous uptake. Subsequent addition of choline, acetylcholine, or protamine, which have a high affinity for CX4 and are capable of entering cells, resulted in a fluorescence switch-on response. This can be traced to the displacement of LCG from CX4 by the analytes. The results establish the principal functionality of indicator displacement assays with synthetic receptors for the detection of the uptake of bioorganic analytes by live cells.*

Indicator displacement assays (IDAs) with synthetic receptors have gained increasing attention in (bio)analytical chemistry[1] because they offer a supramolecular approach for the sensitive detection and differentiation of analytes. IDAs bypass both the need to construct highly specific antibodies for immunoassays and the design of nanotechnological sensing systems, for example those based on graphene oxide[2] or capped mesoporous[3] architectures. The measurement principle is based on the use of an indicator dye bound to a receptor (the "reporter pair"). The receptor, frequently a macrocyclic host, is chosen to have a high affinity for the target analyte, such that competitive binding leads to a release of the dye, which in turn results in a change of its photophysical properties, preferably its fluorescence. A characteristic of such assays is the low selectivity with which the receptor binds different analytes, which can be an advantage because a broad range of analytes can be targeted without the need to synthesize a specific receptor for each of them. On the other hand, it is a disadvantage because the assays are very sensitive to competitive binding by other species with complementary charge and size, which are omnipresent in many fluid matrices and are almost always present in biological samples.[4] Nevertheless, several biologically relevant applications of macrocycles have been brought forward, including the delivery of drugs,[5] improved membrane passage of fluorescent dyes[6] and DNA,[7] the immobilization of cells,[8] protein recognition,[9] and cell imaging.[10]

We have previously designed time-resolved variants of displacement assays, which we refer to as supramolecular tandem assays because they are capable of monitoring enzymatic reactions in real time.[11] Interestingly, the assays performed well not only with purified enzymes but also with crude enzyme extracts[11c] and even with dried cells[11a] expressing a particular enzyme. Although the presence of salts, metabolites, and proteins in biological samples may lead to a sizable instantaneous change of the absolute signal owing to a competitive binding,[11c,12] it is the temporal response of the assay that serves as the robust fingerprint of the enzymatic activity, and this temporal response is what is analyzed.[13] This insight has encouraged the development of additional methods in which the spatiotemporal response of indicator displacement can be put to work. For example, we recently introduced tandem membrane assays, in which the reporter pair is spatially isolated inside the liposomes; in this manner, after addition of a target analyte to the outside bulk solution, its protein-mediated translocation through the biomembranes can be monitored in real time.[14] The combined results, namely a sizable tolerance towards competitive binders and a compartmentalized response, encouraged us to proceed towards the penultimate biological challenge: the transfer of IDAs with synthetic receptors to live cells in order to monitor the cellular uptake of biomolecular analytes. In fact, the application of artificial receptors for monitoring bioorganic analytes or drugs in cellular systems has been identified as a challenge in its own right;[1b,4,10,15] it goes beyond the well-established detection of certain inorganic ions in cells[16] or the use of functional group-specific fluorogenic sensors, such as those introduced for biothiols.[17]

We tested various macrocycle/dye combinations for their compatibility with biomembranes and found that the combination of *p*-sulfonatocalix[4]arene (CX4) and *N*,*N*′-dimethyl-9,9′-biacridinium dinitrate (lucigenin, LCG) gave a reporter pair that showed spontaneous uptake into live Chinese hamster ovary (CHO) and fibroblast cells (V79). The uptake of the reporter pair should allow us to subsequently perform cellular IDAs, while the high biocompatibility and low toxicity of both components, LCG and calixarenes in general,[18] as well as CX4 in particular,[18e,f,19] should be beneficial for live-cell measurements. Indeed, incubation with LCG (250 μM, 24 h) had no adverse effect on the cells. The cellular IDA, which we have now been able to realize, is schematically depicted in Scheme 1. The results relating to the successful uptake of analytes, monitored through the switch-on fluorescence response, are shown in Figure 1.

[*] Dr. A. Norouzy, Prof. Dr. W. M. Nau
Department of Life Sciences and Chemistry, Jacobs University Bremen
Campus Ring 1, 28759 Bremen (Germany)
E-mail: w.nau@jacobs-university.de
Z. Azizi
Centre for Biomolecular Interactions, University of Bremen
Leobener Straße NW2, 28359 Bremen (Germany)

[**] We appreciate the help of D. Gabel (Jacobs University), who provided the V79 cells and cell culture facilities, K. Brix, M. Rehders, J. Fritz, and M. Winterhalter (Jacobs University), K. Maedler (University of Bremen), as well as R. Amann, B. Fuchs and A. Ellrott (Max-Planck-Institute für Marine Mikrobiologie) for instrument access. The authors acknowledge project support from the DFG (W.M.N.) and the DAAD (doctoral fellowship for A.N.).

Supporting information for this article is available on the WWW under http://dx.doi.org/10.1002/anie.201407808.

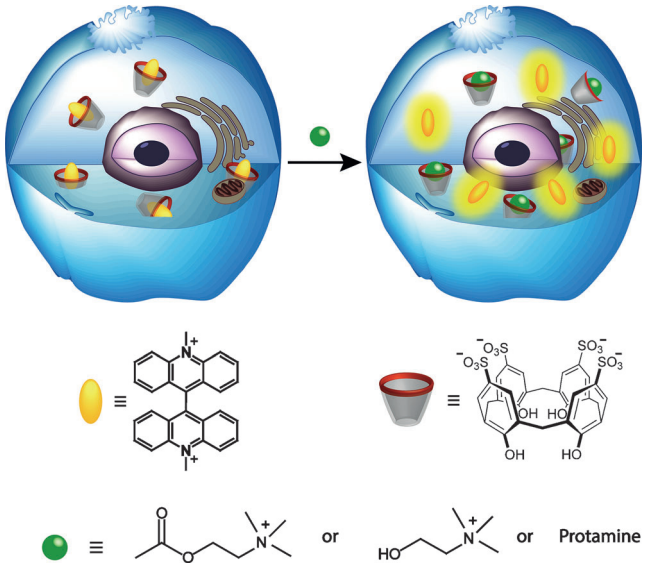

Scheme 1. The uptake of analytes into cells preloaded with the macrocycle–dye complex results in displacement of the dye from the macrocycle and an associated fluorescence increase.

The uptake of dye was confirmed and quantified through incubation of the dye (in the absence and presence of macrocycle), subsequent lysis of the cells, and measurement of the fluorescence after dilution and addition of competitor (to ensure dissociation of the host–dye complex). It should be noted that the fluorescence of the dye is quenched in the supramolecular complex, thus resulting in a switch-off response upon the addition of CX4 and a switch-on response the upon addition of competitor.[20] The uptake of macrocycle (in the presence of dye) was confirmed indirectly from no less than four independent observations: 1) Cells incubated with LCG (800 μM, 30 min) in the presence of CX4 (up to 5-fold excess) displayed an up to twice as efficient uptake of LCG (Table 1),[21] thus suggesting that the host additionally functions as a carrier (reminiscent of DNA transfection with cationic calixarenes).[7] 2) Fluorescence images of cells incubated with LCG in the presence of CX4 afforded much weaker fluorescence (Figure S7 in the Supporting Information). 3) The fluorescence of the lysate of cells incubated with LCG in the presence of CX4 increased substantially upon the addition of competitors, thereby confirming the dissociation of the host–dye complex and thus the presence of CX4 (Figure S4). 4) The observed switch-on fluorescence upon the addition of analytes to the live cells (Figure 1), as opposed to a simple quenching, requires the liberation of the dye from a quenched state, the macrocycle–dye complex.[22]

The surprising finding that the IDA remains operational inside live cells (Figure 1) can be explained by the favorable

Table 1: Uptake efficiency and absolute cellular concentrations of LCG in the absence and presence of CX4.[a]

Cell line	CX4 concentration [mM]	LCG concentration in cells [μM][b]	Uptake [%][b]
V79 cells	0	75	9.4
	4.5	150	19
CHO cells	0	10	1.3
	4.5	20	2.5

[a] Quantified with the lysis method, see the Supporting Information.
[b] Incubation conditions: 800 μM LCG, 30 min.

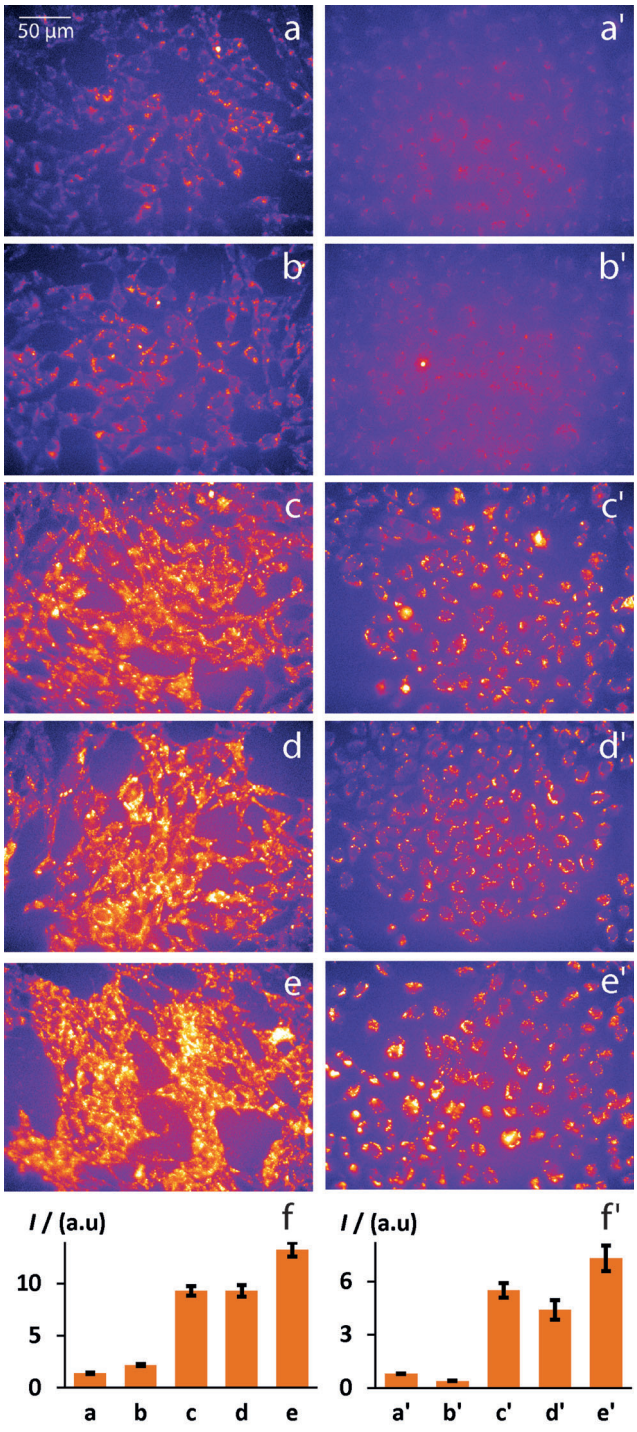

Figure 1. Fluorescence images of V79 cells (left column) and CHO cells (right), both incubated with 50 μM LCG and 250–300 μM CX4 at 37 °C for 15 min, followed by a 10 min incubation with medium (a and a′, as blank controls), 50 mM betaine (b and b′, as negative controls), 50 mM choline (c, c′), 50 mM acetylcholine (d, d′), and 15 min incubation with 200 μM protamine (e, e′). The bar graphs (f, f′) show the relative averaged fluorescence intensity per cell.

characteristics of the specific host/dye system. First, from experiments in pure water, LCG binds CX4 with a high affinity ($K_a = 2.8 \times 10^7\,M^{-1}$)[20] for a synthetic macrocycle,[23] thus facilitating the detection of competitive binders that also display high effective binding constants, such as acetylcholine (ACh, $K_a = 1.0 \times 10^5\,M^{-1}$), choline (Ch, $K_a = 1.0 \times 10^5\,M^{-1}$),[20] and the polycationic peptide protamine ($K_a = 1.24 \times 10^9\,M^{-1}$).[14] Second, CX4 quenches the fluorescence of LCG very efficiently (by a factor of up to 140),[20] which ensures a readily detectable response upon competitive binding. Preliminary experiments in Tyrode's solution and in the media (Figure S6), showed that both properties of the reporter pair are diminished as expected owing to the presence of large amounts of competitive salts, nutrients, and other biomolecules,[12b] but remained at a sufficiently high level ($K_a = 3.0 \times 10^5\,M^{-1}$, fluorescence enhancement factor of 90 in Tyrode's solution and 25 in the media) to retain a response to the target analytes. This encouraged the implementation of the CX4/LCG reporter pair to monitor analyte uptake into live cells.

If the CX4/LCG reporter pair was only physically adsorbed on the cell membrane surface or accessible in the outer cell membrane layer, the incubation of the cells with competitors such as choline, acetylcholine (50 mM),[20] and protamine (200 μM)[14] should lead to an effective release of uncomplexed LCG into the medium because the displacement process itself occurs within milliseconds.[14] However, the analyte solution collected after 10–20 min incubation did not show any LCG fluorescence, thus suggesting that the reporter pair was contained within the cells. By contrast, the cells exposed to the analyte solutions showed significantly enhanced fluorescence, which varied depending on the cell line and the analyte type (Figure 1). These fluorescence enhancements demonstrate that the analytes were taken up within 10–15 min into the cells, where they displaced LCG from the macrocyclic complex to result in enhanced cellular fluorescence. Incubation times longer than 20 min led to relatively smaller fluorescence recoveries, and no significant increase was observed after 5 h of incubation, thus suggesting that the reporter pair proceeds from the cytoplasm into different cellular compartments.[18b] The staining pattern of the released LCG is punctate, in agreement with previous cellular imaging studies of the dye alone.[18d] Although LCG turned out to be photobleached in confocal laser scanning microscopy experiments, the corresponding Z-stacking imaging results (Figure S2) corroborated distribution of the released dye (shortly after analyte addition) through the entire volume of the cell. The fact that dye displacement could also be achieved through cytoplasmic microinjection of the analyte (Figure S8) supports the idea that the initial localization of the CX4/LCG reporter pair is in the cytoplasm.[18a–d]

Indeed, the analytes were selected not only to act as strong competitors, but also because of their efficient cellular uptake. Ch is taken up into non-neuronal cells mainly by specific and nonspecific choline transporters,[24] while ACh crosses the membrane in both directions through organic cation transporters (OCTs),[25] which are expressed in almost all cells.[26] The cellular uptake of protamine is established but mechanistically more diverse, taking place predominantly through rapid endocytosis within 15–30 min,[27] the same time scale as that of the fluorescence recovery in our live-cell IDAs. After endosomal escape,[27b,28] protamine can interact with the reporter pair in the cytoplasm. It should also be noted that betaine was used as a negative control because it is also known to enter cells by a Na^+-dependent active transport mechanism,[29] but does not bind to CX4.[20] Indeed, this analyte (50 mM) afforded no significant fluorescence response in the live cells (Figure 1, parts b and b′), which demonstrates that the method is analyte-selective. The fluorescence enhancements could be semi-quantitatively analyzed (Figure 1, parts f and f′), and the analysis confirmed that, for both cell lines, betaine caused no significant fluorescence response, ACh and Ch caused about the same fluorescence enhancement, and protamine caused the largest fluorescence recovery, even at much lower concentrations. Although the absolute fluorescence responses are composite effects that depend on several factors (including the concentration of the analyte and its binding constant, see above), live-cell-based IDAs in principle offer the possibility for monitoring uptake at different incubation times.

In conclusion, we have established a receptor/dye IDA system that gives an easily measurable response to bioorganic analytes inside live cells. Live-cell-based IDAs could be employed as a simple, economic screening tool to monitor the uptake efficiencies of closely related compounds with similar affinities, such as different trimethylammonium ions or a library of polycationic peptides, the bioactivity of which is presently under intense discussion.

Received: July 31, 2014
Revised: October 14, 2014
Published online: November 27, 2014

Keywords: bioanalytical chemistry · fluorescence · host–guest complexes · macrocycles · supramolecular chemistry

[1] a) B. T. Nguyen, E. V. Anslyn, *Coord. Chem. Rev.* **2006**, *250*, 3118–3127; b) E. V. Anslyn, *J. Org. Chem.* **2007**, *72*, 687–699; c) S. K. Sun, K. X. Tu, X. P. Yan, *Analyst* **2012**, *137*, 2124–2128; d) X. J. Liu, H. T. Ngo, Z. J. Ge, S. J. Butler, K. A. Jolliffe, *Chem. Sci.* **2013**, *4*, 1680–1686; e) D. Leung, J. F. Folmer-Andersen, V. M. Lynch, E. V. Anslyn, *J. Am. Chem. Soc.* **2008**, *130*, 12318–12327; f) R. G. Hanshaw, E. J. O'Neil, M. Foley, R. T. Carpenter, B. D. Smith, *J. Mater. Chem.* **2005**, *15*, 2707–2713.

[2] a) Y. Wang, Z. H. Li, D. H. Hu, C. T. Lin, J. H. Li, Y. H. Lin, *J. Am. Chem. Soc.* **2010**, *132*, 9274–9276; b) X. Sun, Z. Liu, K. Welsher, J. T. Robinson, A. Goodwin, S. Zaric, H. Dai, *Nano Res.* **2008**, *1*, 203–212; c) X. W. Mao, D. M. Tian, H. B. Li, *Chem. Commun.* **2012**, *48*, 4851–4853; d) X. W. Mao, H. B. Li, *J. Mater. Chem. B* **2013**, *1*, 4267–4272.

[3] a) S. Angelos, Y. W. Yang, K. Patel, J. F. Stoddart, J. I. Zink, *Angew. Chem. Int. Ed.* **2008**, *47*, 2222–2226; *Angew. Chem.* **2008**, *120*, 2254–2258; b) A. Agostini, L. Mondragón, A. Bernardos, R. Martínez-Máñez, M. D. Marcos, F. Sancenón, J. Soto, A. Costero, C. Manguan-García, R. Perona, M. Moreno-Torres, R. Aparicio-Sanchis, J. R. Murguía, *Angew. Chem. Int. Ed.* **2012**, *51*, 10556–10560; *Angew. Chem.* **2012**, *124*, 10708–10712; c) Y. Zhou, L. L. Tan, Q. L. Li, X. L. Qiu, A. D. Qi, Y. C. Tao, Y. W. Yang, *Chem. Eur. J.* **2014**, *20*, 2998–3004; d) D. G. He,

X. X. He, K. M. Wang, Z. Zou, X. Yang, X. C. Li, *Langmuir* **2014**, *30*, 7182 – 7189.
[4] a) B. J. Shorthill, C. T. Avetta, T. E. Glass, *J. Am. Chem. Soc.* **2004**, *126*, 12732 – 12733; b) S. H. Zhang, T. E. Glass, *Tetrahedron Lett.* **2010**, *51*, 112 – 114.
[5] a) Q. P. Duan, Y. Cao, Y. Li, X. Y. Hu, T. X. Xiao, C. Lin, Y. Pan, L. Y. Wang, *J. Am. Chem. Soc.* **2013**, *135*, 10542 – 10549; b) J. Zhang, Z. F. Yuan, Y. Wang, W. H. Chen, G. F. Luo, S. X. Cheng, R. X. Zhuo, X. Z. Zhang, *J. Am. Chem. Soc.* **2013**, *135*, 5068 – 5073; c) J. J. Yin, S. Sharma, S. P. Shumyak, Z. X. Wang, Z. W. Zhou, Y. D. Zhang, P. X. Guo, C. Z. Li, J. R. Kanwar, T. X. Yang, S. S. Mohapatra, W. Q. Liu, W. Duan, J. C. Wang, Q. Li, X. J. Zhang, J. Tan, L. Jia, J. Liang, M. Q. Wei, X. T. Li, S. F. Zhou, *PLoS One* **2013**, *8*, e62289.
[6] Z. Y. Li, S. G. Sun, Z. G. Yang, S. Zhang, H. Zhang, M. M. Hu, J. F. Cao, J. Y. Wang, F. Y. Liu, F. L. Song, J. L. Fan, X. J. Peng, *Biomaterials* **2013**, *34*, 6473 – 6481.
[7] a) V. Bagnacani, V. Franceschi, M. Bassi, M. Lomazzi, G. Donofrio, F. Sansone, A. Casnati, R. Ungaro, *Nat. Commun.* **2013**, *4*, 1721; b) L. Nault, A. Cumbo, R. F. Pretôt, M. A. Sciotti, P. Shahgaldian, *Chem. Commun.* **2010**, *46*, 5581 – 5583.
[8] a) P. Neirynck, J. Brinkmann, Q. An, D. W. J. van der Schaft, L. G. Milroy, P. Jonkheijm, L. Brunsveld, *Chem. Commun.* **2013**, *49*, 3679 – 3681; b) Q. An, J. Brinkmann, J. Huskens, S. Krabbenborg, J. de Boer, P. Jonkheijm, *Angew. Chem. Int. Ed.* **2012**, *51*, 12233 – 12237; *Angew. Chem.* **2012**, *124*, 12399 – 12403.
[9] a) D. Bier, R. Rose, K. Bravo-Rodriguez, M. Bartel, J. M. Ramirez-Anguita, S. Dutt, C. Wilch, F. G. Klarner, E. Sanchez-Garcia, T. Schrader, C. Ottmann, *Nat. Chem.* **2013**, *5*, 234 – 239; b) D. W. Lee, K. M. Park, M. Banerjee, S. H. Ha, T. Lee, K. Suh, S. Paul, H. Jung, J. Kim, N. Selvapalam, S. H. Ryu, K. Kim, *Nat. Chem.* **2011**, *3*, 154 – 159; c) S. A. Minaker, K. D. Daze, M. C. F. Ma, F. Hof, *J. Am. Chem. Soc.* **2012**, *134*, 11674 – 11680.
[10] S. S. Agasti, M. Liong, C. Tassa, H. J. Chung, S. Y. Shaw, H. Lee, R. Weissleder, *Angew. Chem. Int. Ed.* **2012**, *51*, 450 – 454; *Angew. Chem.* **2012**, *124*, 465 – 469.
[11] a) A. Hennig, H. Bakirci, W. M. Nau, *Nat. Methods* **2007**, *4*, 629 – 632; b) D. M. Bailey, A. Hennig, V. D. Uzunova, W. M. Nau, *Chem. Eur. J.* **2008**, *14*, 6069 – 6077; c) W. M. Nau, G. Ghale, A. Hennig, H. Bakirci, D. M. Bailey, *J. Am. Chem. Soc.* **2009**, *131*, 11558 – 11570.
[12] a) V. Francisco, A. Pineiro, W. M. Nau, L. Garcia-Rio, *Chem. Eur. J.* **2013**, *19*, 17809 – 17820; b) K. D. Daze, C. E. Jones, B. J. Lilgert, C. S. Beshara, F. Hof, *Can. J. Chem.* **2013**, *91*, 1072 – 1076.
[13] a) R. N. Dsouza, A. Hennig, W. M. Nau, *Chem. Eur. J.* **2012**, *18*, 3444 – 3459; b) D. A. Jose, M. Elstner, A. Schiller, *Chem. Eur. J.* **2013**, *19*, 14451 – 14457; c) B. Vilozny, A. Schiller, R. A. Wessling, B. Singaram, *Anal. Chim. Acta* **2009**, *649*, 246 – 251; d) T. Desmet, W. Soetaert, P. Bojarova, V. Kren, L. Dijkhuizen, V. Eastwick-Field, A. Schiller, *Chem. Eur. J.* **2012**, *18*, 10786 – 10801.
[14] G. Ghale, A. G. Lanctot, H. T. Kreissl, M. H. Jacob, H. Weingart, M. Winterhalter, W. M. Nau, *Angew. Chem. Int. Ed.* **2014**, *53*, 2762 – 2765; *Angew. Chem.* **2014**, *126*, 2801 – 2805.
[15] K. S. Hettie, X. Liu, K. D. Gillis, T. E. Glass, *ACS Chem. Neurosci.* **2013**, *4*, 918 – 923.
[16] a) D. Kim, S. Singha, T. Wang, E. Seo, J. H. Lee, S. J. Lee, K. H. Kim, K. H. Ahn, *Chem. Commun.* **2012**, *48*, 10243 – 10245; b) E. L. Que, D. W. Domaille, C. J. Chang, *Chem. Rev.* **2008**, *108*, 4328 – 4328; c) D. W. Domaille, E. L. Que, C. J. Chang, *Nat. Chem. Biol.* **2008**, *4*, 507 – 507; d) A. K. Mahapatra, J. Roy, P. Sahoo, S. K. Mukhopadhyay, A. Chattopadhyay, *Org. Biomol. Chem.* **2012**, *10*, 2231 – 2236; e) G. Sivaraman, T. Anand, D. Chellappa, *RSC Adv.* **2013**, *3*, 17029 – 17033; f) J. L. Wang, L. P. Long, D. Xie, Y. W. Zhan, *J. Lumin.* **2013**, *139*, 40 – 46; g) M. X. Yu, M. Shi, Z. G. Chen, F. Y. Li, X. X. Li, Y. H. Gao, J. Xu, H. Yang, Z. G. Zhou, T. Yi, C. H. Huang, *Chem. Eur. J.* **2008**, *14*, 6892 – 6900.
[17] a) K. Cui, Z. L. Chen, Z. Wang, G. X. Zhang, D. Q. Zhang, *Analyst* **2011**, *136*, 191 – 195; b) H. Kwon, K. Lee, H. J. Kim, *Chem. Commun.* **2011**, *47*, 1773 – 1775; c) C. Huang, T. Jia, M. Tang, Q. Yin, W. Zhu, C. Zhang, Y. Yang, N. Jia, Y. Xu, X. Qian, *J. Am. Chem. Soc.* **2014**, *136*, 14237 – 14244.
[18] a) R. Lalor, H. Baillie-Johnson, C. Redshaw, S. E. Matthews, A. Mueller, *J. Am. Chem. Soc.* **2008**, *130*, 2892 – 2893; b) A. Mueller, R. Lalor, C. M. Cardaba, S. E. Matthews, *Cytometry Part A* **2011**, *79A*, 126 – 136; c) C. Redshaw, M. R. J. Elsegood, J. A. Wright, H. Baillie-Johnson, T. Yamato, S. De Giovanni, A. Mueller, *Chem. Commun.* **2012**, *48*, 1129 – 1131; d) S. J. Rembish, M. A. Trush, *Free Radical Biol. Med.* **1994**, *17*, 117 – 126; e) A. W. Coleman, S. Jebors, S. Cecillon, P. Perret, D. Garin, D. Marti-Battle, M. Moulin, *New J. Chem.* **2008**, *32*, 780 – 782; f) D.-S. Guo, Y. Liu, *Acc. Chem. Res.* **2014**, *47*, 1925 – 1934.
[19] a) F. Perret, A. W. Coleman, *Chem. Commun.* **2011**, *47*, 7303 – 7319; b) M. H. Paclet, C. F. Rousseau, C. Yannick, F. Morel, A. W. Coleman, *J. Inclusion Phenom. Macrocyclic Chem.* **2006**, *55*, 353 – 357; c) K. Wang, D. S. Guo, X. Wang, Y. Liu, *ACS Nano* **2011**, *5*, 2880 – 2894.
[20] D. S. Guo, V. D. Uzunova, X. Su, Y. Liu, W. M. Nau, *Chem. Sci.* **2011**, *2*, 1722 – 1734.
[21] V79 cells showed more efficient uptake of the dye than CHO cells (Table 1), which could be due, among other factors, to different surface-to-volume ratios of the two cell types (0.65 μm^{-1} for V79 and 0.37 μm^{-1} for CHO cells, see the Supporting Information for size estimations).
[22] While LCG has been demonstrated to undergo cellular uptake by adsorptive endocytosis: I. Braakman, T. Pijning, O. Verest, B. Weert, D. K. F. Meijer, G. M. M. Groothuis, *Mol. Pharmacol.* **1989**, *36*, 537 – 542, there are several potential uptake routes for the CX4/LCG complex (see the Supporting Information).
[23] R. N. Dsouza, U. Pischel, W. M. Nau, *Chem. Rev.* **2011**, *111*, 7941 – 7980.
[24] a) S. A. Müller, K. Holzapfel, C. Seidl, U. Treiber, B. J. Krause, R. Senekowitsch-Schmidtke, *Eur. J. Nucl. Med. Mol. Imaging* **2009**, *36*, 1434 – 1442; b) P. R. Lockman, D. D. Allen, *Drug Dev. Ind. Pharm.* **2002**, *28*, 749 – 771; c) P. Schloss, W. Mayser, A. Niehuis, H. Betz, *Biochem. Biophys. Res. Commun.* **1994**, *199*, 1320 – 1325.
[25] K. S. Lips, C. Volk, B. M. Schmitt, U. Pfeil, P. Arndt, D. Miska, L. Ermert, W. Kummer, H. Koepsell, *Am. J. Respir. Cell Mol. Biol.* **2005**, *33*, 79 – 88.
[26] I. Wessler, C. J. Kirkpatrick, *Br. J. Pharmacol.* **2008**, *154*, 1558 – 1571.
[27] a) H. Amos, *Biochem. Biophys. Res. Commun.* **1961**, *5*, 1 – 4; b) H. Amos, K. E. Kearns, *Exp. Cell Res.* **1963**, *32*, 14 – 32; c) J. Nagai, T. Komeda, Y. Katagiri, R. Yumoto, M. Takano, *Biol. Pharm. Bull.* **2013**, *36*, 1942 – 1949.
[28] a) J. Guy, D. Drabek, M. Antoniou, *Mol. Biotechnol.* **1995**, *3*, 237 – 248; b) Y. W. Cho, J. D. Kim, K. Park, *J. Pharm. Pharmacol.* **2003**, *55*, 721 – 734.
[29] P. G. Petronini, E. Deangelis, A. F. Borghetti, K. P. Wheeler, *Biochem. J.* **1994**, *300*, 45 – 50.

Angewandte Chemie
Eine Zeitschrift der Gesellschaft Deutscher Chemiker

Supporting Information

69451 Weinheim, Germany

Indicator Displacement Assays Inside Live Cells**

*Amir Norouzy, Zahra Azizi, and Werner M. Nau**

anie_201407808_sm_miscellaneous_information.pdf

Supporting Information

Table of Contents

1. Materials

Frozen Chinese hamster ovary (CHO) cells were purchased from Sigma-Aldrich. Chinese hamster fibroblast (V79) cells were kindly made available by Detlef Gabel, Jacobs University Bremen. Cultivation dishes (60 cm^2) and Falcon tubes as well as penicillin/streptomycin and trypsin (1000 U ml^{-1}) were purchased from Biochrom AG. Ham's F10 and F12 media, fetal bovine serum (FBS), sterile glutamine solution, acetylcholine perchlorate, and protamine sulfate (from herring) were purchased from Sigma-Aldrich. Imaging µ-dishes (35 mm, high wall and low wall, for micro injection) were purchased from *ibidi*. Choline chloride was from Fluka.

2. Cell Cultivation and Preparation for Imaging

V79 cells (Figure S1) were cultivated in Ham's F10 medium, 10% FBS, while CHO cells (Figure S1) were grown in Ham's F12 medium, 10% FBS, and 2 mM L-Glutamine. Dishes were kept in a humid, 5% CO_2 incubator at 37 °C until the cells reached a confluence of about 90%. The cells were subsequently trypsinized and diluted by 1:10 into the *ibidi* dishes followed by 2-3 days incubation until 60-80% confluent monolayers were obtained.

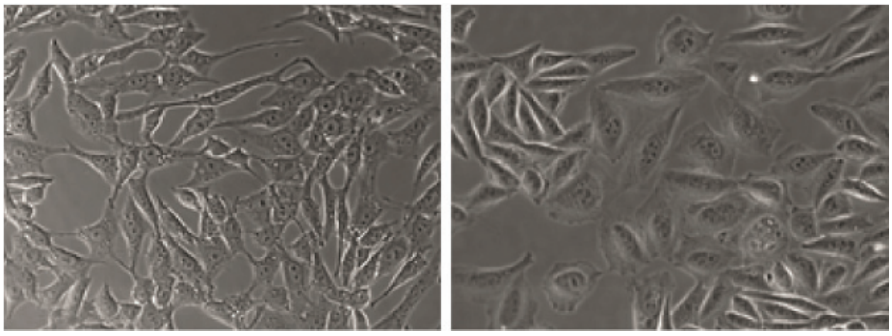

Figure S1. Bright-field images with 40X object magnification of V79 cells (left) and CHO cells (right).

3. Loading with Host and Dye and Subsequent Dye Displacement by Analytes

For loading with CX4/LCG, the V79 and CHO cells in the *ibidi* dishes were incubated for 15 min at 37 °C with a mixture of 50 µM LCG and 250-300 µM CX4, dissolved in medium. An excess of host was needed for efficient fluorescence quenching, as judged from the cell images (Figure S7). The cells were then washed 3 times with fresh medium and incubated for 10-15 minutes at 37 °C with 50 mM ACh, 50 mM Ch, or 200 µM (0.9 mg ml^{-1}) protamine, dissolved in medium pre-warmed to 37°C. Subsequently, the supernatant analyte solutions were collected and tested for LCG to confirm that the dye was retained in the cells (and not, for example, weakly adsorbed on the outer cell membrane). Finally, the cells were washed 3 times with Tyrode's solution and immediately used for imaging under Tyrode's solution (Figure 1).

4. Microscopy

4.1. Fluorescence microscopy

Cell images were taken in a dark room on an Axiovert 200 microscope (Zeiss) equipped with an Evolution™ QEi camera with 1.4 megapixels and 1392×1040 dimension. Filter set 44 (Zeiss) in combination with a 500-nm beam splitter was used for excitation at 435-500 nm and emission at 480-580 nm. To reduce photobleaching of LCG, the snapshot was taken immediately upon exposure to the excitation light, using identical light exposure (500 ms, unless stated differently) and gain settings.

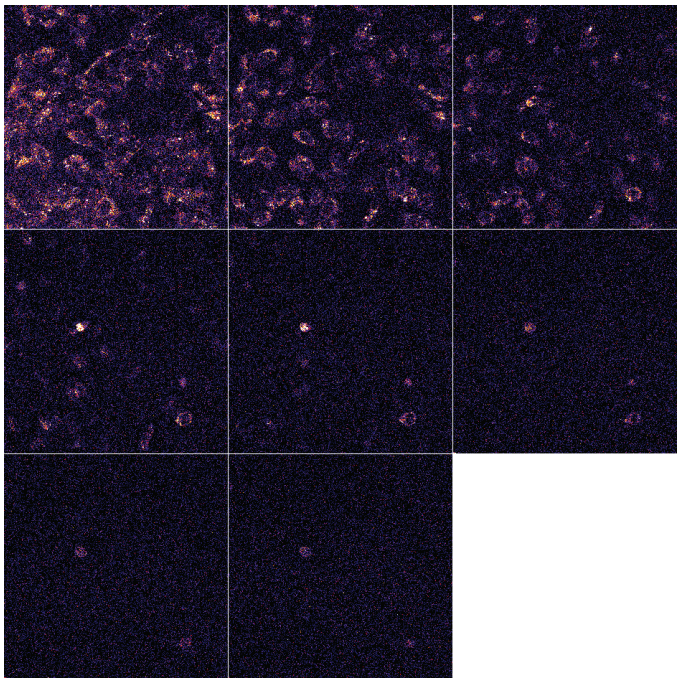

Figure S2. Fluorescence images of a V79 cell monolayer were recorded by CLSM 3D scanning after incubation with CX4/LCG and subsequently 50 mM Ch. From left to right in each row, one layer of the cells was scanned from bottom of the dish to the top (Z stacking).

4.2 Confocal Laser Scanning Microscopy (CLSM)

The uptake of Ch was also monitored by 3D scanning using a confocal laser scanning microscope (Zeiss LSM 780) by 405-nm laser excitation (Figure S2). Since the dye was significantly photobleached already after the third scan, the confocal measurements were not preferred for the comparative measurements of analyte uptake. Nevertheless, vertical scanning, from bottom to top, showed the distribution of the dye in the entire volume of the cells. This provided circumstantial evidence that the dye does not accumulate in the cell membrane but rather distributes in the cytoplasm with a punctate pattern.

5. Image Processing and Analysis

The 16-bit fluorescence-microscopic images were added to an imageJ stack[1] with normalized background for further processing (Figure 1, selected color was “fire”). The average fluorescence intensities (Figure 1 f and f') were obtained by binning of the entire fluorescence images in 8-bit type, and by choosing the threshold manually (the selection of automated thresholding procedures provided qualitatively comparable results, but with lower contrast, see Figure S3). The abundance of each histogram bar was multiplied with the relative intensity (between the threshold value and the maximum value of 255), and finally, divided by the number of cells (counted manually). The error bars correspond to the standard deviation from the mean value calculated by the imageJ program for each individual image.

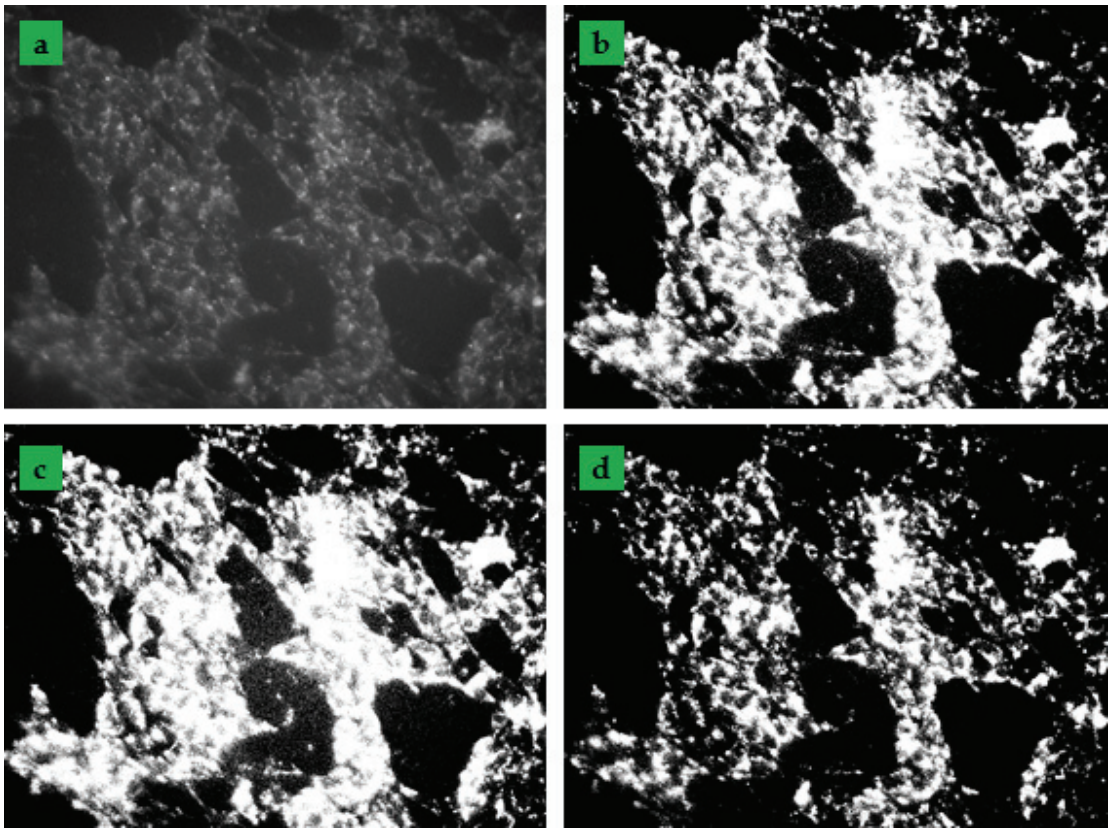

Figure S3. Fluorescence images of V79 cells. An 8-bit image (a, raw data) was subjected to different thresholding methods: Otsu[2] (b), Li[3] (c), and manually (d).

6. Calculation of Uptake of LCG in the Absence and Presence of CX4

Comparable numbers of V79 or CHO cells were cultivated in three 60 cm^2 dishes. In Dish 1 the cells were incubated with 800 µM LCG, in Dish 2 they were incubated with CX4/LCG ([LCG] = 800 µM, [CX4]/[LCG] = 5/1), and Dish 3 was used as a reference, without additive incubation (Figures S4b,d). After 30 min incubation, Dish 1 and 2 were washed three times with warm medium (37 °C) to remove residual LCG and CX4/LCG. Following trypsinization, the homogenously suspended cells were counted on a cytometer to estimate the total number of cells on each dish. For dye content analysis, the suspended cells were lysed with Triton X-100 to collect their cytoplasmic components.[4]

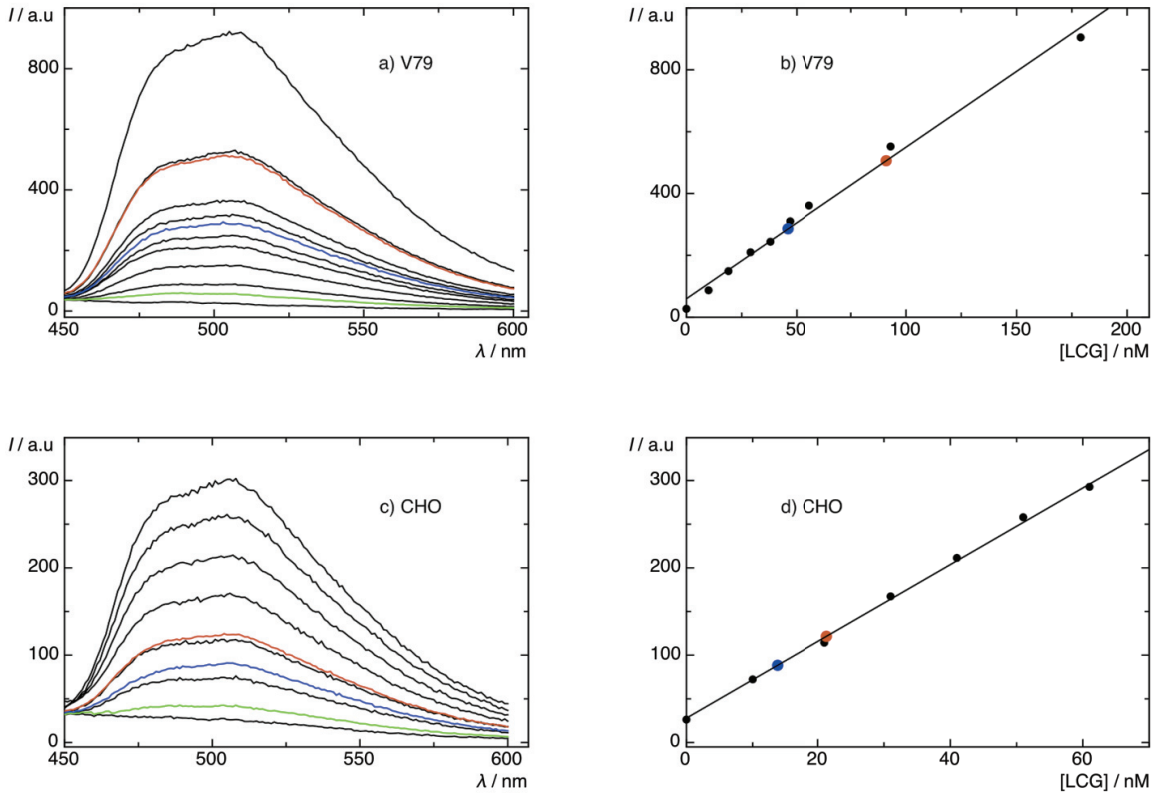

Figure S4. a,c) Fluorescence spectra of lysed V79 and CHO cells after incubation with LCG (800 µM) in the absence (blue) and presence of a 5-fold excess of CX4 (green) and after addition of excess protamine (4 mM, red). The black spectra are for different LCG concentrations in the lysed reference solutions. b,d) Calibration curves, obtained from the fluorescence maxima (λ_{max} = 505 nm) of the black spectra in a,c); the blue and red data points mark the interpolated LCG concentrations in the absence (blue) and presence of a 5-fold excess of CX4 after addition of excess protamine (4 mM, red), respectively.

Fluorescence spectra of all lysates (λ_{exc} = 369 nm) were obtained after dilution to 3 ml (to allow cuvette measurement) and filtering (0.20 µm syringe filter, tested not to adsorb the dye). In a second step, an excess of protamine (4 mM) was added to the obtained lysed solutions from all dishes in order to affect a complete dissociation of the CX4/LCG complex, resulting in a significant increase due to dye release for Dish 2 only (from green to red spectra in Figure S4a,c); incidentally, this experiment corroborates the presence of CX4 in the cytoplasm. In contrast, the fluorescence intensity in Dish 1, which contained no CX4, remained unchanged, because control experiments showed that the direct addition of competitors (up to 10 mM Ch or ACh and 4 mM protamine) cause no significant fluorescence quenching. To determine the absolute uptake of LCG, different LCG concentrations were added to the lysed *reference* solutions (Dish 3, without additives). This allowed us to construct calibration curves (Figure S4, right) for the dye fluorescence intensity in this medium (black spectra in Figure S4a,c). The absolute concentrations of LCG after uptake into the cells (Table 1 of main text) were estimated by employing spherical cell volumes derived from reported average cell diameters (9.3 µM for V79 and 14.0 µM for CHO).[5]

7. Potential Uptake Routes of LCG in the Absence and Presence of CX4

Due to the established use of LCG, among others for the detection of mitochondrial superoxide generation in cells[6] its cellular uptake mechanism has already been investigated in detail and identified as proceeding by adsorptive endocytosis.[7] The presence of CX4 results not only in an uptake of the macrocycle but also an enhanced uptake of LCG (see main text), the mechanism for which is yet not clarified in detail.

Although CX4 by itself does not permeate through lipid bilayer membranes,[8] it has been demonstrated that it can pass through anion channels under certain conditions.[9] Moreover, especially in the presence of hydrophobic guests,[10] CX4 is able to form charge-neutralized host-guest aggregates, which have been shown to facilitate cellular uptake.[10b] To evaluate a possible aggregate formation, we have investigated the host-guest system by UV titrations, which, however, did not reveal any light scattering in the typical concentration range, but, instead, clearly defined isosbestic points at 373, 392 and 464 nm (Figure S5). Similarly, dynamic light scattering experiments did not afford any evidence for the formation of large aggregates. We therefore have at present no evidence for the involvement of CX4/LCG aggregates. Frequently, the formation of such aggregates is facilitated by π-π stacking interactions between guest molecules (for a review of guests promoting aggregate formation see ref.[10a]). For LCG, this possibility is prevented by the twisted arrangements of the aryl groups, which is also evident from the experimental crystal structure.[11]

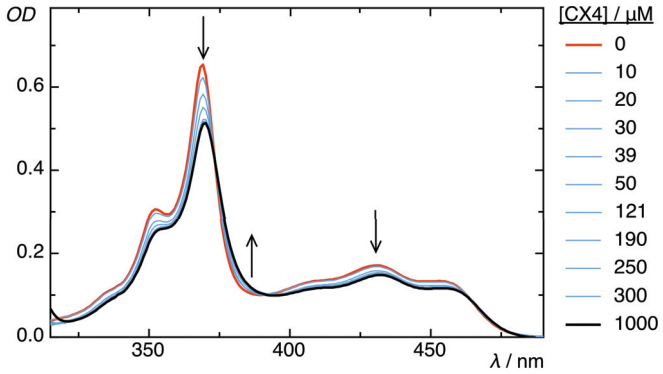

Figure S5. UV-Vis titration of 50 μM LCG with CX4 (up to 1 mM); the arrows depict the trend of the *OD* changes in the different spectral regions.

It should also be noted that the uptake mechanism of several labeled calixarene derivatives into several cell lines, including CHO, THP-1 and HeLa, has been extensively studied by Mueller and coworkers.[12] A non-specific, membrane carrier-mediated uptake with an initial homogeneous distribution in the cytoplasm, followed by appearance in the Golgi and, finally, in the acidic vesicles was suggested.

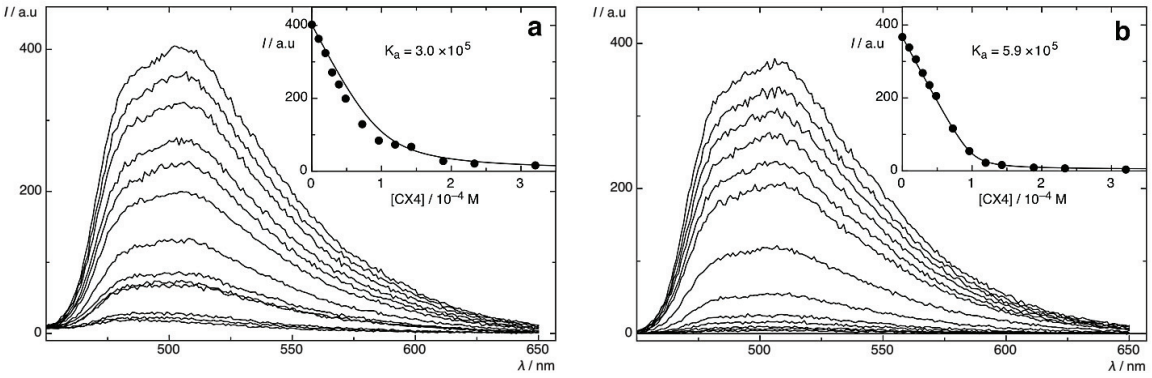

Figure S6. Direct fluorescence titration of LCG (100 μM) with CX4 in Ham's medium (a) and in Tyrode's solution (b) pH= 7, λ_{ex} =369 nm. The inset shows the associated titration curve, and nonlinear fitting according to a 1:1 binding stoichiometry.

8. Gradual Decrease of LCG Fluorescence in Cells

Figure S6 shows direct titrations of LCG by CX4 in Ham's medium[13] and in Tyrode's solution[14] and the determinations of the apparent binding constants (insets). Due to the presence of ca. 150 mM salts, nutrients, amino acids, vitamins, 10% fetal bovine serum, etc. in Ham's medium, the host-dye binding constant is reduced in the medium compared to neat water (see main text), but remains large (> 3 × 10^5 M^{-1}). Based on the titrations, an excess of CX4 needed to be employed to ensure efficient quenching of LCG fluorescence and, thus, to facilitate a readily

detectable fluorescence recovery upon analyte uptake. Figure S7 shows the fluorescence of V79 and CHO cells incubated with different host/dye ratios. A 4:1 ratio for V79 and 6:1 ratio for CHO was preferable to affect a strong (> 50%) fluorescence quenching.

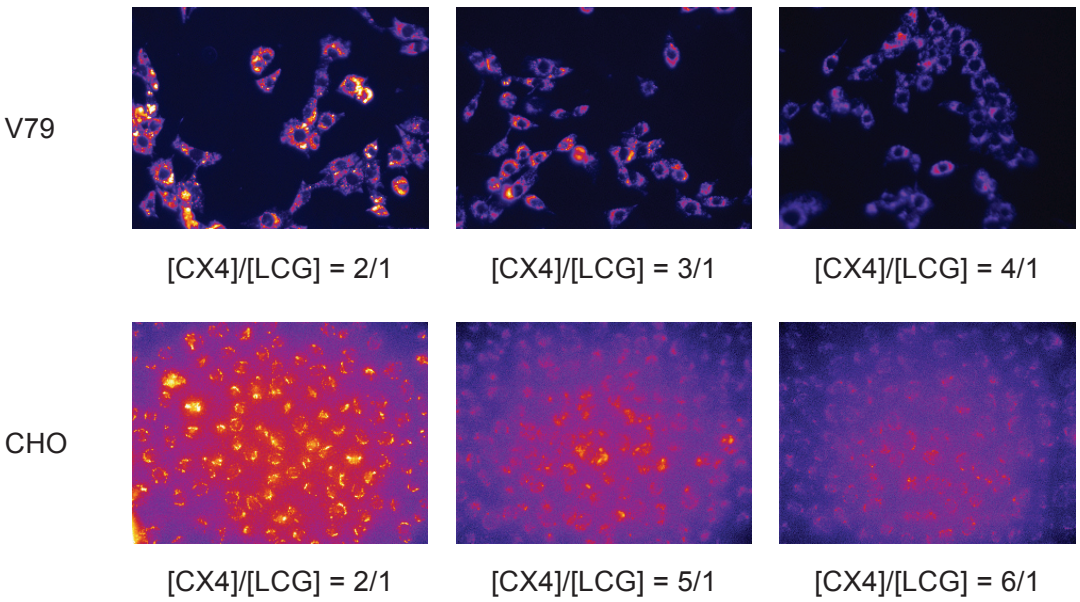

Figure S7. Fluorescence of V79 and CHO cells incubated with different superstoichiometric amounts of host at a constant dye concentration (50 μM); light exposure was 100 ms for V79 cells and 500 ms for CHO cells.

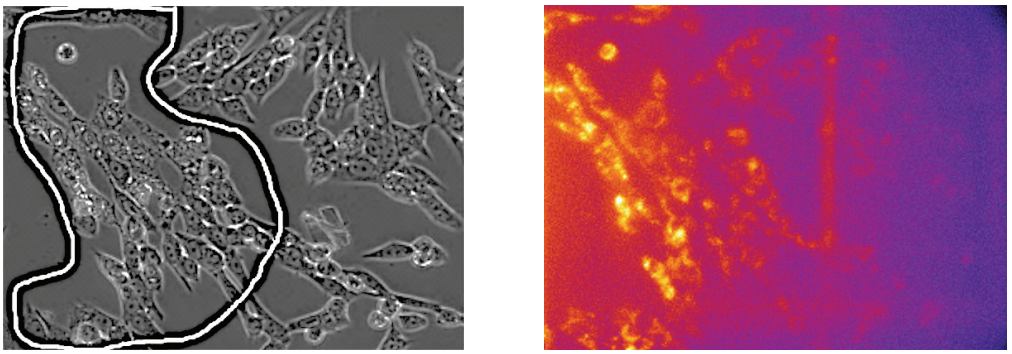

Figure S8. Bright-field (left) and fluorescence image (right) of V79 cells incubated with CX4/LCG solution ([LCG] = 10 μM, [CX4]/[LCG] = 5/1, 10 min) and after microinjection with ACh (area with injected cells encircled on the left).

9. Dye Release by Microinjection

For microinjection experiments, V79 cells were incubated with CX4/LCG solution, washed with Tyrode's solution, and 100 mM ACh solution was injected into the cytoplasm of selected cells by

using a FemtoJet Eppendorf microinjector (60 hpa capillary pressure, injection pressure 190 hpa, 3 seconds). A strong fluorescence recovery was observed (Figure S8). Since this method was prone to cellular damage and because the timing between incubation and injection turned out to be critical but difficult to ensure by this method, it was not preferred for follow-up experiments.

10. Effects at High Protamine Concentrations

It is known that high (mM) concentrations of protamine can damage cells by causing membrane rupture. Therefore, we also applied high concentrations and, indeed, dead cells were observed (Figure S9). Interestingly, these cells showed the largest fluorescence enhancements (see arrows in Figure S9), presumably due to additional release of dye from the endosomes.[12b] The comparison of two cell lines showed further that V79 cells are more sensitive to protamine than CHO cells, since almost all V79 cells were adversely affected. Analytes causing cell lysis do therefore need to be investigated with particular care to avoid false positive results.

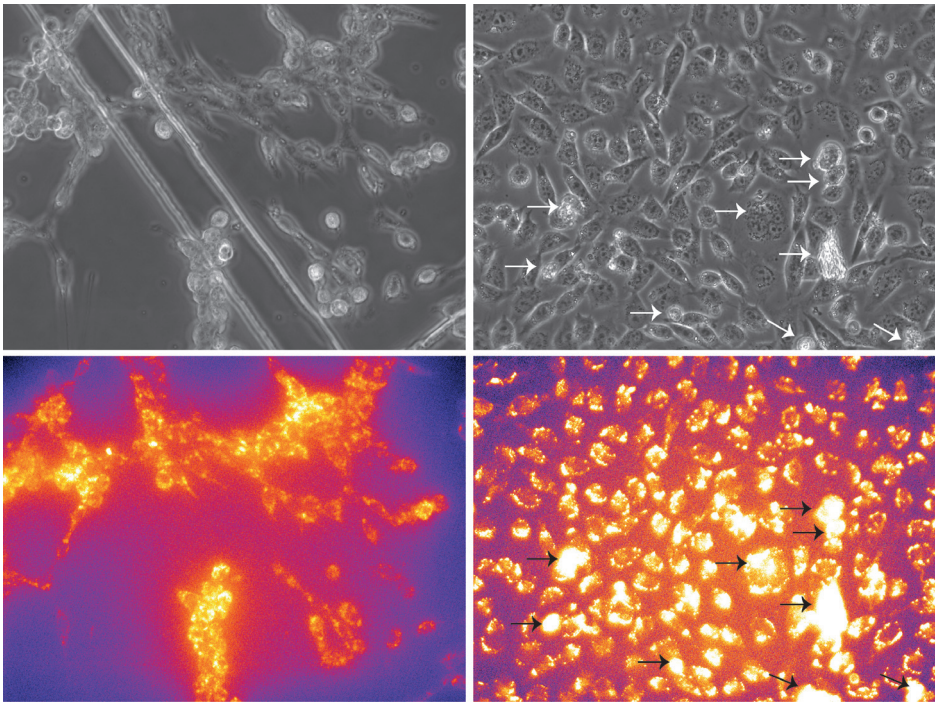

Figure S9. Bright-field (top) and fluorescence images of V79 cells (left column) and CHO cells (right), both incubated with 50 µM LCG and 250-300 µM CX4 at 37 °C for 15 min, followed by a 20-min incubation with 4 mM protamine. Dead CHO cells resulting from protamine-induced cell damage are marked by arrows.

11. References

[1] C. A. Schneider, W. S. Rasband, K. W. Eliceiri, *Nat. Methods* **2012**, *9*, 671-675.

[2] J. H. Xue, Y. J. Zhang, *Pattern Recognit. Lett.* **2012**, *33*, 793-797.

[3] C. H. Li, P. K. S. Tam, *Pattern Recognit. Lett.* **1998**, *19*, 771-776.

[4] H. Ji, *Cold Spring Harb. Protoc.* **2010**, *2010*, pdb.prot5466.

[5] a) D. Bettega, P. Calzolari, S. M. Doglia, B. Dulio, L. Tallone, A. M. Villa, *Int. J. Radiat. Biol.* **1998**, *74*, 397-403; b) Y. Han, X. M. Liu, H. Liu, S. C. Li, B. C. Wu, L. L. Ye, Q. W. Wang, Z. L. Chen, *J Biosci Bioeng* **2006**, *102*, 430-435.

[6] S. J. Rembish, M. A. Trush, *Free Radical Biol. Med.* **1994**, *17*, 117-126.

[7] I. Braakman, T. Pijning, O. Verest, B. Weert, D. K. F. Meijer, G. M. M. Groothuis, *Mol. Pharmacol.* **1989**, *36*, 537-542.

[8] a) Y. L. Ying, J. J. Zhang, F. N. Meng, C. Cao, X. Y. Yao, I. Willner, H. Tian, Y. T. Long, *Sci. Rep.* **2013**, *3*, 1662; b) B. J. Laventie, C. Potrich, C. Atmanene, M. Saleh, O. Joubert, G. Viero, C. Bachmeyer, V. Antonini, I. Mancini, S. Cianferani-Sanglier, D. Keller, D. A. Colin, T. Bourcier, G. Anderluh, A. van Dorsselaer, M. Dalla Serra, G. Prevost, *Biochem. J.* **2013**, *450*, 559-571; c) G. Ghale, A. G. Lanctot, H. T. Kreissl, M. H. Jacob, H. Weingart, M. Winterhalter, W. M. Nau, *Angew. Chem. Int. Ed.* **2014**, *53*, 2762-2765.

[9] G. Droogmans, J. Prenen, J. Eggermont, T. Voets, B. Nilius, *Am. J. Physiol.-Cell Ph.* **1998**, *275*, C646-C652.

[10] a) D.-S. Guo, Y. Liu, *Acc. Chem. Res.* **2014**, *47*, 1925-1934; b) Patents: FR2904782-A1; WO2008020126-A2; WO2008020126-A3; EP2073783-A2; CA2660295-A1; US2010292272-A1.

[11] D. S. Guo, V. D. Uzunova, X. Su, Y. Liu, W. M. Nau, *Chem. Sci.* **2011**, *2*, 1722-1734.

[12] a) R. Lalor, H. Baillie-Johnson, C. Redshaw, S. E. Matthews, A. Mueller, *J. Am. Chem. Soc.* **2008**, *130*, 2892-2893; b) A. Mueller, R. Lalor, C. M. Cardaba, S. E. Matthews, *Cytom. Part A* **2011**, *79A*, 126-136; c) C. Redshaw, M. R. J. Elsegood, J. A. Wright, H. Baillie-Johnson, T. Yamato, S. De Giovanni, A. Mueller, *Chem. Commun.* **2012**, *48*, 1129-1131.

[13] R. G. Ham, *Exp. Cell Res.* **1963**, *29*, 515-526.

[14] 137 mM NaCl, 2.7 mM KCl, 1 mM $MgCl_2$, 1.8 mM $CaCl_2$, 0.2 mM Na_2HPO_4, 12 mM $NaHCO_3$, 5.5 mM D-glucose. The Tyrode's solution was prepared according to the receipt NO 10479 from Cold Spring Harbor Protocols (doi:10.1101/pdb.rec10479).

Part II
Acknowledgments

I would never have been able to finish my thesis without the guidance and support of my supervisors, coauthers and committee members, help from friends, and support from my family.

I would love to express my gratitude to my first supervisor at Universität Klinikum Hamburg Eppendorf, Prof. Dr. Axel R. Zander for his care and guidance. I know that it was hard for him to support me in the last few years after his retirement. Really much thankful for all his support and encouragement.

I would also express my deep gratitude to my second supervisor at University of Bremen. Prof. Dr. Kathrin Maedler who was with me in my difficult times, supervised and encouraged me during my whole PhD project. She has provided me a place and an environment without stress. During these years, I have learned a lot of things in both scientific and non-scientific lifestyle from her. Thanks for all of that.

Here, I would like to give special thank to Prof. Dr. Elke Oetjen for reviewing my thesis, Prof. Dr. Sørge Kelm and Dr. Antonio Caliani for their time and consideration and my coauthers, Prof. Dr. Christof Westenfelder at University of Utah, Dr. Claudia Lange at Universität Klinikum Hamburg Eppendorf and Dr. Amin Ardestani, Dr. Anke Meyer and Dr. Federico Paroni at University of Bremen for their help, support, care and guidance as well as warmly thank Anita, Ursula, Angela, Gita, Payal, Jenny, Wei, Alieh, Nesrine, Michael, Katrin, Katharina, Katrischa, Shakiba, Ting, Vrushali, Niels, Durga, Karthika, Dammie, Janina, Erna, Yong Hua, Sahar and other nice friends and colleagues in Bremen, Hamburg, Dresden and my nice friends in Iran.

At the end, I am especially thankful for my father, a person that gave me freedom and inspirations ncesabout life, he taught me to be a good person is the most important thing in the life. I am thankful for my sister, brother and mother for all their supports, help and care.

Above all, my endless thank is for my husband, Amir, who was with me throughout my happiness and difficulties, in my health and disease.